Design Of Experiments And Modelling Of The Direct Methanol Fuel Cell

Thesis By

Mahesh Ratanlal Shivhare

In Partial Fulfilment of the Requirements

for the Degree of

Doctor of Philosophy

School of Chemical Engineering and Advanced Materials

Newcastle University, UK

September 2008

ABSTRACT

Environmentally friendly polymer electrolyte membrane fuel cells (PEMFCs) have the potential to revolutionise mobile power sources. One of the more promising PEMFC candidates is the direct methanol fuel cell (DMFC). Significant commercial interest has been expressed in the DMFC as a consequence of it becoming a possible replacement technology for batteries and internal combustion engines. The DMFC is a simple system that utilises liquid fuel and which requires minimal ancillary equipment, and hence are more suited to the logistics of portable and vehicular applications than hydrogen fuel cells. However, significant technological challenges remain that must be addressed prior to the DMFC becoming more commercially exploitable. These challenges include improving the poor anode kinetics of methanol oxidation and reducing methanol crossover.

To aid the understanding of the various factors limiting the widespread application of the DMFC, the statistical method of design of experiments was applied. A fractional factorial design was implemented to understand the main effects and interactions of a number of operating parameters on the overall performance of the DMFC, in which the effect of the crossover of methanol through the membrane was considered. The statistical models developed facilitated the detection of key two-factor interactions of temperature with methanol concentration, type of oxidant and cathode back pressure, which suggested that an improvement in DMFC performance was achievable by reducing the effect of methanol crossover. Based on the outcomes of the parametric study, response surface methodology was applied to optimise catalyst layer formulation. The response surface method highlighted the significance of high catalyst loading and the non-linear behaviour of the Nafion® content. Furthermore, the advantage of adding PTFE in the anode catalyst formulation, to make the anode morphology favourable for carbon dioxide gas evolution, was demonstrated.

Steady state semi empirical models for the anode based on methanol oxidation kinetics and cathode considering the effect of methanol crossover through the membrane were also developed. The kinetic models for the anode illustrated the significance of water and surface intermediates in the methanol oxidation reaction on a dual site Pt-Ru catalyst and highlighted the subtle balance between the methanol adsorption-dehydrogenation step and the subsequent oxidative removal step. The

cathode model developed provided insight into the effect of methanol crossover on the cathode open circuit potential and helped in reliable estimation of the cathode polarisation curve. Finally a combination of these two models was used in the prediction of the cell polarisation characteristic as a function of cell potential, temperature and amount of methanol crossed over through the membrane.

PUBLICATIONS

Journal Articles

1. Shivhare M. R., Allen R. G., Scott K., Morris A. J., and Martin E. B., *A kinetic model for the direct methanol fuel cell anode based on surface coverage.* Journal of Electroanalytical Chemistry, 2006. 595: p. 145-151.
2. Shivhare M. R., Jackson C.L., Scott K., and Martin E.B., *Simplified model for the direct methanol fuel cell anode.* Journal of Power Sources, 2007. 173: p. 240–248.

Conference Papers

1. Shivhare M. R., Allen R. G., Scott K., Morris A. J., and Martin E. B., *A kinetic model for the direct methanol fuel cell anode based on surface coverage.* 7th European Symposium on Electrochemical Engineering, October 2005, Toulouse, France.
2. Shivhare M. R., Jackson C.L., Martin E. B., and Scott K., *Experimental design methodology for parametric study of direct methanol fuel cells*, NORDIC PEMFC 2006 Conference, September 2006, Stockholm, Sweden.
3. Duțeanu N.M., Shivhare M.R. Jackson C.L., and Scott K., *Fuels for the future*, NORDIC PEMFC 2006 Conference, September 2006, Stockholm, Sweden.
4. Shivhare M. R., Jackson C.L., Martin E. B., and Scott K., *Optimal design for direct methanol fuel cell electrodes*, NORDIC PEMFC 2006 Conference, September 2006, Stockholm, Sweden.
5. Shivhare M. R., Jackson C.L., Martin E. B., and Scott K., *Direct methanol fuel cell performance improvement using design of experiments*, H_2 Expo 2006, International Conference and Trade Fair on Hydrogen and Fuel Cell Technologies, October 2006, Hamburg, Germany.
6. Shivhare M. R., Jackson C.L., Scott K., and Martin E. B., *Simplified one dimensional model for the direct methanol fuel cell anode*, 2006 Fuel Cell Seminar, November 2006, Honolulu, Hawai.
7. Shivhare M. R., Jackson C.L., Duțeanu N.M., Scott K., and Martin E. B., *Recent advances in low temperature PEM fuel cells at Newcastle University*, Update to

the International Energy Agency (IEA) Annex meeting XVI, November 2006, Jülich, Germany.

8. Shivhare M. R., Martin E. B., and Scott K., *Fuelling the future*, SET For Britain, Britain's Younger Engineers at the House of Commons, December 2006, UK.

ACKNOWLEDGEMENTS

The past four years in my life have been a wonderful experience both personally and professionally. I had the opportunity of working with one of the most renowned research groups in the field of fuel cell and system modelling and analysis in the UK and make friends from across the globe. I would therefore like to take this opportunity to thank all the people who have been of great help and support throughout this research project.

I would first like to thank my supervisors Prof Elaine Martin and Prof Keith Scott without whose continuous guidance this research would have been an insurmountable task. Thank you for sharing your insight and enthusiasm and giving me the opportunity to work in this unique collaborative project. I am thankful to Prof Julian Morris, Prof Gary Montague, Prof Jie Zhang and Dr Suresh Thennadil, who have also been of great help especially during our technical discussions in this project.

My acknowledgement also goes to the excellent Chemical Engineering administrative and IT team, Clare McCartney, Justine McGruther, Kay Garrick, Janice Terwick, Claire Polly, Margret Carruthers, Vince Scott and Daniel Padgett, who were always easily approachable and had "ready made" solutions to my "unique" problems! Angela Bott and Debra Gray thanks for sorting out meeting dates from Elaine's diary. Thank you to the technician team, Paul Sterling, Rob Dixon and Stewart Latimer for assistance in the laboratory.

My colleagues and friends have always been a great source of support and motivation and have made Newcastle a home away from home. Ahmed, Daniel, Sophia, Chris Wong, Elitsa, Maria, Cheng, Aidong, Chris O'Malley and Tao, thanks for your truly inspiring and entertaining company in the office. Chris Jackson, Dave, Ruth, Narcis, Eileen, Raghu, and Moody, without you I would have definitely caused a mishap in the Lab! Chris and Dave, thanks for your continuous help and selfless donation of time, this project would not have been completed without your help.

Most of all, I am grateful to my parents, brother and sister who have always encouraged me. My parents have been a true source of inspiration and guidance and when I planned to move to Newcastle for post graduate studies they fully supported my dreams and inspired me with the saying *"You are the Creator of your Life"*. This quote helped me especially when life in Newcastle and PhD seemed a little tough. Pummy and Vijayji, thanks for always believing in me. Finally, Sourima, without your love, understanding and support I wouldn't have achieved this. Thanks for putting up with me and sacrificing your countless weekends!

Financial support for the project from the Centre of Process Analytics and Control Technology (CPACT), UK and conference bursaries from Society of Chemical Industry (SCI) is much appreciated.

"तूही अपनि जीवन का शिल्पकार है "

स्वमी विवेकान्नद

"*You are the Creator of your Life*"

Swami Vivevakanand

TABLE OF CONTENTS

LIST OF FIGURES

LIST OF TABLES

NOMENCLATURE

a	activity of the reactants and products
A_{Mem}	area of the membrane / m^{-2}
b	Tafel slope / V dec^{-1}
C	reactant concentration/ M, mol dm^{-3}
D_{Me}	diffusion coefficient of methanol / m^2 s^{-1}
E	electrode potential / V
E^o	standard electrode potential / V
E_a	activation energy / kJ mol^{-1}
F	Faraday's constant / 96485 C mol^{-1}
G	Gibbs free energy / kJ mol^{-1}
H	enthalpy of reaction / kJ mol^{-1}
i	current / A
i_o	exchange current / A
j	cell current density / A m^{-2}
j_o	exchange current density / A m^{-2}
j_{Lim}	limiting current density / A m^{-2}
j_{Cross}	crossover current density / A m^{-2}
k	reaction rate constants / mol $m^{-2}s^{-1}$
l_{Mem}	thickness of the membrane / m
l_a	thickness of anode backing layer / m
n	moles of electrons /mol
N	molar flux
P	partial pressure of reactant / N m^{-2}
R	gas constant / 8.3145 J $mol^{-1}K^{-1}$
R_e	cell resistance / Ω
S	entropy of reaction / kJ $mol^{-1}K^{-1}$
T	temperature / K, °C
v	volumetric flow rate / m^3 s^{-1}

x	mole fraction
z	moles of electrons exchanged during reaction /mol

GREEK

α	transfer coefficient
β	symmetry factor
ρ	density / kg m^{-3}
λ	drag coefficient
η	Overpotential / V
η_{Act}	Activation overpotential / V
η_{Ohm}	Ohmic overpotential / V
η_{Conc}	Concentration overpotential / V
γ	activity coefficient
Γ	site density / mol m^{-2}
θ_M	surface coverage of methanol
θ_{CO}	surface coverage of carbon monoxide
$\theta_{OH,Pt}$	surface coverage of hydroxyl ion on the Pt site
$\theta_{OH,Ru}$	surface coverage of hydroxyl ion on the Ru

Acronyms:

AFC	Alkaline Fuel Cell
ANOVA	Analysis of Variance
BOP	Balance of Plant
CCD	Central Composite Design
DF	Degrees of Freedom
DMFC	Direct Methanol Fuel Cell
DOE	Design of Experiments
FFD	Fractional Factorial Design
FTIR	Fourier Transform Infrared Spectroscopy
GDL	Gas Diffusion Layer

IC	Internal Combustion
IR	Infrared Spectroscopy
LSD	Least Significant Difference
M	Methanol concentration/ mol dm^{-3}
MCFC	Molten Carbonate Fuel Cell
MEA	Membrane Electrode Assembly
N117	Nafion® 117 membrane
OCV	Open Circuit Voltage
PAFC	Phosphoric Acid Fuel Cell
PEM	Polymer Electrolyte Membrane
PEMFC	Proton Exchange or Polymer Electrolyte Membrane Fuel Cell
PTFE	Polytetrafluoroethylene
RHE	Reference Hydrogen Electrode
RSM	Response Surface Methodology
SOFC	Solid Oxide Fuel Cell

Chapter 1
INTRODUCTION

1.1. Fuelling the Future

"World marketed energy consumption is projected to increase by 57% from 2004 to 2030. Total energy demand in the non-Organization for Economic Cooperation and Development (OECD) countries (China, India, Brazil and others) increases by 95%, compared with an increase of 24% in the OECD countries (UK, US, Canada, Japan and others)"- International Energy Outlook 2007, May 2007 [1].

According to the Official Energy Statistics from the US government [1], the total world's energy use will rise from 447 quadrillion British thermal units (Btu) in 2004 to 559 quadrillion Btu in 2015 and then to 702 quadrillion Btu in 2030 despite the relatively high world oil and natural gas prices. This growth in global energy demand is largely as a result of the strong projected economic growth of non-Organization for Economic Cooperation and Development countries including China, India and Brazil. The increase in global energy demand due to increasing human population, industrialisation, mobility and economic development is in conflict with the earth's ecosystem and finite fossil fuel resources. A consequence of the increase in energy usage has led to an increase in greenhouse gases such as carbon dioxide and methane and gave birth to the onset of global warming. Global warming was once a term used only by a limited number of scientists who had concerns over the effects of decades of pollution on long-term weather patterns. Today, global warming is a well recognized and debated phenomena and is used to describe a significant increase in the earth's climatic temperature over a relatively short period of time as a result of the activities of humans [2]. Thus civilization now faces a major challenge, to protect the environment while sustaining a plentiful supply of clean, pollution free, energy.

The first major step to reduce CO_2 and other greenhouse gas emissions worldwide was taken in 1997. Thirty-five industrialized nations committed to reducing their output of

greenhouse gases by varying degrees. This expanded to over 160 countries in 2007 under the Kyoto Protocol and now covers over 55% of global greenhouse gas (GHG) emissions [3]. More recently in the G8 summit held in Japan in July 2008, the leaders of the G8 countries and a number of developing countries agreed to seek substantial cuts in the emissions of greenhouse gases in an effort to tackle climate change. To reduce the emission of greenhouse gases, there is a need to develop non-fossil fuel power sources such as hydro-electric power, solar power, hydrogen engines and fuel cells [1, 2, 4].

1.2. Fuel Cell Technology

Fuel cells are power sources with the potential to replace traditional devices based on combustion of fossil fuels, particularly in the areas of automobiles and portable electronics. Fuel cells are electrochemical devices that convert chemical energy into electrical energy. Fuel cells are theoretically energy efficient compared to internal combustion engines as they are not driven by temperature differences and thus are not subject to Carnot's limit of efficiency [4]. In addition, there is no combustion of fuel hence the common pollutants such as sulphur dioxide and nitrous oxides are not produced. These advantages, together with the reduction in greenhouse gases and fuel consumption due to higher efficiencies have generated significant interest in fuel cells for stationary as well as mobile applications [5-9].

The fuel cell was first invented in 1839 by Sir William Grove, Professor of Experimental Philosophy, at the Royal Institution in London [10]. The fundamental components of a fuel cell are the electrolyte and two electrodes, an anode and cathode, sandwiched between flow field/current collector plates (Figure 1.1). A fuel such as hydrogen (or a derivative of H_2) is fed to the anode of the fuel cell and an oxidant, such as pure oxygen (or oxygen from air), is fed to the cathode. Due to the presence of a catalyst, the hydrogen atoms split into protons and electrons according to the reaction:

$$Anode: \quad H_2 \rightarrow 2H^+ + 2e^- \qquad \ldots 1.1$$

The electrons (e^-) and the protons (H^+) produced from reaction 1.1, take different paths towards the cathode. The proton (H^+) production at the anode creates a positive

potential which pushes the outer layer of protons away from the anode. The protons (H^+) transfer to the cathode side of the cell through the electrolyte by remaining attached to a water molecule (diffusion) or by being positioned between water molecules (electro osmotic drag).

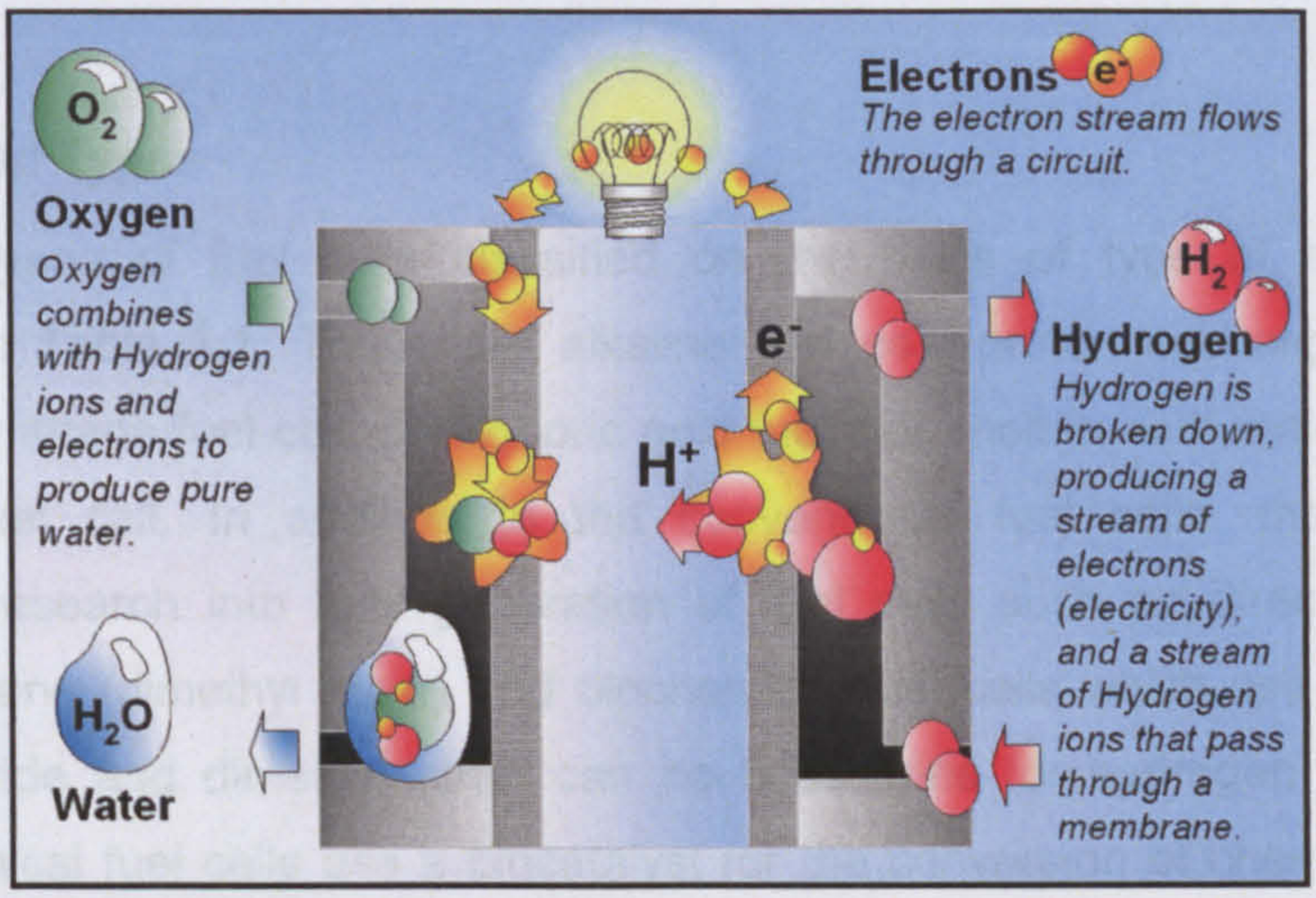

Figure 1.1: Schematic diagram showing the fuel cell working principle

The acid in the electrolyte serves to provide structure as well as a barrier to electrons. Due to this barrier, the electrons at the anode are forced to move from the anode reaction sites through the anode current collector and an external circuit. The energy that is generated is used to power an electric motor or light bulb, for example. After expending this energy, the electrons enter the cathode current collector through an external circuit to the cathode reaction sites. The electrons coming from the anode then react with the protons, originating from the electrolyte, and the oxygen molecule from the cathode to produce water:

$$Cathode: \quad \tfrac{1}{2}O_2 + 2H^+ + 2e^- \rightarrow H_2O \qquad \ldots 1.2$$

The electrons do not pass through the electrolyte because the acid chains hold their electrons tightly and thus constitute an electric insulator. Overall the cell reaction is given by:

$$Overall\ Cell: \quad H_2 + \tfrac{1}{2}O_2 \rightarrow H_2O \qquad \ldots 1.3$$

Thus the fuel cell is a type of galvanic cell where spontaneous chemical reactions occur at the electrodes [4, 10]. The fuel (H_2 or a derivative of H_2) is oxidised at the anode and

the oxidising agent (pure O_2 or O_2 from air) is reduced at the cathode. The electrolyte defines the key properties, particularly the operating temperature of the fuel cell. For this reason, the fuel cells are named by their electrolyte and in some cases the type of fuel utilised [4, 10-12].

1.2.1 Fuel Cell Types

The various types of fuel cells classified on the basis of type of electrolyte are summarised in Table 1.1. These are alkaline fuel cell, proton exchange or polymer electrolyte membrane fuel cell, phosphoric acid fuel cell, molten carbonate fuel cell and solid oxide fuel cell. In addition to the conventional fuel cells, there has been considerable research into new generation of fuel cells such as direct borohydride, methoxy methane (dimethyl ether) and biochemical fuel cells which use different fuels [11]. Borohydride and dimethyl ether can be substitutes for hydrogen and methanol fuels. Biochemical fuel cells use a biocatalyst for the conversion of chemical energy to electrical energy [13]. Materials such as methanol, organic acids, or glucose can be used as a fuel and molecular oxygen or hydrogen peroxide (H_2O_2) can be used as a oxidant. Biochemical fuel cells present an opportunity to obtain power in remote locations at low cost. They are also ideal candidates for electrically operated devices that can be implanted in the human body such as a pacemaker, where advantage can be taken of the natural fuel substances present in the body and thus can continue to draw power for as long as the subject lives [13].

Of all the fuel cells summarised in Table 1.1, the Proton Exchange Membrane Fuel Cell (PEMFC) that uses hydrogen as the clean fuel, is most widely used for transport and portable applications [14-17]. The unique feature of the PEMFC, as compared to other types of fuel cells is that it has a solid proton conducting electrolyte. The PEMFC generally operates at low temperature (below 100 °C) and generates a specific power (W kg^{-1}) and power density (W cm^{-2}) that is higher than other types of fuel cell. Generally, the use of hydrogen raises issues concerning safe transportation and storage of the fuel [5, 18, 19]. An alternative approach is to reform/oxidise a liquid fuel into hydrogen in situ. However this needs additional equipments thereby increasing the size and weight of the overall system and cost. Consequently a cell that can directly oxidise a liquid fuel, e.g. methanol is attractive [6, 17, 20].

Fuel Cell and Temperature	Electrolyte	Electrochemical Reaction	Application	Advantages	Disadvantages
Alkaline Fuel Cell (AFC) Temperature: <100 °C	Aqueous solution of potassium hydroxide soaked in a matrix	$Anode: \quad H_2 + 2(OH)^- \rightarrow 2H_2O + 2e^-$ $Cathode: 0.5O_2 + H_2O + 2e^- \rightarrow 2(OH)^-$ $Cell: \quad H_2 + 0.5O_2 \rightarrow H_2O$	Military, space, transportation	Cathode reaction faster in alkaline electrolyte hence the performance is high	Expensive removal of CO_2 from fuel and air streams required
Polymer Electrolyte Membrane Fuel Cell (PEMFC) Temp: 60-100 °C	Solid organic polymer, poly-perfluorosulphonic acid	$Anode: \quad H_2 \rightarrow 2H^+ + 2e^-$ $Cathode: 0.5O_2 + 2H^+ + 2e^- \rightarrow H_2O$ $Cell: \quad H_2 + 0.5O_2 \rightarrow H_2O$	Electric utility, portable power, transportation	Solid electrolyte reduces corrosion and management problems, Low temperature, and Quick start-up	Low temperature requires expensive catalyst, High sensitivity to fuel impurities
Phosphoric Acid Fuel Cell (PAFC) Temperature: 175 - 200 °C	Liquid phosphoric acid soaked in a matrix	$Anode: \quad H_2 \rightarrow 2H^+ + 2e^-$ $Cathode: 0.5O_2 + 2H^+ + 2e^- \rightarrow H_2O$ $Cell: \quad H_2 + 0.5O_2 \rightarrow H_2O$	Electric utility, Transportation	High efficiency in cogeneration of electricity and heat, Impure hydrogen can also be used	Platinum catalyst, Low current and power, large size and weight
Molten Carbonate Fuel Cell (MCFC) Temperature: 600 - 1000 °C	Liquid solution of lithium, sodium and/or potassium carbonate soaked in a matrix	$Anode: H_2 + CO_3^{2-} \rightarrow H_2O + CO_2 + 2e^-$ $Cathode: 0.5O_2 + CO_2 + 2e^- \rightarrow CO_2$ $Cell: \quad H_2 + 0.5O_2 + CO_2 \rightarrow H_2O + CO_2$	Electric utility	High efficiency due to high temperature, flexibility of using more types of fuels and inexpensive catalysts	High temperature enhances corrosion and breakdown of cell component
Solid Oxide Fuel Cell (SOFC) Temperature: 600 - 1000 °C	Solid zirconium oxide to which a small amount of ytrria is added	$Anode: \quad H_2 + O^{2-} \rightarrow H_2O + 2e^-$ $Cathode: 0.5O_2 + 2e^- \rightarrow O^{2-}$ $Cell: \quad H_2 + 0.5O_2 \rightarrow H_2O$	Electric utility	High efficiency due to high temperature, flexibility of using more types of fuels and inexpensive catalysts, Solid electrode reduces corrosion and management problems	High temperature enhances corrosion and breakdown of cell component

Table 1.1: Characteristics and applications of various types of fuel cell [4, 10, 12]

1.2.2 Direct Methanol Fuel Cell

The direct methanol fuel cell (DMFC) has basically evolved from PEMFC technology with similar electrode construction and materials. The first report on the DMFC was in 1954 [21]. In the 1960's, a DMFC stack with a power density of 40 mW cm^{-2} was developed with the main focus on portable military application [22]. The convenience of using liquid fuel i.e. easy handling, storage and the simplified overall design compared to the PEMFC, attracted significant attraction. Moreover the theoretical gravimetric energy density of methanol (6000 Wh kg^{-1}) was ten times higher than that of the rechargeable Li-ion battery (600 Wh kg^{-1}) [9]. Consequently, since the 1960's, considerable research has been undertaken into the technological development of the DMFC. Various sizes of DMFC demonstration units have been developed culminating in a DMFC power unit for a bus in the late 1990's [23]. In 1999, by utilising a polymer electrolyte membrane such as Nafion® and a Pt-Ru anode catalyst, a significant increase in DMFC power output was achieved by the Los Alamos Laboratory [4]. This has materialised in an increased research in DMFC technology [6, 9].

1.3. The DMFC Challenges and Limitations

The best single cell DMFC performances in terms of peak power density under high pressure using a Nafion® membrane were 300-450 mW cm^{-2} and 200-300 mW cm^{-2} in the presence of oxygen and air feed at the cathode respectively [11]. Despite this significant progress in the development of DMFC technology, there are a number of issues that limit its commercial exploitation [6, 9, 19, 24-27]. These are:

i) **Poor anodic methanol oxidation:** The electrochemical oxidation of methanol at the anode is complicated and involves the transfer of six electrons. Even the most favourable binary catalysts of Pt-Ru show kinetic limitations for methanol oxidation. In addition to the slow kinetic reaction, there is also poisoning of the reactive catalyst sites by the adsorbed intermediates and possible formation of by-products (formaldehyde, formic acid and methyl formate) due to partial oxidation of the methanol, which reduces the overall efficiency of the cell [28]. In addition, the ambiguous methanol oxidation reaction mechanism has also limited the modelling approach and there are still conflicting views about the

exact reaction pathways and rate determining step for the complex methanol oxidation mechanism [19, 29].

ii) **Fuel cell cost:** To overcome the limiting anode kinetics, relatively large quantities of catalyst materials are required. This significantly increases the cost of the fuel cell compared to its competitors such as batteries and internal combustion engines.

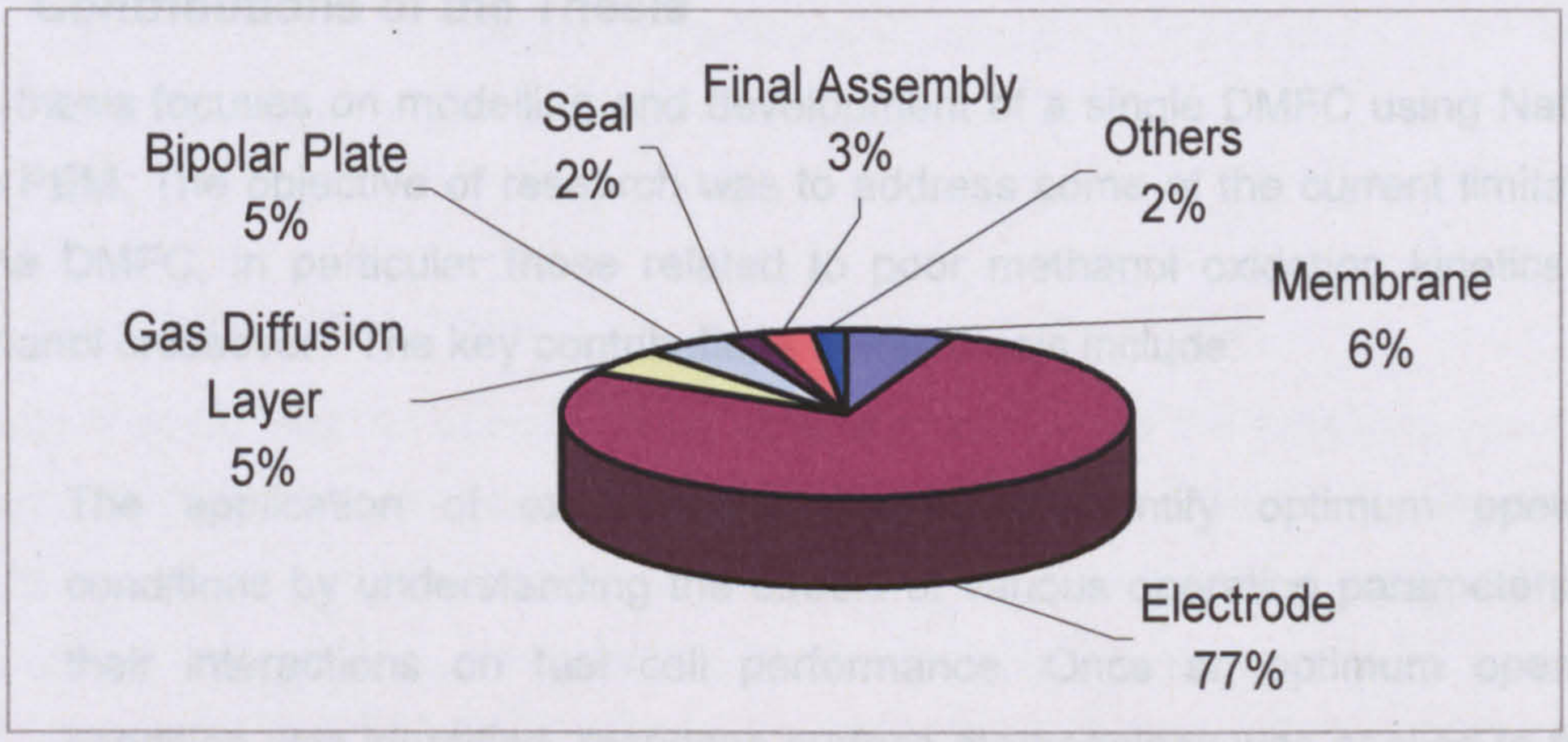

Figure 1.2: Cost distribution for a single cell in a stack to generate 80kW output [30]

In a fuel cell, the electrodes dominate the cost due to the high platinum loading (Figure 1.2). In addition, the balance of plant components including pumps, blowers and compressors also contributes significantly to the overall fuel cell cost [30].

iii) **Carbon dioxide production:** The oxidation of methanol at the anode leads to the formation of carbon dioxide. The aqueous methanol mixture has low solubility with respect to carbon dioxide hence, even at low current densities, carbon dioxide bubbles are formed both within and on the outer surface of the electrodes [24, 31]. Consequently cell performance is affected as the carbon dioxide bubbles can block the pathway for methanol to transfer to the catalyst thereby increasing mass transport limitation.

iv) **Methanol Crossover:** Methanol crossover is one of the major problems with a Nafion® based DMFC. Ideally a polymer electrolyte membrane (PEM) has to combine good proton conductivity with low electronic conductivity. Among the Currently available commercial products, Nafion® manufactured by DuPont and

analogous materials are still widely used [19]. With Nafion®, methanol easily transports through the PEM by means of electro-osmotic drag with protons and diffusion along with water molecules. This crossover of methanol results in a mixed potential in which simultaneous methanol oxidation and oxygen reduction can occur on the Pt catalyst at the cathode leading to a significant decrease in the overall cell potential and the loss of fuel.

1.4. Contributions of the Thesis

This thesis focuses on modelling and development of a single DMFC using Nafion® as a PEM. The objective of research was to address some of the current limitations of the DMFC, in particular those related to poor methanol oxidation kinetics and methanol crossover. The key contributions of this thesis include:

- The application of experimental design to identify optimum operating conditions by understanding the effects of various operating parameters and their interactions on fuel cell performance. Once an optimum operating condition was identified, response surface methodology was applied to find a suitable catalyst layer formulation to achieve higher fuel cell output. The proposed technique of experimental design highlighted significant effects and interactions influencing fuel cell output, by taking into account the variability associated with the experiments; and hence provided a more realistic methodology compared to the one-factor-at-a time approach used by most researchers [32-36].

- One of the challenges in DMFC technology is to improve the poor methanol oxidation reaction at the anode by understanding the complex methanol oxidation reaction kinetics. To address this, two detailed kinetic models that describe the surface coverage resulting from binary Pt-Ru catalyst site were proposed [37]. The analysis of the initial detailed kinetic models identified that a simplification in anode modelling can be made with some of the kinetic parameters eliminated. Based on this approach, simplified three parameter model was proposed for application to real-time DMFC simulations that is applicable to whole stack or system studies [38].

- To identify the effect of mixed potential on DMFC performance, a semi-empirical model to predict fuel cell performance with respect to cell potential,

methanol concentration and cell temperature was proposed. The model helped estimate the open circuit potential and cathode polarisation in the presence of methanol.

- The demonstration of a novel programming approach for fuel cell modelling. The proposed implementation of LabVIEW® simplified the modelling and simulation by use of graphical user interface (GUI) as compared to a text-based programming language such as Matlab [39] . LabVIEW® based models, due to the dataflow modelling structure are quick and can be linked to control applications and real time simulation.

1.5. Structure of the Thesis

Chapter 1 introduces the concept of fuel cell technology and the various types of the fuel cell. In Chapter 2, a detailed description of the DMFC in particular focusing on current practices, experimental procedures and operational aspects of the DMFC is introduced. The remainder of the thesis is then split into two parts.

The first part, Chapters 3 and 4, focuses on the application of experimental design. Chapter 3 investigates the effect of various operating parameters and their interactions on the performance of the DMFC using a fractional factorial experimental design. The results from the fractional factorial design analysis are then validated to confirm the appropriateness of the experimental design for optimising the overall performance of the DMFC. In Chapter 4, the focus is on response surface methodology for the optimisation of the membrane electrode assembly. The multiple responses, such as peak power, anode and cathode performances, were analysed to identify a suitable catalyst formulation for both the anode and cathode, thus demonstrating the application of response surface methodology in fuel cell technology.

The second part, Chapters 5 and 6, of the thesis focuses on the steady state modelling of a DMFC. In Chapter 5, two kinetic models for the DMFC anode, using a dual site approach and based on the surface coverage of the catalyst site, are proposed. The models help identify the limiting reaction and estimate the kinetic parameters. Additionally it also predicts the performance of the anode and describes the surface coverage of the intermediates (such as CO and OH) as a function of cell temperature, anode potential and methanol concentration. Based on the outcome of

the detailed kinetic models, a reduced three parameter kinetic model is also proposed, which swiftly returns the cell current density utilising cell temperature, anode potential and methanol concentration as inputs. Chapter 6 proposes a DMFC cell model using the detailed methanol oxidation and oxygen reduction kinetics. The model also takes into account the effect of the mixed potential on cell performance and the methanol concentration profile across the cell. The models were developed using LabVIEW® and it was concluded that a fairly accurate model was achieved based on the experimental data.

Finally in Chapter 7, conclusions are drawn from the overall research and future areas for DMFC research are proposed.

Chapter 2
THE DIRECT METHANOL FUEL CELL

2.1. Introduction

The direct methanol fuel cell (DMFC) although commercially attractive, has some limitations, as explained in Chapter 1, hindering its widespread application in power generation. These limitations are associated with its complicated reaction mechanism and cell design. However before attempting to analyse the behaviour and model of the DMFC, it is important to understand the mechanism and design principles behind the DMFC. Hence in this chapter, the basic principles of DMFC operation are explored. The various inefficiencies related to the DMFC are also investigated. In addition a brief literature review focusing on semi-empirical modelling is presented to identify potential areas of improvement in terms of DMFC modelling.

2.2. General Overview

The DMFC belongs to the class of polymer electrolyte membrane fuel cells (PEMFC) and uses methanol as a fuel instead of using hydrogen. Since the 1960's [14, 15], the development of DMFC's has provided significant research opportunities due to the following advantages of using methanol in a fuel cell [5, 6, 8, 9, 18, 19]:

(i) The most important characteristics by which energy generating devices are compared is energy density, i.e. the amount of energy in watt-hours (Wh) packaged per unit weight (kg) and unit volume (L). Methanol is a liquid fuel with a gravimetric and volumetric energy density (6000 Wh kg^{-1} and 4800 Wh L^{-1}) that is higher than that for rechargeable batteries such as Lithium-Ion (110 Wh kg^{-1} and 300 Wh L^{-1}). Thus a fuel cell operating with methanol could provide higher operational life compared with a battery of the same size, thereby providing advantages in terms of cost and weight.

(ii) Successful development of a DMFC will eliminate the need for an on-board fuel-processor sub-system that is required for the production of hydrogen. Since the weight and volume of the fuel-processor sub-system are approximately the same as the electrochemical stack sub-system, their elimination from the fuel

cell system will increase the overall efficiency of the fuel cell system as less energy input will be required to run the whole system.

(iii) The DMFC is an ideal portable power source for civilian and defence applications including laptop computers, cellular phones and portable power. The DMFC has considerably higher energy density than the most advanced rechargeable batteries (nickel–metal hydride and lithium ion) that are currently used for such applications. In particular it outperforms other batteries in the kilo-watt range [40]. DMFC performance is also stable compared to some of the other technologies in the field of PEMFC. In this research work, the relative stability of a single DMFC for ~200 hrs operating under various conditions was tested. The results are presented in Appendix A, which shows the stabile performance of DMFC at varying load conditions. Similar research on a DMFC stack by other groups has shown that the DMFC achieves stable power output up to 8000 hrs [40, 41]. Moreover the DMFC has a fast dynamic response to variable load changes [42], This behaviour is evident from observing the changes to sudden load conditions, Appendix A.

(iv) The DMFC emits zero pollutants. Research by leading groups in DMFC development [4, 40] suggests that there are no traceable emissions of methane, higher hydrocarbons, NO_x or similar substances when operated within a closed environment. Hence DMFC power systems are in line with current laws and regulations and will contribute to green power generation.

Figure 2.1 shows a schematic diagram of a DMFC where methanol (CH_3OH) and water (H_2O) react electrochemically at the anode to produce carbon dioxide (CO_2), protons (H^+) and electrons (e^-):

$$Anode: \quad CH_3OH + H_20 \longrightarrow CO_2 + 6H^+ + 6e^- \qquad E^o = 0.02\ V \qquad \ldots 2.1$$

The carbon dioxide produced in the methanol oxidation reaction at the anode could react with alkaline electrolytes to form carbonates hence in the DMFC an acidic electrolyte such as Nafion® membrane is used to aid carbon dioxide rejection [6, 19]. The acidic electrolytes also act as a barrier (electronic insulator) to the electrons produced in reaction 2.1 due to which the electrons are forced to reach the cathode via an external circuit. In contrast, the acidic electrolyte serves as a carrier for the protons. The rate of proton transfer is a function of electrolyte membrane thickness, the amount of water in the membrane, current density, cell temperature and the

number of ions transported [10]. The protons and electrons on reaching the cathode react with oxygen (typically air) to produce water:

$$Cathode: \qquad 1.5O_2 + 6H^+ + 6e^- \longrightarrow 3H_2O \qquad E^o = 1.23\ V \qquad \ldots 2.2$$

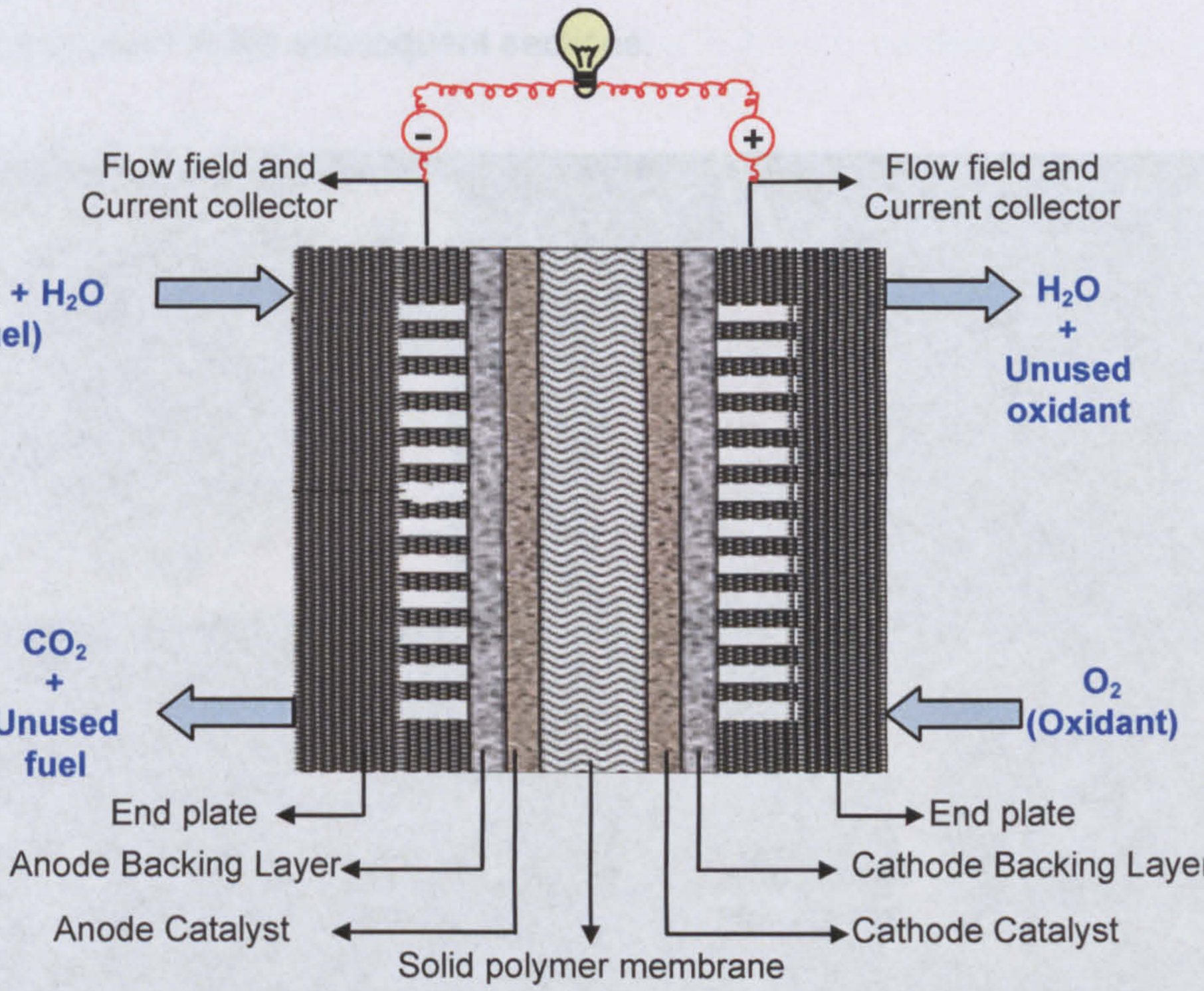

Figure 2.1: Schematic representation of a direct methanol fuel cell

The electrons produced at the anode carry the free energy change of the chemical reaction and while passing through an external circuit, the energy generated can be used to power an electric motor or light a bulb, for example. The overall cell reaction, given by reaction 2.3, shows that methanol and oxygen react to produce water and carbon dioxide:

$$Cell: \qquad CH_3OH + 1.5O_2 \longrightarrow CO_2 + 2H_2O \qquad E^o = 1.21\ V \qquad \ldots 2.3$$

These reactions are promoted by the incorporation of platinum based electro catalyst materials in the electrodes [4, 27, 28, 43-45].

2.3. DMFC Components

In a DMFC, the Membrane Electrode Assembly (MEA), which is a combination of an anode, membrane and cathode, forms the heart of the cell. The MEA assembly, Figures 2.2.e and 2.2.f, is sandwiched between porous backing layers and the flow

field/current collectors using PTFE (Polytetrafluroethylene) gaskets, Figure 2.2.d, which act as seals. The hardware of the fuel cell is the backing layer and flow field/current collectors (Figure 2.2.a). These are designed to maximize the current that can be obtained from the heart of the fuel cell [4]. A detailed description of each component is given in the subsequent sections.

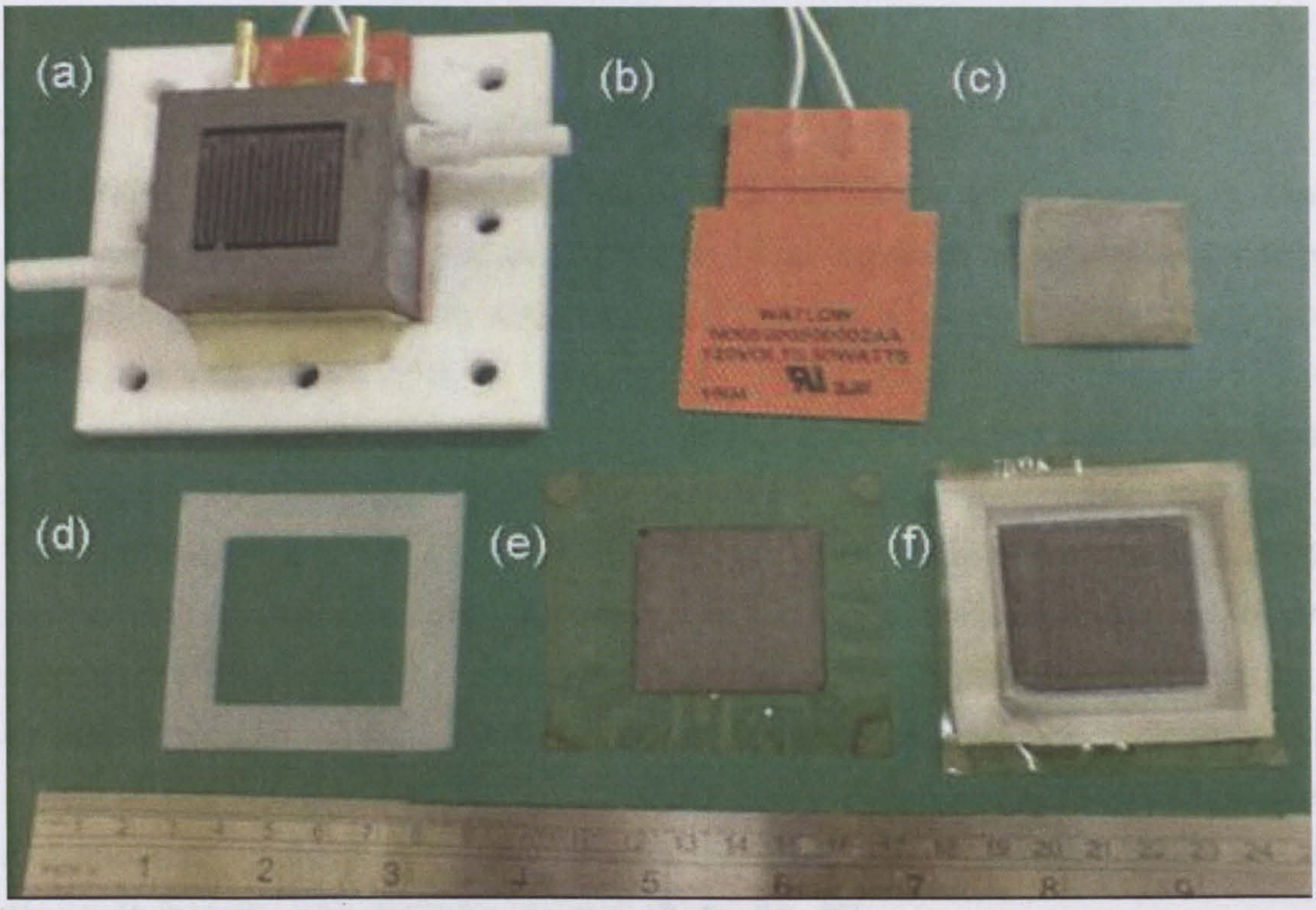

Figure 2.2: Basic DMFC Components. (a) Flow field and current collector with a heating pad (b) Heating pad, (c) Titanium mesh for anode (d) PTFE Gasket for sealing, (e) MEA (f) MEA after 180hrs of continuous operation.

2.3.1 Membrane Electrode Assembly

The combination of the anode/membrane/cathode is referred to as the membrane electrode assembly (Figure 2.2.d) and its construction and composition is of crucial importance to the fuel cell performance [4, 10, 27]. The key goals in terms of design include:

i) To minimize all forms of inefficiencies and maximize power density,

ii) To minimize the Pt catalyst loading (and thus minimise the cost per kW of the PEMFC) in the gas diffusion electrodes by high utilization of the surface areas of the nano-sized particles of the electrocatalyst,

iii) To achieve effective thermal and water management,

iv) To maximise the lifetime of the PEMFC to satisfy the requirements of a particular transportation or portable power application.

It is in this area of science and technology that major advances were made in the late 1980's and in the early 1990's [14, 15]. The following section provides a brief description of the components of MEA.

2.3.1.1 Solid Polymer Electrolyte Membrane

The DMFC utilises a solid perfluorosulfonic acid membrane as the electrolyte. The membrane, which is typically 30 to 200 microns thick, provides an electrolyte capable of withstanding high pressure differentials with no free corrosive liquids which can attack the cell components [6, 19]. Besides acting as an acid electrolyte, the perfluorsulfonic acid membrane separates the fuel from the oxidant gas. Membranes are typically solid, hydrated sheets of a sulfonated fluoropolymer similar to Teflon. The acid concentration of a particular membrane is characterised by its equivalent weight (EW), grams of dry polymer/mole of ion exchange sites. Generally, a thinner membrane with a lower equivalent weight results in higher cell performance. However thinner membranes can materialise in higher methanol crossover from the anode to the cathode and can give rise to mixed potential effects, which is the simultaneous oxidation of methanol and the reduction of oxygen at the same electrode thereby reducing fuel efficiency [6, 19, 25, 46].

The most commonly used perfluorosulfonic acid electrolyte membrane is Nafion® from DuPont [9, 19]. Other perfluorosulfonic membranes used include Gore-Select® (Gore), BAM® (Ballard), Aciplex®-S (Asahi Chemical Industry Co.) and Flemion® (Asahi Glass Company) [6, 9, 19]. The typical chemical structure of some of these membrane is illustrated in Figure 2.3 and it comprises of three regions [4, 16]:

i) a Teflon like, fluorocarbon backbone comprising hundreds of repeating $-CF_2-CF-CF_2-$ units,

ii) $\underset{\displaystyle CF_3}{-O-CF_2-\overset{}{CF}-O-CF_2-CF_2-}$ side chains which connect the molecular backbone to the sulfonic acid ion region,

iii) ion clusters consisting of sulfonic acid ions, $SO_3^- - H^+$.

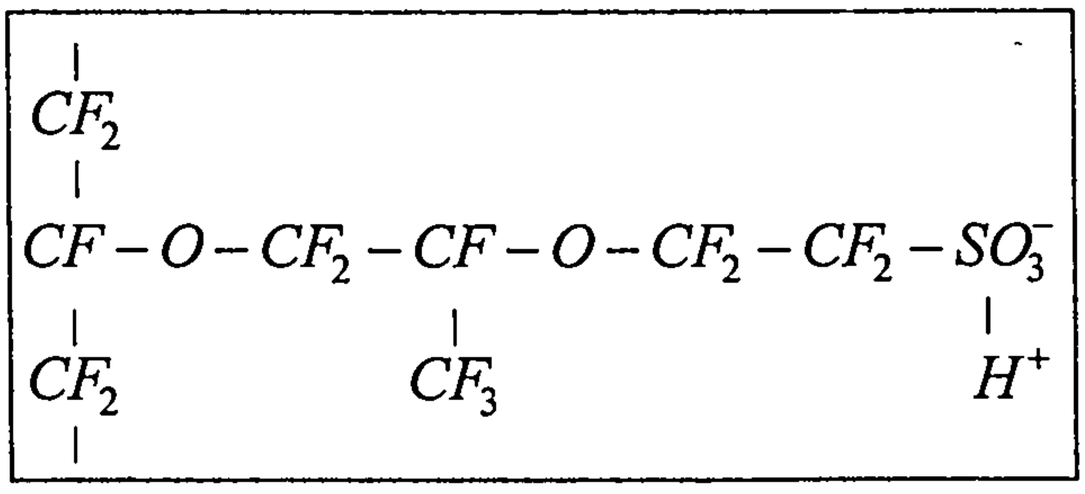

Figure 2.3: Chemical Structure of membrane material (Nafion® by DuPont) [4]

The negative SO_3^- ions are permanently attached to the side chain and cannot move. However, when the membrane becomes hydrated by absorbing water, the hydrogen ions connected to the sulfonic acid region ($SO_3^- - H^+$) become mobile. Due to this movement of the hydrogen ions, bonded with the water molecules, from one SO_3^- site to another SO_3^- site, within the polymer membrane, the polymer electrolyte membrane becomes an excellent conductor of hydrogen ions.

2.3.1.2 Electrodes and Electrode Structure

Platinum (Pt) and platinum ruthenium (Pt-Ru) alloys are the most studied and appropriate electro-catalysts for DMFC electrodes [6, 19, 29, 43, 47, 48]. The rationale is that with a Pt-Ru alloy electro-catalyst, the water discharge at the anode occurs at low potentials on the Ru sites with methanol chemisorption taking place on the adjoining Pt sites. The removal of carbon monoxide requires the presence of OH species at low potential. This is possible due to the presence of Ru sites since OH groups are preferably formed on ruthenium (Ru) at fairly low electrode potentials (~0.3 V vs. Normal Hydrogen Electrode). Hence a binary catalyst such as Pt-Ru is considered to be the best option for the DMFC anode.

The electrodes in a fuel cell can dominate the cost due to high platinum loadings [30]. The electrode structure is formed by evenly distributing the fine catalyst particle on the surface of larger particles of fine carbon powder. A carbon based powder, such as Ketjen Black, Vulcan XC-72 or Acetylene Black, has been widely used [4, 6, 9]. The catalyst is finely divided and spread out so that a high proportion of the surface area is in contact with the reactants. The final electrode structure is made by two alternative methods, although the end result is essentially the same [10, 11].

i) Separate electrode method:

For this method, the carbon-supported catalyst mixture is fixed to a porous and conductive backing layer such as carbon cloth or carbon paper. To minimise the contact losses and to form a three phase reactive zone, Nafion® is added to the catalyst mixture. Polytetrafluoroethylene (PTFE) is often added because it is hydrophobic and hence would repel water to the surface where it can be removed. The catalyst mixture is fabricated on the carbon cloth or carbon paper by using a proprietary technique such as tape casting, brushing or painting [10]. In addition to providing the basic structure for the electrode, the carbon paper or cloth also distributes by diffusion the gas onto the catalyst. Due to this, they are often termed as the "gas diffusion layer" [10]. The final separate electrodes fabricated by this method are then fixed to each side of a piece of polymer electrolyte membrane using a hot pressing method [10, 11].

ii) Building the electrode directly onto the membrane:

The alternative method is to build the electrode directly onto the membrane that is the platinum on the carbon catalyst is fixed directly to the electrolyte. Consequently the electrode is manufactured directly onto the membrane as opposed to them being manufactured separately. The catalyst, which is often (but not always) mixed with hydrophobic PTFE, is applied to the electrolyte membrane using rolling, spraying or painting [10]. Once the catalyst is fixed to the membrane, a gas diffusion layer is applied. This is a carbon cloth or paper, and is approximately 0.2 to 0.5 mm thick, which is similar to the separate electrode method.

The resulting structure from both methods is shown in Figure 2.2.d and depicted schematically in Figure 2.4. The carbon supported catalyst particles are connected to the electrolyte on one side with the gas diffusion layer on the other side, resulting in three-phases that are highly reactive. Apart from the afore mentioned methods, in the last decade, there has been an increase in the use of electrochemical methods such as electrochemical deposition to fabricate the precious metal catalyst layer directly onto the membrane or onto the gas diffusion electrode [49-51] . The electrochemical deposition technique has significantly reduced the precious metals loading in the fuel cell and has also increased the performance of the DMFC. To tackle the production of carbon dioxide at the anode, the use of a titanium mesh on which the catalyst is deposited by electrochemical deposition technique has been proposed [31].

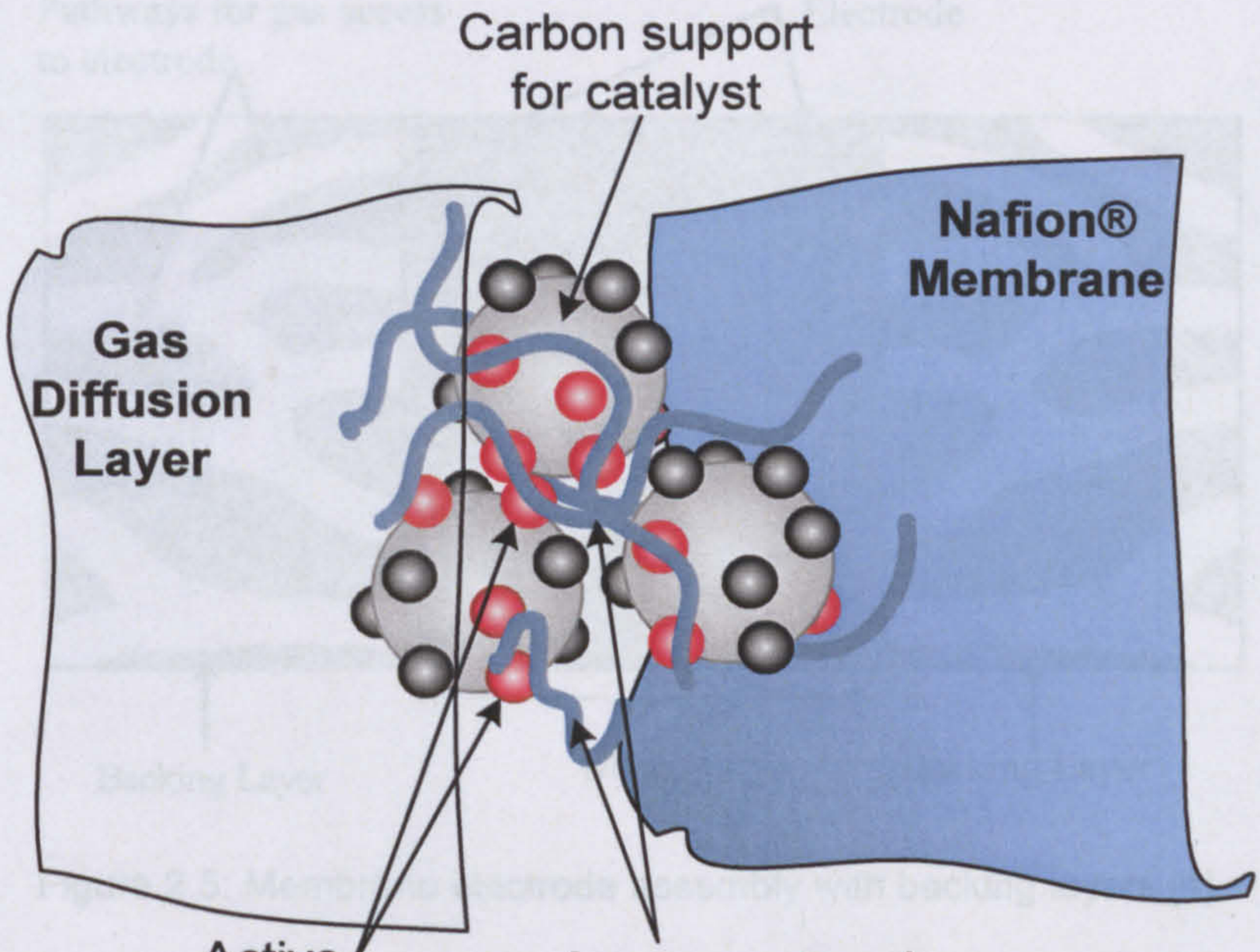

Figure 2.4: Simplified structure of a PEM fuel cell electrode [10]

2.3.2 Backing Layers

The hardware of the fuel cell, that is the backing layers and the flow field/current collectors, are designed to maximize the current that can be obtained from a MEA. The backing layers, which are positioned alongside the anode and the cathode (Figure 2.5) are typically made of porous paper or carbon cloth that is typically 100 to 300 microns thick [27, 50, 52]. ETEK type "A" carbon cloth and Toray carbon paper are the most commonly used material for the backing layer [16, 27, 52]. Carbon is used since it is a relatively stable material and helps in the conduction of electrons from the anode.

To ensure the effective diffusion of reactants to the catalyst site on the MEA, the backing layers are often coated with carbon powder treated with PTFE. The addition of PTFE binder to carbon promotes areas of relatively high and low hydrophobicity which in turn assists in gas and liquid flow to the various catalyst sites on the MEA [10]. This gas diffusion layer also forms an electrical connection between the carbon-supported catalyst and the bipolar plate, or another current collector. In addition, it transports the water produced away from the electrolyte surface and forms a protective layer over the very thin layer of catalyst.

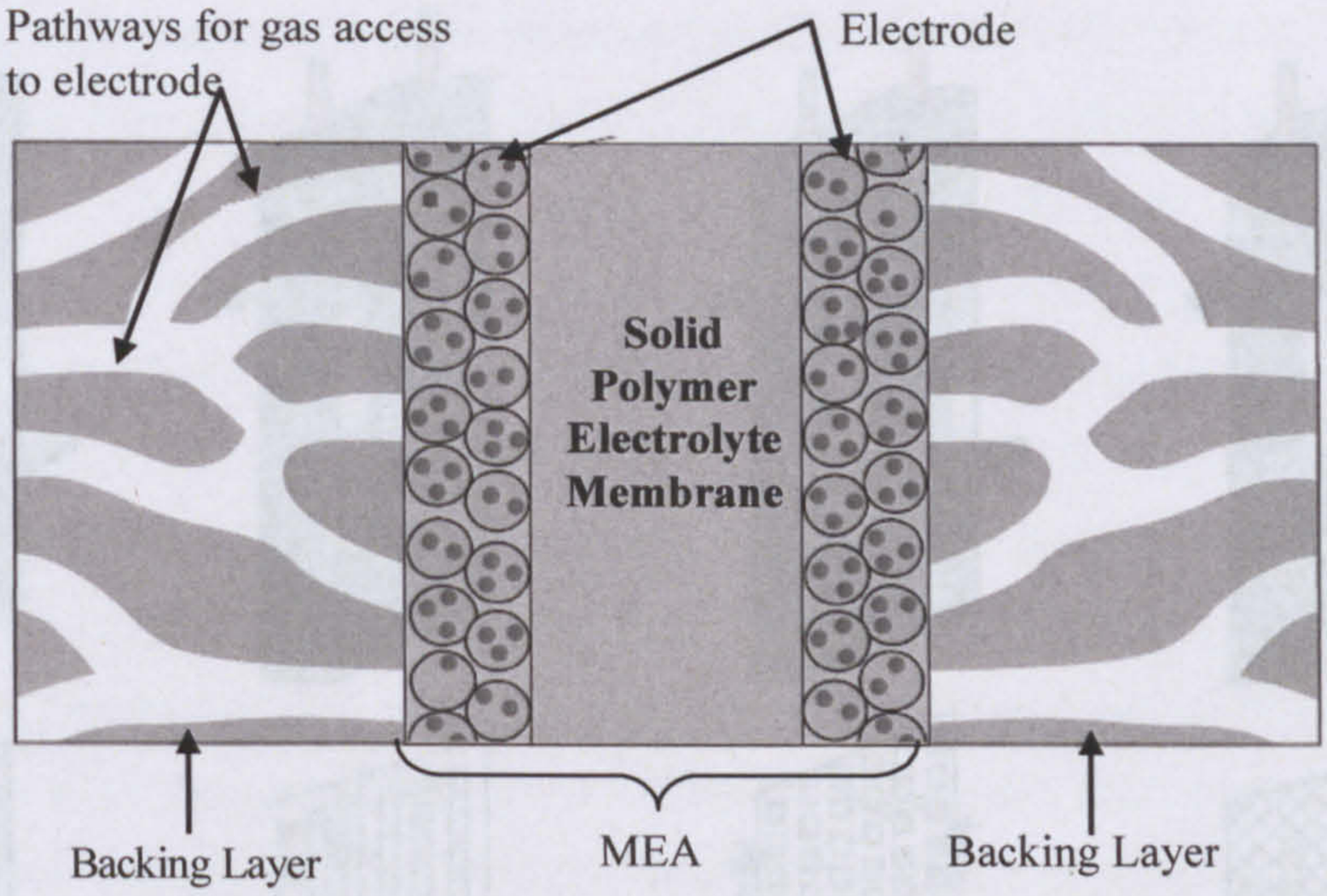

Figure 2.5: Membrane electrode assembly with backing layers [4].

2.3.3 The Flow Fields/Current Collectors

Pressed against the outer surface of each backing layer is a piece of hardware, generally made of graphite (Figure 2.2.a), called a current collector plate [4, 10]. The primary task of this plate is to provide a reactant flow field and electronic conduction. The side of the plate next to the backing layer comprises of a number of channels machined into the plate, which transport the reactants in and out of the cell. The pattern of the flow field in the plate as well as the width and depth of the channels have a significant impact on the effectiveness of the distribution of the reactant gases across the active area of the MEA. They also affect water flow to the membrane and water removal from the cathode [53, 54].

The most common flow field patterns/designs are parallel, serpentine, spot and mesh (Figure 2.6). The main advantage of using a serpentine design is the forced flow direction. In addition, compared with the spot flow field design, a homogeneous current density distribution is obtained [55]. The interaction between the flow field and gas diffusion layer is significant and affects the performance of the DMFC and hence the design of the flow field is important [55]. In cells operating at higher temperatures and flow rates, structures such as parallel flow are preferred as they provide low resistance to the flow resulting in lower pressure losses [53]. Some researchers prefer the use of a mesh electrode structure as it provides greater surface area for gas evolution reaction, excellent mass transport rates and better gas release [24, 54, 56].

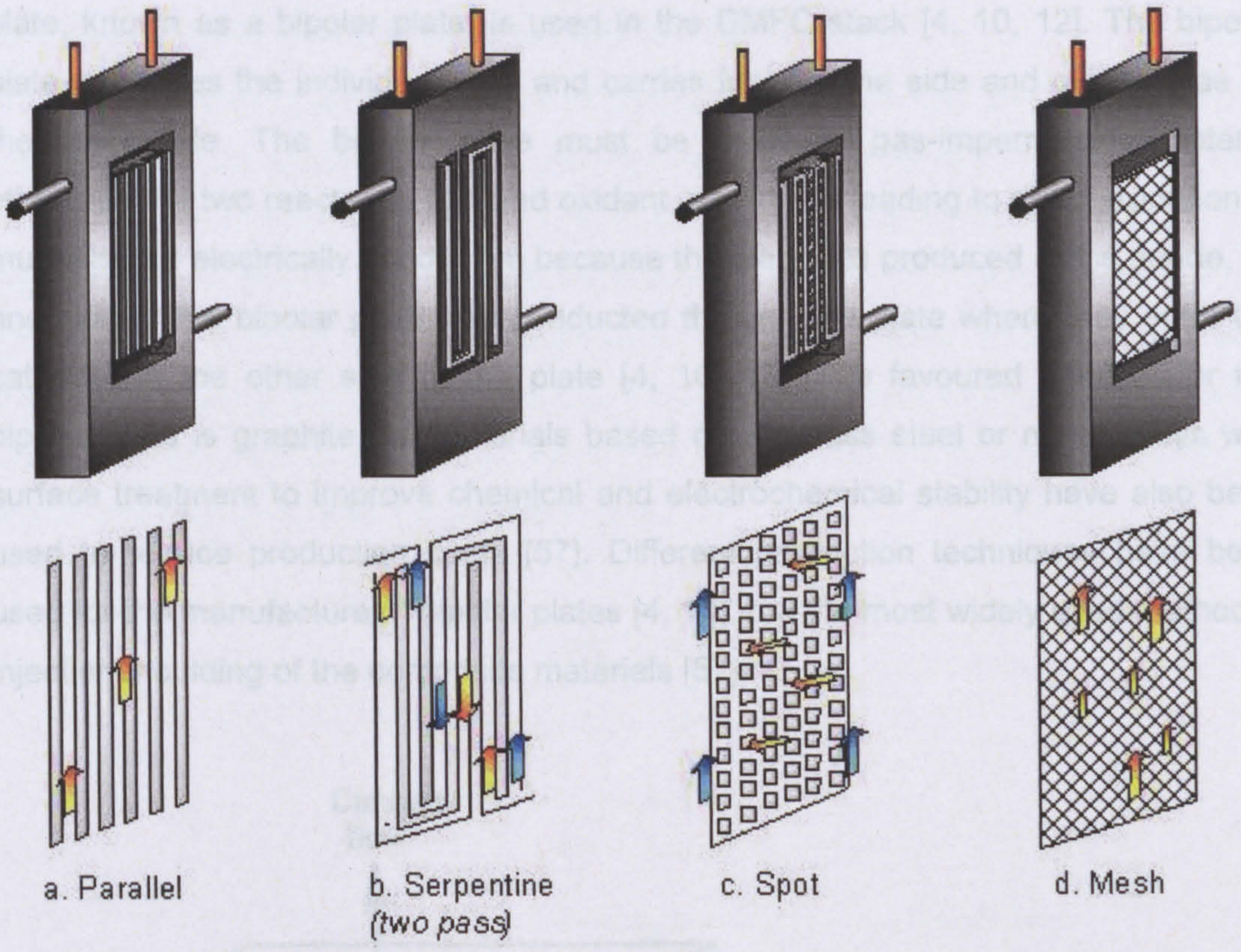

Figure 2.6: Examples of flow field designs structures [10].

The second task of this plate is that of current collection. Electrons produced by the oxidation of the fuel (methanol) must be conducted through the anode via the backing layer and then through the plate before they exit to do some work, such as produce energy to light a bulb, and re-enter at the cathode plate. In a single fuel cell, these two plates are the final components that make up the cell.

2.4. Direct Methanol Fuel Cell Stack

The voltage from a single cell is approximately 0.7 V, which is sufficient to support a small light bulb. As most applications require a much higher voltage, the required voltage is obtained by connecting individual fuel cells in series to form a fuel cell stack (Figure 2.7). When the cells are stacked in series, the operating voltage increases to the product of 0.7 V and the number of cells stacked.

If the cells are placed side by side to increase the operating voltage, a separator plate is required to connect the cells electrically in series and to prevent the mixing of reactants. This separator plate increases the overall volume and weight of the stack. To overcome this problem the integrated structure of a flow field and a separator

plate, known as a bipolar plate, is used in the DMFC stack [4, 10, 12]. The bipolar plate separates the individual cells and carries fuel on one side and oxidant gas on the other side. The bipolar plate must be made of gas-impermeable material otherwise the two reactants, fuel and oxidant, would mix leading to direct oxidation. It must also be electrically conductive because the electrons produced at the anode, on one side of the bipolar plate, are conducted through the plate where they enter the cathode on the other side of the plate [4, 10, 12]. The favoured material for the bipolar plate is graphite but materials based on stainless steel or metal alloys with surface treatment to improve chemical and electrochemical stability have also been used to reduce production costs [57]. Different production techniques have been used for the manufacture of bipolar plates [4, 10], but the most widely used method is injection moulding of the composite materials [57].

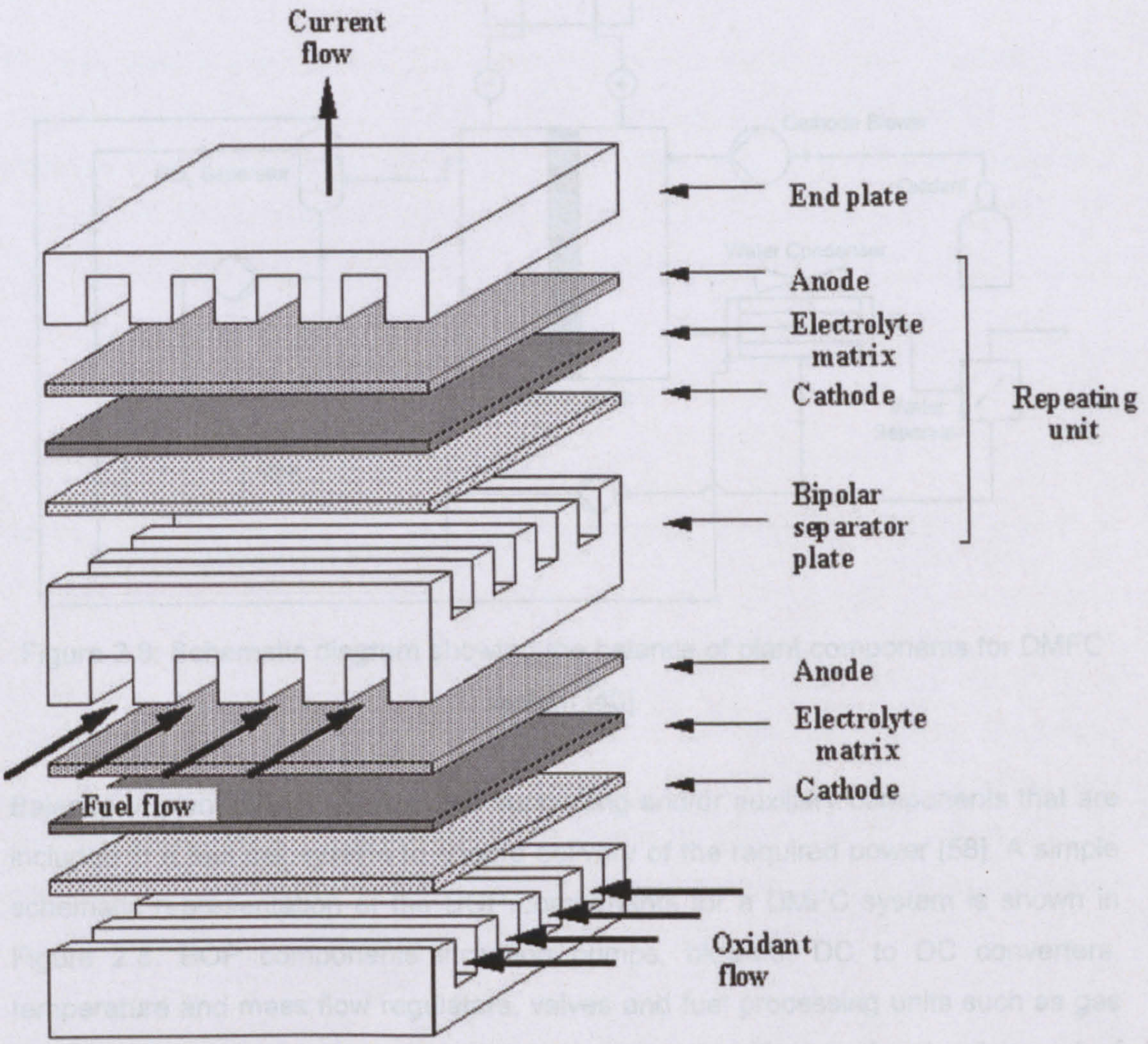

Figure 2.7: Schematic diagram of fuel cell stack [58]

2.5. Balance of Plant and Other Components

A DMFC includes other components including gaskets, clamps, and endplates [10]. Gaskets act as a sealant between the MEA and plates (Figure 2.2.d), and they are usually made of Teflon or silicon rubber so that they are corrosion resistant and impermeable to gases. The endplates are used to provide mechanical support to the fuel cell and to keep the cell compressed. Generally thicker endplates are used thereby increasing the weight of the cell. However advanced structures, such as the Dbow-concept, for the end plates have been proposed. These significantly reduce the weight and volume of the endplates [59] .

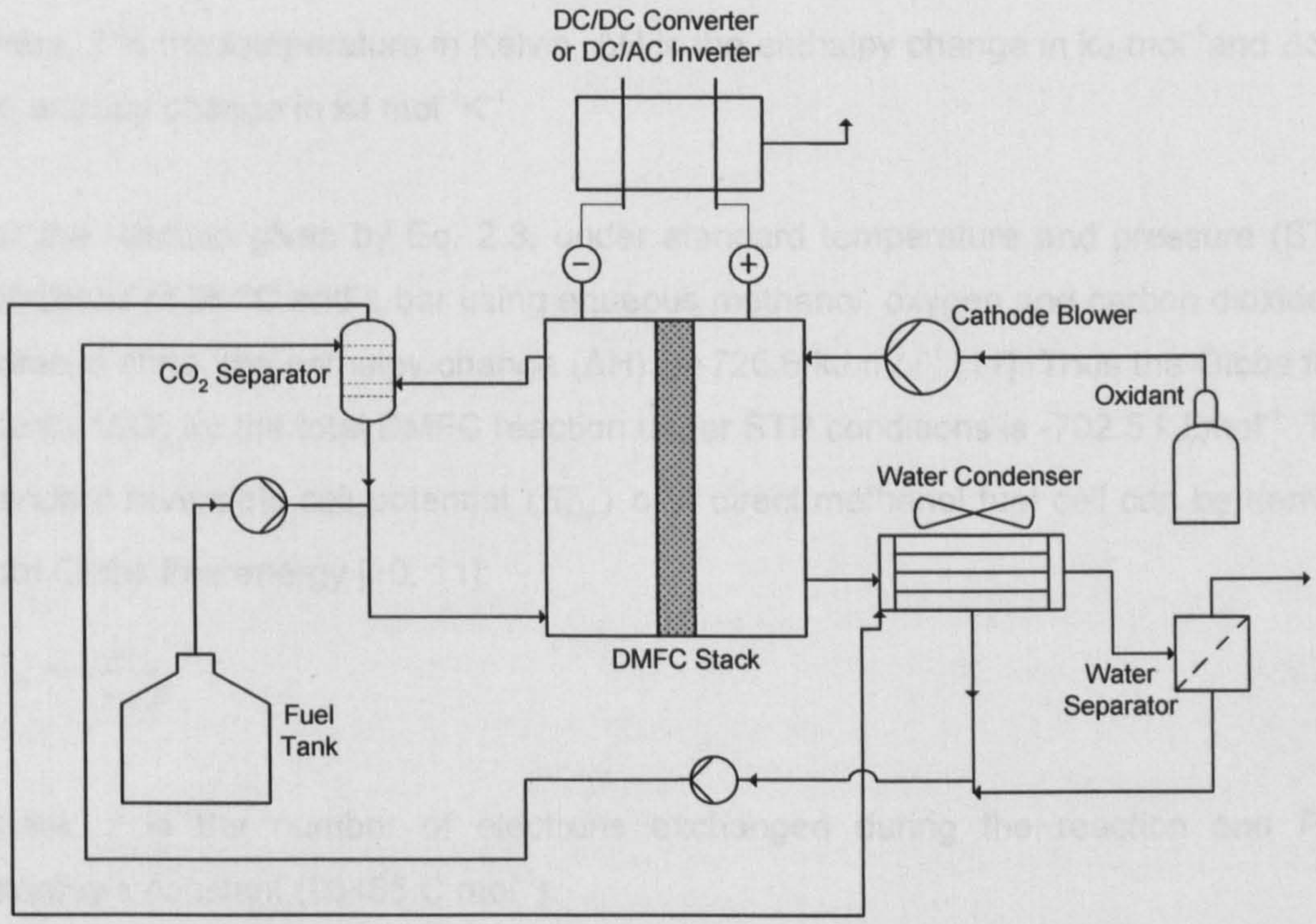

Figure 2.8: Schematic diagram showing the balance of plant components for DMFC system [40].

Balance of plant (BOP) refers to the supporting and/or auxiliary components that are included in a fuel cell system to ensure delivery of the required power [58]. A simple schematic representation of the BOP components for a DMFC system is shown in Figure 2.8. BOP components including pumps, blowers, DC to DC converters, temperature and mass flow regulators, valves and fuel processing units such as gas humidifiers, liquid vaporizer and/or compressors are critical to the development of compact, reliable and portable fuel cell systems. Power output from the complete fuel cell system depends on the operating conditions, which in turn depends on the BOP

components. Additional power is required to operate some of the BOP components such as pumps, compressor and the fuel processing unit and hence the fuel cell system has to be oversized to power them decreasing the efficiency of the overall system [4, 10, 12].

2.6. Operational DMFC Voltage

The maximum non-expansion work obtainable from a process at constant pressure and temperature is given by Gibbs free energy (ΔG) [60]:

$$\Delta G = \Delta H - T \times \Delta S \qquad \ldots 2.4$$

where, T is the temperature in Kelvin, ΔH is the enthalpy change in kJ $mol^{-1}$and ΔS is the entropy change in kJ $mol^{-1}K^{-1}$.

For the reaction given by Eq. 2.3, under standard temperature and pressure (STP) conditions of 25 °C and 1 bar using aqueous methanol, oxygen and carbon dioxide in gaseous state, the enthalpy change (ΔH) is -726.6 kJ mol^{-1} [11]. Thus the Gibbs free energy (ΔG) for the total DMFC reaction under STP conditions is -702.5 kJ mol^{-1}. The standard reversible cell potential (E^{o}_{rev}) of a direct methanol fuel cell can be derived from Gibbs free energy [10, 11]:

$$E^{o}_{rev} = -\frac{\Delta G}{z \times F} \qquad \ldots 2.5$$

where, z is the number of electrons exchanged during the reaction and F is Faraday's constant (96485 C mol^{-1}).

Under STP conditions, solving Eq. 2.5 gives the open circuit voltage (OCV) for a DMFC as 1.21 V. This is similar to the OCV for hydrogen fed polymer electrolyte membrane fuel cells (1.23 V). For the above reactions both the enthalpy change (ΔH) and entropy change (ΔS) can be considered constant within a certain temperature as long as no phase change occurs in any of the species involved. Thus it can be said that the free energy is a linear function of temperature:

$$\frac{\partial(\Delta G)}{\partial T} = \Delta S^{o} \qquad \ldots 2.6$$

Combining Eq. 2.5 and Eq. 2.6:

$$E_{rev} = E^{o}_{rev} + \frac{\Delta S^{o}}{z \times F}\left(T - T^{o}\right) \qquad \ldots 2.7$$

At STP, the entropy of reaction for a DMFC is -0.081 kJ $mol^{-1}K^{-1}$ [11]. Consequently from Eq 2.7, an increase in cell temperature results in the decrease in the reversible open circuit voltage (E_{rev}). Similarly to examine the effect of methanol concentration on the reversible OCV, if the Nernst equation [11] is applied to Eq. 2.3 under ideal conditions (i.e. complete separation of the anode and the cathode chambers) then:

$$E_{rev} = E^{o}_{rev} + \frac{R \times T}{z \times F} \ln\left(\frac{a^{1.5}_{O_2} \times a_{CH_3OH}}{a^{2}_{H_2O} \times a_{CO_2}}\right) \qquad \ldots 2.8$$

where, *R* is the gas constant (8.3145 J $mol^{-1}K^{-1}$) and *a* is the activity of the reactants and products in Eq. 2.3.

From Eq. 2.8 it can be concluded that for increasing methanol concentration, the reversible OCV should increase. However in reality compared to the ideal thermodynamic relationship, given by Eq. 2.7 and Eq. 2.8, the DMFC exhibits different behaviour for both changes in the temperature and methanol concentration. This is due to some inefficiency which tends to reduce the actual voltage of the DMFC from the ideal open circuit voltage of 1.21 V as shown in Figure 2.9. These non-ideal effects or inefficiencies are separated into three categories; activation polarisation, ohmic polarisation, concentration polarisation and methanol crossover.

The characteristic S-shape of the stationary current-voltage trajectory, Figure 2.9, resulting from these three major irreversibilities or inefficiencies, is a classical method to represent the performance of a fuel cell [10, 12]. The curve shows limiting mechanisms occurring during the operation of a fuel cell. The combination of all three polarisations has distinguishable effects on the performance of the cell since each is dominant at different current stages.

2.6.1 Activation Polarisation

Activation polarisation occurs due to the energy intensive activity associated with the making and breaking of the chemical bonds at the cathode and anode. At the anode, aqueous methanol enters the reaction site and forms ions and electrons with the aid of the Pt based catalyst. The same procedure occurs at the cathode catalyst site.

Incoming oxygen reacts with the electrons and protons on the Pt catalyst to form water. The amount of energy required for the forming and destroying all these bonds comes from the fuel and thus the overall energy that the cell can produce is reduced.

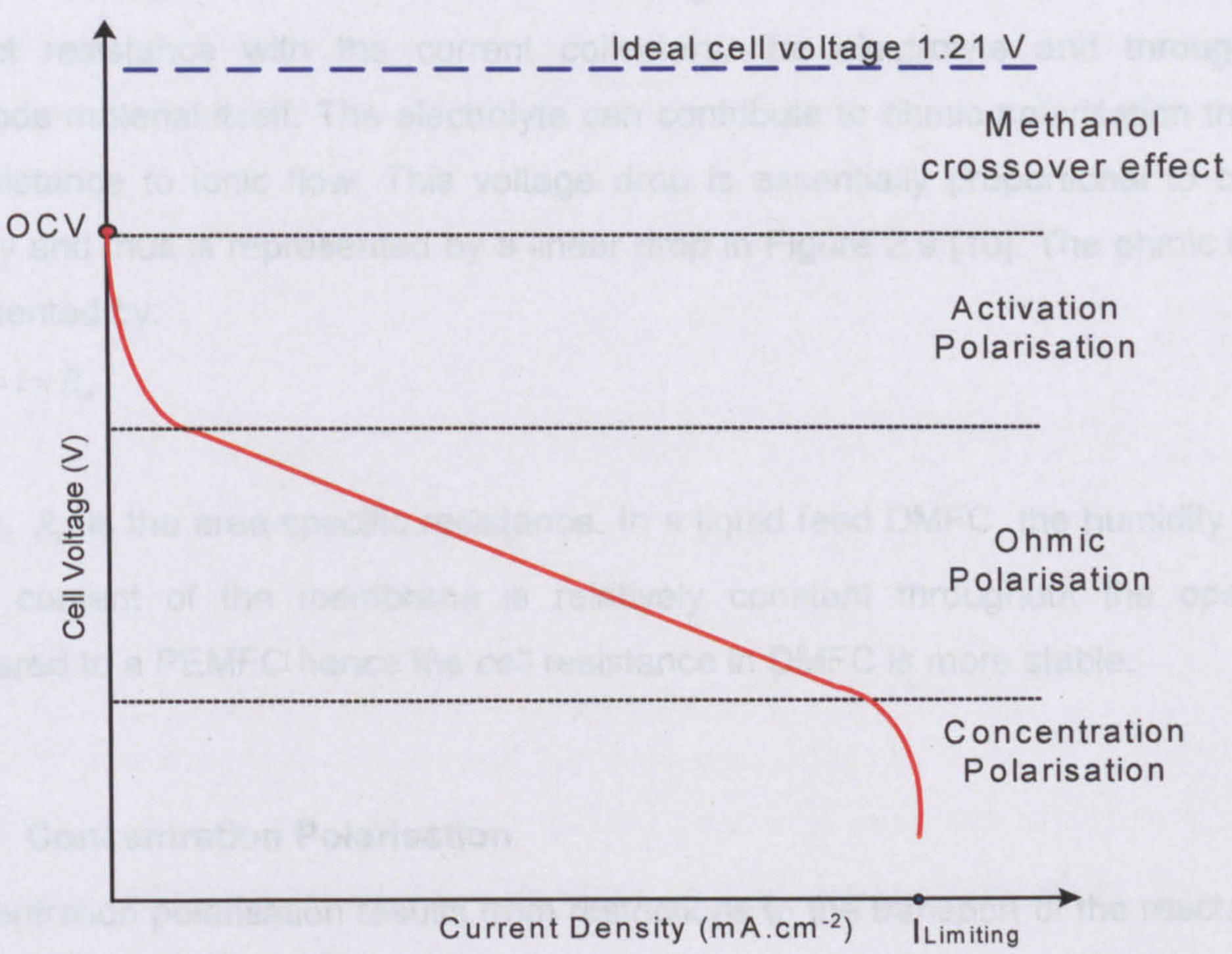

Figure 2.9: Characteristics of DMFC polarisation (current-voltage) curve

In low and medium temperature fuel cells, the activation overvoltage is the most important irreversibility and cause of voltage drop. Activation overvoltage at both electrodes is important in cells using fuels other than hydrogen, such as methanol [11]. From Figure 2.9 it can be observed that the voltage drop in the activation region is highly non-linear. Activation polarisation (η_{Act}) is described by the Tafel equation:

$$\eta_{Act} = \frac{RT}{\alpha n F} \ln\left(i / i_o\right) \qquad \ldots 2.9$$

where, i_o is the exchange current density in A cm^{-2} and α is the charge transfer coefficient. The charge transfer coefficient is the proportion of electrical energy applied that is harnessed when changing the rate of an electrochemical reaction. The value of α depends on the reaction involved and the material of the electrode, but it is in the range of 0 to 1.0 [10, 11].

2.6.2 Ohmic Polarisation

Ohmic polarisation is caused by electrical losses in the cell. The resistance of the current collecting plates, electrodes and the electrolyte are all factors that contribute to the electrical loss. The resistance resulting from the electrodes is due to the contact resistance with the current collectors, the electrolyte and through the electrode material itself. The electrolyte can contribute to ohmic polarisation through its resistance to ionic flow. This voltage drop is essentially proportional to current density and thus is represented by a linear drop in Figure 2.9 [10]. The ohmic loss is represented by:

$$\eta_{Ohm} = i \times R_e \qquad \ldots 2.10$$

where, R_e is the area-specific resistance. In a liquid feed DMFC, the humidity or the water content of the membrane is relatively constant throughout the operation compared to a PEMFC hence the cell resistance in DMFC is more stable.

2.6.3 Concentration Polarisation

Concentration polarisation results from restrictions to the transport of the reactants to the reaction sites. This usually occurs at high current density since the formation of product water and excess humidification blocks the reaction sites. Concentration polarisation is also termed as "mass transport" loss since the reduction in the concentration is a result of the failure to transport sufficient reactant to the electrode surface. Concentration polarisation is a significant factor in fuel cell performance if the fuel cell is operated with a low reactant flow rate or when a low concentration of fuel is used. Concentration polarisation is given by:

$$\eta_{Conc} = \frac{RT}{nF} \ln\left(1 - {}^{i}\!/\!_{i_{Lim}}\right) \qquad \ldots 2.11$$

Where, i_{Lim} is the cell limiting current density in A cm^{-2} (Figure 2.9). Concentration polarisation is also affected by the MEA fabrication technique, gas diffusion layer and flow field geometry [6].

2.6.4 Methanol Crossover

Methanol crossover is the transfer of methanol through the membrane from the anode to cathode. Apart from the non-ideal effects or inefficiencies discussed in sections 2.6.1 to 2.6.3, the crossover of methanol is also a major cause of

inefficiency as it is essentially wasted and the cathode catalysts are poisoned by the carbon atoms in the methanol [46, 61]. Methanol crossover is mainly a result of diffusion and electro-osmotic drag [6, 19].

Methanol transfer by diffusion is a result of the concentration gradient across the membrane. The diffusion flux through the membrane can be modelled by using Fick's law [62]:

$$N_{Me} = -D^{e}_{Me} \times \frac{C^{a}_{Me}}{l_{Mem}} \times A_{Mem} \qquad \ldots 2.12$$

where, D^{e}_{Me}, the methanol diffusion coefficient ($cm^2\ sec^{-1}$), is a function of temperature, C^{a}_{Me} is the concentration of methanol at the anode, A_{Mem} is the area of the membrane and l_{Mem} is the thickness of the membrane.

Assuming that the methanol concentration is approximately the same at the interface between the anode catalyst layer and the membrane as in the feed concentration, the methanol diffusion coefficient (D^{e}_{Me}) can be calculated by combining Eq. 2.12 with Faraday's equation [62]:

$$D^{e}_{Me} = -\frac{i \times l_{Mem}}{zFC^{a}_{ME}} \times A_{Mem} \qquad \ldots 2.13$$

where, i is the cell current density, A cm^{-2}.

Ren et al., (2000) [63], Narayanan et al., (1995) [64] and Ling et al., (2004) [65] measured the methanol flux for different membrane thicknesses and showed that the methanol crossover rate is inversely proportional to the membrane thickness, indicating that diffusion is dominant [66]. Apart from diffusion, a certain amount of methanol transfers through the membrane by accompanying the water molecule, which in turn is attached to a proton migrating from the anode to the cathode. This phenomenon is known as electro-osmotic drag. It can also occur due to physical similarities in molecular size and dipole moment between the water and methanol molecule. Due to these similarities, it is assumed that the drag coefficient for water (λ_{H_2O}) and methanol (λ_{Me}) are approximately equal. The protons migrating through the membrane cannot distinguish between these two molecules and the amount of

methanol passing through the membrane is calculated as the methanol fraction (X_{Me}) in the liquid [67, 68]:

$$N_{Me,drag} = \frac{i \times A_{Mem}}{F} \times \lambda_{H_2O} X_{Me} \quad \ldots 2.14$$

where, λ_{H_2O} is the water drag coefficient which typically lies between 2 to 5 depending on the cell temperature and pressure [68, 69].

A significant amount of research has been undertaken to measure the crossover of the methanol through the membrane and its impact on DMFC performance [25, 26, 62, 69-73]. In this research, a technique similar to Qi et al., [62] was used to measure crossover. In this case, the cathode was supplied with nitrogen feed and the anode was supplied with a regular feed of aqueous methanol. By reversing the poles of the power supply, the methanol, which had crossed over to the cathode was forced to oxidize at the cathode at high potentials, 900 to 1000 mV. The limiting current (I_{Cross}) resulting from this methanol oxidation at the cathode was measured. This approximately represents the rate of the methanol crossover at open circuit. Other techniques used to measure the crossover of methanol are gas chromatography, FTIR and IR spectroscopy. These devices detect the level of carbon dioxide produced at the cathode due to the oxidation of the methanol that has crossed over [26, 72, 74].

2.7. Literature Review on DMFC Models

The performance of the DMFC depends on a large number of parameters including physical and electrochemical parameters (e.g. composition of the catalyst layer, kinetic reaction, single or dual site catalyst), design parameters (e.g. catalyst layer and backing layer thickness, flow field design, membrane thickness, porosity of gas diffusion later) and operating parameters of the overall cell (e.g. cell temperature and pressure, flow rate of reactants, concentration of methanol). In a DMFC many of these parameters are intimately coupled, resulting in the need to search for the 'optimal' cell design and operating conditions. A better understanding of the relationship between these parameters is essential and can be achieved by combining mathematical modelling approaches with a detailed experimental programme. Mathematical modelling and simulation can help understand the effect of

the different physical and electrochemical phenomena, occurring inside the cell, on fuel cell performance and hence influence its design and optimization [75-78].

Different types of modelling approaches, such as analytical models, semi-empirical models and mechanistic models, that focuses on one or more aspects or components (catalyst, stack, polarisation, crossover, etc) pertaining to the cell have been reported in the literature [78]. The mechanistic and semi-empirical modelling approaches are further subdivided into 1-dimensional models, where all regions of interest are combined and solved in a single domain, or 2 or 3-dimensional models, where sets of equation for each region of interest are utilised [75]. This thesis focuses on one-dimensional semi-empirical model which facilitates in the prediction of the fuel cell performance as a function of different operating conditions. Hence the literature review concentrates on this aspect.

Scott et al., [79-84] have developed a number of simplified one dimensional, single phase models to study transport and electrochemical reactions in a DMFC. Furthermore Scott et al., [79] proposed an empirical model that was developed from the empirical models of a PEMFC (Table 2.1), to predict the cell voltage versus current density performance of a DMFC [85-87]. The resulting model was solved using non-linear regression algorithms (Appendix B) and was fairly accurate compared to other models.

Model Equation	References
$E = E_0 - b\log(i) - R_e i$	Srinivasan et al., [87]
$E = E_0 - b\log(i) - R_e i - m\times\exp(ni)$	Kim et al., [85]
$E = E_0 - b\log(i) - R_e i + \alpha\, i^k \ln(1-\beta\, i)$	Squadrito et al., [86]
$E_{cell} = E_o - b\log(i) - R_e i + C_1 \times \ln(1 - C_2)$	Scott et al., [79]
$E_{cell} = E_o - b\log(1 - k_b i) - R_e i - E^o_{MC} \times (1 - e^{-\alpha \times i/T})$	Hwan Kim et al., [88]

Table 2.1: The empirical and semi-empirical model equations for PEMFC and DMFC

Based on Srinivasan's [87] model, Kim et al., [85], Squadrito et al., [86] and Scott et al., [79] proposed different semi-empirical relationships, to predict the cell polarisation curve. These are summarised in Table 2.1. The first three terms in these models

account for the open circuit voltage (E_0), activation polarisation ($-b\log i$) and ohmic losses ($-R_e i$). The three terms in Kim et al., [85], Squadrito et al., [86] and Scott et al., [79] are similar to those in Srinivasan et al., [87] model. To improve model fit to the DMFC polarisation curve, a fourth term was proposed by Scott et al., [79] that takes into account the mass transport limitations present in fuel cell operation. However this simplified model has a mathematical limitation and was unable to fit the open circuit voltage (OCV) as shown in Appendix B. This limitation to predict the OCV was addressed by Hwan Kim et al., [88] who proposed a semi-empirical approach which included the methanol crossover effect to model the DMFC polarisation curve. Tu et al., [89] also developed a semi-empirical model to overcome the limitation of Scott et al., [79] model. They proposed a model to distinguish between the individual voltage losses due to methanol crossover and the overpotential of both the anode and the cathode.

Scott et al., [80, 82] also proposed a semi-empirical model for a DMFC based on Tafel type kinetics and mass transport coefficients. In Scott et al., [80, 82], they derived the parameter for a new membrane electrode assembly to predict the DMFC performance. One different area of modelling from Scott's group was in the dynamic modelling of a DMFC using a semi empirical approach (Simouglou et al., [90, 91]). The model was developed using the statistical approach of canonical variate analysis (CVA) and it provided one-step-ahead predictions of the dynamic voltage response of the cell.

Another group active in the field of DMFC modelling is based at the Research Centre Jülich, Germany [46, 67, 69, 71, 92-97]. Most of their models are one dimensional physico-chemical models that predict the cell polarisation curve. Kulikovsky [46, 67, 95-97] developed a model for the cathode side to understand the different reactive zones in the cathode compartment as well as developing models that focus on the anode side and the mixed potential effects. Baxter et al., [98] proposed a single phase mathematical model for a liquid-feed DMFC anode. They used a macro-homogeneous model to describe the reaction and transport in the catalyst layer of a vapour-feed anode and predicted the amount of methanol crossover through the membrane for any given current density.

Sundmacher et al., [99] observed that pulsed methanol feeding could achieve a significant increase in the cell voltage and a considerable reduction in methanol

consumption. Kauranen et al., [29] reported a model describing both the oxygen reduction and the methanol oxidation in the cathode of a DMFC and concluded that the oxygen reduction current is decreased in the presence of methanol oxidation due to surface poisoning. This model was based on a dual site approach which suggested that for a Pt-Ru dual catalyst for the anode, the Ru sites act as a centre for CO oxidation and Pt the sites act as a centre for the adsorption and dehydrogenation of methanol. Using this dual site approach, Kauranen et al., proposed a model for the anode and predicted the surface coverage of individual species with changes in cell potential. Alternatively, Nordlund et al., [100, 101] used a single site mechanism, which suggested that adsorption and dehydrogenation of methanol and CO oxidation occurs both on the Pt-Ru catalyst sites. Using this single site concept, they studied the influence of the porous anode structure on anode polarisation with mathematical modelling and experimental verification.

More recently computational fluid dynamic (CFD) modelling techniques have provided a different approach to mechanistic modelling of the fuel cell [75]. Wang et al., [102] proposed a comprehensive two phase model for a DMFC using CFD. The model considered convection and diffusion of both the gas and liquid phases in addition to the cathode and anode reactions. Similarly Murgia et al., [103] described a one-dimensional, two-phase, multi-component steady-state model based on phenomenological transport equations for the catalyst layer, diffusion layer, and polymer membrane for a liquid-feed DMFC. Meyers and Newman [104-106] developed a theoretical framework that described the equilibrium of multi-component species in the membrane. The transport of species in the membrane based on concentrated-solution theory, transport phenomena in the porous electrodes and membrane swelling was taken into consideration as well. In addition they also proposed a simple kinetic based model to predict the anode polarisation curve for a DMFC. Based on the Myers and Newman simplified anode model Garcia et al., [107] proposed a one dimensional cell model for inclusion in a real time simulation for system or stack studies. The model accounted for methanol oxidation at the anode, methanol crossover through the membrane and the mixed potential at the cathode.

Although a significant amount of research has been undertaken in DMFC modelling, a number of unresolved issues remain, particularly in support of the emerging portable designs and systems. Modelling work in the area of micro-fluidic theory for portable systems including the effects of channel geometry and wettability characteristics of the gas diffusion layer on fluid flow in the anode or cathode remains

a challenge [77]. Another area is the numerical modelling of two-phase flows (both at the anode and the cathode) with parallel experimental studies on the visualization of these phenomena. Despite significant research there is still limited understanding of the mechanism of methanol oxidation on dual site Pt-Ru catalyst [19]. Improved and validated mechanistic models are also required to enable better design of fuel cells and its components [78]. For systems analysis and real time simulation where calculation economy is necessary, there is also a need for a simplified model that has as inputs, a limited number of parameters, such as potential, methanol concentration and cell temperature to reliably predict the cell current density.

To address some of these issues, in this research work, kinetic based models to understand the mechanism of methanol oxidation on dual site Pt-Ru catalyst are developed in Chapter 5 [37]. In addition, a simplified model with a limited number of parameters as inputs is also proposed in chapter 5 to predict the cell current density [38]. A semi-empirical model taking into effect the methanol crossover effect to overcome the limitation of Scott et al., [79] model is proposed in Chapter 6.

2.8. Conclusions

The DMFC is a promising power generation system with a range of possible applications. To overcome the current limitations of DMFC there is a need to identify improvements in overall reaction kinetics (catalyst), mass transport limitations (gas diffusion layer and flow field designs), membrane properties and design (crossover) of DMFC. This is possible with steady state models focusing on the specific area of interest. For example, a kinetic based model for the DMFC anode can help identify the rate determining reaction step and the behaviour of the different reaction intermediates on the catalyst site, which in turn can help understand the methanol oxidation mechanism.

A steady state model to understand the impact of mixed potential due to methanol crossover can help identify those conditions, which can either inhibit the reaction of methanol on the cathode or assist in finding an alternative catalyst. Such modelling approaches will allow detailed studies to be undertaken pertaining to the development of DMFC's. In addition, with the potential to be used in a real time simulation, these detailed models will be of interest in predicting the cell performance in whole system or fuel stack studies.

In theory, as discussed in section 2.2, the working principles of the DMFC appear simple but in reality it is supported by a complex mechanism which, to date, is not clearly understood. DMFC performance is influenced by physical, electrochemical, design and operating parameters and their interactions. Consequently optimisation of the process is challenging due to the number of permutations involved. One approach to attain a better understanding of the interactions is through the application of experimental design.

The cell operating conditions including temperature, pressure, methanol concentration and reactant flow rates can be manipulated to optimise cell performance but at the cost of high methanol crossover resulting in a loss of system efficiency. The adoption of a systematic approach through design of experiments can help identify the most suitable conditions for DMFC operation taking into account the negative effects such as methanol crossover. The optimisation of a MEA is another key area where experimental design can be applied. Since there are different ways to construct a MEA, as discussed in section 2.3.1, each of the variables involved in MEA fabrication and their interaction have a significant impact on the overall performance of a DMFC. It is hypothesised that through the application of statistical design the key variables and their interactions can be studied, thereby identifying combination that achieves overall MEA optimisation. In the following Chapters 3 and 4, this proposed technique of experimental design has been put to test and attempt has been made to show that experimental design can be a valuable tool for understanding complex parameters and their interactions affecting the DMFC operation.

Chapter 3
PARAMETRIC STUDY USING DESIGN OF EXPERIMENTS

3.1. Introduction

Two key barriers to the commercial exploitation of a DMFC, as identified in Chapter 1, are its poor anode performance and the methanol crossover through the Nafion® membrane [5, 9, 26, 40, 50]. To overcome these limitations, recent trends have been to focus on the optimisation of the Membrane Electrode Assembly (MEA) and to investigate alternative membrane fabrication techniques. This has resulted in less research being undertaken into parametric studies. However, recent parametric studies by Ge et al., (2005) [33] have shown that some limitations of the DMFC can be addressed by modifying basic operating conditions.

A number of studies have been undertaken in the past to investigate the effects of various operating conditions such as cell temperature, methanol concentration, cathode back pressure, flow rates of reactant and type of oxidant on the performance of the DMFC [32, 41, 92, 108, 109]. However, the majority of these have not fully addressed the current limitations in DMFC technology due to one or more of the following reasons:

i) The majority of the parametric studies looking to understand the issues limiting DMFC performance were based on a one-factor-at-a-time (single factor analysis) experimental approach [32-34, 36, 108, 109]. These studies fail to take account of any interactions between operating conditions that have an effect on the performance of the DMFC. Additionally in these parametric studies, conclusions drawn were solely based on the cell polarisation data. Cell polarisation data alone is not sufficient to explain various phenomena. Other factors to be considered include methanol crossover, which affects the overall cell performance.

ii) Researchers studying the development of DMFCs using a parametric approach, rarely make use of standard test conditions. To maximise DMFC performance, some published work have reported results of experiments

undertaken at extreme values of operating conditions at the cost of system efficiency or alternatively with high catalyst loadings [32, 36, 108-110]. To address this situation the European Commission is aiming to standardise methodologies and fuel cell testing procedures (Fuel Cell Testing, Safety and Quality Assurance, FCTES^{QA}) [111].

iii) The number of experimental runs required to investigate the range of factors involved in a DMFC performance study is significant and hence such studies are expensive. For example in recent work Ge et al., (2005) [33], undertook 63 experimental runs to investigate 5 operating factors. Despite the large number of experimental runs, they were unable to explain the significant interactions between the parameters. Additionally their study did not include significant factors such as type of oxidant and the pressure at cathode.

iv) Variability in the performance of a DMFC is another critical issue. Variability arises due to several factors such as non-identical functioning of the electrodes (anode and cathode), which is mainly due to the complex structure of the MEA, inconsistency in MEA fabrication and the complex reaction mechanism. Additionally, variability due to loss of performance of the DMFC through continuous use of the same MEA as a result of catalyst poisoning is also an issue [35].

In summary, there is a need for a statistical framework that allows the main effects and interactions between various operating factors on DMFC performance to be examined and analysed, as well as a method that takes into account the underlying variability. Cell polarisation alone is not the only key indicator of DMFC performance. Other criteria such as anode polarisation and methanol crossover are also required to be considered.

The objectives of this chapter are therefore to:

- Apply statistical experimental design to enable the impact of different operating factors such as temperature, pressure, methanol concentration, air/oxygen supply, flow rate of reactants and their interactions on the performance of a single DMFC to be investigated.
- Identify an 'industrially' realistic set of operating conditions that give 'maximum' power, 'high' anode limiting current and 'low' methanol crossover rate.
- Confirm the results of the statistical analysis and hence optimise overall fuel cell performance by limiting the methanol crossover effect

3.2. Design of Experiments

DMFC studies have made extensive use of one-factor-at-a-time approaches (i.e. single factor analysis). This approach is based on selecting a baseline set of levels, for each factor in the experiment, then varying each individual factor over its range but keeping the other factors at a constant baseline level. The data generated by this method is then used to illustrate how the response variable of interest is affected by each factor. The major limitation of this strategy is that it fails to consider any possible interactions between the factors due to the number of permutations required [112, 113]. In a DMFC, factors interact and hence a single factor analysis would fail to capture such behaviour. Compounding this challenge is the need to incorporate, within the analysis, the fact that significant variability is associated with DMFC experimentation.

One definition of statistical design of experiments (DOE) is "the process of planning the experiment so that appropriate data that can be analysed by statistical methods will be collected, resulting in valid and objective conclusions" [113]. In an experimental design, the factors chosen for study are varied systematically to allow the investigation of both single factors and their interactions. Planning and design is the key to the successful implementation of experimental design. In particular the selection of factors, their levels, and the choice of response variable determine the structure and form of the experiment.

3.2.1 Selection of Response Variables

There are number of metrics to measure the performance of a DMFC including fuel cell efficiency, fuel utilisation, cell limiting current, current density at a particular cell voltage and peak power output. Power density, which is a product of cell voltage and cell current density, gives a good indication of performance for various current densities, whilst the anode limiting current and methanol crossover are the best indicators of cell limiting current and fuel cell efficiency respectively. Consequently peak power density, methanol crossover rate and anode limiting current were selected as the response variables. The rationale for selecting the last two was to overcome the issue that operating parameters can be pushed to extremes to ensure maximum power is achieved, even though the parameters are unrealistic for application in practice.

3.2.2 Selection of Factors and their Levels

After selecting the response variables, the factors and their levels are determined. The factors considered in this parametric study, that are thought to influence maximum power output, methanol crossover rate and anode limiting current, are summarised in Table 3.1 along with their levels. The factors were identified utilising the results from previous parametric studies [32-34, 108, 109]. To investigate the effect of oxidant on the peak power output, a categorical factor, type of oxidant at the cathode, was included in the design. The next step in the design phase is the selection of the experimental design.

Factors	Low Level (-)	Centre point (0)	High Level (+)
Cell Temperature (°C)	60	75	90
Methanol feed concentration (M)	1	2	3
Type of oxidant at cathode *(Categorical)*	Air	--	Oxygen
Flow rate of methanol (ml min^{-1})	3.4	5.0	6.60
Flow rate of oxidant (ml min^{-1})	300	400	500
Back pressure at cathode (MPa)	0.1	0.15	0.2

Table 3.1: The factors and levels selected for the parametric study

3.2.3 Choice of experimental design

Factorial designs are one of the most efficient methods to study the effect of two or more factors and their interactions on the outcome (response) of an experiment [113]. In a 2^k factorial design, 'k' factors are investigated at two levels, termed high and low. One of the issues with 2^k designs is that the number of experiments doubles with each additional factor [112, 113] thereby impacting on the length of time to perform the study and the quantity of materials or other resources required. In these situations, partial or fractional factorial designs may be more appropriate. A fractional factorial design is characterised by its resolution level which is defined in terms of the confounding pattern, that is the inability to distinguish between the effects of certain factors [112, 113]. For example, for a Resolution III study each main effect is confounded with one or more higher order interaction. Resolution III are efficient designs enabling a significant number of factors to be tested using a limited number of experiments. In practice they are used to investigate robustness and realise the initial screening of the factors. A Resolution IV design, allow the main effects to be investigated but the 2-factor interactions are confounded with each other. Resolution

IV designs provide greater confidence with respect to the impact of the main effects compared to a Resolution III design. In fractional factorial design, after full factorial designs, Resolution V studies are considered to be the next most desirable as they allow all the main effects and 2-factor interactions to be investigated.

For this research, the six factors detailed in Table 3.1 were investigated. A 2^{k-1} fractional factorial design with two centre points will result in a Resolution V design. This design can be augmented to a full factorial or a central composite design to allow the investigation of additional higher order interactions that may be of interest. Moreover replicates of the centre points allow the variability in the design to be calculated and also identify any curvature in the resulting model. The experimental runs were randomised to satisfy the statistical requirement of independence. Table 3.2, summarises the design matrix for the parametric study and Table C.1 in the Appendix C gives the measured responses.

Standard Runs	Randomised Runs	Type	Cell Temperature (°C)	Methanol Concentration (M)	Methanol Flow Rate ($ml.min^{-1}$)	Oxidant Flow Rate ($ml.min^{-1}$)	Back Pressure at Cathode (Mpa)	Type of Oxidant (Categorical)
1	23	Fact	90	1	3.4	300	0.2	AIR
2	34	Center	75	2	5	400	0.15	OXYGEN
3	32	Fact	90	1	3.4	500	0.1	AIR
4	11	Center	75	2	5	400	0.15	AIR
5	15	Fact	60	3	3.4	500	0.1	AIR
6	22	Fact	60	3	3.4	300	0.1	OXYGEN
7	6	Fact	90	3	3.4	300	0.1	AIR
8	27	Fact	90	3	6.6	300	0.1	OXYGEN
9	13	Fact	90	3	3.4	500	0.1	OXYGEN
10	17	Fact	90	1	3.4	500	0.2	OXYGEN
11	10	Fact	60	3	6.6	300	0.1	AIR
12	5	Fact	90	3	3.4	300	0.2	OXYGEN
13	4	Fact	60	3	6.6	500	0.1	OXYGEN
14	7	Fact	60	3	6.6	500	0.2	AIR
15	12	Fact	60	1	3.4	300	0.2	OXYGEN
16	31	Fact	60	1	6.6	500	0.2	OXYGEN
17	21	Fact	60	1	3.4	500	0.2	AIR
18	2	Fact	90	1	3.4	300	0.1	OXYGEN
19	33	Fact	60	3	3.4	500	0.2	OXYGEN
20	1	Fact	60	1	3.4	300	0.1	AIR
21	29	Fact	60	1	3.4	500	0.1	OXYGEN
22	25	Fact	60	1	6.6	500	0.1	AIR
23	26	Fact	60	3	3.4	300	0.2	AIR
24	16	Fact	90	3	6.6	500	0.1	AIR
25	8	Fact	60	1	6.6	300	0.1	OXYGEN
26	18	Fact	90	1	6.6	300	0.2	OXYGEN
27	28	Fact	90	1	6.6	300	0.1	AIR
28	30	Fact	90	1	6.6	500	0.2	AIR
29	14	Fact	90	1	6.6	500	0.1	OXYGEN
30	9	Fact	90	3	6.6	300	0.2	AIR
31	20	Fact	90	3	3.4	500	0.2	AIR
32	35	Center	75	2	5	400	0.15	OXYGEN
33	36	Fact	90	3	6.6	500	0.2	OXYGEN
34	24	Center	75	2	5	400	0.15	AIR
35	3	Fact	60	3	6.6	300	0.2	OXYGEN
36	19	Fact	60	1	6.6	300	0.2	AIR

Table 3.2: 2^{k-1} fractional factorial design matrix for the parametric study

3.3. Experimental Setup

A single graphite (Ralph Coiden) fuel cell assembly etched with seven parallel channels (30mm X 1mm X 2mm) creating an active surface area of 9 cm^2, Figure 3.1, was used. The MEA is placed between two graphite or flow field current collectors where the ridges between the channels of the graphite cell assembly provide the electrical contact to the MEA. The electrical contacts to the current load, are made using gold-plated metallic bolts screwed into the graphite blocks. Flexible electrical heaters (Watson Marlow) are mounted at the rear of the graphite blocks to maintain the desired cell temperature, which is controlled through a PID controller and monitored by a thermocouple positioned inside one of the two graphite blocks. The heaters are pressed against the graphite blocks by using two steel backing plates which are compressed to a torque of 2 Nm to evenly distribute the load and maintain the sealing across the MEA surface.

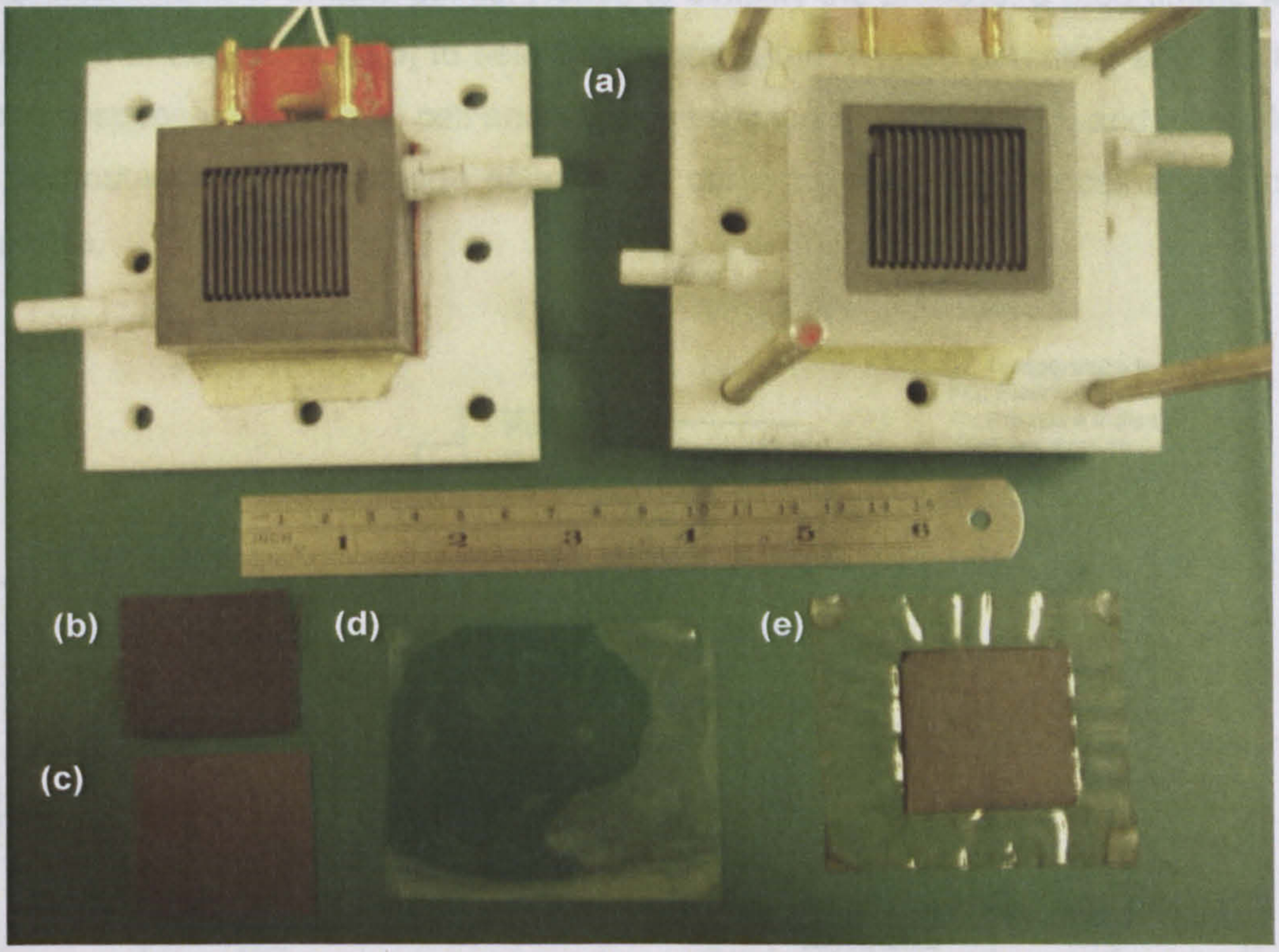

Figure 3.1: DMFC single cell assembly (a) Graphite fuel cell assembly, (b) Carbon cloth, ETEK ELAT LT 1400 W (woven), (c) Toray paper, TGP 090 20% WP, (d) Nafion® 117 membrane and (e) Final assembled MEA.

3.3.1 MEA Fabrication

An in-house manufactured membrane electrode assembly (MEA) was used [114] in this study. The electrodes were fabricated using 1 $mg_{Pt}cm^{-2}$ Pt-Ru/C catalyst (60

%.wt) with 1:1 platinum to ruthenium atomic ratio at the anode and 1 $mg_{Pt}cm^{-2}$ Pt/C catalyst (60 %.wt) at the cathode. Catalyst layers containing 20 %.wt Nafion® ionomer were applied onto a micro porous layer of 0.5 $mg_{KB}cm^{-2}$ (Ketjen Black) with 20 %.wt polytetrafluoroethylene (PTFE) binder deposited onto a TGP-090 20% wet proof gas diffusion layer. The electrodes were hot pressed on to a Nafion® 117 membrane at 140 °C under a load of 50 kg cm^{-2} for 10 minutes and allowed to cool under pressure.

3.3.2 Fuel Cell Test Rig

The fuel cell test rig [114], as shown in Figure 3.2, was used to perform in situ experiments. To improve the repeatability and speed of testing, an automated system was designed and installed. Data were collected potentiostatically and at a potentiodynamic sweep rate of 2 mV s^{-2}. The collection of data at this rate resulted in a significant number of data points. Hence to simplify the process, a programme was developed in LabVIEW [115] to select the data at the desired potential, such as the anode response at 700 mV, cell and anode response at 10 mA cm^{-2}, and also allow the computation of the cathode polarisation curve by summing the cell and anode response.

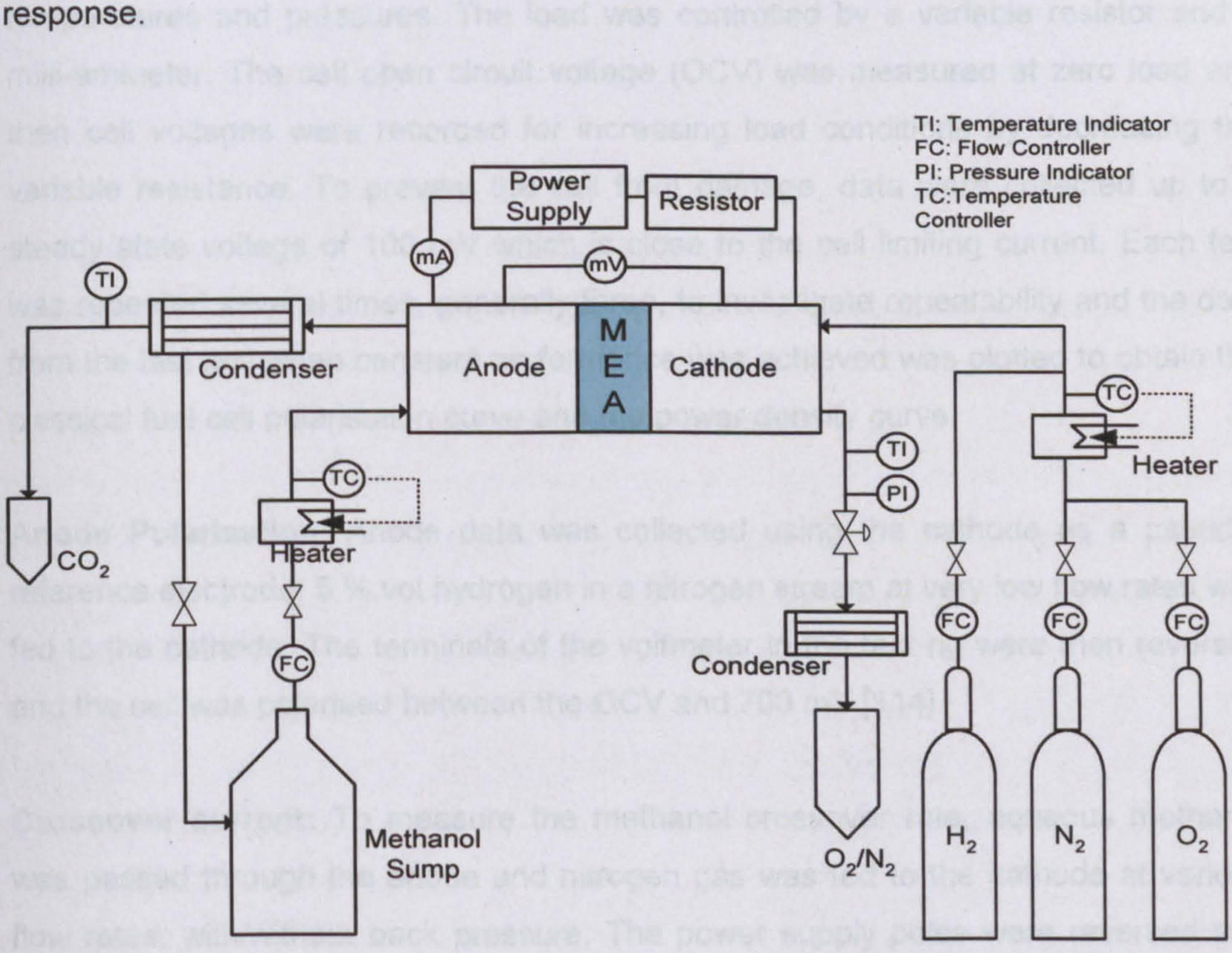

Figure 3.2: Schematic representation of the DMFC test rig [114]

In the fuel cell test rig, Figure 3.2, a Watson Marlow 101 U/R peristaltic pump was used to pump aqueous methanol from a glass sump to the anode compartment of the fuel cell. The un-reacted methanol was returned to the feed solution. The carbon dioxide produced during the reaction was vented into the atmosphere after the methanol/CO_2 mixture had been passed through the condensing unit. Unheated and non-humidified air or oxygen (BOC) was supplied to the cathode from a regulated, filtered compressed air supply, through a rotameter for flow measurement. Exhaust from the cathode was passed through a condenser with/without back pressure depending on the experimental run before venting it into the atmosphere.

3.3.3 Experimental Procedure

The following three experimental procedures were implemented to realise informative conclusions about fuel cell operation.

Cell Polarisation: Steady state galvanic polarisation was used to evaluate the performance of the DMFC. The cell was fed with aqueous methanol at the anode and air/O_2 at the cathode, for specific methanol concentrations, reactant flow rates, cell temperatures and pressures. The load was controlled by a variable resistor and a milli-ammeter. The cell open circuit voltage (OCV) was measured at zero load and then cell voltages were recorded for increasing load conditions by decreasing the variable resistance. To prevent the cell from damage, data were collected up to a steady state voltage of 100 mV which is close to the cell limiting current. Each test was repeated several times, generally three, to investigate repeatability and the data from the last test when constant performance was achieved was plotted to obtain the classical fuel cell polarisation curve and the power density curve.

Anode Polarisation: Anode data was collected using the cathode as a pseudo-reference electrode. 5 %.vol hydrogen in a nitrogen stream at very low flow rates was fed to the cathode. The terminals of the voltmeter in the test rig were then reversed and the cell was polarised between the OCV and 700 mV [114].

Crossover current: To measure the methanol crossover rate, aqueous methanol was passed through the anode and nitrogen gas was fed to the cathode at various flow rates, with/without back pressure. The power supply poles were reversed and the methanol which had crossed through the membrane from the anode to cathode was oxidised at the cathode. The cell was polarised at high potentials, ~900 to

1000 mV, and the limiting current obtained for complete oxidation of crossover methanol at the cathode was measured. This limiting crossover current was used in the calculation of methanol crossover [62].

After setting the operating conditions for each experimental run, Table 3.2, the cell polarisation data, anode polarisation data and methanol crossover current were collected. Performing the crossover current procedure at the end of each experimental sequence slightly improved cell performance. This was potentially due to removal of solvents or methanol residues deposited on the active catalyst site [114]. To reduce this post-effect of cell cleaning and methanol crossover, the cell was set to new operating conditions and allowed to stabilise for approximately 2 hrs. After stabilising, 10 to 15 cell polarisation cycles were performed until constant reproducible performance was achieved.

3.4. Analysis of Fractional Factorial Design

A fractional factorial, $2^{k-1} = 2^{6-1} = 32$ run, with two centre points for each level of categorical factor (type of oxidant) and defining relation I=ABCDEF was used to analyse the DMFC peak power performance. The statistical analysis was performed using Design Expert software (version 6.0.11) from Stat Ease, Inc [116].

The DMFC, as discussed previously has significant variability associated with its response due to the complex fabrication technique, reaction mechanism and experimental error. The variability associated with DMFC performance can be observed from the two centre point runs executed for the two levels of type of oxidant, Figures 3.3.a and 3.3.b. The centre point experimental runs at a cell temperature of 75 °C using 2 M methanol at a flow rate of 5 ml min^{-1} with oxidant at a flow rate of 400 ml min^{-1}, Figures 3.3.a and 3.3.b, illustrates the variability in the performance of DMFC, when utilising the same MEA. It can be observed that there is less variation in the anode response compared to the peak power and cell response, indicating that the variation in cathode performance is the key reason behind the variability in cell performance. Experimental design allows the effect of both factors and their interactions on the DMFC response to be analysed whilst taking into account the associated variability.

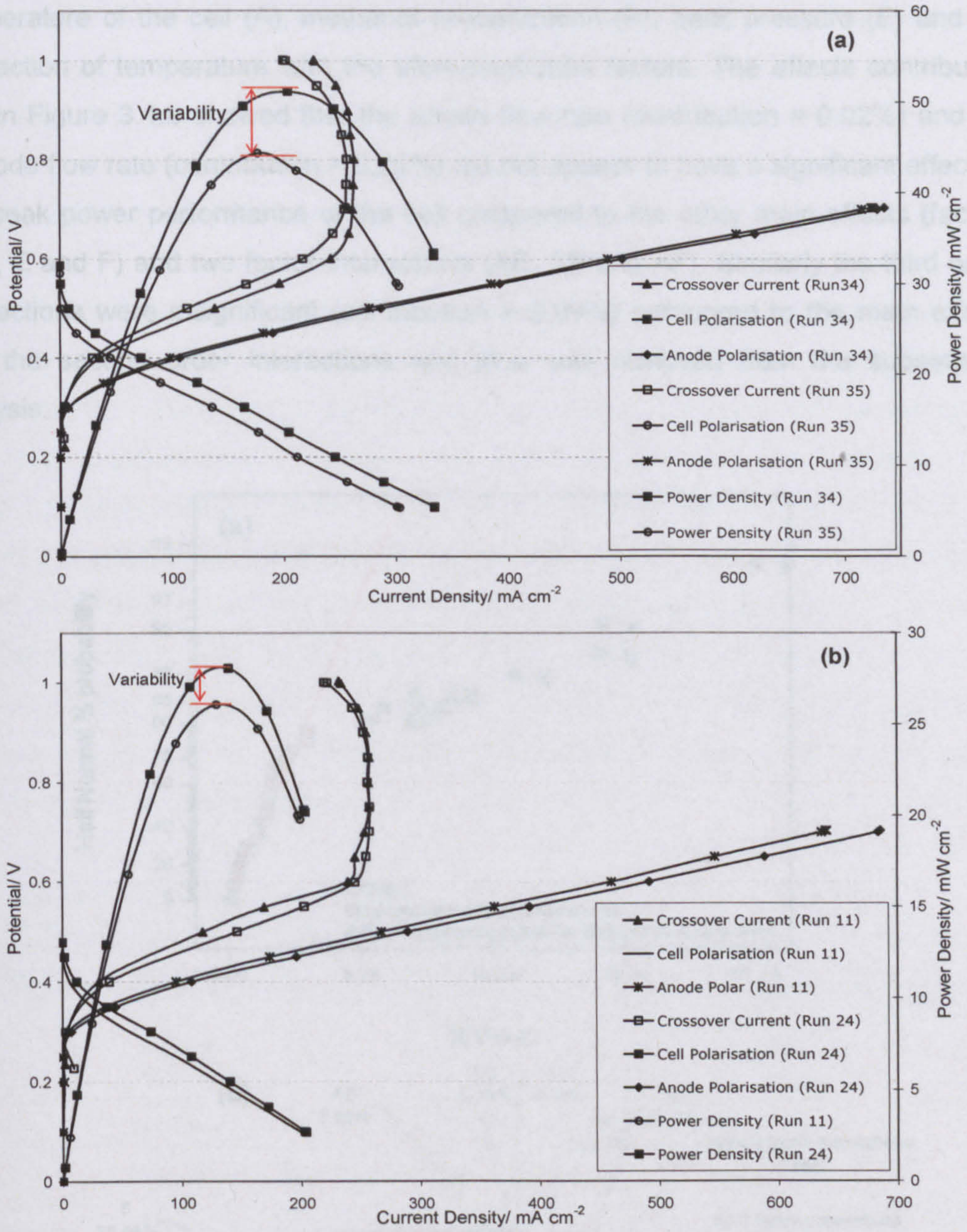

Figure 3.3: DMFC characteristics curves for centre point runs showing the variability associated with DMFC performance using (a) oxygen at cathode and (b) air at cathode.

3.4.1 Peak Power Analysis

The half normal plot and the effects contribution plot for the peak power analysis are shown in Figures 3.4.a and 3.4.b respectively. A half normal probability plot is a graph with y-axis scaled by cumulative probability so that data that do not influence the response fall on the straight normal line [113, 117] . Half normal plot helps in visual identification of influential effects and interactions which fall away from the normal straight line. It can be observed that the influential factors affecting the peak power performance on the basis of half normal plot were type of oxidant (F),

temperature of the cell (A), methanol concentration (B), back pressure (E) and the interaction of temperature with the aforementioned factors. The effects contribution plot in Figure 3.4.b showed that the anode flow rate (contribution = 0.02%) and the cathode flow rate (contribution = 0.20%) did not appear to have a significant effect on the peak power performance of the cell compared to the other main effects (factors A, B, E and F) and two factor interactions (AE, AB and AF). Similarly the third order interactions were insignificant (contribution = 2.09%) compared to the main effects and the second order interactions and thus was removed from the subsequent analysis.

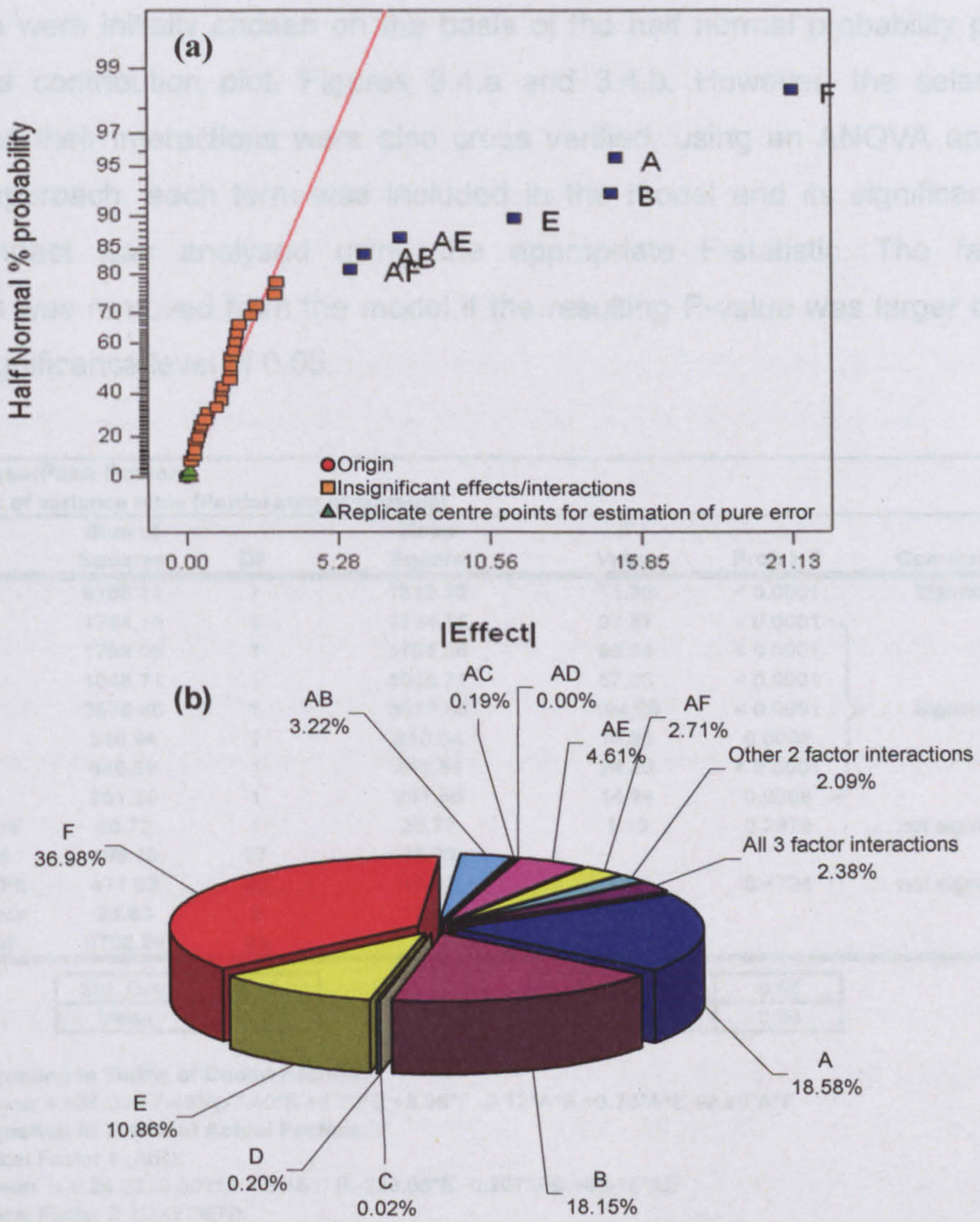

Figure 3.4: Influential factors and interactions affecting the peak power of the DMFC. (a) Half normal plot and (b) Effects contribution plot.

The analysis of variance (ANOVA) output from Design Expert based on the factors selected using the half normal plot is given in Table 3.3. The ANOVA is a commonly used statistical tool to analyse the effect of factors and their interactions on the measured response [113, 117]. The various statistical calculations used in the ANOVA table are described in detail in the Appendix D.

From the ANOVA table in Table 3.3 it can be concluded that all the factors (A, B, E, and F) and two factor interactions (AB, AE, and AF) are significant with the P-values being less than the selected significance level of 0.05. Similarly the overall model, including the aforementioned terms, is also significant ($P<0.05$). The factors and their interaction were initially chosen on the basis of the half normal probability plot and the effects contribution plot, Figures 3.4.a and 3.4.b. However, the selection of factors and their interactions were also cross verified, using an ANOVA approach. For this approach, each term was included in the model and its significance and overall impact was analysed using the appropriate F-statistic. The factor or interaction was removed from the model if the resulting P-value was larger than the chosen significance level of 0.05.

Response:Peak Power
Analysis of variance table [Partial sum of squares]

Source	Sum of Squares	DF	Mean Square	F Value	Prob > F	Comment
Model	9185.11	7	1312.16	71.36	< 0.0001	.... Significant
A	1794.15	1	1794.15	97.57	< 0.0001	
B	1753.06	1	1753.06	95.34	< 0.0001	
E	1048.71	1	1048.71	57.03	< 0.0001	
F	3570.86	1	3570.86	194.20	< 0.0001	.... Significant
AB	310.94	1	310.94	16.91	0.0003	
AE	445.59	1	445.59	24.23	< 0.0001	
AF	261.80	1	261.80	14.24	0.0008	
Curvature	20.72	1	20.72	1.13	0.2978	.... not significant
Residual	496.46	27	18.39			
Lack of Fit	471.63	25	18.87	1.52	0.4734	.... not significant
Pure Error	24.83	2	12.41			
Cor Total	9702.29	35				

Std. Dev.	4.29
Mean	35.27

R-Squared	0.95
Adj R-Squared	0.94

Final Equation in Terms of Coded Factors:
Peak Power = +35.00 +7.49*A -7.40*B +5.72*E +9.96*F -3.12*A*B +3.73*A*E +2.86*A*F
Final Equation in Terms of Actual Factors:
Categorical Factor 1 (AIR):
Peak Power = + 24.33 -0.022*A + 8.184* B -258.66*E -0.207*AB +4.975*AE
Categorical Factor 2 (OXYGEN):
Peak Power = + 15.648 + 0.359*A +8.184*B -258.66*E -0.208*AB +4.975*AE

Table 3.3: Analysis of Variance (ANOVA) output for peak power analysis

The addition of centre points allows the presence of curvature/non-linearity in the response to be investigated. The ANOVA output shows that there is no evidence of

curvature in the peak power data (P= 0.2978 >0.05). The lack of fit test compares the error from the excess design points, i.e. those not used in the model, with the pure error from the replicated design points [112, 113, 117]. The ANOVA output in Table 3.3 shows that the lack of fit test is not significant; hence the variation in the excess design points does not significantly differ from the variation in the replicated points.

The validity of the model fit is further investigated through a residual analysis, Figure 3.5. From Figure 3.5.a. it can be seen observed the residuals are normally distributed whilst the random scatter of the residuals, Figures 3.5.b. indicates that the residuals exhibit constant variance, confirming that the underlying model assumptions are satisfied. A plot of residual versus experimental run is depicted in Figures 3.5.c. The plot should be random but the presence of a trend in Figure 3.5.c indicates that there is potentially a run dependent variable present in the experimentation. At the end of each experimental run the methanol crossover current was measured by passing nitrogen at the cathode side. This procedure cleaned the cathode side by removing any extra solvents or methanol residues deposited on the active catalyst site and has previously been observed to improve the DMFC performance [114]. This slight improvement in performance and the use of the same MEA for the whole analysis may have been the reason for the trend. The experimental runs were randomised as shown in Table 3.2 and were performed over a number of weeks without blocking as the experiment was carried out by a single experimenter utilising the same cell. Thus in addition to the improvement in the performance being associated with cell cleaning, the change in raw materials or other uncontrolled effects like temperature of the laboratory and efficiency of the experimenter could also contribute to the trend.

3.4.1.1 Effect of Two Factor Interactions

A resolution-V design was selected for the peak power analysis as it ensured that 2-factor interactions were not aliased with other effects. Figure 3.6 shows the 2-factor interactions affecting the DMFC peak power response using air and oxygen at the cathode. Due to the presence of second order interactions, these factors are investigated to identify the 'optimal combination' to ensure 'maximum peak power'.

The '•' in these plots depict the centre point experimental runs at 75 °C, using 2 M methanol at a flow rate of 5 ml min^{-1} and oxidant at the a rate of 400 ml min^{-1} with 0.15 MPa back pressure for air and oxygen respectively. The spread of these centre point runs indicate the variability present in the design. The experiments were

performed using the same MEA. However the variability may be due to the non-identical behaviour of the electrodes (anode and cathode) under same operating conditions, the degradation of the electrodes due to methanol crossover and catalyst poisoning or uncontrollable factors such as variation in the laboratory temperature. As stated previously, the experimental design took account of this variability.

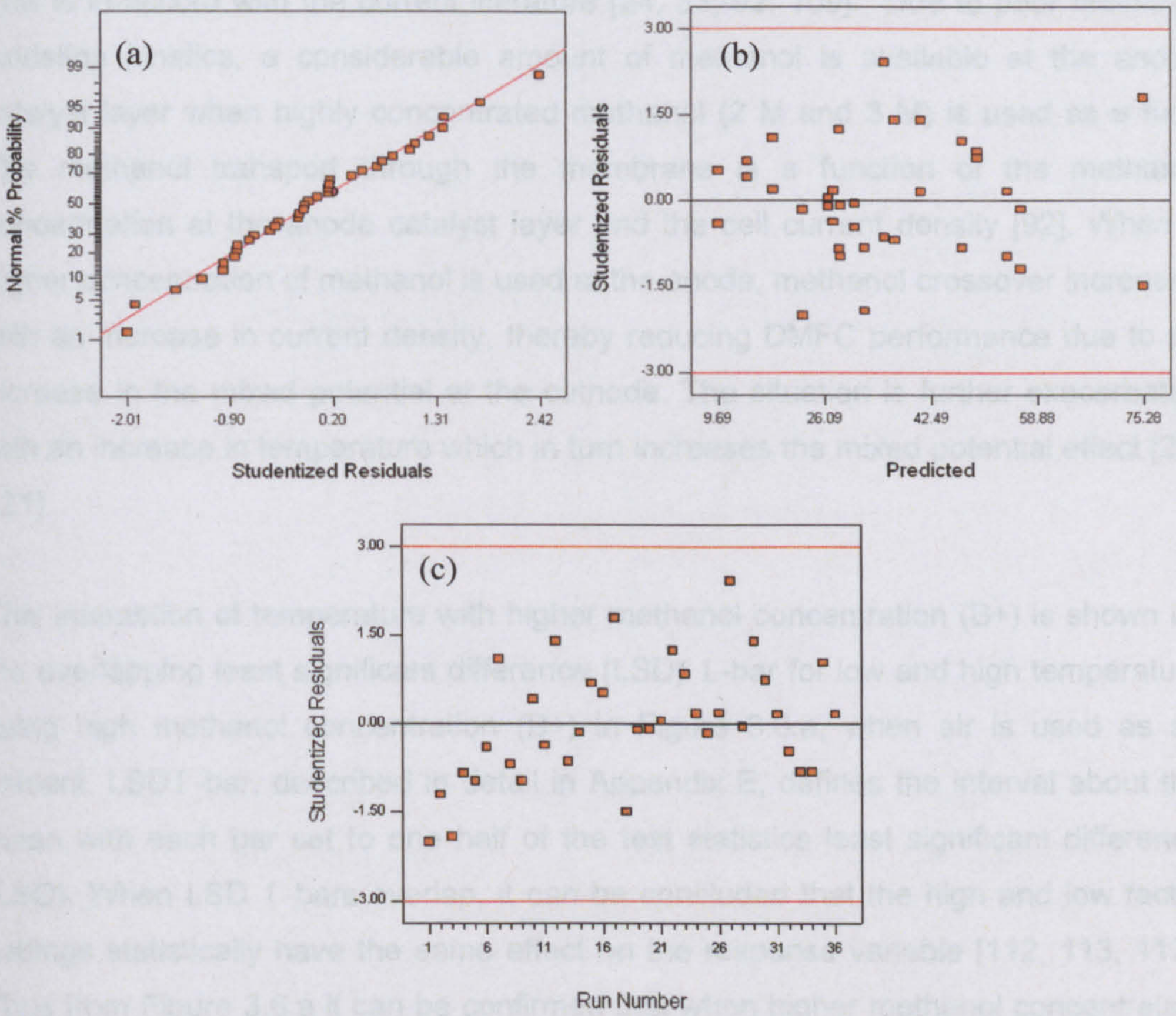

Figure 3.5: Residual analysis (a) Normal scores plot of residuals, (b) Residuals vs. predicted values and (c) Residuals vs. run order

3.4.1.1.1 Cell temperature and Methanol concentration

Figures 3.6.a and 3.6.b demonstrate the influence of cell temperature (A) and methanol concentration (B) on peak power output, using air and oxygen at cathode respectively. It can be observed that a combination of low methanol concentration (1 M) and high cell temperature (90 °C) favours high peak power for both types of oxidant (air/oxygen) at the cathode. It has been reported that a higher temperature (90 °C) improves both the methanol oxidation kinetics and the oxygen reduction kinetics at the anode and cathode respectively [34, 118-120]. In addition, an increase

in temperature increases the membrane proton conductivity and thus the peak power [6, 33]. However, this advantage of high temperature is not beneficial at higher methanol concentration, as shown in Figures 3.6.a and 3.6.b. These figures indicate that due to the interaction of temperature with methanol concentration a combination of high temperature only with lower methanol concentration (1 M) is favourable for obtaining improved peak power from the DMFC irrespective of the type of oxidant. This is in accord with the current literature [24, 33, 92, 109]. Due to poor methanol oxidation kinetics, a considerable amount of methanol is available at the anode catalyst layer when highly concentrated methanol (2 M and 3 M) is used as a fuel. The methanol transport through the membrane is a function of the methanol concentration at the anode catalyst layer and the cell current density [92]. When a higher concentration of methanol is used at the anode, methanol crossover increases with an increase in current density, thereby reducing DMFC performance due to an increase in the mixed potential at the cathode. The situation is further exacerbated with an increase in temperature which in turn increases the mixed potential effect [25, 121].

This interaction of temperature with higher methanol concentration (B+) is shown by the overlapping least significant difference (LSD) I-bar for low and high temperature using high methanol concentration (B+) in Figure 3.6.a, when air is used as an oxidant. LSD I-bar, described in detail in Appendix E, defines the interval about the mean with each bar set to one half of the test statistics least significant difference (LSD). When LSD I-bars overlap, it can be concluded that the high and low factor settings statistically have the same effect on the response variable [112, 113, 117]. Thus from Figure 3.6.a it can be confirmed that when higher methanol concentration is used at anode the cell temperature statistically have the same effect on the peak power due to increase in crossover and mixed potential effect at cathode. Overall it can be observed that, a reduction in methanol crossover through the membrane and increase in peak power can be achieved at high temperature with a combination of lower methanol concentrations (1 M). The influence of methanol concentration on crossover is later verified by analysing the crossover current response in section 3.4.2.

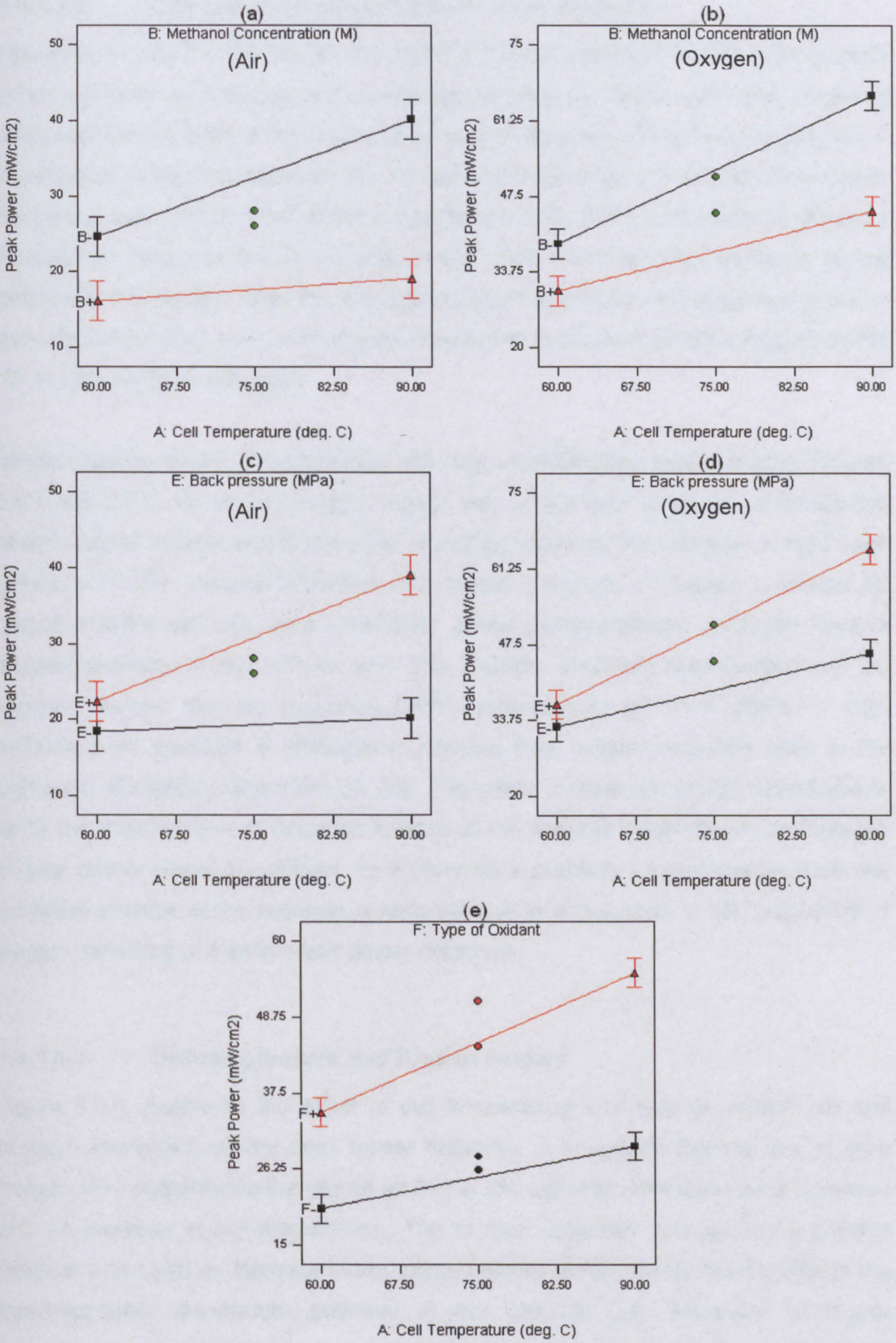

Figure 3.6: Effect of two factor interactions on peak power analysis. (a) Cell temperature vs. methanol concentration (air), (b) cell temperature vs. methanol concentration (oxygen),(c) cell temperature vs. cathode back pressure (air), (d) cell temperature vs. cathode back pressure (oxygen) and (e) cell temperature vs. oxidant type. '●' depicts centre point experimental runs.

3.4.1.1.2 Cell temperature and Cathode back pressure

Figures 3.6.c and 3.6.d, illustrate the effect of the cathode back pressure (E) on peak power using air and oxygen at the cathode respectively. From both plots, it can be observed that the effect of cathode back pressure depends on cell temperature (A). A combination of high temperature (90 °C) and high back pressure (0.2 MPa) increases the peak power from the cell whilst at low temperature (60 °C), a high back pressure in isolation does not influence peak power. This effect of back pressure at low temperature is evident from the overlapping least significant difference bar (LSD I-bar) of the high (E+) and low (E-) back pressure at a low level of cell temperature (60 °C) in Figures 3.6.c and 3.6.d.

Similar positive slopes of temperature with high cathode back pressure (E+), Figures 3.6.c and 3.6.d, for air and oxygen signify that a high back pressure increases the power output irrespective of the type of oxidant used at the cathode. A high back pressure at the cathode increases the partial pressure of oxygen available for reduction at the cathode. More specifically, a high partial pressure of oxygen, favours oxygen reduction at the cathode and also impedes methanol chemisorption on the cathode surface thereby improving DMFC performance [6]. In a DMFC, a high cathode back pressure is desirable to achieve high oxygen reduction rates in the presence of methanol crossover [6, 25]. This effect is observed at high temperatures since the improvement of oxidation kinetics at the cathode materialise in an increase in peak power output. In contrast, for a lower back pressure and cell temperature, the oxidation kinetics at the cathode is reduced due to a reduction in the availability of oxygen, resulting in a lower peak power response.

3.4.1.1.3 Cell temperature and Type of oxidant

Figure 3.6.e, examines the effect of cell temperature and type of oxidant (air and oxygen) interaction on the peak power response. It is evident that the use of pure oxygen (F+) outperforms the use of air (F-) at the cathode. This distinction increases with an increase in cell temperature. The oxygen reduction reaction has a positive reaction order and an increase in the oxygen partial pressure significantly affects the thermodynamic equilibrium potential at the cathode [34]. Moreover at higher temperatures, the rate of water and methanol permeation increases through the membrane. At elevated temperatures (above 60 °C), methanol and water vaporise at the cathode decreasing the oxygen solubility in the liquid diffusion film at the active cathode catalyst surface. When pure oxygen is used, the concentration gradient

remains sufficiently steep to saturate the cathode catalyst with enough oxygen so that it can compete with the presence of methanol on the active cathode catalyst site.

In contrast, when air is used at the cathode, the relatively small amount of oxygen in air reduces the driving force of oxygen diffusion through the electrodes and as a result, the oxidant partial pressure at the cathode catalyst is lower [34]. This reduction in oxygen availability worsens with additional dilution by the methanol and water vapour resulting in poor DMFC performance [33, 109].

3.4.1.2 Effect of Methanol Flow Rate

The methanol flow rate in the parametric design was not observed to affect the peak power performance. The approximately horizontal regression line for methanol flow rate with both air and oxygen as oxidant, Figures 3.7.a and 3.7.b, confirms that it is not an influential factor affecting cell performance.

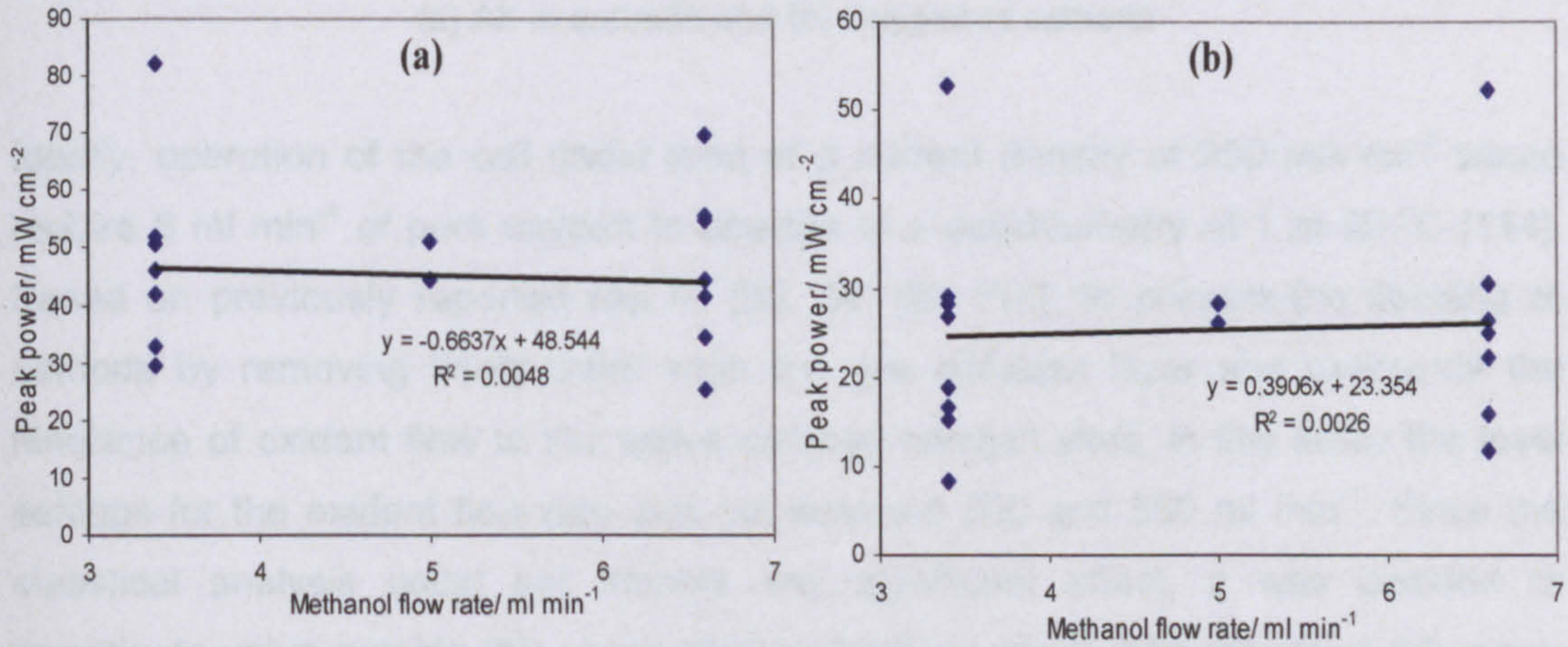

Figure 3.7: Results showing the effect of methanol flow rate on the peak power performance. (a) Air at cathode and (b) Oxygen at cathode

The settings for methanol flow rate (3.4 to 6.6 ml min^{-1}) was too narrow (range = 3.2 ml min^{-1}) to allow the identification of whether methanol flow rate impacts on peak power performance. This result was in accordance with that reported by Ge et al., (2005) [33], where it was observed that an methanol flow rate in the range 5 to 8 ml min^{-1} did not have a significant effect on DMFC performance. This was in contrast to the results attained for a range of 0.5 to 10 ml min^{-1}. To verify this, additional experiments were carried (Appendix F), which showed that DMFC performance is affected by the methanol flow rate but only when operated at high flow rates.

3.4.1.3 Effect of Oxidant Flow Rate

Similar to methanol flow rate, the parametric design did not identify any significant influence of the oxidant flow rate on peak power performance, Figure 3.8.

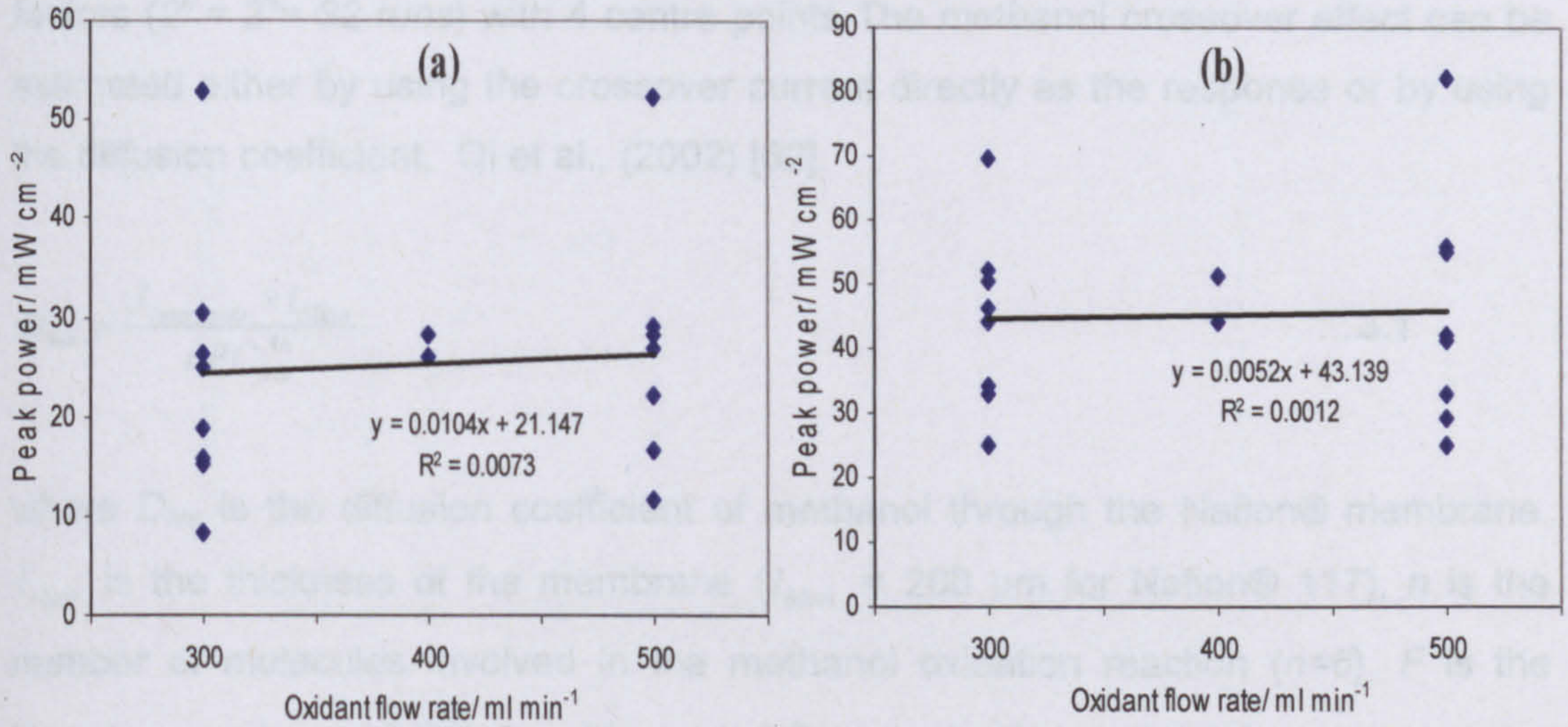

Figure 3.8: Results showing the effect of oxidant flow rate on the peak power performance. (a) Air at cathode and (b) Oxygen at cathode

Ideally, operation of the cell under load at a current density of 200 mA cm^{-2} would require 8 ml min^{-1} of pure oxygen to operate at a stoichiometry of 1 at 90 °C [114]. Based on previously reported results [33, 34, 56, 114], to prevent the flooding of cathode by removing liquid water from the gas diffusion layer and overcome the hindrance of oxidant flow to the active cathode catalyst sites, in this study the level settings for the oxidant flow rate was set between 300 and 500 ml min^{-1}. Since the statistical analysis could not identify any significant effect, it was decided to investigate value outside this range (200 to 2000 ml min^{-1}). The results of this study are given in Appendix F, which confirmed that oxidant flow rate does affect peak power performance, but only if operated at high oxidant flow rates. A high oxidant flow rate increases the partial pressure of oxygen on the cathode side and effectively removes the product water formed at the cathode thereby increasing DMFC performance [34]. However a balance of methanol flow rate and oxidant flow rate is required as an excess of these reactants would have a significant negative effect on system efficiency.

3.4.2 Crossover Current Analysis

Along with peak power, the crossover current for each of the experimental runs, was also measured by passing nitrogen instead of oxidant at the cathode. Hence type of oxidant (F) was removed from the analysis resulting in a full factorial design using 5 factors ($2^k = 2^5 = 32$ *runs*) with 4 centre points The methanol crossover effect can be estimated either by using the crossover current directly as the response or by using the diffusion coefficient, Qi et al., (2002) [62].

$$D_{Me} = \frac{J_{crossover} \times l_{Mem}}{nFC_{Me}^{An}} \qquad \ldots 3.1$$

where D_{Me} is the diffusion coefficient of methanol through the Nafion® membrane, l_{Mem} is the thickness of the membrane (l_{Mem} = 200 μm for Nafion® 117), n is the number of molecules involved in the methanol oxidation reaction (n=6), F is the Faraday constant (96487 C mol^{-1}), and C_{Me}^{An} is the concentration of methanol at the anode catalyst layer.

In this study, the concentration of methanol at the anode catalyst layer was assumed to be the same as the concentration of methanol at feed. Based on this assumption, the results for crossover current and the diffusion coefficient result in the same conclusions since crossover current is the only variable which varied for different methanol concentrations. Consequently only the results for the direct measurement of crossover current are reported.

Figure 3.9.a, identifies the influential factors and interactions that impact on crossover current. The key factors and interactions are methanol concentration (B), temperature of cell (A) and their interaction (AB). Figure 3.9.b shows the percentage contribution of the various factors and the interactions on the methanol crossover current. It can be observed from the effects contribution plot that methanol concentration (B) is important in terms of influencing methanol crossover with an effective contribution of 73.27%. Based on the half normal plot and effects contribution plot, an ANOVA was undertaken, Table 3.4.

From the ANOVA, it can be concluded that the temperature of the cell and the concentration of methanol along with their interaction were significant. The ANOVA also identified that significant curvature was present ($P=0.0026<0.05$). To investigate

further the results of the ANOVA, a model residual analysis was performed, Figure 3.10.

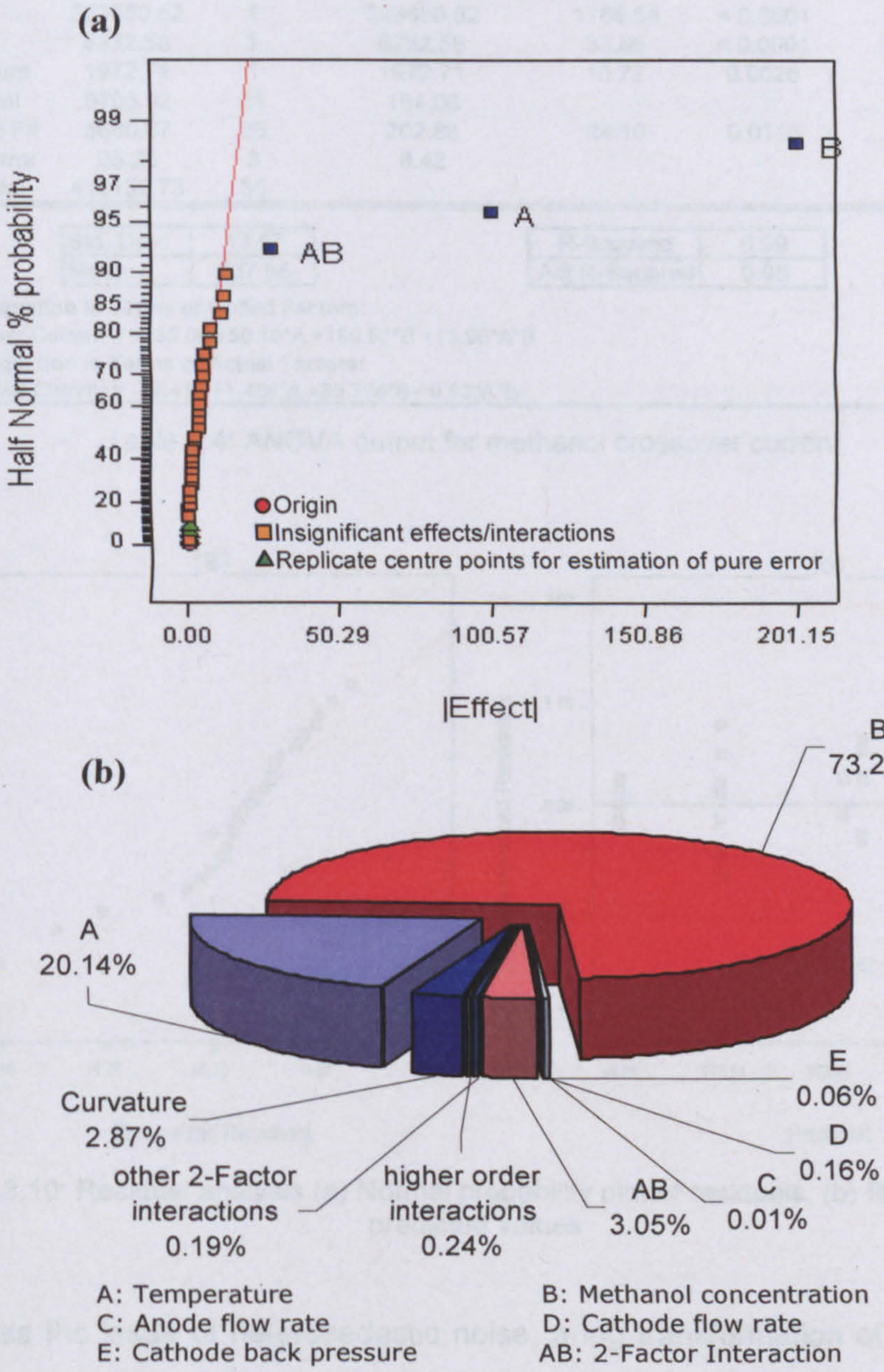

Figure 3.9: Influential factors and interactions affecting the methanol crossover current response (a) Half normal plot and (b) Effects contribution plot

The normal probability plot of the residuals, Figure 3.10.a, showed that the residuals were not normal. The residual vs. fitted values, in Figure 3.10.b, illustrated the presence of heterosedastic noise [117]. Consequently the underlying statistical assumptions of independence, identically distributed, normality and constant variance were not satisfied.

Response: Methanol Crossover Current
Analysis of variance table [Partial sum of squares]

Source	Sum of Squares	DF	Mean Square	F Value	Prob > F	Comment
Model	410479.10	3	136826.37	743.37	< 0.0001	.... Significant
A	80566.00	1	80566.00	437.71	< 0.0001	.... Significant
B	323680.52	1	323680.52	1758.54	< 0.0001	.... Significant
AB	6232.58	1	6232.58	33.86	< 0.0001	.... Significant
Curvature	1972.71	1	1972.71	10.72	0.0026	.... Significant
Residual	5705.92	31	184.06			
Lack of Fit	5680.67	28	202.88	24.10	0.0115	.... Significant
Pure Error	25.25	3	8.42			
Cor Total	418157.73	35				

Std. Dev.	13.57
Mean	237.68

R-Squared	0.99
Adj R-Squared	0.98

Final Equation in Terms of Coded Factors:
Crossover Current = +235.06 +50.18*A +100.57*B +13.96*A*B
Final Equation in Terms of Actual Factors:
Crossover Current = -77.413 +1.484*A +30.794*B +0.93*A*B

Table 3.4: ANOVA output for methanol crossover current

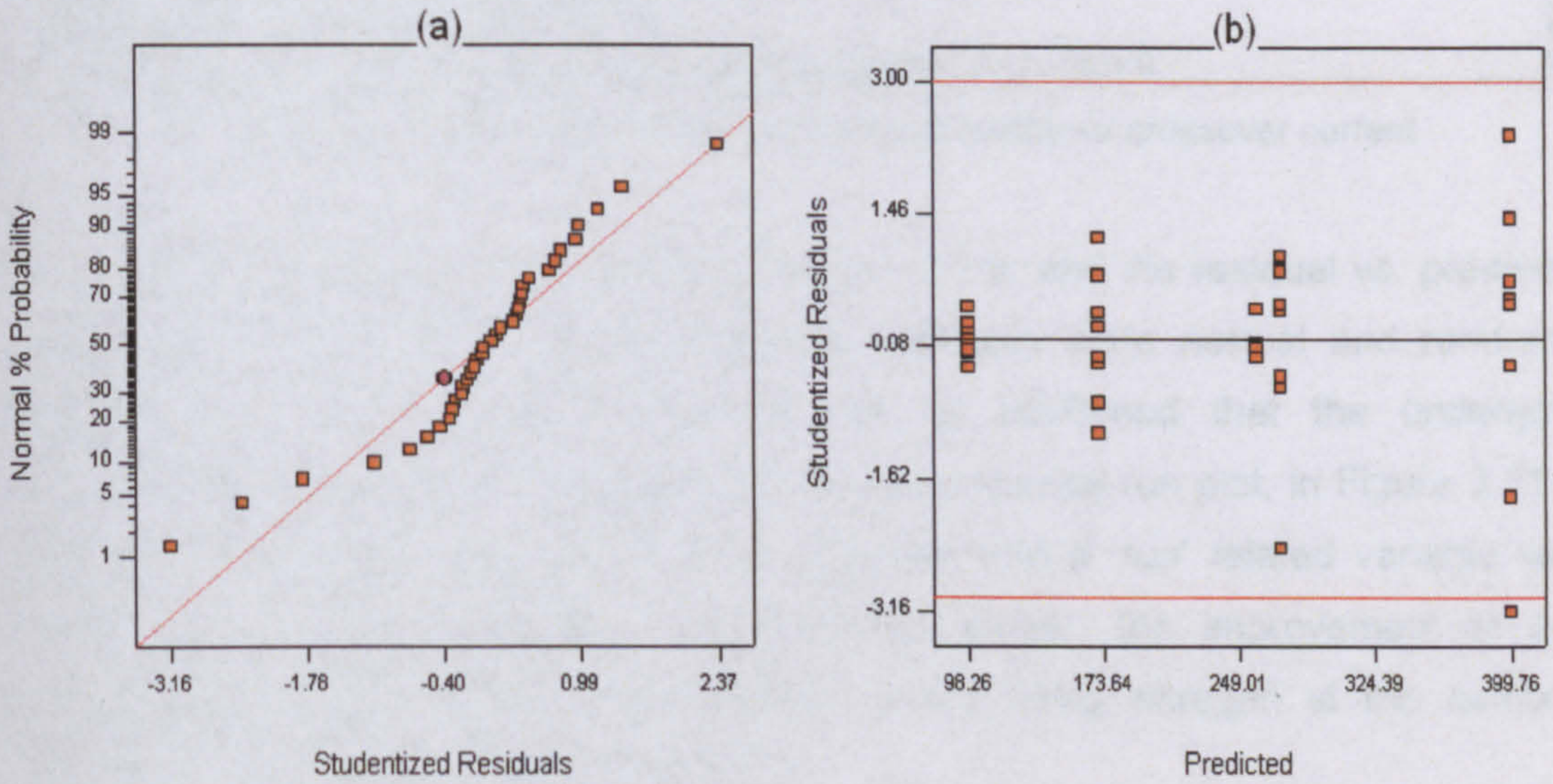

Figure 3.10: Residual analysis (a) Normal probability plot of residuals, (b) Residuals vs. predicted values

To address the issue of heterosedastic noise, a log transformation of the response was taken [112, 117, 122]. An increase in variability with an increase in cell current density can be a potential cause for the heterosedastic noise in the response. Table 3.5, reports the analysis for the log transformed crossover current response.

The ANOVA, in Table 3.5, showed that the cell temperature (A), methanol concentration (B) and their interaction (AB) were significant. Additionally the model also identified that the curvature was present in the design due to the quadratic nature of cell temperature (A^2). The overall model was significant and was able to

describe 99% of the variability about the mean. A residual analysis was performed to further validate the model, Figure 3.11.

Response: Methanol Crossover Current (Log_{10} Transformed)

Analysis of variance table [Partial sum of squares]

Source	Sum of Squares	DF	Mean Square	F Value	Prob > F	Comment
Model	1.69	4	0.42	966.38	< 0.0001	.... Significant
A	0.33	1	0.33	759.24	< 0.0001	.... Significant
B	1.31	1	1.31	3004.78	< 0.0001	.... Significant
A2	3.42E-02	1	0.03	78.19	< 0.0001	.... Significant
AB	1.02E-02	1	0.01	23.34	< 0.0001	.... Significant
Residual	1.36E-02	31	4.37E-04			
Lack of Fit	1.35E-02	28	4.82E-04	20.47	0.0146	.... Significant
Pure Error	7.06E-05	3	2.35E-05			
Cor Total	1.70	35				

Std. Dev.	0.02
Mean	2.33

R-Squared	0.99
Adj R-Squared	0.99

Final Equation in Terms of Coded Factors:

$Log_{10}(Crossover\ Current) = +2.41 +0.10*A +0.20*B -0.098*A^2 -0.018*A*B$

Final Equation in Terms of Actual Factors:

$Log_{10}(Crossover\ Current) = -1.132 +0.075*A +0.292*B -4.36E-04*A^2 -1.19E-03*A*B$

Table 3.5: ANOVA output for log transformed methanol crossover current

The normal probability plot of residual, Figure 3.11.a, and the residual vs. predicted value plot, Figure 3.11.b, showed that the residuals were normal and randomly distributed. On the basis of which it can be confirmed that the underlying assumptions were satisfied. The residual vs. experimental run plot, in Figure 3.11.c, depicts a slight increasing trend, which suggests that a 'run' related variable was present in the experimentation. As described earlier, the improvement in cell performance by measuring the crossover current using nitrogen at the cathode potentially could be a reason for this trend.

3.4.2.1 Effect of Cell Temperature and Methanol Concentration

The 2D contour plot, in Figure 3.12.a, illustrates the influence of the interaction of methanol concentration and cell temperature on log crossover rate. The plot suggests that a combination of high cell temperature (90 °C) and low methanol concentration (1 M) will result in a low crossover current whilst the combination of low cell temperature (60 °C) and high methanol concentration (3 M) gives higher crossover rate. With the use of a higher methanol concentration at the anode un-reacted methanol at the anode is always available which passes to the cathode via diffusion or electro-osmotic drag through the Nafion® membrane. This increase in methanol crossover due to higher methanol concentration results in an increase in

the mixed potential at the cathode thereby affecting the peak power output as observed in Figure 3.6.

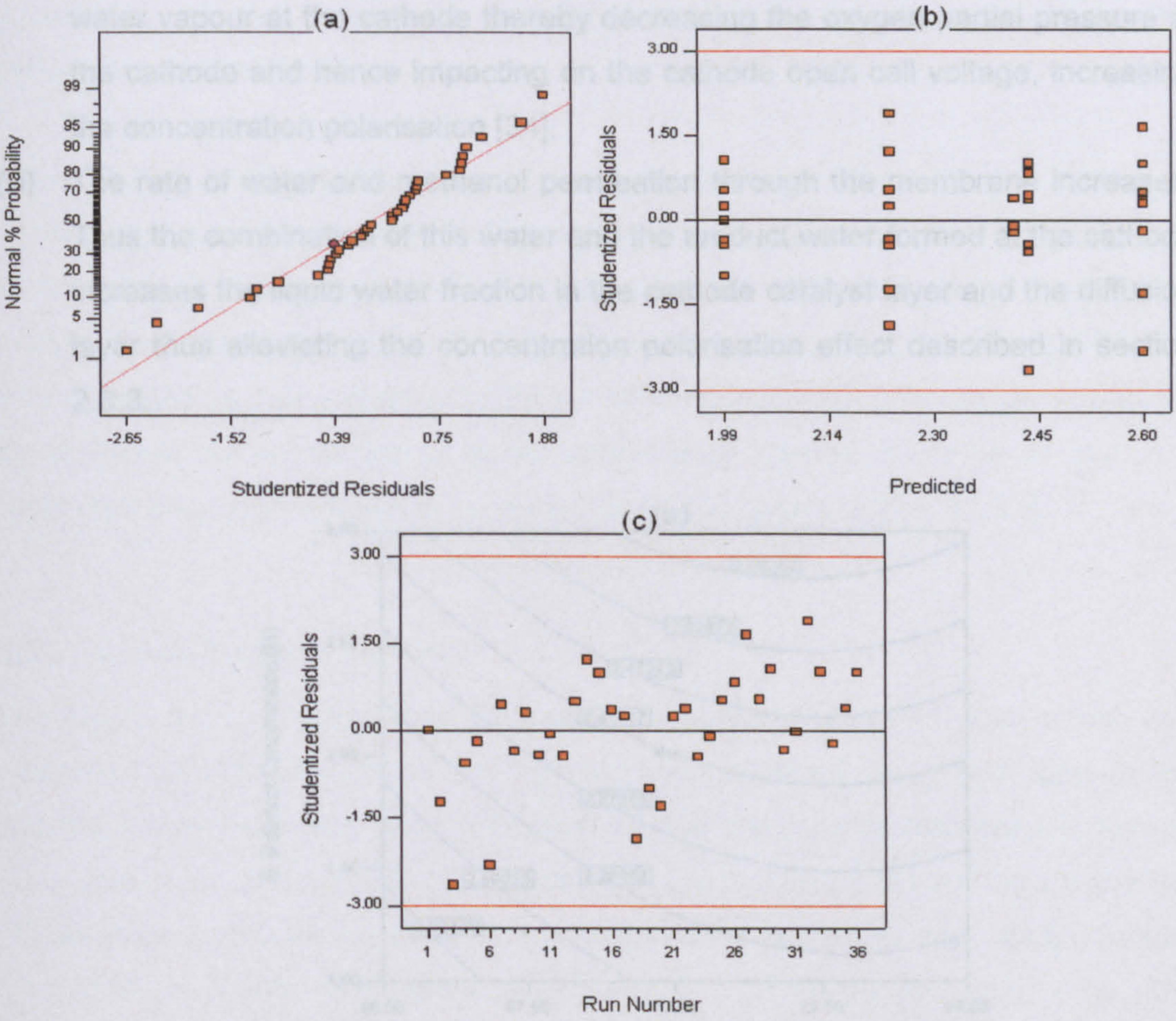

Figure 3.11: Residual analysis (a) Normal probability plot of residuals, (b) Residuals vs. predicted values and (c) Residual vs. experimental run order

The main effect plot of cell temperature in Figure 3.21.b illustrates the impact of the quadratic nature of cell temperature on log crossover current response. The process of crossover depends on the availability of methanol at the interface between the anode catalyst layer and the electrolyte membrane. At high cell temperature and current density the availability of methanol at the interface between anode catalyst layer and the electrolyte membrane is low due to which a quadratic behaviour is observed in cell temperature [123].

An increase in temperature also has the following negative effects on the performance of the DMFC:

(i) An increase in cell temperature results in an increase in the permeability of methanol through the Nafion® membrane, thus the mixed potential at the

cathode increases due to the high methanol crossover resulting in poor performance [33].

(ii) An increase in cell temperature increases the partial pressure of methanol and water vapour at the cathode thereby decreasing the oxygen partial pressure at the cathode and hence impacting on the cathode open cell voltage, increasing the concentration polarisation [34].

(iii) The rate of water and methanol permeation through the membrane increases. Thus the combination of this water and the product water formed at the cathode increases the liquid water fraction in the cathode catalyst layer and the diffusion layer thus alleviating the concentration polarisation effect described in section 2.6.3.

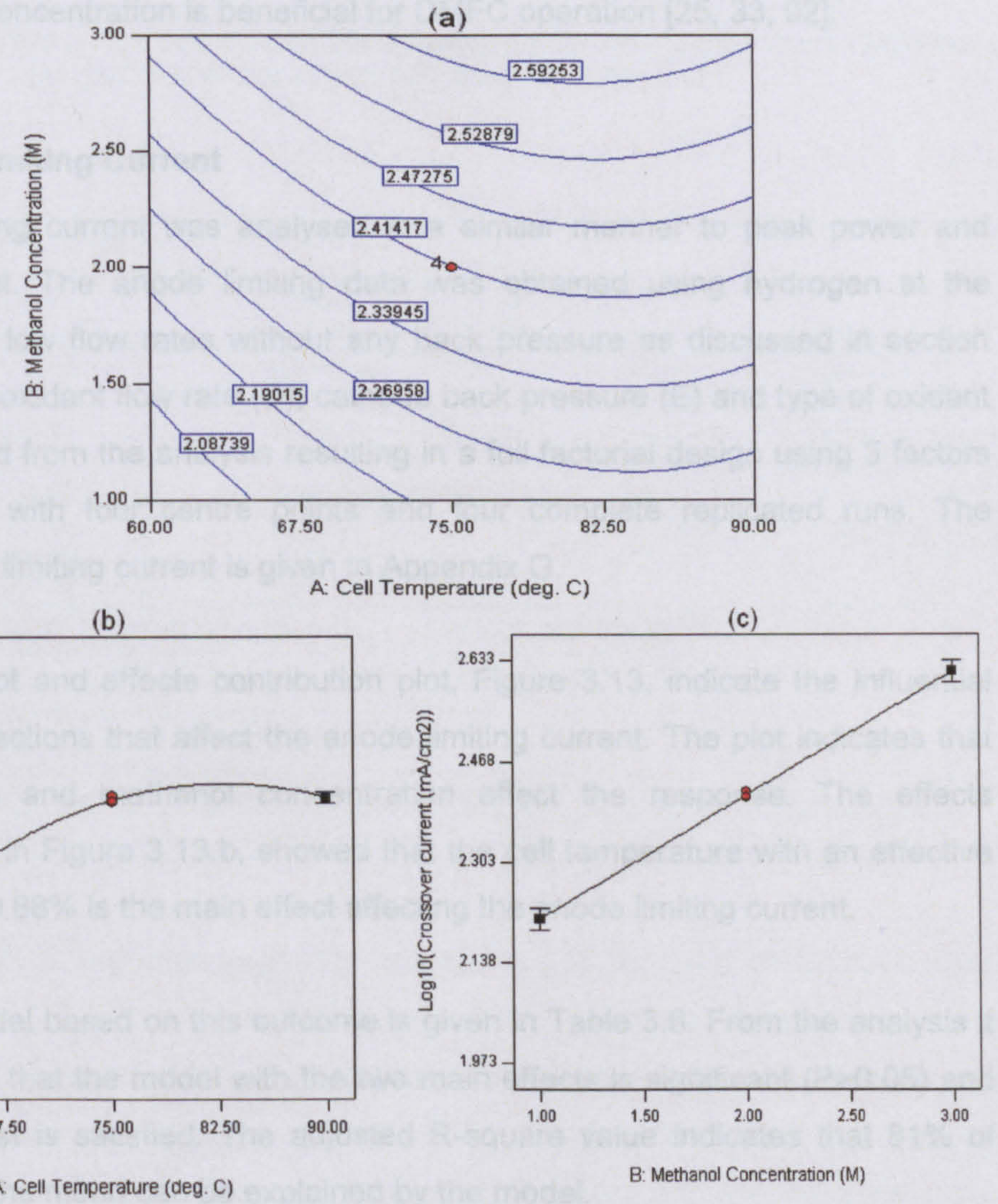

Figure 3.12: Effect plot for log transformed crossover current response (a) 2D contour plot of interaction of cell temperature with methanol concentration, (b) Main effect plot of cell temperature and (c) Main effect plot for methanol concentration. The '•' in the plot represent centre point experimental runs.

These negative effects of a high temperature require to be balanced against the positive effects that were observed in Figure 3.6, where it was observed that an increase in cell temperature improves the reaction kinetics as well as proton conductivity of the membrane thereby resulting in an improvement in the performance of the DMFC.

Figure 3.12.c illustrates the effect of concentration of methanol on log crossover current. It can be observed that an increase in methanol concentration materialises in an increase in log crossover current [25, 32, 92, 109]. The steep gradient for methanol concentration (Figure 3.12.c), compared to that for cell temperature (Figure 3.12.b), indicates that a change methanol concentration has a significant impact on log crossover current compared to cell temperature. Overall, it can be concluded a lower methanol concentration is beneficial for DMFC operation [25, 33, 92].

3.4.3 Anode Limiting Current

The anode limiting current was analysed in a similar manner to peak power and crossover current. The anode limiting data was obtained using hydrogen at the cathode for very low flow rates without any back pressure as discussed in section 3.3.3. Hence the oxidant flow rate (D), cathode back pressure (E) and type of oxidant (F) were removed from the analysis resulting in a full factorial design using 3 factors ($2^k = 2^3 = 8$ *runs*) with four centre points and four complete replicated runs. The response, anode limiting current is given in Appendix G.

A half normal plot and effects contribution plot, Figure 3.13, indicate the influential factors and interactions that affect the anode limiting current. The plot indicates that cell temperature and methanol concentration affect the response. The effects contribution plot, in Figure 3.13.b, showed that the cell temperature with an effective contribution of 69.88% is the main effect affecting the anode limiting current.

The ANOVA model based on this outcome is given in Table 3.6. From the analysis it can be observed that the model with the two main effects is significant ($P>0.05$) and the lack of fit test is satisfied. The adjusted R-square value indicates that 81% of variability about the mean can be explained by the model.

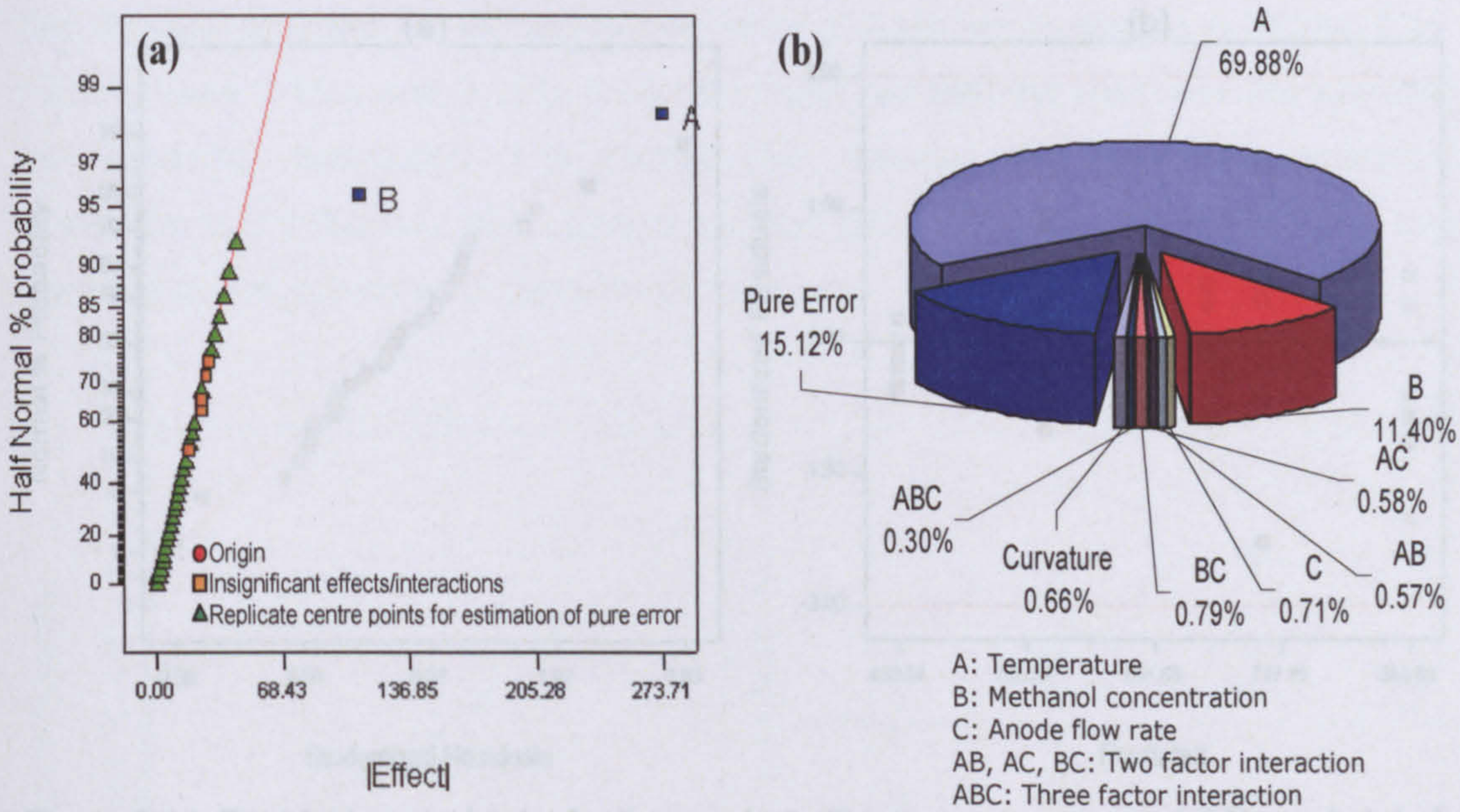

Figure 3.13: Influential factors and interactions affecting the anode limiting current response. (a) Half normal plot and (b) Effects contribution plot.

Response: Anode Limiting Current at 700 mV
Analysis of variance table [Partial sum of squares]

Source	Sum of Squares	DF	Mean Square	F Value	Prob > F	Comment
Model	697132.16	2	348566.08	72.01	< 0.0001	.... Significant
A	599326.36	1	599326.36	123.81	< 0.0001	.... Significant
B	97805.80	1	97805.80	20.21	< 0.0001	.... Significant
Curvature	5627.72	1	5627.72	1.16	0.2890	...Not significant
Residual	154897.95	32	4840.56			
Lack of Fit	25245.46	5	5049.09	1.05	0.4085	...Not significant
Pure Error	129652.49	27	4801.94			
Cor Total	857657.84	35				

Std. Dev.	69.57
Mean	656.10

R-Squared	0.82
Adj R-Squared	0.81

Final Equation in Terms of Coded Factors:
Anode lim @700mv = +651.68 +136.85*A +55.29*B
Final Equation in Terms of Actual Factors:
Anode lim @700mv = -143.158 +9.124*A +55.285*B

Table 3.6: ANOVA output for the anode limiting current response.

To verify the fit of the anode limiting current model a residual analysis was performed, Figure 3.14. The normal probability plot of residuals, Figure 3.14.a, and the residual vs. predicted plot, Figure 3.14.b, showed that the residuals were not normal and exhibited heterosedastic noise [117]. On the basis of this it can be concluded that the anode limiting current model, in Table 3.6, did not satisfy the underlying statistical assumptions.

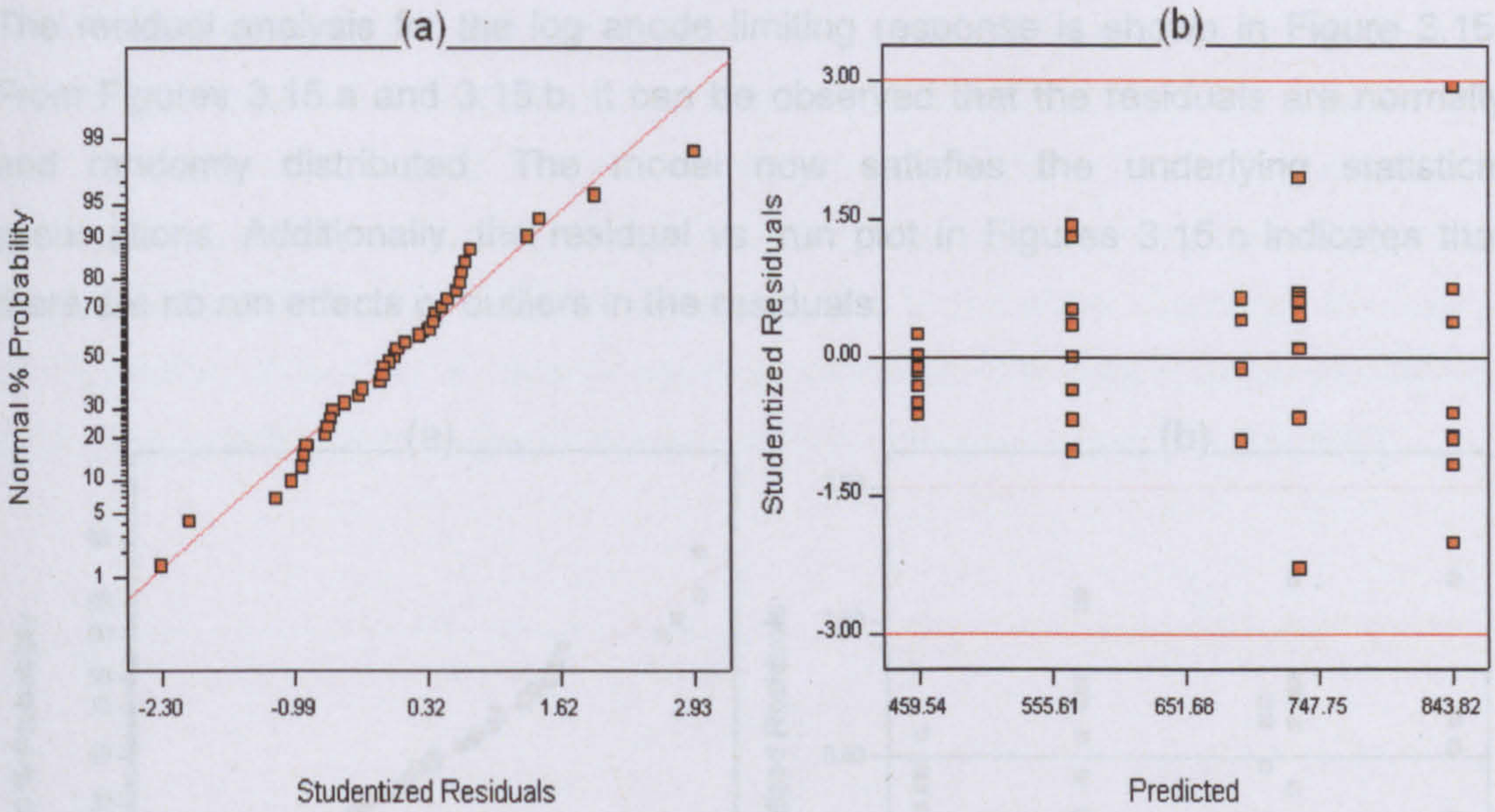

Figure 3.14: Residual analysis plot for the anode limiting current response (a) Normal plot of residuals and (b) Residuals vs. predicted value

To satisfy the statistical assumption of normality and randomly distributed residual and address the issue of heterosedastic noise a log transformation of anode limiting current was performed [112, 117, 122]. Table 3.7, shows the ANOVA output for the log anode limiting current response. The model showed that the factors cell temperature (A) and methanol concentration (B) had a significant effect ($P<0.05$) on the log anode limiting current. Additionally it indicated that the curvature was insignificant ($P=0.1049 >0.05$). The model passed the lack of fit test and was able to predict higher variability (83%) about the mean. To further confirm the fit of the model a residual analysis was performed.

Response: Anode Limiting Current at 700 mV (Log_{10} Transformed)
Analysis of variance table [Partial sum of squares]

Source	Sum of Squares	DF	Mean Square	F Value	Prob > F	Comment
Model	3.31E-01	2	1.65E-01	85.24	< 0.0001	.... Significant
A	2.79E-01	1	2.79E-01	143.97	< 0.0001	.... Significant
B	5.14E-02	1	5.14E-02	26.52	< 0.0001	.... Significant
Curvature	5.40E-03	1	5.40E-03	2.79	0.1049	...Not significant
Residual	6.21E-02	32	1.94E-03			
Lack of Fit	1.63E-02	5	3.27E-03	1.93	0.1227	...Not significant
Pure Error	4.58E-02	27	1.69E-03			
Cor Total	3.98E-01	35				

Std. Dev.	4.40E-02
Mean	2.80E+00

R-Squared	0.84
Adj R-Squared	0.83

Final Equation in Terms of Coded Factors:
Log_{10}(Anode lim @700mv) = +2.80 +0.093*A +0.040*B
Final Equation in Terms of Actual Factors:
Log_{10}/(Anode lim @700mv) = +2.253 +6.23E-03*A +0.04*B

Table 3.7: ANOVA output for the log anode limiting current response.

The residual analysis for the log anode limiting response is shown in Figure 3.15. From Figures 3.15.a and 3.15.b, it can be observed that the residuals are normally and randomly distributed. The model now satisfies the underlying statistical assumptions. Additionally, the residual vs. run plot in Figures 3.15.c indicates that there are no run effects or outliers in the residuals.

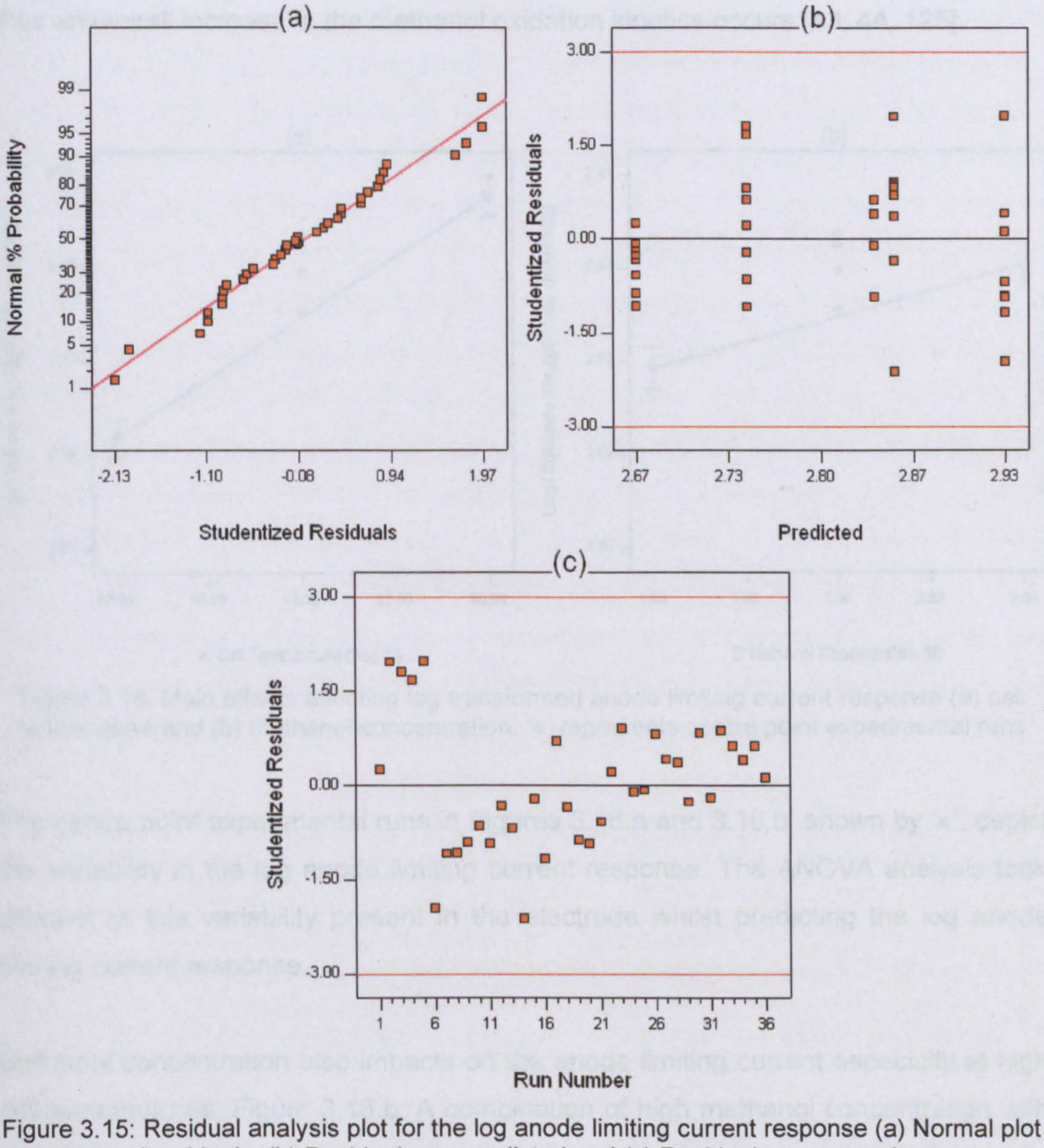

Figure 3.15: Residual analysis plot for the log anode limiting current response (a) Normal plot of residuals, (b) Residuals vs. predicted and (c) Residuals vs. run order

3.4.4 Influence of Cell temperature and Methanol Concentration

Figure 3.16.a, illustrates the effect of cell temperature on the log anode limiting current response. It can be seen that an increase in temperature increases the log anode limiting current response. An increase in temperature enhances the methanol

oxidation kinetics and hence the anode limiting current increases [29, 119]. In a DMFC, the methanol oxidation reaction takes place on a dual site Pt-Ru catalyst [44, 47, 119, 124]. Compared to Pt, the Ru catalyst is less active for methanol oxidation reaction at low temperatures. For high temperatures, Ru produces increased activity for the methanol oxidation reaction especially due to the water discharge reaction at the Ru active sites. Hence a higher reaction temperature results in better activity and thus an overall increase in the methanol oxidation kinetics occurs [43, 44, 125].

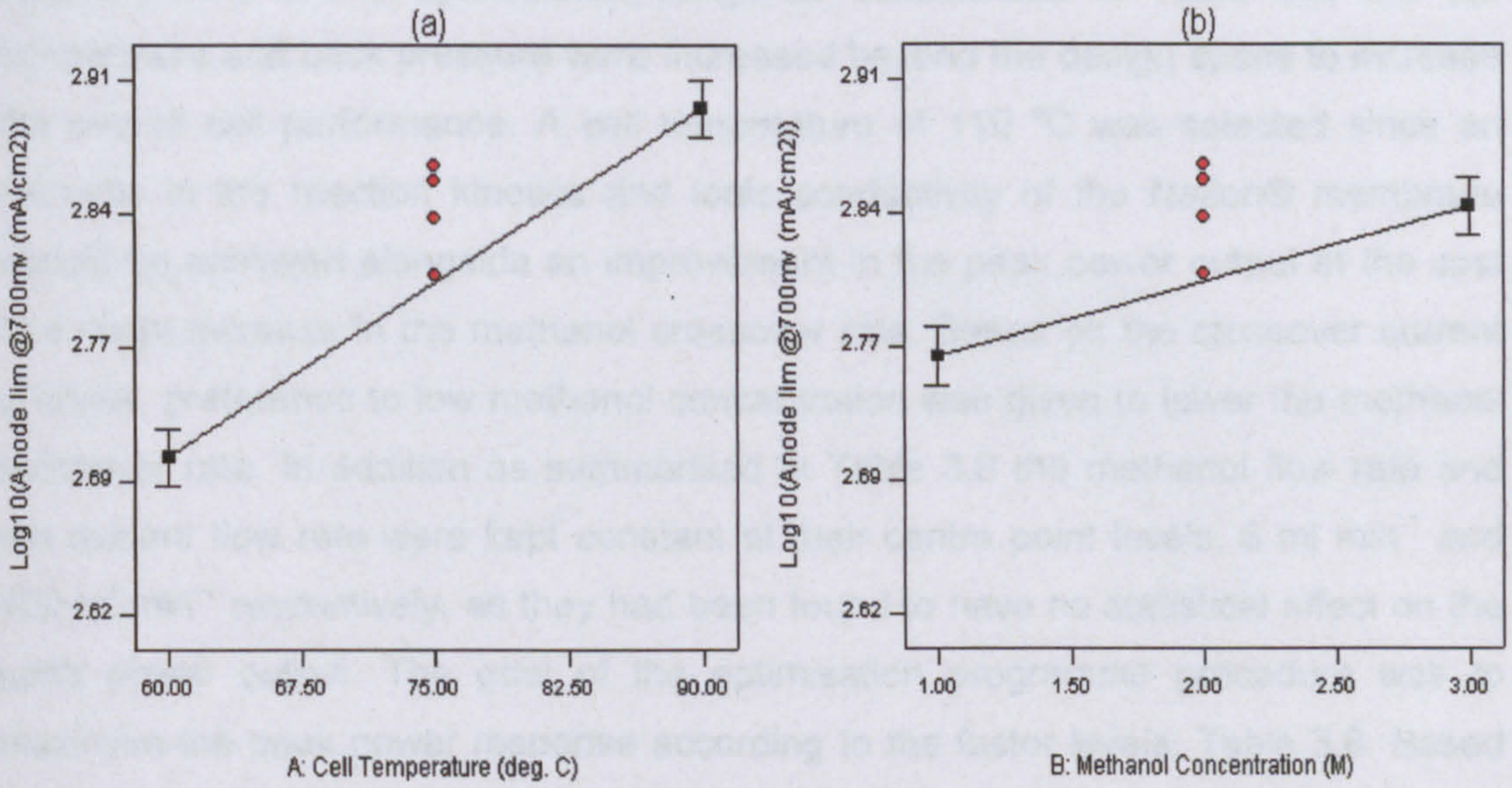

Figure 3.16: Main effects affecting log transformed anode limiting current response (a) cell temperature and (b) methanol concentration. '•' represents centre point experimental runs

The centre point experimental runs in Figures 3.16.a and 3.16.b, shown by '•', depict the variability in the log anode limiting current response. The ANOVA analysis took account of this variability present in the electrode whilst predicting the log anode limiting current response.

Methanol concentration also impacts on the anode limiting current especially at high cell temperatures, Figure 3.16.b. A combination of high methanol concentration with high cell temperature improves the methanol oxidation kinetics and supply the anode catalyst with an adequate amount of methanol at high current density thus improving the anode limiting current. However, as observed in the crossover current analysis, section 3.4.2, this availability of excess methanol can be detrimental to the overall cell performance due to increase in methanol crossover through the membrane. Thus it is necessary to balance the positive effect of increasing methanol

concentration for improving anode performance with the negative effect of methanol crossover through the membrane to overall increase the cell performance.

3.5. Optimising Peak Power Performance

An optimisation was performed on the peak power output combining the outcomes from the methanol crossover effect and anode limiting current. It was observed that an increase in cell temperature and cathode back pressure increases the peak power output. Hence in the optimisation study, as summarised in Table 3.8, the cell temperature and back pressure were increased beyond the design space to increase the overall cell performance. A cell temperature of 110 °C was selected since an increase in the reaction kinetics and ionic conductivity of the Nafion® membrane should be achieved alongside an improvement in the peak power output at the cost of a slight increase in the methanol crossover rate. Based on the crossover current analysis, preference to low methanol concentration was given to lower the methanol crossover rate. In addition as summarised in Table 3.8 the methanol flow rate and the oxidant flow rate were kept constant at their centre point levels, 5 ml min^{-1} and 400 ml min^{-1} respectively, as they had been found to have no statistical effect on the peak power output. The goal of the optimisation programme procedure was to maximise the peak power response according to the factor levels, Table 3.8. Based on the model in the ANOVA table, the 95% confidence intervals within which the response is expected to fall 95% of the time are also calculated [116].

Factor	Name	Level	Low Level	High Level
A	Cell Temperature (°C)	**110 °C**	60	90
B	Methanol Concentration (M)	**1 M**	1	3
C	Methanol flowrate (ml min^{-1})	**5 ml min^{-1}**	6	12
D	Oxidant flowrate (ml min^{-1})	**400 ml min^{-1}**	300	500
E	Back pressure (Mpa)	**0.22 Mpa**	0	0.2
F	Type of Oxidant (Categorical)	**OXYGEN**	AIR	OXYGEN

Note: One or more factor value(s) is outside of the design space.

	Prediction	SE Mean	95% CI low	95% CI high
Peak Power (O_2)	**103.983 mW cm^{-2}**	4.271	95.220	112.746
Peak Power (Air)	**70.716 mW cm^{-2}**	4.271	61.953	79.479

Table 3.8: Numerical optimisation of DMFC power output by restricting the methanol concentration

The results from the optimisation are shown in Table 3.8 and Figure 3.17. On the basis of the regression model for the peak power reported in Table 3.3, the peak

power is predicted for the different combinations of factors in Table 3.8. Since there is one categorical factor, type of oxidant at two levels (air and oxygen), the response is predicted separately for each oxidant as well as the standard error of mean and the confidence interval.

Figure 3.17 indicates that by increasing the cell temperature and cathode back pressure to 110 °C and 0.22 MPa respectively and using a lower concentration of methanol (1M), peak power of 103.98 mW cm^{-2} and 70.18 mW cm^{-2} can be achieved using oxygen and air respectively as an oxidant.

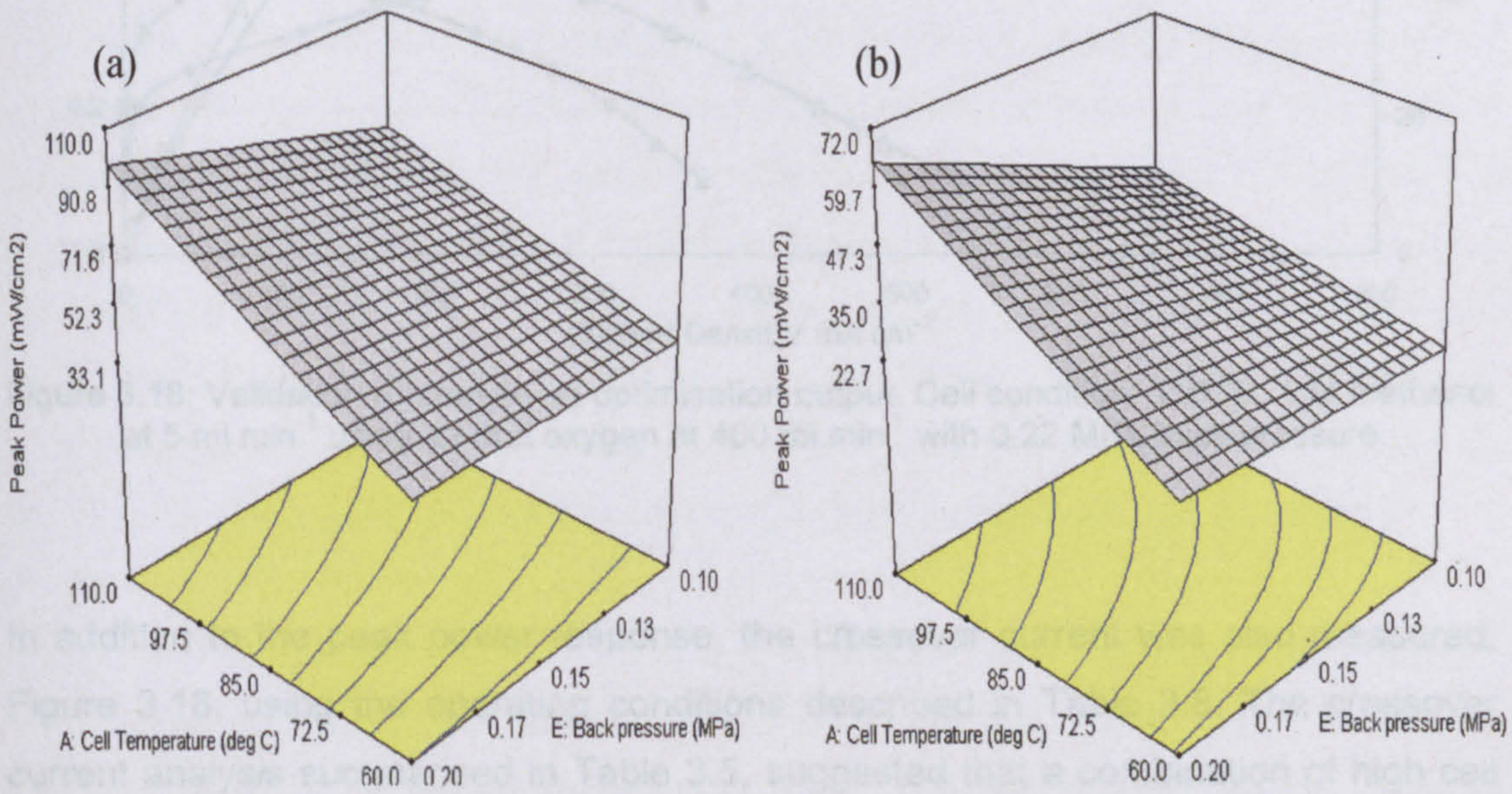

Figure 3.17: Predicted peak power from optimisation process at 110 °C, 0.22 MPa back pressure with 1 M methanol at 5ml min^{-1} using 400 ml min^{-1} of (a) oxygen and (b) air at cathode respectively.

To verify the output from the optimisation, a validating experimental run was performed. Figure 3.18 shows the validation experimental run using the factor levels summarised in Table 3.8. A peak power output of 105.12 mW cm^{-2} using oxygen and 69.03 mW cm^{-2} using air at the cathode was achieved as shown in Figure 3.18. The validation run gave an output which lay within the 95% confidence interval (95.22 to112.75 mW cm^{-2} for oxygen and 61.95 to 79.48 mW cm^{-2} for air) as predicted by the optimisation procedure and thus suggested that model, in Table 3.3, for peak power was a good fit.

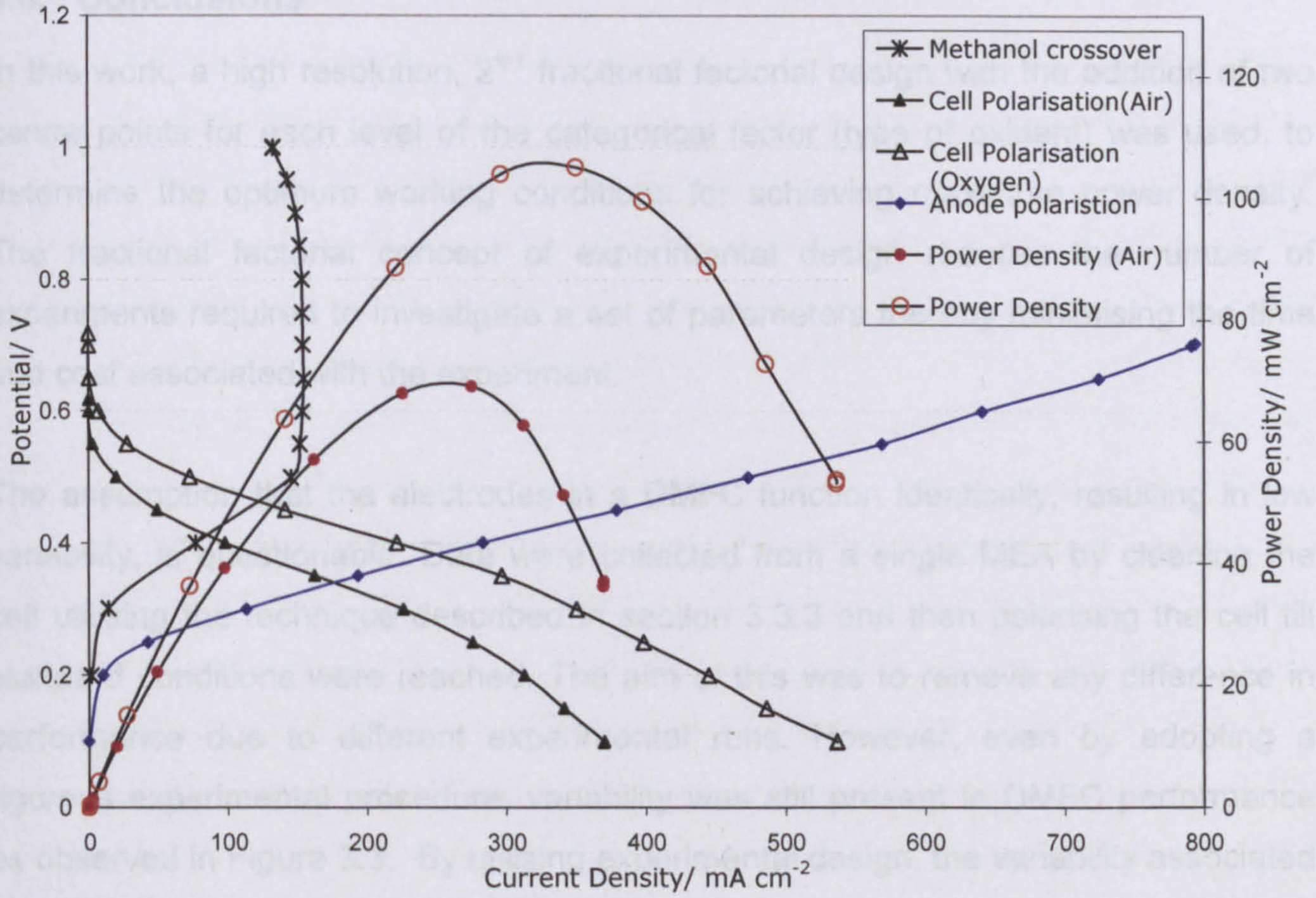

Figure 3.18: Validation run based on optimisation output. Cell condition: 110 °C, 1 M methanol at 5 ml min^{-1} using air and oxygen at 400 ml min^{-1} with 0.22 MPa back pressure

In addition to the peak power response, the crossover current was also measured, Figure 3.18, using the operating conditions described in Table 3.8. The crossover current analysis summarised in Table 3.5, suggested that a combination of high cell temperature (90 °C) and low methanol concentration (1M) would result in a low crossover current (177.87 mA cm^{-2}). However, a lower crossover current is attained from the optimisation study (154.57 mA cm^{-2}) compared to that predicted by the contour plot in Figure 3.12.a, suggesting that the effect of high back pressure (beyond the initial design space) played an important role in reducing the methanol crossover effect. Cruickshank et al., (1998) [70] observed that an increase in cathode back pressure reduced the methanol crossover rate and thus increased the DMFC performance. Conversely, the statistical analysis of crossover current, in Table 3.5, did not identify any effect of back pressure on methanol crossover rate. This was likely to be due to the narrow range considered in the design explaining why a lower crossover current than that predicted by the crossover current analysis was achieved in the optimisation study.

3.6. Conclusions

In this work, a high resolution, 2^{k-1} fractional factorial design with the addition of two centre points for each level of the categorical factor (type of oxidant) was used, to determine the optimum working conditions for achieving maximum power density. The fractional factorial concept of experimental design reduces the number of experiments required to investigate a set of parameters thereby minimising the time and cost associated with the experiment.

The assumption that the electrodes in a DMFC function identically, resulting in low variability, is questionable. Data were collected from a single MEA by cleaning the cell utilising the technique described in section 3.3.3 and then polarising the cell till standard conditions were reached. The aim of this was to remove any difference in performance due to different experimental runs. However, even by adopting a rigorous experimental procedure, variability was still present in DMFC performance as observed in Figure 3.3. By utilising experimental design, the variability associated with DMFC operation was taken into account when determining the optimum configuration of the design parameters to attain maximum power density. Based on the results of the experimental design, the following conclusions can be drawn:

- The temperature of the cell and its interaction with methanol concentration, type of oxidant and back pressure affected the peak power from the cell. The peak power analysis showed that higher cell temperature (90 °C) leads to improved performance of the DMFC. The analysis of anode limiting current supported the peak power analysis and suggested that an increase in cell temperature had a significant impact on the anode limiting current (log transformed) response. In contrast to both the peak power and anode limiting current analysis, the crossover current (log transformed) analysis showed that an increase in temperature gives rise to the undesirable effect of methanol crossover. Thus it is necessary to balance the positive effect of an increase in reaction kinetics and proton conductivity with the negative effect of methanol crossover through the membrane when optimising the overall DMFC performance. For this specific cell design, for low methanol concentration (1 M), the analysis indicated that a high cell temperature (90 °C) is beneficial for optimising fuel cell performance as the positive effects of temperature are greater than the negative effect of methanol crossover.

- Methanol concentration is also a key factor in determining peak power output, methanol crossover and anode limiting current. The analysis indicated that 1 M methanol yields "maximum" peak power and reduces the methanol crossover. Additionally, an improvement in log anode limiting current response with increase in methanol concentration was observed which suggested that a balance to limit the crossover current whilst improving the anode performance is needed. Argyropoulos et al., (1999) [56] and Ge et al., (2005) [33] concluded that the optimum concentration of methanol lay in the range 1 to 2 M. However they failed to establish the effect of the interaction between methanol concentration and cell temperature on peak power and methanol crossover. A combination of low methanol concentration and high cell temperature results in high peak power and reduces the crossover of methanol through the membrane. Overall it can be concluded that the use of low methanol concentration (1 M) at high cell temperature (90 °C) benefits not only the peak power output but also inhibits the adverse effect of methanol crossover through the membrane.

- The flow rates of the reactants (methanol and air/oxygen) were not observed to affect any of the responses considered. However an extra experimental run reported in Appendix F showed that the performance of the DMFC increased with an increase in flow rate of both reactants thus suggesting that the narrow range of the flow rates (3.4 to 6.6 ml min^{-1} for methanol and 300 to 500 ml min^{-1} for oxidant) considered was the issue. This demonstrates the importance of selecting appropriate levels and ranges in an experimental design. The range should be large enough (for example 2 to 10 ml min^{-1} for methanol and 100 to 700 ml min^{-1} for oxidant) so that a difference in the response can be identified and analysed.

- The cathode back pressure impacted on the peak power output from the DMFC. It was observed that the back pressure alone does not influence the peak power response. Of importance is the combination of high back pressure and high cell temperature. In addition the back pressure at the cathode plays an important role in reducing the methanol crossover through the membrane. This effect of back pressure was not identified from the statistical analysis due to the narrow range of the factor but was evident from the optimisation procedure which showed that an increase in back pressure

(outside the range considered in the design) reduces the methanol crossover through the membrane.

- The type of oxidant significantly affected DMFC performance. In this work, the use of oxygen outperformed that of air at the cathode and this effect was dominant at high temperatures due to the interaction of type of oxidant with the cell temperature. The use of pure oxygen in combination with a high cell temperature makes effective use of the high partial pressure of the oxygen and thus improves the overall performance of the DMFC. In addition, when pure oxygen is used, the concentration gradient of oxygen remains sufficiently steep to saturate the cathode catalyst with an appropriate amount of oxygen even in the presence of crossed over methanol and additional water at the active cathode catalyst site, thereby increasing the performance of the DMFC.

- Finally the optimisation study clearly demonstrates the appropriateness of the approach of experimental design in direct methanol fuel cell technology. In this work, by taking into account the variability associated with DMFC operation, all the main effects and interactions of the six operating parameters on DMFC performance were investigated utilising only 36 experimental runs. Conclusions were drawn from anode polarisation characteristics and methanol crossover data as opposed to just relying on cell polarisation data. By utilising a limited number of experiments, labour, time and costs associated with the study were reduced.

In conclusion, the application of experimental design has enabled the investigation of the main effects and interactions of different operating parameters on peak power performance of a single DMFC. The different operating parameters including temperature, pressure, methanol concentration, air/oxygen supply, flow rates of reactants provided information on the optimum settings to achieve "maximum" peak power. However, these settings depend significantly on the design of the membrane electrode assembly (MEA). The design of the MEA depends on various factors including amount of catalyst, type of catalyst, content of PTFE or Nafion® binder. Higher peak power than those achieved by manipulating the operating variables can be achieved by optimising the MEA design. Therefore further optimisation of these design criteria is needed to achieve higher cell output. This is addressed in the next chapter through the application of experimental design techniques.

Chapter 4
RESPONSE SURFACE METHODOLOGY FOR OPTIMISING DMFC PERFORMANCE

4.1. Introduction

The basic physical structure of a DMFC consists of a multi-component membrane electrode assembly (MEA), sandwiched between a flow field and a current collector. The MEA comprises a catalyst layer, micro porous layer (MPL) and a gas diffusion layer (GDL) for each electrode that is positioned on either side of a proton exchange membrane. Optimal performance of the catalyst layer of the DMFC is a critical issue and is influenced by both the choice of catalyst and the fabrication technique, which allows maximum utilisation of the catalyst material. There are a number of factors, including the loading of catalyst, the Nafion® content, coating method, and their interactions involved in the optimisation of the catalyst layer. Additionally the interaction of catalyst layer with the adjoining MPL is also of significance in the optimisation of the MEA. The MPL controls the transfer of the reactants and by-products and hence the emissions of both the anode and the cathode. The catalyst and gas diffusion layers combine to produce a composite catalysed gas diffusion electrode, which is required to be optimised for use in gas, vapour and liquid environments. Typically laborious and costly screening tests are performed to identify the best catalysed gas diffusion electrode formulations. These have previously been performed based on a single factor analysis approach [27, 34, 52, 126-133]. However as discussed in section 3.1, this approach fails to consider the interaction effect and incorporate the variability of the measured response. Thus there is a need for an alternative technique that predicts the MEA formulation that results in enhanced cell performance. The aim of this chapter therefore is to demonstrate the use of the experimental design technique, Response Surface Methodology (RSM), to identify the catalyst layer formulation that optimises the overall DMFC output.

4.2. Experimental Study

The catalyst layer of a DMFC involves the three phases; protons, electrons and gases, and the extent to which these phases are maintained is a function of materials

and fabrication technique [6, 9, 19]. These three phase zones are crucial for the overall DMFC performance as they control the flow of reactants and products to the active catalyst site, and protons and electrons from reacting site. The various ingredients and the fabrication technique involved in the catalyst formulation which have an impact on the formation of three phase zone and thus on the overall performance of the DMFC are [6, 9, 17, 19, 27, 41, 52, 92, 134] :

i) Catalyst loading (0.5, 1, 2 or 3 mg cm^{-2})
ii) Nafion® content (10, 20, 40 or 50 %.wt)
iii) Polytetrafluoroethylene (PTFE) content (0,10, or 20 %.wt)
iv) Supported or unsupported catalyst layer
v) Metal loading (20, 40 or 60 %.wt)
vi) Type of solvent (Acetone, Isopropyl alcohol, Water)
vii) Coating of catalyst on MPL or directly to membrane
viii) Method of applying catalyst (spraying, brushing, tapecasting)

4.2.1 Choice of Factors and their Levels

From the literature review [4, 6, 9, 19, 40], the catalyst and metal loading along with the Nafion® content used in the catalyst layer formulation appear to be the most influential factors. These materials due to high cost at present are the most significant contributors to the overall cost of the system and thus are also the key limiting factor in terms of commercialisation [40]. Practically, a high catalyst loading corresponds to good performance due to an increase in the number of active catalyst sites. Optimisation of the catalyst loading and the Nafion® content depends on the electrode morphology, which is a function of the method used to manufacture the electrode [6, 135, 136]. The activity of the catalyst layer depends on the structure of the Nafion® ionomer "film" that provides the proton conduction from the active catalyst sites. Thus, the Nafion® content in the catalyst layer helps the formation of the three dimensional structure of the electrode. As Nafion® is hydrophilic, its presence in the catalyst layer also aids the retention of moisture. In contrast, a high Nafion® content can result in pore blockage and prevent the gases accessing the catalyst, resulting in poor performance. Several researchers have used polytetrafluoroethylene (PTFE i.e. Teflon) in the formulation of the catalyst layer to provide a gas flow network [136, 137]. The use of PTFE is still open to debate as some researchers believe that its use blocks the catalyst and reduces the active electrode surface area. To investigate these aspects, catalyst loading, Nafion®

content and the addition of PTFE at different levels were considered in the experimental design, Table 4.1.

Factors	Low Level	Centre point	High Level
Loading of Catalyst (mg cm^{-2})	0.5	1.25	2
Nafion® Content (%.wt)	10	25	40
PTFE Content (%.wt)	0	10	20

Table 4.1: Factors considered in the experimental design

Commercially available catalyst materials commonly used in DMFCs take two forms, supported and unsupported. Unsupported catalysts are finely divided powder with no supporting material present. The catalyst layer thus obtained is thinner but this approach can be expensive. To overcome the cost issue supported catalysts that make maximum use of the noble metal are utilised. However with a supported catalyst too much can result in a thicker electrocatalyst layer which can increase the mass transport and ohmic resistance [31]. Thus to balance this and the cost issue, a carbon supported catalyst with a high weight percent of catalyst (60% wt) is desirable.

More recently it has been shown [114] that a dry spraying technique using acetone as a solvent, resulted in better performance of the DMFC. For this study the type, solvent and method of applying the catalyst were fixed. Although the application of the catalyst layer directly on the membrane results in better performance [8, 138], due to experimental limitations, this factor was fixed with the catalyst layer being deposited on the MPL.

Additional to the factors above, the composition of the micro porous layer (MPL) and the gas diffusion layer (GDL) are also of importance as they control the access of the reactants and the by-product. The appropriate structure of the MPL and GDL can result in a reduction of the electrical resistance, provide the necessary hydrophobic or hydrophilic behaviour that will materialise in the correct transfer of the gas and liquid and hence the by-products and reactants to the active catalyst layer. The objective of this study was to investigate the application of experimental design for catalyst layer formulation and hence MPL and GDL formulation were fixed and fabricated using an in-house technique [114].

In this study, the effect of different catalyst formulations on the anode, cathode and the overall cell were of interest. Consequently anode and cell polarisation data were collected using the procedure described in section 3.3. More specifically the experiments were performed at 90 °C using 1 M methanol feed at the anode with a flow rate of 5 ml min^{-1} and oxygen at the cathode as the oxidant with a flow rate of 400 ml min^{-1} and a back pressure of 0.2 MPa. These operating parameters were identified from the study reported in Chapter 3.

4.2.2 Selection of the Response Variable

The main objective of the experiment was to optimise the overall performance of the DMFC, i.e. peak power, and to separately optimise cathode and anode catalyst formulation. The latter two contribute to the overall cell output. For the anode, since catalyst formulation mainly affects the kinetic region, anode performance at 0.25 V was taken as the response. A similar approach was adopted for the cathode. A measure of the cathode response at 10 mA cm^{-2} was attained, by summing the cell and anode polarisation data, using the values from the respective polarisation curves. The experimental technique described in section 3.3 was used to collect data and after each experimental run, the methanol crossover current was measured by passing nitrogen gas through the cathode. This allowed the impact of different catalyst layer formulations on methanol crossover to be investigated.

4.2.3 Experimental Design Structure

This experiment focused on three factors, catalyst loading, Nafion® content and PTFE content at different levels summarised in Table 4.1. Additionally from the literature review [6, 9, 16, 19, 135], it was indicated that electrode activity was non-linearly related to at least one of the factors, catalyst loading or Nafion® content. Consequently a full factorial design comprising of 8 runs (2^3) and four centre point was selected. The centre points were included to analyse the non-linear effect on the response and assess the variability associated with the overall experiment. Table 4.2, summarises the experimental design and Table G.1 in Appendix G gives the results.

Standard experimental runs	Randomised experimental runs	Block	Type of run	A: Catalyst loading (mg cm^{-2})	B: Nafion® Content %.wt	C:PTFE Content %.wt
1	4	Block 1	Fact	0.5	10	0
2	1	Block 1	Fact	2	10	0
3	8	Block 1	Fact	0.5	40	0
4	9	Block 1	Fact	2	40	0
5	6	Block 1	Fact	0.5	10	20
6	10	Block 1	Fact	2	10	20
7	7	Block 1	Fact	0.5	40	20
8	5	Block 1	Fact	2	40	20
9	2	Block 1	Center	1.25	25	10
10	3	Block 1	Center	1.25	25	10
11	11	Block 1	Center	1.25	25	10
12	12	Block 1	Center	1.25	25	10

Table 4.2: Full factorial design with centre points for catalyst layer formulation

4.3. Analysis of the Full Factorial Design

The statistical analysis of the design given in Table 4.2 was performed using Design Expert (version 6.0.11) [116]. To analyse the variability in the measured responses four centre point experimental runs using 1.25 mg cm^{-2} of catalyst loading, 25 %.wt Nafion® content and 10 %.wt PTFE in catalyst formulation were performed. Figure 4.1.a, provide an indication of the variability associated with the peak power response (mean = 67.53 mW cm^{-2}, standard deviation = 8.56 mW cm^{-2}), and methanol crossover current response (mean = 133.2 mA cm^{-2}, standard deviation = 12.49 mA cm^{-2}). Similarly Figure 4.1.b, depicts the variability in the cathode response at 10 mA cm^{-2} (mean = 0.823 V, standard deviation = 0.021 V) and the anode response at 0.25 V (mean = 4.753 mA cm^{-2}, standard deviation = 0.943 mA cm^{-2}). The differences in fabrication technique, non identical functioning of electrodes and experimental error can be a potential reason behind this variation. A detailed analysis of the different responses taking account of this variability is given in the following sections.

4.3.1 Peak Power Analysis

The half normal probability plot in Figure 4.2.a identifies those factors that affect the peak power performance, factors A (catalyst loading) and C (PTFE content). The plot also indicated that the factor B (Nafion® content) and other higher order interactions (AB, BC, AC and ABC) between the factors (shown by orange squares lying on straight line in Figure 4.2.a) did not affect the peak power response. This was further validated by the contribution plot in Figure 4.2.b, which showed the major contribution of catalyst loading (50.12%) and PTFE content (4.15%) on the peak power response.

Additionally, the non-linear behaviour (curvature = 43.97%) was evident from the peak power response, as observed from the contribution plot. The next step was to develop an analysis of variance (ANOVA) model.

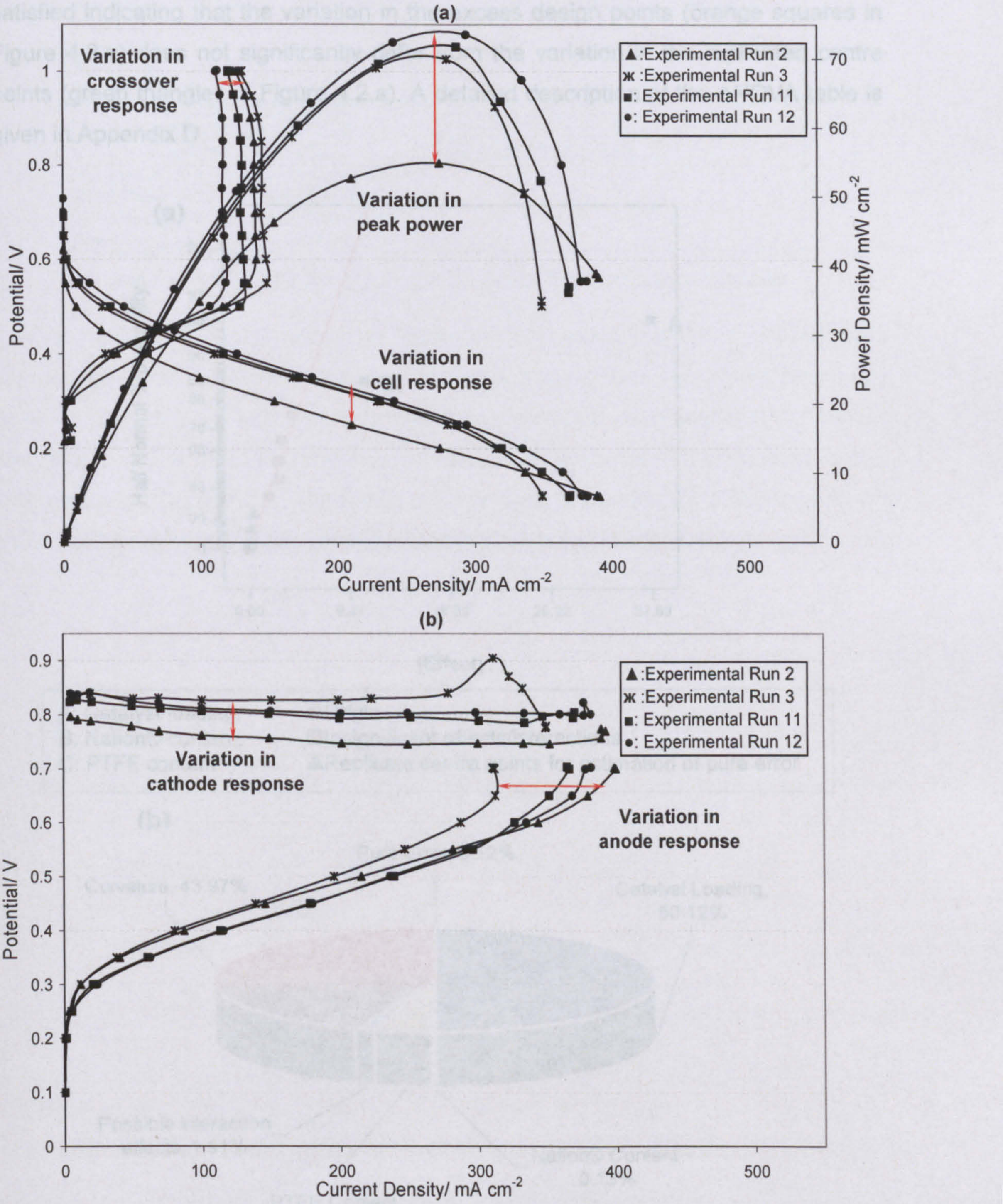

Figure 4.1: Centre point runs (a) variation in peak power response and methanol crossover current response (b) variation in anode and cathode response.

The results of the ANOVA confirmed that catalyst loading (A) and PTFE content (C) have a significant ($P<0.05$) impact on the response and also that curvature/non-linearity is present in the model. The model given in Table 4.3 explains 88% (adjusted R-square) of the variability about the mean and the lack of fit test was satisfied indicating that the variation in the excess design points (orange squares in Figure 4.2.a) does not significantly differ from the variation in the replicated centre points (green triangles in Figure 4.2.a). A detailed description of the ANOVA table is given in Appendix D.

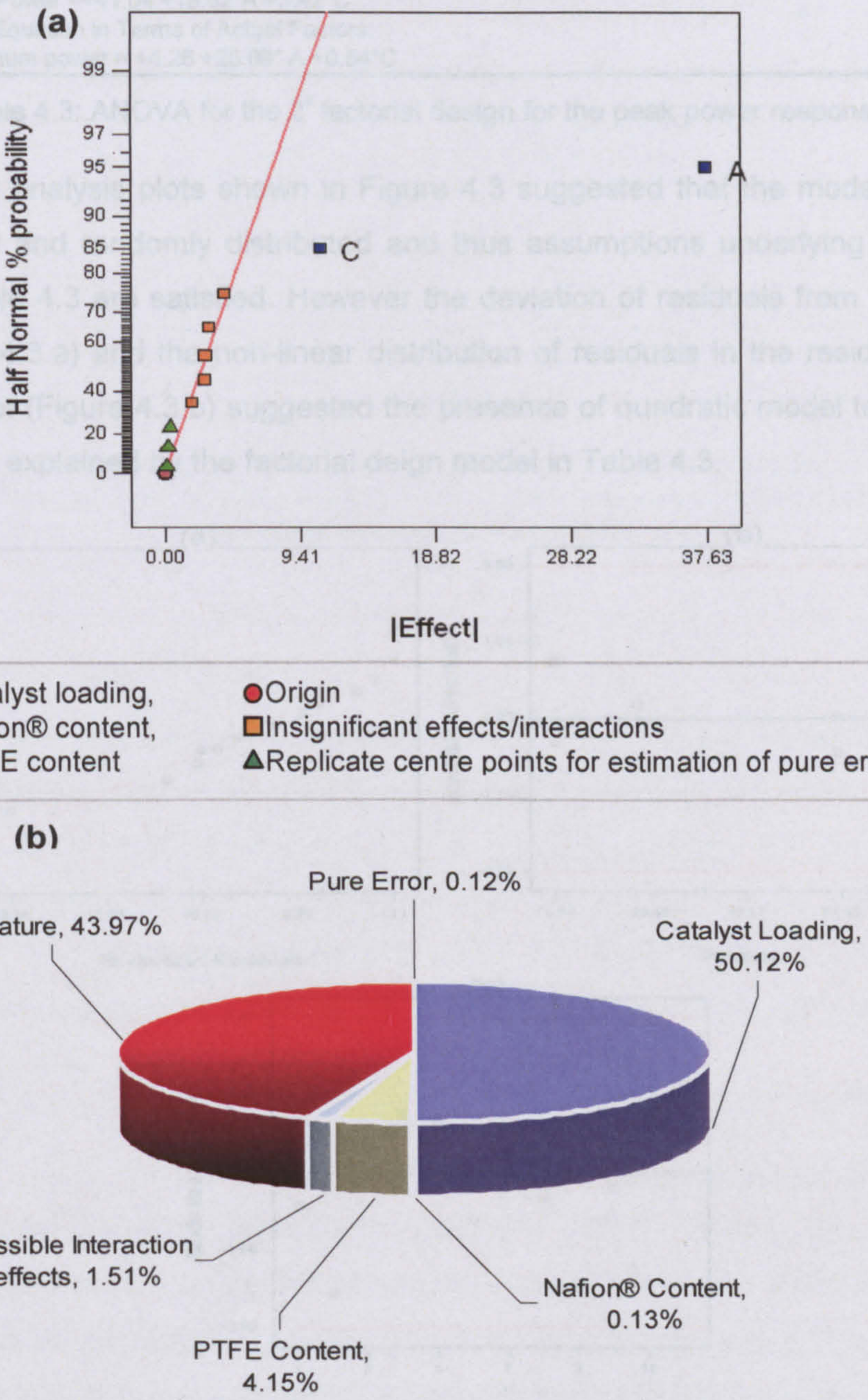

Figure 4.2: Influential factors and interaction affecting the peak power response. (a) Half normal probability plot and (b) Pie chart of the contribution of different effects

Response:Maximum power
Analysis of variance table [Partial sum of squares]

Source	Sum of Squares	DF	Mean Square	F Value	Prob > F	Comment
Model	3066.83	2	1533.41	39.28	< 0.0001	...Significant
A	2832.03	1	2832.03	72.54	< 0.0001	...Significant
C	234.79	1	234.79	6.01	0.0398	...Significant
Curvature	1871.96	1	1871.96	47.95	0.0001	...Significant
Residual	312.33	8	39.04			
Lack of Fit	92.71	5	18.54	0.25	0.9133	...Not significant
Pure Error	219.63	3	73.21			
Cor Total	5251.12	11				

Std. Dev.	6.25
Mean	49.87

R-Squared	0.91
Adj R-Squared	0.88

Final Equation in Terms of Coded Factors:
Peak Power =+41.04 +18.82*A +5.42*C
Final Equation in Terms of Actual Factors:
Maximum power = +4.26 +25.09* A +0.54*C

Table 4.3: ANOVA for the 2^k factorial design for the peak power response

The residual analysis plots shown in Figure 4.3 suggested that the model residuals are normally and randomly distributed and thus assumptions underlying the model given in Table 4.3 are satisfied. However the deviation of residuals from the normal plot (Figure 4.3.a) and the non-linear distribution of residuals in the residual versus predicted plot (Figure 4.3.b) suggested the presence of quadratic model terms which could not be explained by the factorial deign model in Table 4.3.

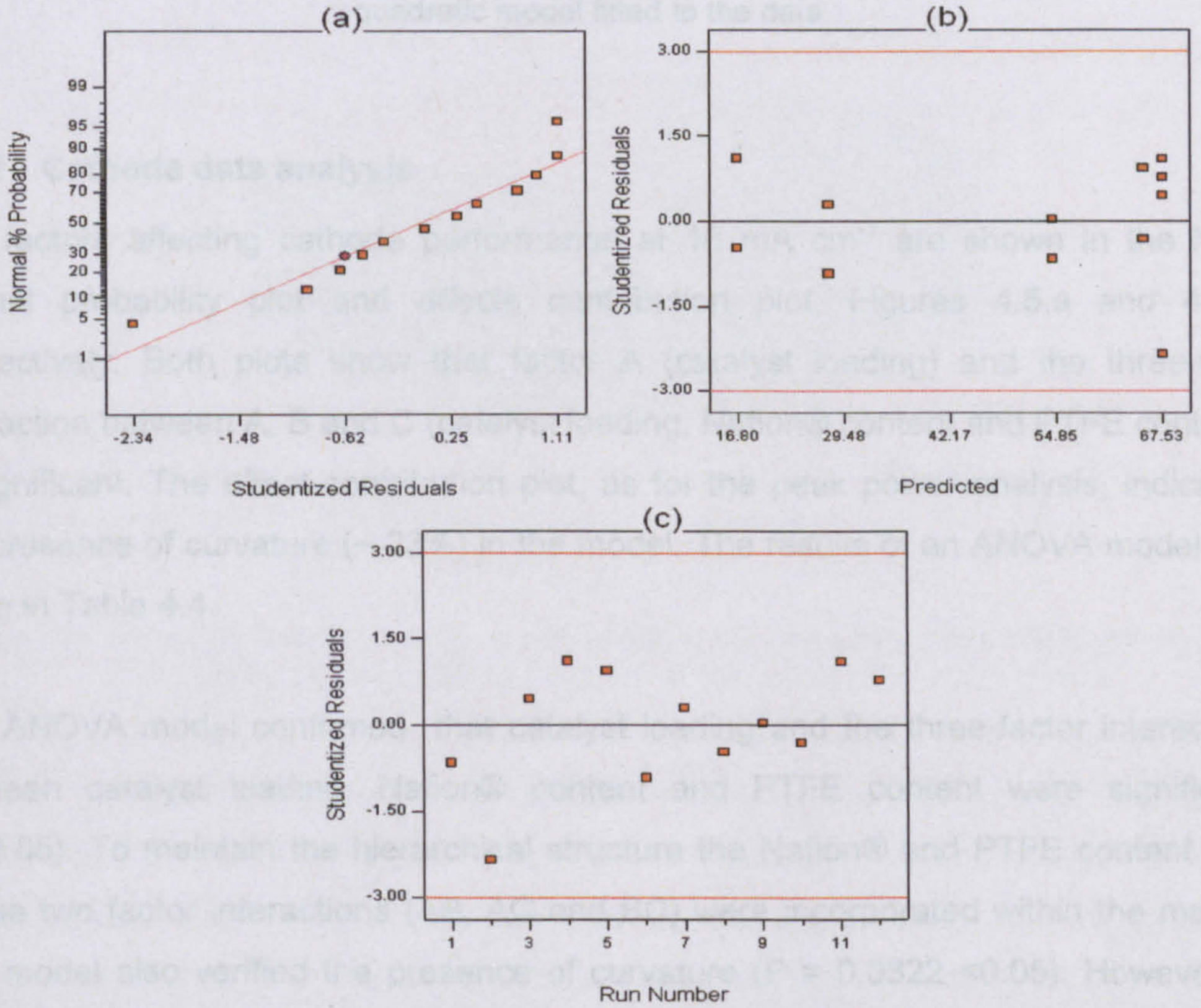

Figure 4.3: Residual analysis of peak power response (a) Normal probability plot of residuals, (b) Residual vs. predicted values and (c) Residual vs. experimental run order

Additionally, a plot of catalyst loading versus peak power response, Figure 4.4, indicated the presence of a quadratic response that was not captured by the factorial design (Table 4.3). These results suggested the need of additional experimental runs to investigate the curvature/non-linearity in the design.

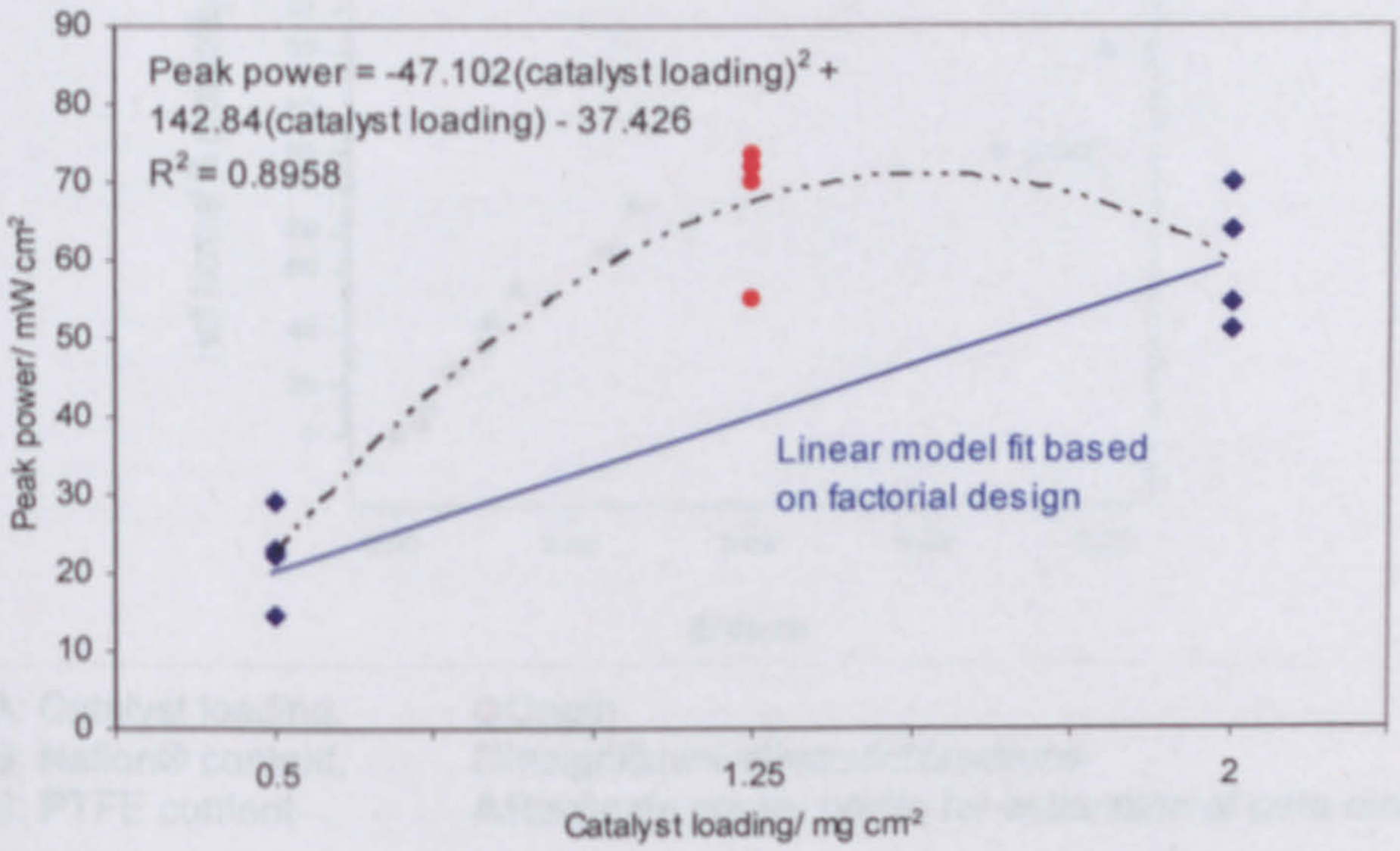

Figure 4.4: Catalyst loading vs. peak power response. '●' represents response from centre point experimental runs, blue line depicts fit using linear model and dotted black line is a quadratic model fitted to the data.

4.3.2 Cathode data analysis

The factors affecting cathode performance at 10 mA cm^{-2} are shown in the half-normal probability plot and effects contribution plot, Figures 4.5.a and 4.5.b respectively. Both plots show that factor A (catalyst loading) and the three-way interaction between A, B and C (catalyst loading, Nafion® content and PTFE content) is significant. The effect contribution plot, as for the peak power analysis, indicates the presence of curvature (~ 23%) in the model. The results of an ANOVA model are given in Table 4.4.

The ANOVA model confirmed that catalyst loading and the three-factor interaction between catalyst loading, Nafion® content and PTFE content were significant ($P<0.05$). To maintain the hierarchical structure the Nafion® and PTFE content and all the two factor interactions (AB, AC and BC) were incorporated within the model. The model also verified the presence of curvature ($P = 0.0322 <0.05$). However in this case the model was not significant ($P = 0.930 >0.05$). This was probably due to

inadequacy of the linear model, in Table 4.4, to take account of curvature present in the design.

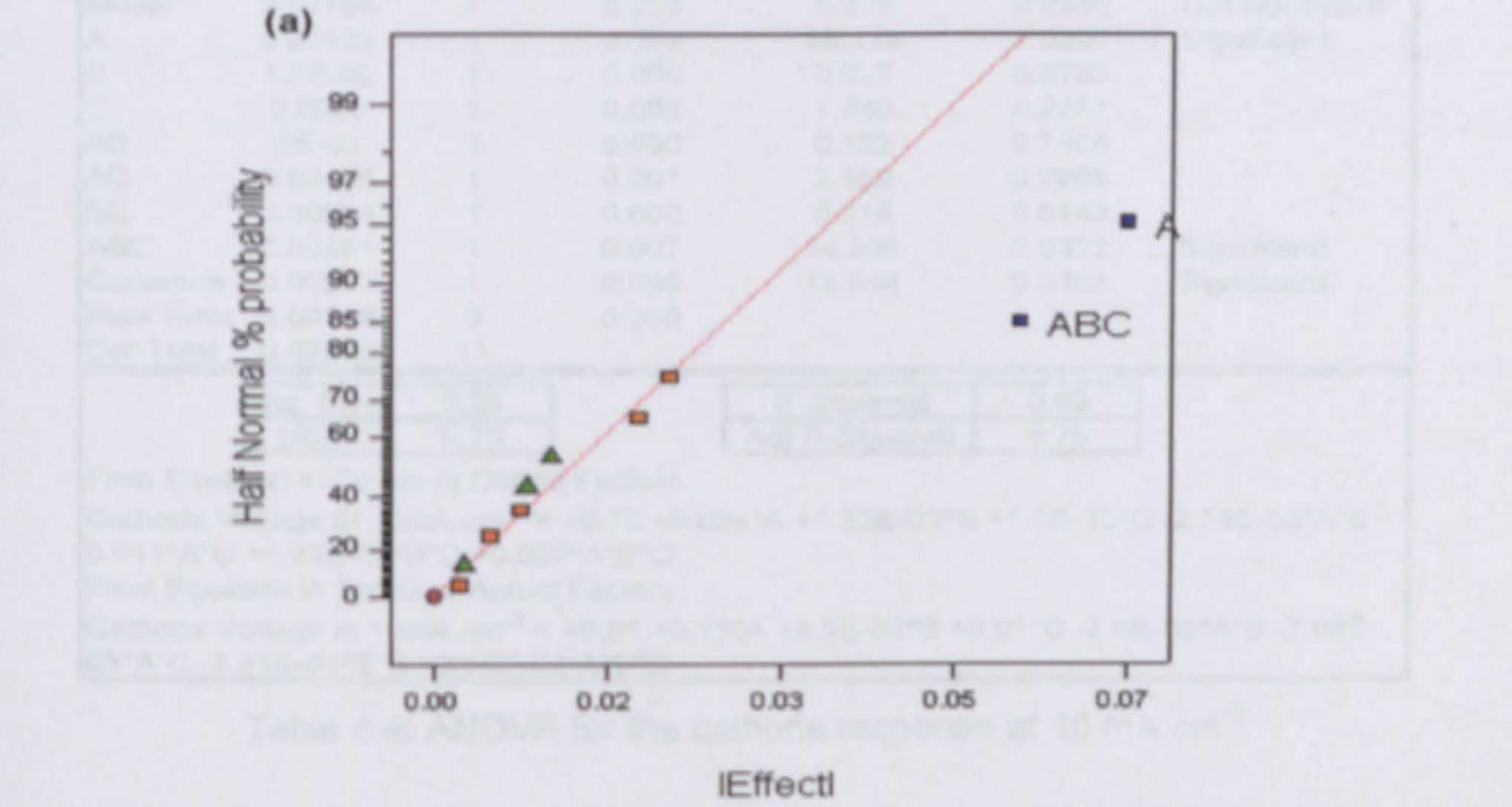

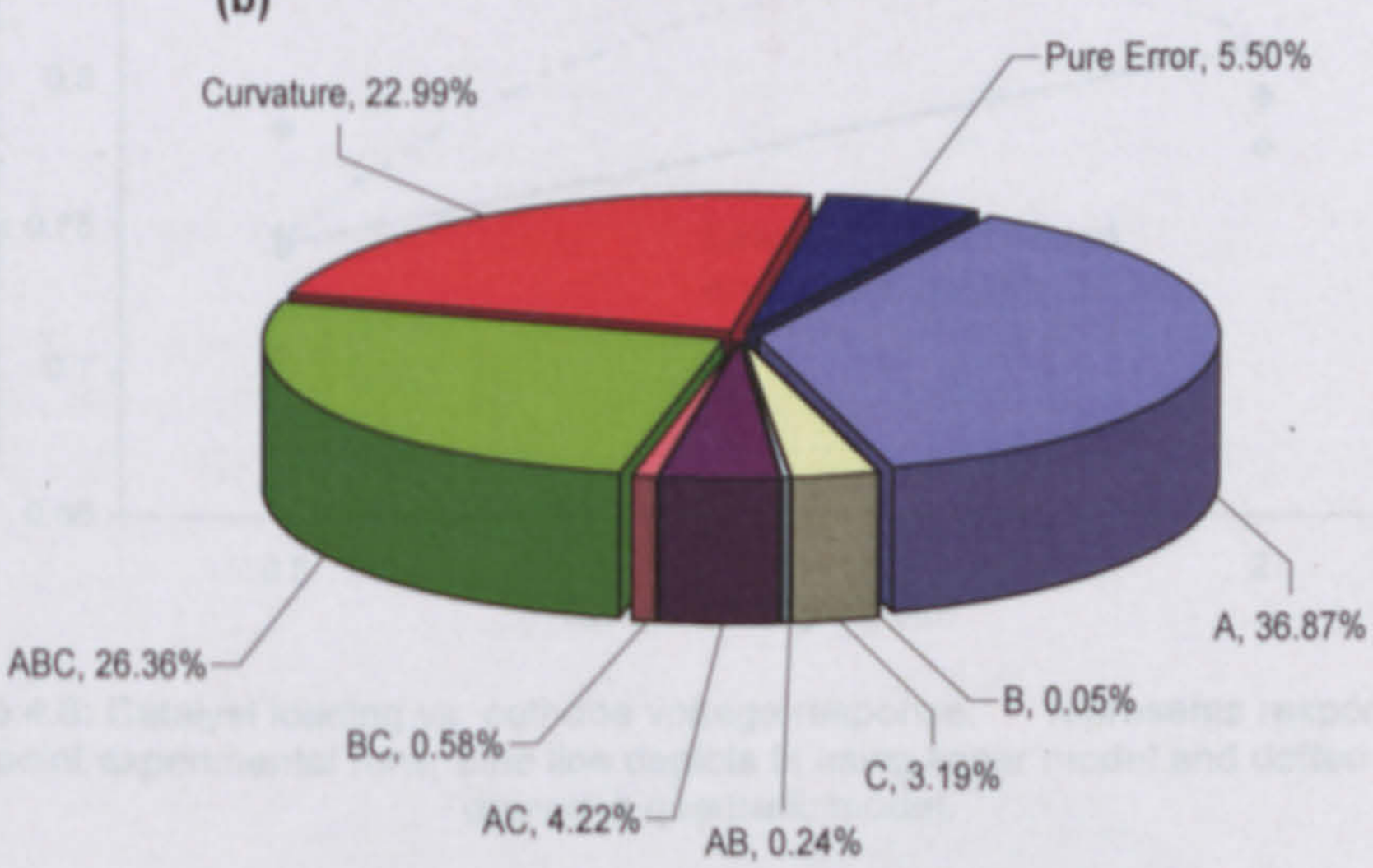

Figure 4.5: Influential factors and interaction affecting the cathode voltage response. (a) Half normal probability plot and (b) Pie chart of the contribution of the effects

A plot of catalyst loading versus the cathode voltage (10 mA cm^{-2}) response, given in Figure 4.6, demonstrates the presence of a quadratic relationship. To take account of this behaviour, additional experimental runs were required to analyse the curvature and identify a model that describes cathode behaviour at 10 mA cm^{-2}.

Response:Cathode Voltage at 10mA cm^{-2}
Hierarchical Terms Added after Manual Regression: B, C, AB, AC and BC
Analysis of variance table [Partial sum of squares]

Source	Sum of Squares	DF	Mean Square	F Value	Prob > F	Comment
Model	0.01794	7	0.003	5.574	0.0930	...Not significant
A	0.00925	1	0.009	20.119	0.0207	...Significant
B	1.2E-05	1	0.000	0.027	0.8795	
C	0.0008	1	0.001	1.740	0.2787	
AB	6E-05	1	0.000	0.132	0.7408	
AC	0.00106	1	0.001	2.302	0.2265	
BC	0.00014	1	0.000	0.314	0.6142	
ABC	0.00661	1	0.007	14.385	0.0322	...Significant
Curvature	0.00577	1	0.006	12.544	0.0383	...Significant
Pure Error	0.00138	3	0.000			
Cor Total	0.02508	11				

Std. Dev.	0.02
Mean	0.79

R-Squared	0.93
Adj R-Squared	0.76

Final Equation in Terms of Coded Factors:
Cathode Voltage at 10mA cm^{-2} = +0.78 +0.034*A +1.25E-03*B +1.0E-02*C -2.75E-03*A*B -0.011*A*C +4.25E-03*B*C +0.029*A*B*C
Final Equation in Terms of Actual Factors:
Cathode Voltage at 10mA cm^{-2} = +0.61 +0.13*A +3.3E-03*B +0.01*C -2.8E-03*A*B -7.92E-03*A*C -2.91E-04*B*C +2.56E-04*A*B*C

Table 4.4: ANOVA for the cathode response at 10 mA cm^{-2}

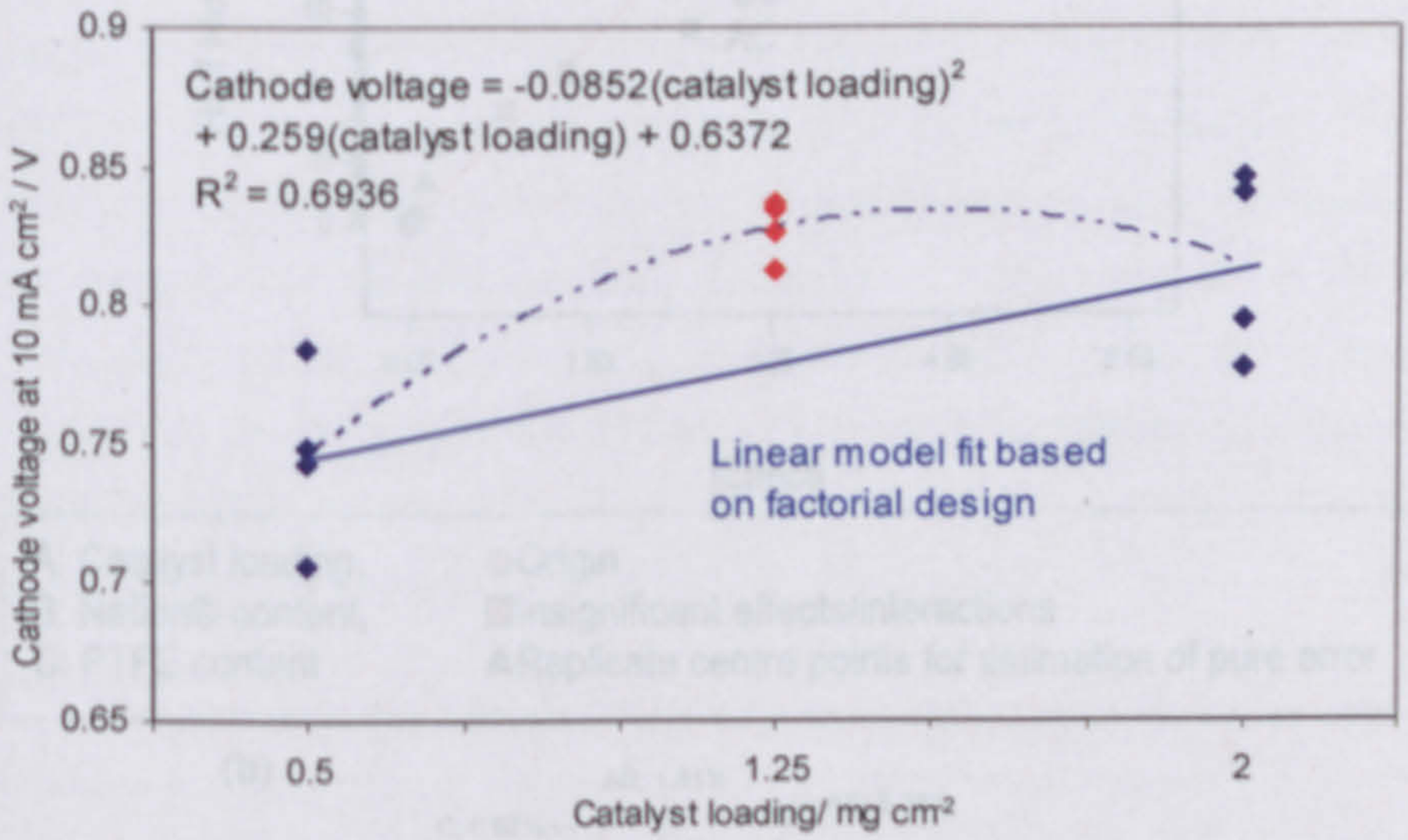

Figure 4.6: Catalyst loading vs. cathode voltage response. '●' represents response from centre point experimental runs, blue line depicts fit using linear model and dotted black line depicts a quadratic model.

4.3.3 Anode data analysis

To analyse the effect of different catalyst formulation on the anode response, the anode response at 0.25 V was measured. The half normal probability plot and the effects contribution plot, in Figures 4.7.a and 4.7.b, suggested that the catalyst loading (A), Nafion® content (B), their two-way interactions with PTFE content (C) and the three way interaction between A, B and C had an impact on the anode performance at 0.25 V. This was confirmed by the ANOVA model, Table 4.5.

The ANOVA model, in Table 4.5, supported the conclusions attained from the half normal probability plot and effects contribution plot. The high adjusted R-square value suggested that the linear model was a good fit. Compared to the peak power and cathode data analysis, the curvature was not identified as an influential feature (P=0.3435>0.05) in the model.

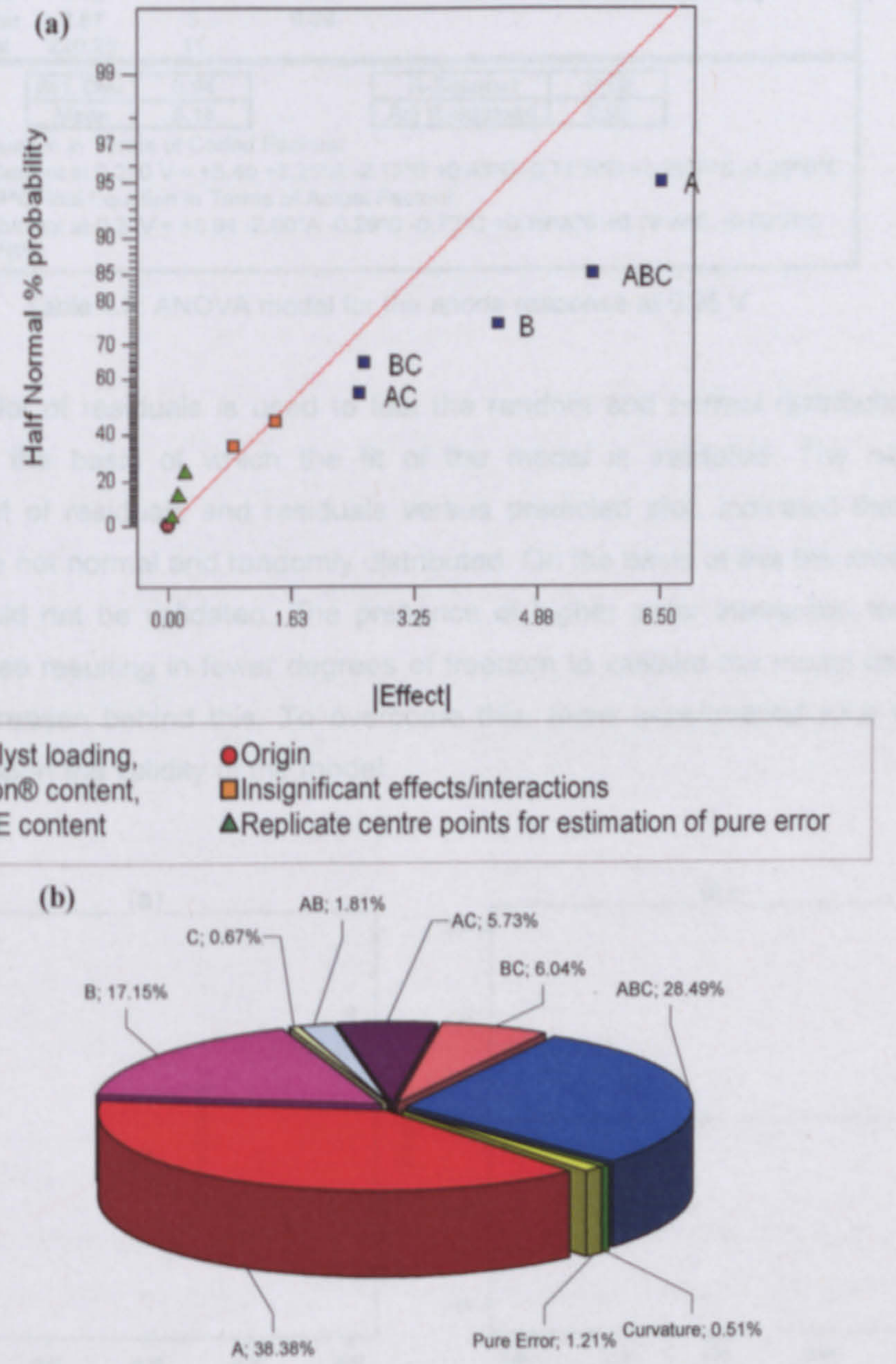

Figure 4.7: Influential factors and interaction affecting the anode response. (a) Half normal probability plot and (b) Pie chart of the contribution of the effects. (AB, AC and BC: two-factor interactions and ABC: three-factor interaction)

Response:Anode response at 0.25V
Hierarchical Terms Added after Manual Regression: C and AB
Analysis of variance table [Partial sum of squares]

Source	Sum of Squares	DF	Mean Square	F Value	Prob > F	Comment
Model	216.46	7	30.92	34.75	0.0072	...Significant
A	84.54	1	84.54	94.99	0.0023	...Significant
B	37.78	1	37.78	42.45	0.0073	...Significant
C	1.47	1	1.47	1.65	0.2891	
AB	3.99	1	3.99	4.48	0.1245	
AC	12.63	1	12.63	14.19	0.0327	...Significant
BC	13.30	1	13.30	14.95	0.0306	...Significant
ABC	62.75	1	62.75	70.51	0.0035	...Significant
Curvature	1.12	1	1.12	1.26	0.3435	...Not significant
Pure Error	2.67	3	0.89			
Cor Total	220.25	11				

Std. Dev.	0.94	R-Squared	0.99
Mean	5.18	Adj R-Squared	0.96

Final Equation in Terms of Coded Factors:
Anode Current at 0.250 V = +5.40 +3.25*A -2.17*B +0.43*C -0.71*A*B +1.26*A*C -1.29*B*C -2.80*A*B*CFinal Equation in Terms of Actual Factors:
Anode Current at 0.25V = +8.94 -2.00*A -0.29*B -0.73*C +0.19*A*B +0.79*A*C +0.02*B*C -0.025*A*B*C

Table 4.5: ANOVA model for the anode response at 0.25 V

The normal plot of residuals is used to test the random and normal distribution of residuals; on the basis of which the fit of the model is validated. The normal probability plot of residuals and residuals versus predicted plot, indicated that the residuals were not normal and randomly distributed. On the basis of this the model in Table 4.5 could not be validated. The presence of higher order interaction for the anode response resulting in fewer degrees of freedom to validate the model can be the potential reason behind this. To overcome this, more experimental runs were needed to support the validity of the model.

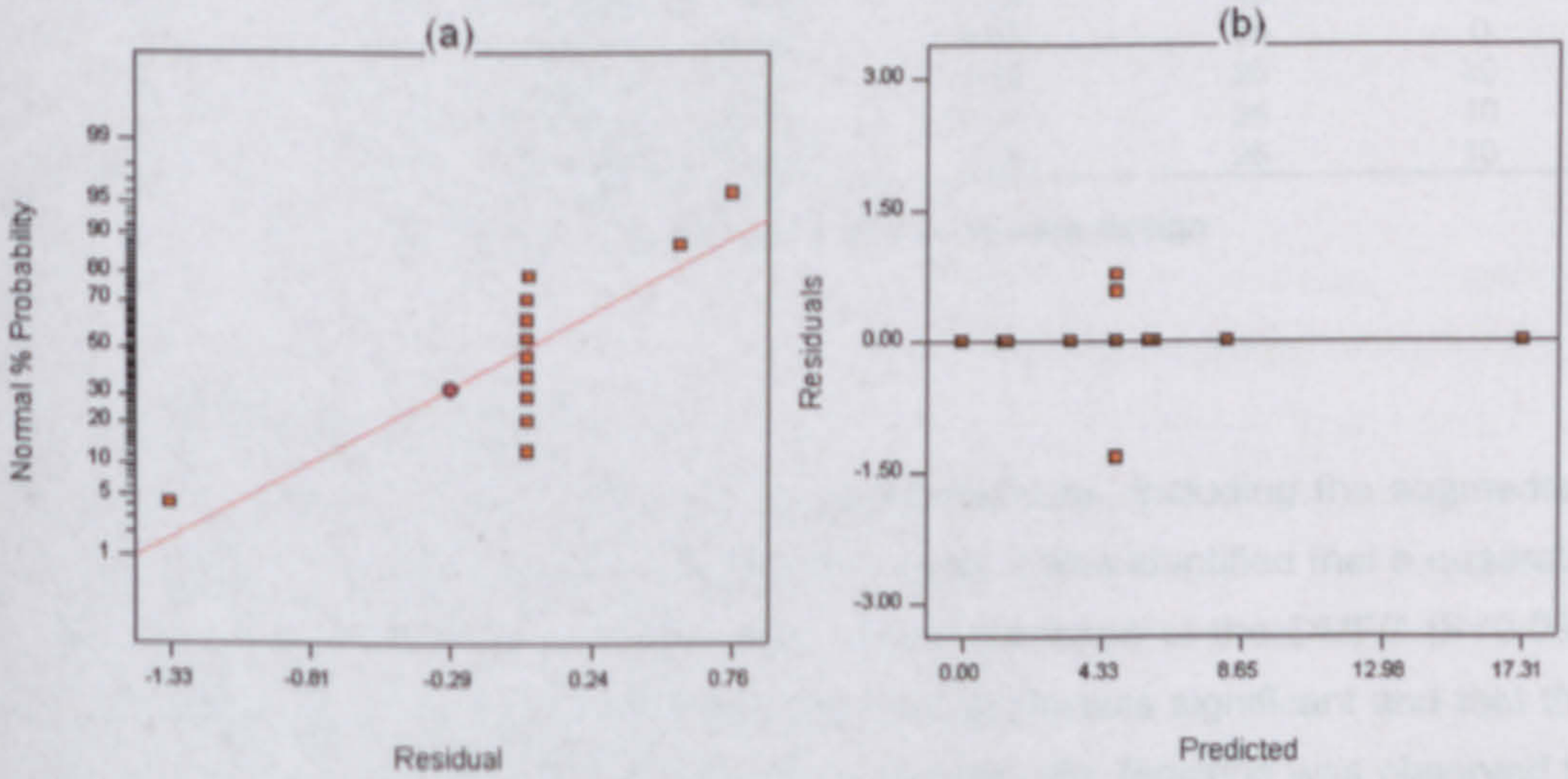

Figure 4.8: Residaul analysis plot for the anode response

4.4. Central Composite Design

Analysis of the peak power and cathode responses indicated that curvature was present in the model. Additionally the analysis of anode response suggested that extra experimental runs were required to identify an appropriate anode model that satisfied the underlying statistical assumption of normal and random distributed residuals. Hence to explore these aspects further, the full factorial design given in Table 4.2 was augmented, with a central composite design (CCD) [112, 113, 139]. The revised design is summarised in Table 4.6. The experimental runs 2, 3, 11 and 12 in Table 4.2 for the full factorial design at the centre point (1.25 mg cm^{-2} Catalyst loading, 25 %.wt Nafion® content, 10%.wt PTFE) suggested that there was a repeatability and reproducibility issue with the experiments. To address this issue the augmented design included two additional centre points. To reduce the impact of changes in raw materials, experimenter performance and overall variability in the analysis due to additional set of experiments, being run at a later stage, the augmented design runs were blocked. Blocking is advantageous when there is a known factor, such as changes in raw materials or experimenter performance, that may influence the experimental result, but the effect is not of interest. The responses for these additional runs were measured according to the procedure described in section 3.3, and the results are summarised in Appendix G.

Standard experimental runs	Randomised experimental runs	Block	Type of run	A: Catalyst loading (mg cm^{-2})	B: Nafion® Content %.wt	C:PTFE Content %.wt
13	17	Block 2	Axial	0.5	25	10
14	14	Block 2	Axial	2	25	10
15	18	Block 2	Axial	1.25	10	10
16	16	Block 2	Axial	1.25	40	10
17	19	Block 2	Axial	1.25	25	0
18	15	Block 2	Axial	1.25	25	20
19	13	Block 2	Center	1.25	25	10
20	20	Block 2	Center	1.25	25	10

Table 4.6: Augmented central composite design

4.4.1 Peak Power Analysis

The analysis of peak power for the 20 experimental runs, including the augmented CCD, is given in Table 4.7. From the ANOVA model, it was identified that a quadratic model was best suited for predicting peak power response of the DMFC ($P<0.05$). The ANOVA showed that the factor catalyst loading (A) was significant and that the model was quadratic with respect to Nafion® Content (B). Blocking was observed to have an insignificant influence on the model. To maintain the statistical principle of

hierarchy, the main effect Nafion® Content (B) was included. The CCD model also showed that in this study the addition of PTFE, (i.e. 0 to 20%wt) does not have a significant influence on peak power performance. The adjusted R-square value suggested that the model explained 75% of the variability and the lack of fit suggested that the variation in the excess design points was not significant compared to the replicated points.

Response:Peak Power
Analysis of variance table [Partial sum of squares]

Source	Sum of Squares	DF	Mean Square	F Value	Prob > F	Comment
Block	199.90	1	199.90	1.82		
Model	6282.35	3	2094.12	19.06	< 0.0001	...Significant
A	3176.95	1	3176.95	28.91	< 0.0001	...Significant
B	24.37	1	24.37	0.22	0.6445	...Not significant
B2	3081.03	1	3081.03	28.04	< 0.0001	...Significant
Residual	1648.48	15	109.90			
Lack of Fit	1427.85	11	129.80	2.35	0.2123	...Not significant
Pure Error	220.62	4	55.16			
Cor Total	8130.73	19				

Std. Dev.	10.48
Mean	52.45

R-Squared	0.79
Adj R-Squared	0.75

Final Equation in Terms of Coded Factors:
Peak Power = +65.56 +17.82*A -1.56*B -27.19*B^2
Final Equation in Terms of Actual Factors:
Peak Power = -37.08 +23.77*A +5.94*B -0.12*B^2

Table 4.7: ANOVA model for the peak power response using CCD

To further validate the CCD model, a residual analysis was performed, as shown in Figure 4.9. The normal probability plot, Figure 4.9.a, showed that the residuals were normal. The residual versus predicted value and the residual versus run order plot in Figures 4.9.b and 4.9.c showed that there was no structure remaining unexplained by the model. Thus it can be concluded that the CCD model was a good fit and was able to adequately describe the experimental data.

The ANOVA in Table 4.7 also showed that there was no significant interaction between catalyst loading (A) and Nafion® content (B). This was confirmed from the main effect plot of catalyst loading and Nafion® content, Figures 4.10.a, and 4.10.b. In Figure 4.10.a, the least significant difference (LSD) is represented by the 'I'bar, the definition of which is given in Appendix F. Overlap of the LSD I-bar indicates no significant difference between the different levels [112, 113, 117]. The LSD I–bar for low catalyst loading in Figure 4.10.a and Figure 4.10.b do not overlap with those for high catalyst loading, hence it can be concluded, with 95% confidence level that the mean of high catalyst loading is significantly different and higher than that at low

catalyst loading. Additionally on the basis of gradient of the main effects plot of catalyst loading in Figure 4.10.a it can be concluded that a high catalyst loading of 2 mg cm^{-2} gives greater peak power.

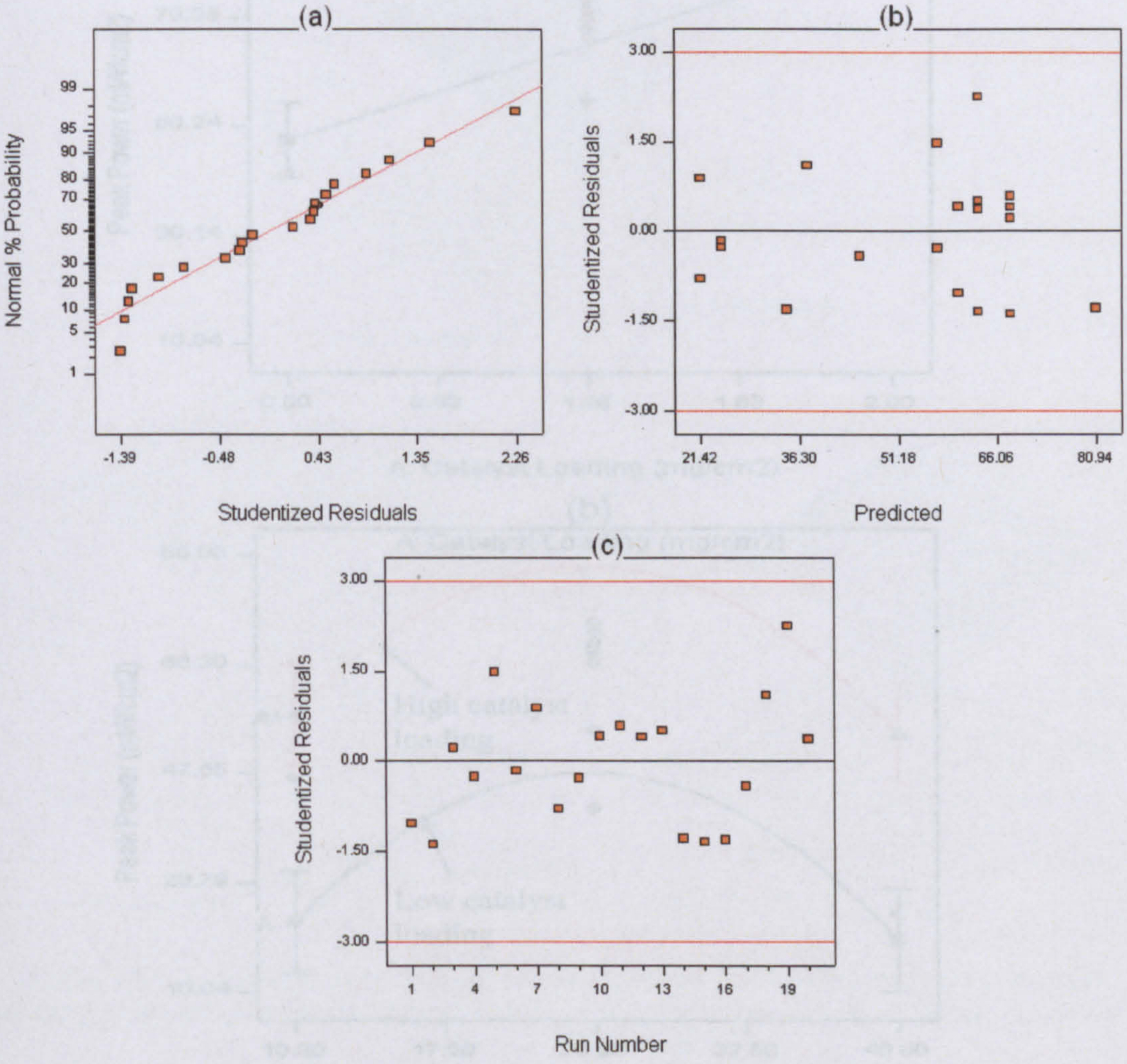

Figure 4.9: Residual analysis of the peak power CCD model (a) Normal probability plot of residuals, (b) Residual vs. predicted values and (c) Residual vs. experimental run order

The red and green dots, Figures 4.10.a and 4.10.b, represents the centre point and axial point experimental runs using 1.25 mg cm^{-2} catalyst loading, 25 %.wt Nafion® content and 10 %.wt PTFE in the catalyst formulation. The centre point runs show the amount of variability in the design, which is accounted for in the quadratic model in Table 4.7. The points outside the LSD I – bar, in Figure 4.10.a, can be attributed to this variability in the design [113, 117, 139]. The overlapping structure of LSD I – bar in Figure 4.10.b indicated that both high and low Nafion® content resulted in similar low peak power response. However the summit at centre of the main effect plot suggested that the most favourable Nafion® content for achieving peak power was between 20 to 30%.wt [132, 140].

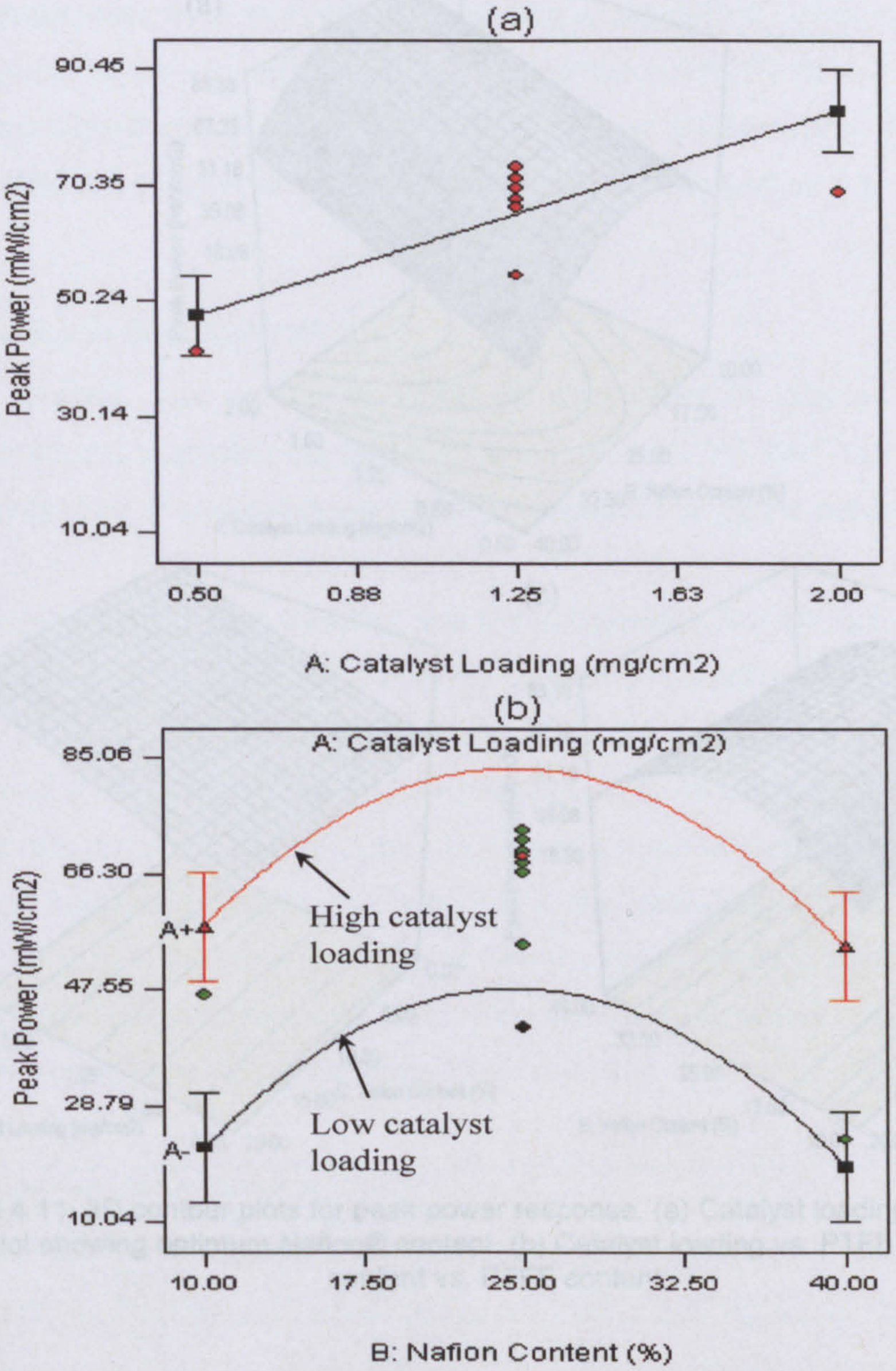

Figure 4.10: Main effects plot for peak power response (a) Catalyst loading and (b) Nafion® content at different levels of catalyst loading. The dots represent the response from the experimental runs with dots at the centre level denoting the six centre point runs.

In this work, the prime objective was to demonstrate how the application of Design of Experiments can help identify the best combination of the three factors in catalyst formulation in conjunction with process understanding. The 3D contour plot (Figure 4.11) obtained from the quadratic model in Table 4.7 confirms the area of operation which gives the maximum peak power performance. From Figure 4.11.a, it is clear that for this study, high catalyst loading (2 mg cm^{-2}) was beneficial with best performance being achieved when the Nafion® content was of the order of 20 to 30 % wt.

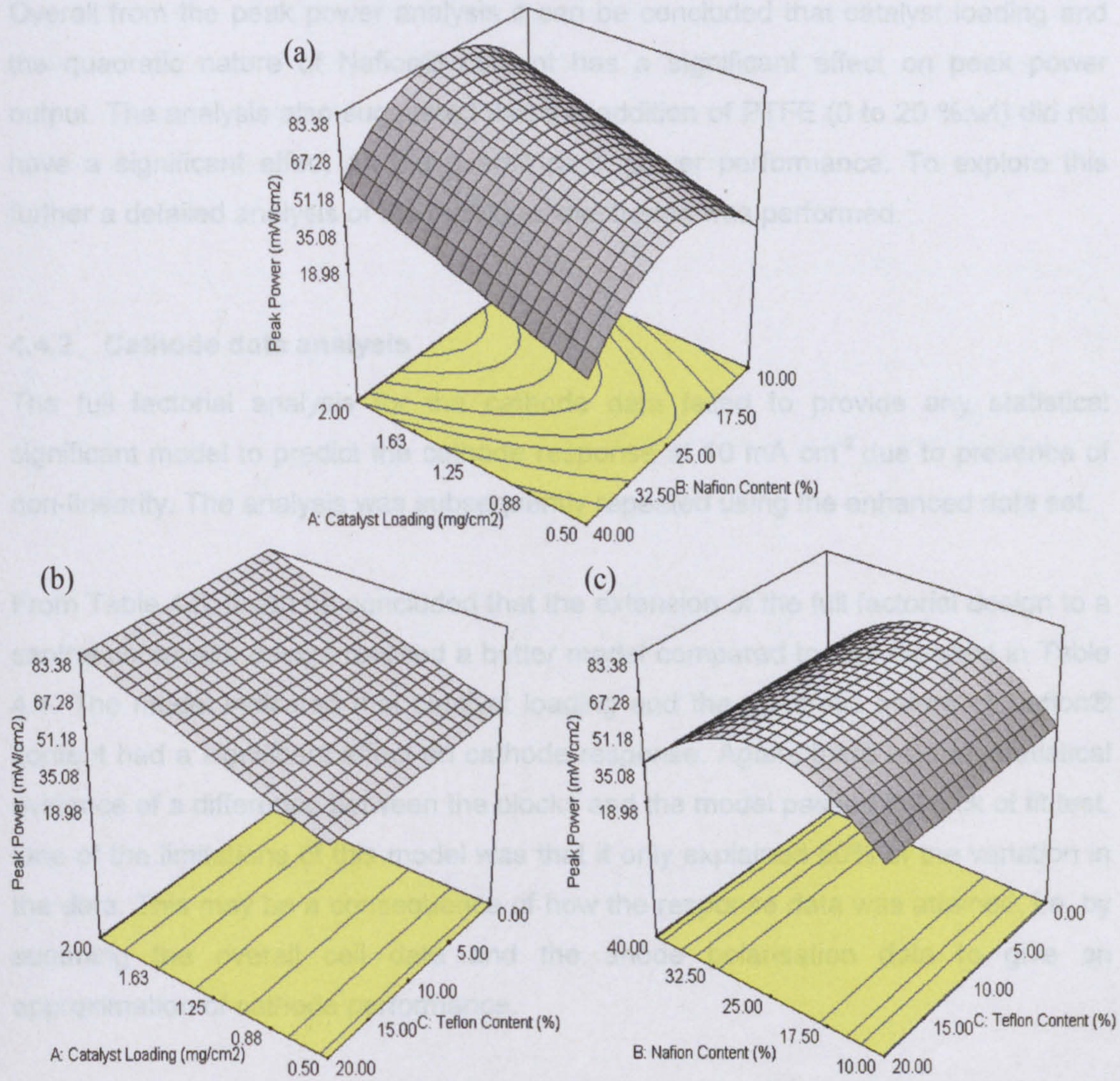

Figure 4.11: 3D contour plots for peak power response. (a) Catalyst loading vs. Nafion® content plot showing optimum Nafion® content, (b) Catalyst loading vs. PTFE and (c) Nafion® content vs. PTFE content

This conclusion is aligned with the literature where a high Nafion® content can cause greater mass transport problems across the film covering the catalysts, restricting the access of methanol and oxygen, Similarly low Nafion® content can result in a poor network of Nafion® ionomer and low proton conduction in the catalyst layer and reduce performance [140]. The model also showed that the addition of PTFE did not have any noticeable effect on peak power performance. The loading of PTFE in this experiment was restricted to 20%.wt maximum and from Figures 4.11.b and 4.11.c, it can be observed that the addition of PTFE to both the anode and cathode catalyst formulation gave a similar response in terms of peak power for all levels of catalyst loading and Nafion® content.

Overall from the peak power analysis it can be concluded that catalyst loading and the quadratic nature of Nafion® content has a significant effect on peak power output. The analysis also suggested that the addition of PTFE (0 to 20 %.wt) did not have a significant effect on the overall peak power performance. To explore this further a detailed analysis of the individual electrodes was performed.

4.4.2 Cathode data analysis

The full factorial analysis for the cathode data failed to provide any statistical significant model to predict the cathode response at 10 mA cm^{-2} due to presence of non-linearity. The analysis was subsequently repeated using the enhanced data set.

From Table 4.8, it can be concluded that the extension of the full factorial design to a central composite design realised a better model compared to that reported in Table 4.4. The model indicated that catalyst loading and the quadratic nature of Nafion® content had a significant effect on cathode response. Again, there was no statistical evidence of a difference between the blocks and the model passed the lack of fit test. One of the limitations of this model was that it only explained 50% of the variation in the data. This may be a consequence of how the response data was attained, i.e. by summing the overall cell data and the anode polarisation data to give an approximation of cathode performance.

Response:Cathode Voltage at 10mA cm^{-2}
Hierarchical Terms Added after Manual Regression: B
Analysis of variance table [Partial sum of squares]

Source	Sum of Squares	DF	Mean Square	F Value	Prob > F	Comment
Block	1.64E-03	1	1.64E-03	1.50		
Model	2.27E-02	3	7.56E-03	6.90	0.0039	...Significant
A	1.08E-02	1	1.08E-02	9.87	0.0067	...Significant
B	6.72E-04	1	6.72E-04	0.61	0.4457	..added due to hlerachy
B2	1.12E-02	1	1.12E-02	10.21	0.0060	...Significant
Residual	1.64E-02	15	1.10E-03			
Lack of Fit	1.49E-02	11	1.35E-03	3.42	0.1229	...Not significant
Pure Error	1.58E-03	4	3.95E-04			
Cor Total	4.08E-02	19				

Std. Dev.	0.03
Mean	0.80

R-Squared	0.58
Adj R-Squared	0.50

Final Equation in Terms of Coded Factors:
Cathode Voltage at 10mA cm^{-2} =+0.82 +0.033*A -8.2E-03*B -0.052*B^2
Final Equation in Terms of Actual Factors:
Cathode Voltage at 10mA cm^{-2} = +0.64 +0.04*A +0.01*B -2.3E-04*B^2

Table 4.8: ANOVA model for the cathode response at 10 mA cm^{-2} using CCD

To confirm the statistical validity of the CCD model, a residual analysis was performed. The normal probability plot, Figure 3.12.a, the residual versus predicted value, Figures 4.12.b, and residual versus run order plot, 4.12.c, showed that the residuals were normal and randomly distributed thus validating the fit of the model.

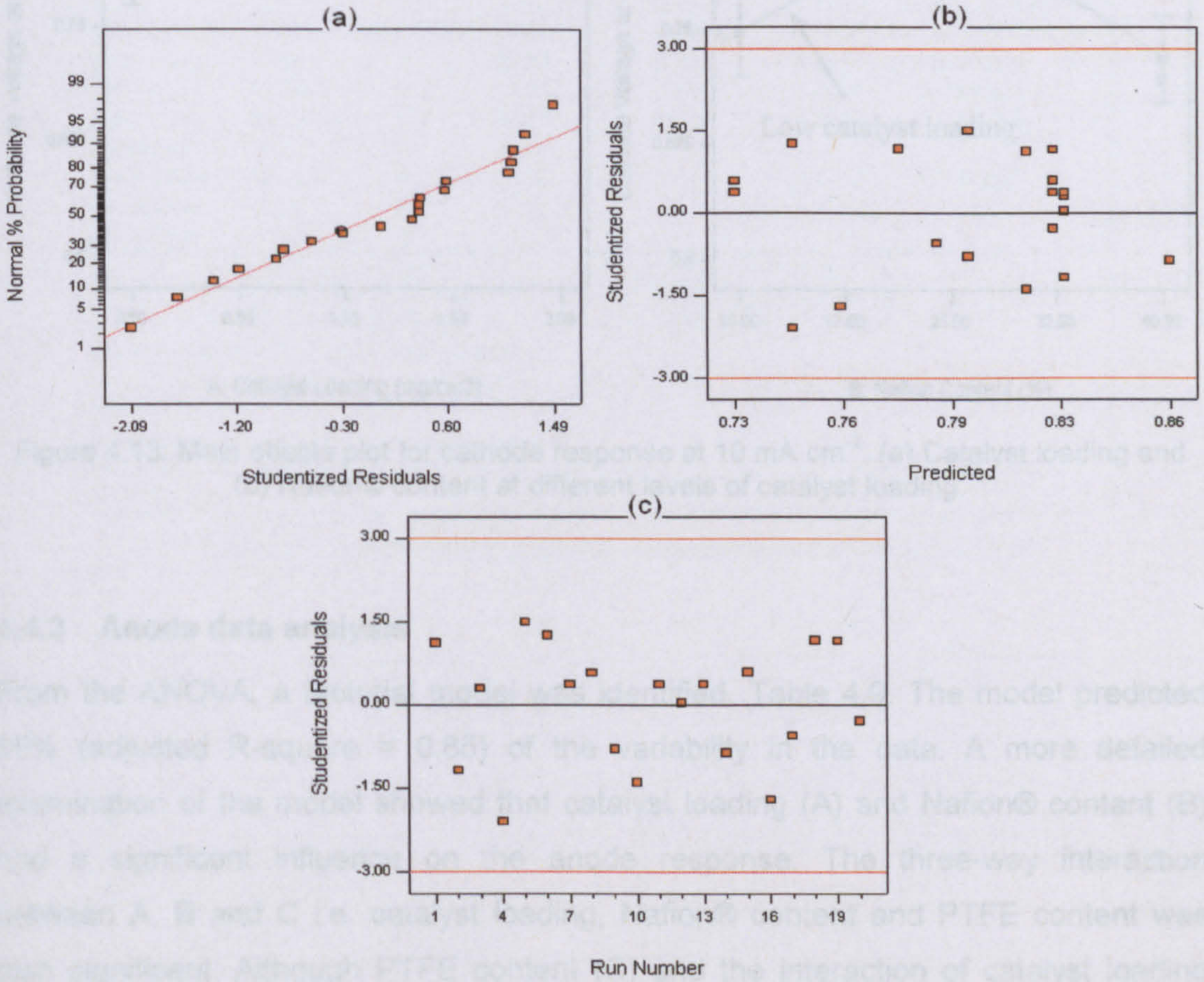

Figure 4.12: Residual analysis plot the cathode response CCD model (a) Normal probability plot of residuals, (b) Residual vs. predicted values and (c) Residual vs. experimental run order

The main effects plot for the catalyst loading, Figure 4.13, suggests that a high catalyst loading results in better cathode performance. A high catalyst loading increases the number of active Pt catalyst sites thereby improving the oxygen reduction kinetics which in turn increases cathode performance [6, 9, 19, 40]. Moreover the high catalyst loading also compensates for the mixed potential at the cathode caused by the methanol crossover phenomena and helps sustain cathode performance. The plot of Nafion® content and catalyst loading shows the quadratic nature of Nafion® content and suggests that to obtain a high cathode response at 10 mA cm^{-2}, a Nafion® content between 20 to 30 %.wt is beneficial. The dots at the centre of the main effects plot illustrate the high level of variation in the cathode response arising from the variation in MEA fabrication.

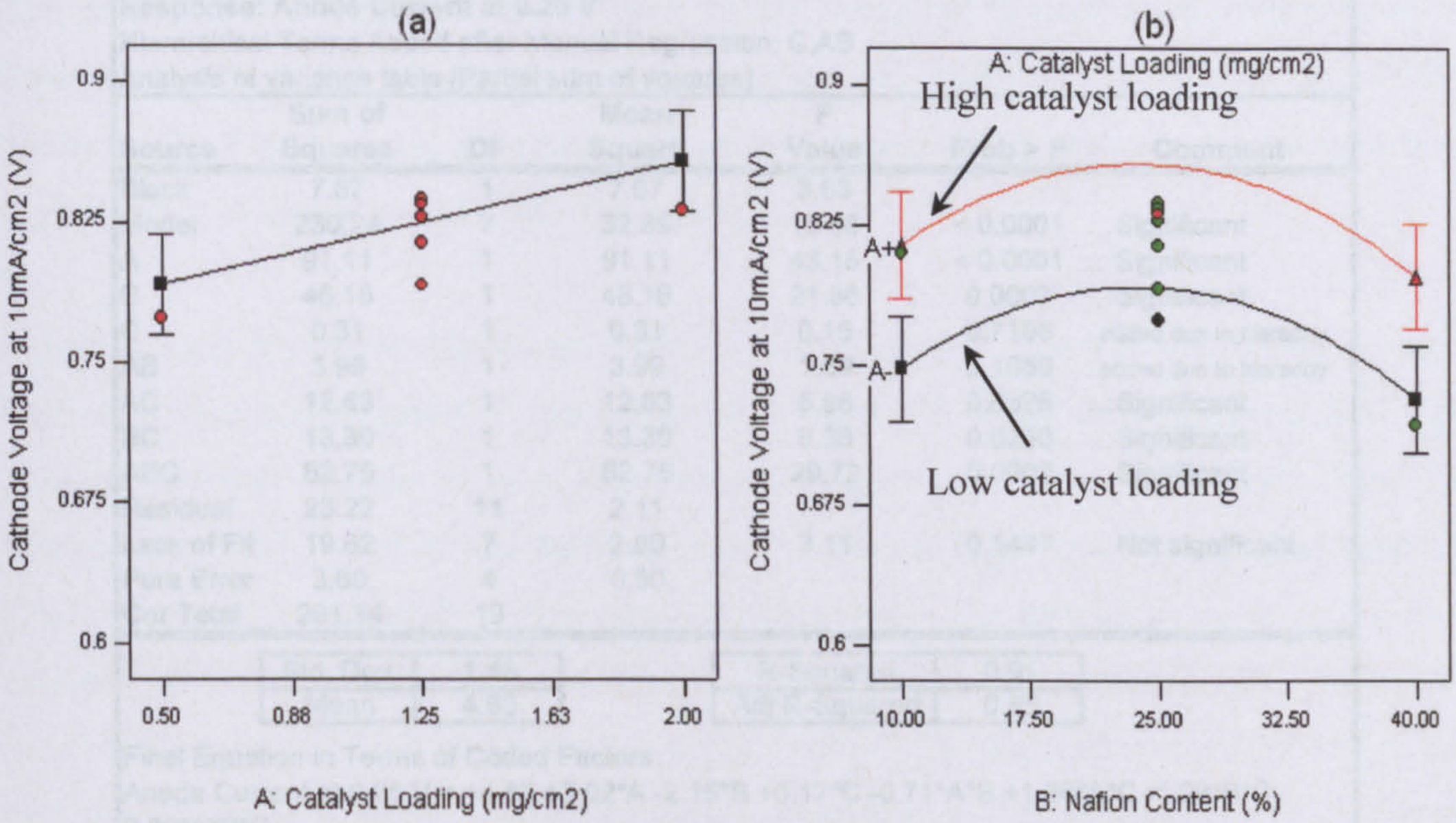

Figure 4.13: Main effects plot for cathode response at 10 mA cm^{-2}. (a) Catalyst loading and (b) Nafion® content at different levels of catalyst loading.

4.4.3 Anode data analysis

From the ANOVA, a factorial model was identified, Table 4.9. The model predicted 85% (adjusted R-square = 0.85) of the variability in the data. A more detailed examination of the model showed that catalyst loading (A) and Nafion® content (B) had a significant influence on the anode response. The three-way interaction between A, B and C i.e. catalyst loading, Nafion® content and PTFE content was also significant. Although PTFE content (C) and the interaction of catalyst loading with Nafion® content were not significant, they were included to maintain the hierarchical structure. These results and the overall anode model align with the full factorial model in Table 4.5.

To statistically validate the model, a residual analysis was performed. The normal probability plot of residuals in Figure 4.14.a showed that the residuals were normally distributed. The residual versus predicted value plot and residual versus run order plot, Figures 4.14.b and 4.14.c, indicated that the residuals were randomly distributed. On the basis of these plots it can be concluded the model in Table 4.9 was good fit.

Response: Anode Current at 0.25 V
Hierarchical Terms Added after Manual Regression: C,AB
Analysis of variance table [Partial sum of squares]

Source	Sum of Squares	DF	Mean Square	F Value	Prob > F	Comment
Block	7.67	1	7.67	3.63		
Model	230.24	7	32.89	15.58	< 0.0001	...Significant
A	91.11	1	91.11	43.15	< 0.0001	...Significant
B	46.16	1	46.16	21.86	0.0007	...Significant
C	0.31	1	0.31	0.15	0.7106	..added due to hierachy
AB	3.99	1	3.99	1.89	0.1966	..added due to hierachy
AC	12.63	1	12.63	5.98	0.0325	...Significant
BC	13.30	1	13.30	6.30	0.0290	...Significant
ABC	62.75	1	62.75	29.72	0.0002	...Significant
Residual	23.22	11	2.11			
Lack of Fit	19.62	7	2.80	3.11	0.1447	...Not significant
Pure Error	3.60	4	0.90			
Cor Total	261.14	19				

Std. Dev.	1.45
Mean	4.68

R-Squared	0.91
Adj R-Squared	0.85

Final Equation in Terms of Coded Factors:
Anode Current at 0.25 V = +4.55 +3.02*A -2.15*B +0.17*C -0.71*A*B +1.26*A*C -1.29*B*C -2.80*A*B*C
Final Equation in Terms of Actual Factors:
Anode Current at 0.25 V = +8.69 -2.31*A -0.29*B -0.76*C +0.19*A*B +0.79*A*C +0.02*B*C -0.02*A*B*C

Table 4.9: ANOVA for the anode response at 0.25 V using CCD

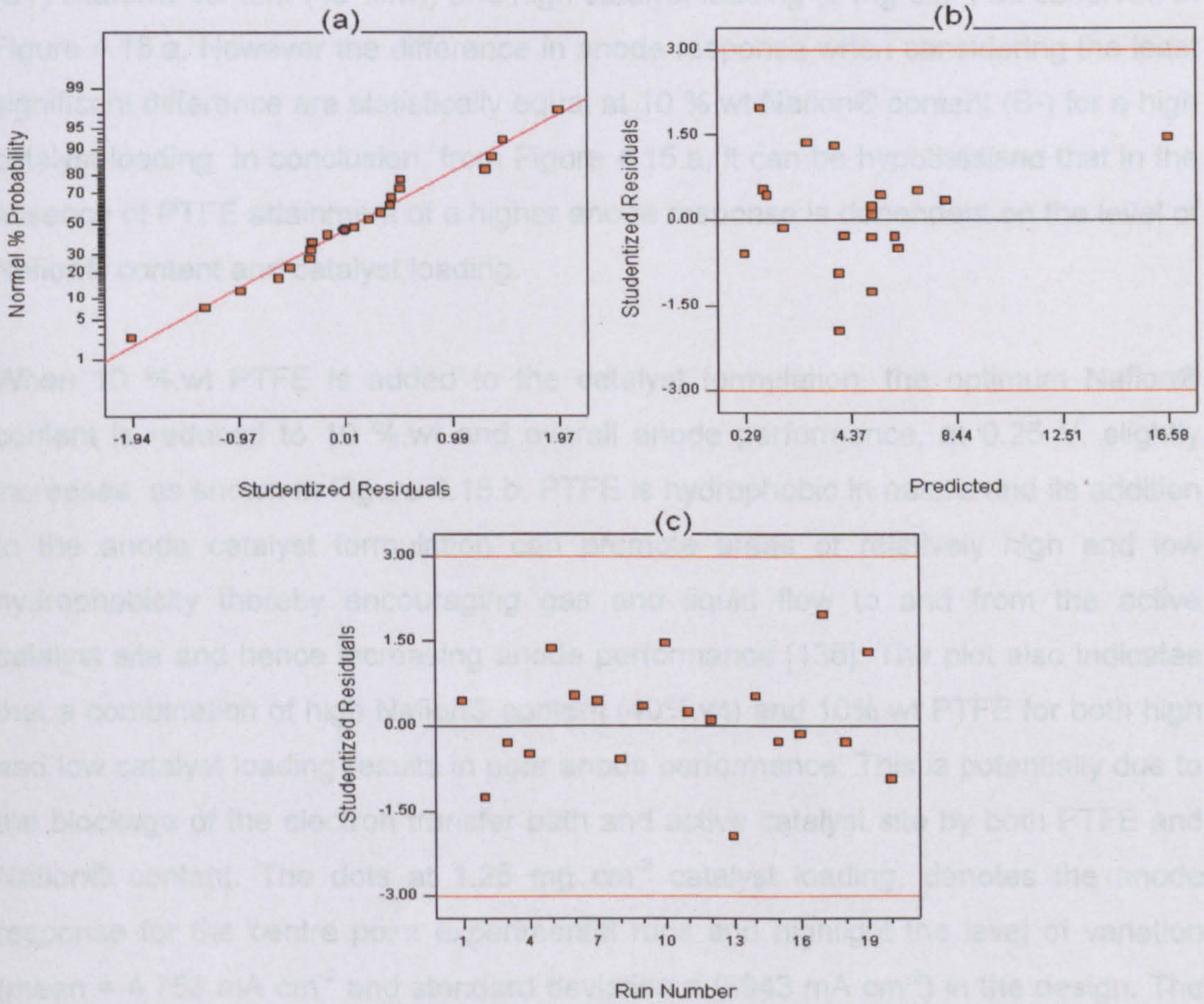

Figure 4.14: Residual analysis plot for the CCD anode model (a) Normal probability plot of residuals, (b) Residual vs. predicted values and (c) Residual vs. experimental run order

The influence of various factors on the anode response is explained on the basis of three-factor interaction between catalyst loading (A), Nafion® content (B) and PTFE content (C), Figure 4.15, as focussing on the main effect plots in the presence of higher order interactions can be misleading.

Figure 4.15.a, indicates that when PTFE is not present (0 %.wt) in the anode catalyst formation, the combination of low Nafion® content (10 %.wt) with both low and high catalyst loading results in a similar anode response. This is evident from the overlapping LSD I-bar of low Nafion® content (B-) at high and low catalyst loading. The presence of Nafion® in the catalyst layer aids the formation of a continuous network for proton conductivity resulting in higher anode performance [132, 140-142]. From the analysis of the experiments a combination of low Nafion content (10 %.wt) and low catalyst loading (0.5 mg cm^{-2}) resulted in an adequate proton network. However as the level of catalyst loading is increased to 2 mg cm^{-2}, anode performance decreases (Figure 4.15.a) due to insufficient Nafion® to form a continuous proton network. This effect is reduced through the contribution of high (B+) Nafion® content (40 %.wt) and high catalyst loading (2 mg cm^{-2}) as observed in Figure 4.15.a. However the difference in anode response when considering the least significant difference are statistically equal at 10 %.wt Nafion® content (B-) for a high catalyst loading. In conclusion, from Figure 4.15.a, it can be hypothesised that in the absence of PTFE attainment of a higher anode response is dependent on the level of Nafion® content and catalyst loading.

When 10 %.wt PTFE is added to the catalyst formulation, the optimum Nafion® content is reduced to 10 %.wt and overall anode performance, at 0.25 V, slightly increases, as shown in Figure 4.15.b. PTFE is hydrophobic in nature and its addition to the anode catalyst formulation can promote areas of relatively high and low hydrophobicity thereby encouraging gas and liquid flow to and from the active catalyst site and hence increasing anode performance [136]. The plot also indicates that a combination of high Nafion® content (40%.wt) and 10%.wt PTFE for both high and low catalyst loading results in poor anode performance. This is potentially due to the blockage of the electron transfer path and active catalyst site by both PTFE and Nafion® content. The dots at 1.25 mg cm^{-2} catalyst loading, denotes the anode response for the centre point experimental runs and highlight the level of variation (mean = 4.753 mA cm^{-2} and standard deviation = 0.943 mA cm^{-2}) in the design. The

ANOVA model in Table 4.9 takes account of this variation when modelling the anode response.

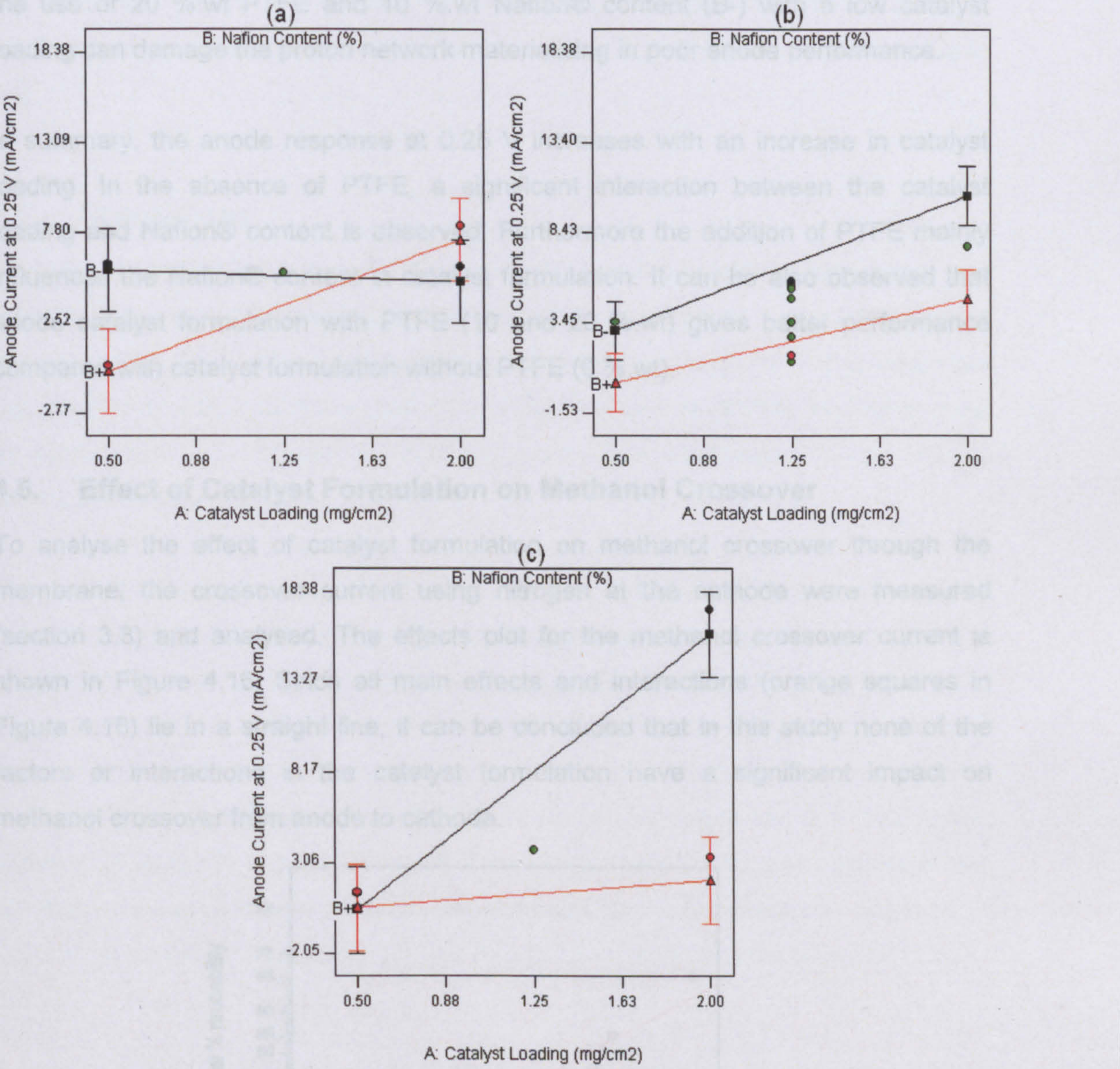

Figure 4.15: Three factor interaction plot for the anode response. Interaction of catalyst loading with Nafion® content at (a) 0 %.wt PTFE, (b) 10 %.wt PTFE and (c) 20 %.wt PTFE

When a high level of PTFE (20%.wt) is added to the anode catalyst formulation, the optimum Nafion® content of 10% (B-), with a combination of high catalyst loading (2 mg cm^{-2}), results in highest anode response (Figure 4.15.c). The increase in the addition of PTFE increases the size of hydrophobic pores forming a continuous channel in the catalyst layer. These channels provide additional room for carbon dioxide gas evolved during the reaction to leave the anode catalyst site, improving the mass transfer within the electrode and thereby increasing the anode response

[136]. From the three factor interaction, the use of low catalyst loading (0.5 mg cm^{-2}) with high PTFE (20 %.wt) and high (B+) Nafion® content (40 %.wt) appears to result in the active catalyst site being blocked and resulting in poor performance. Similarly the use of 20 %.wt PTFE and 10 %.wt Nafion® content (B-) with a low catalyst loading can damage the proton network materialising in poor anode performance.

In summary, the anode response at 0.25 V increases with an increase in catalyst loading. In the absence of PTFE, a significant interaction between the catalyst loading and Nafion® content is observed. Furthermore the addition of PTFE mainly influences the Nafion® content in catalyst formulation. It can be also observed that anode catalyst formulation with PTFE (10 and 20 %.wt) gives better performance compared with catalyst formulation without PTFE (0 %.wt).

4.5. Effect of Catalyst Formulation on Methanol Crossover

To analyse the effect of catalyst formulation on methanol crossover through the membrane, the crossover current using nitrogen at the cathode were measured (section 3.3) and analysed. The effects plot for the methanol crossover current is shown in Figure 4.16. Since all main effects and interactions (orange squares in Figure 4.16) lie in a straight line, it can be concluded that in this study none of the factors or interactions in the catalyst formulation have a significant impact on methanol crossover from anode to cathode.

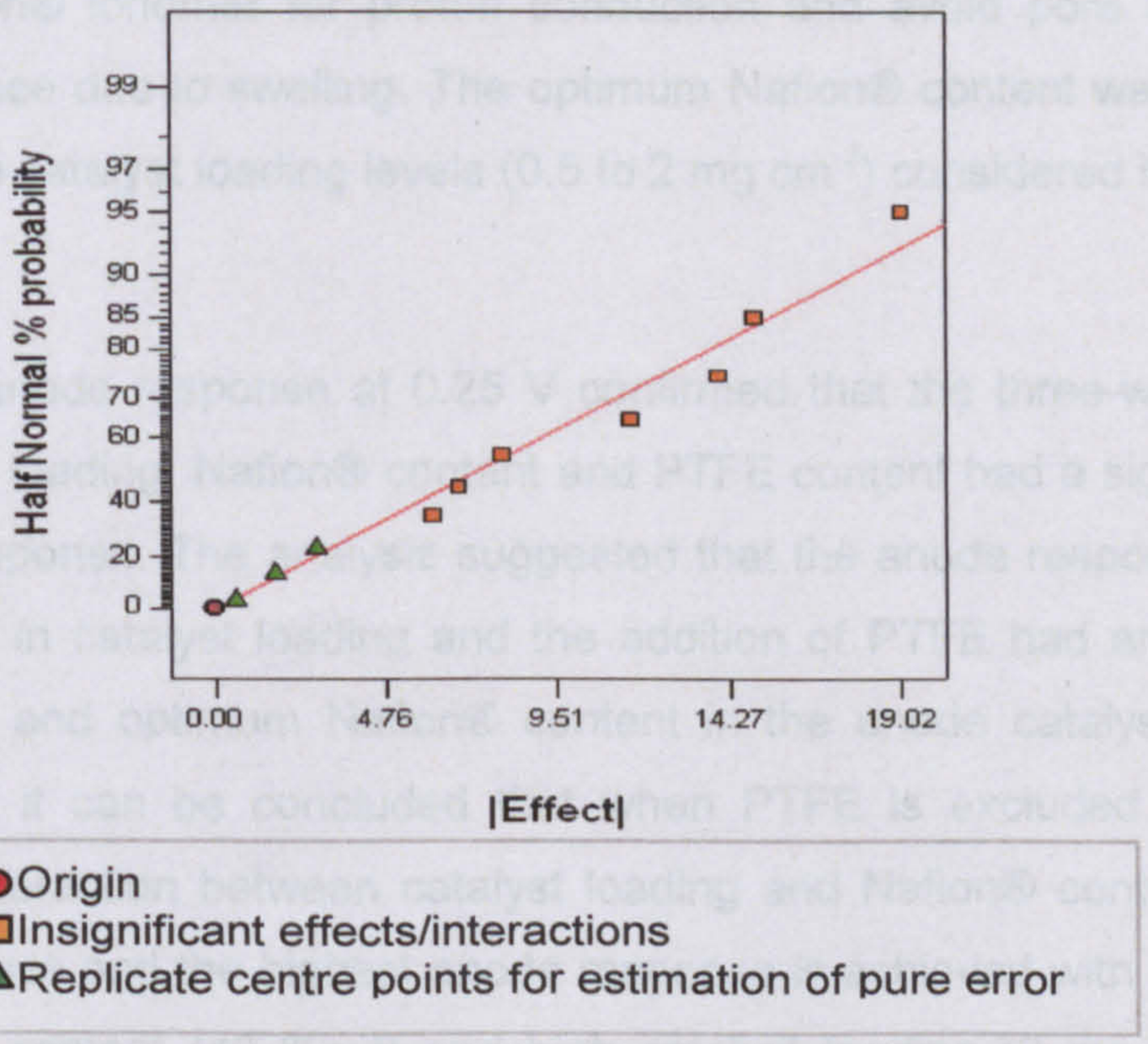

Figure 4.16: Half normal probability plot for identifying effects and interactions affecting the methanol crossover response.

As observed in Chapter 2, the methanol crossover through the membrane was mainly influenced by the concentration of methanol, cell temperature and their two-factor interaction. In this study the operating parameters methanol concentration and cell temperature were held constant at 1 M and 90 °C respectively. This resulted in an almost constant crossover rate for all the experimental runs summarised in Table 4.2.

4.6. Conclusions

An initial analysis of a full factorial design with four centre points for peak power and cathode data revealed that there was curvature in at least one of the factors considered in the design. Additionally a full factorial study for the anode data suggested that additional experimental runs were needed to validate the higher order interaction model. To address these issues the full factorial design was increased to a central composite design.

The central composite design for the peak power and cathode data at 10 mA cm^{-2} response suggested that high catalyst loading had a significant effect on both the responses. The responses increased with an increase in catalyst loading from 0.5 to 2 mg cm^{-2}. Both models also identified that the non-linear behaviour of Nafion® content was significant. The models suggested that an optimum level of Nafion® content was needed for effective utilisation of the catalyst which can provide a proper network of Nafion® ionomer for proton conduction and avoid pore blockage and electrical resistance due to swelling. The optimum Nafion® content was between 20 to 30 %.wt for the catalyst loading levels (0.5 to 2 mg cm^{-2}) considered in the design.

Analysis of the anode response at 0.25 V confirmed that the three-way interaction between catalyst loading, Nafion® content and PTFE content had a significant effect on the anode response. The analysis suggested that the anode response increased with an increase in catalyst loading and the addition of PTFE had an influence on anode response and optimum Nafion® content in the anode catalyst formulation. From the model it can be concluded that when PTFE is excluded from catalyst formation, the interaction between catalyst loading and Nafion® content influences the anode response and the highest anode response is achieved with a combination of high Nafion® content (40 %.wt) and high catalyst loading (2 mg cm^{-2}). On the contrary, with the addition of PTFE (10 and 20 %.wt) the optimal Nafion® content

changed to 10 %.wt and resulted in better anode performance for both high and low catalyst loading compared to catalyst formulation without PTFE.

In this study, the experimental runs needed for the CCD were separately blocked to take account of the variability due to factors such as experimenter performance and raw material. Analysis of blocks for all responses in the central composite design suggested that there was no significant difference between the blocks.

In conclusion, the application of response surface methodology helped in understanding the critical interactions and non-linearity present in the design. Additionally, the design of experiment technique took account of the variability associated with the experiment and identified statistically significant models. The overall cell, anode and cathode data analysis revealed that catalyst loading is a critical factor which affects the cell and individual electrode response. To further understand the effect of this critical parameter on DMFC catalyst formulation, comprehensive knowledge of the methanol oxidation mechanism and the oxygen reduction mechanism at the anode and cathode respectively is needed. This is addressed in the subsequent chapters through the application of semi-empirical modelling techniques for both anode and cathode of the DMFC.

Chapter 5
KINETIC MODELS FOR THE ANODE BASED ON SURFACE COVERAGE

5.1. Introduction

The relatively slow rate of anodic methanol oxidation is one of the limitations presently hindering the widespread application of the DMFC [5, 6, 8, 40, 143]. Consequently to optimise DMFC performance, a clear understanding of the rate limiting reaction and methanol oxidation reaction mechanism on platinum or its alloys is required. Understanding the reaction mechanism will help to generate better catalysts. Additionally, understanding the limiting reaction step will help determine the control strategy thereby improving the overall DMFC performance. One approach may be by periodically removing the adsorbed reaction intermediate species [6, 120, 143]. Based on the pioneering work of Bagotzky et al., (1977) [144] a number of mechanisms have been proposed to describe the methanol oxidation process. At present Pt-Ru alloy is considered to be the state-of-the-art candidate for practical anode catalysis in the DMFC and the common consensus is that the electro-oxidation of methanol on Pt-Ru occurs via a dual site mechanism [18, 43-45, 120, 143, 145]. Despite this significant advancement, only a limited number of kinetic models have been reported to describe the rate limiting process and to predict anode fuel cell polarisation behaviour [81, 99-101, 104].

In this chapter, kinetic models for the DMFC anode are proposed with the aim of developing kinetic equations based on the reaction mechanism which returns the rate determining reaction step. In this chapter, two detailed kinetic models based on surface coverage, described by a dual site mechanism, are proposed [37, 38]. The kinetic models are temperature dependent and effectively describe the surface coverage of all the intermediate species involved in the methanol oxidation reaction in addition to identifying the rate limiting step. An analysis of the detailed surface coverage models indicated that the anode model can be simplified by not taking into account some of the kinetic parameters included in the initial kinetic models. Based on this approach, a simplified model derived from the similar reaction mechanism that returns current density is consequently proposed [38]. Simulations of the surface

coverage for different species and anode performance from the proposed dual site kinetic equations are also developed for high methanol concentrations. The models were developed using the graphical programming language, LabVIEW [115] and validated using experimental data generated using a conventional porous anode for various methanol concentrations (0.5, 1 and 2 M) and temperatures (30, 60 and 90 °C) [31].

5.2. Oxidation of Methanol at the Anode

Several schemes have been proposed for the oxidation of methanol at the anode [6, 29, 43, 47, 125, 145, 146]. The basic mechanism for methanol oxidation can be summarised in terms of two functionalities; the electrosorption of methanol onto the substrate and the subsequent addition of oxygen to the adsorbed carbon-containing intermediates to generate carbon dioxide. In practice, only a few electrode materials are capable of adsorbing methanol. In acidic media, only platinum (Pt) and platinum-based catalysts have been found to exhibit reasonable activity, and hence the majority of mechanistic studies have concentrated on these materials [47, 48, 125, 147-149]. With respect to Pt, the adsorption of methanol is believed to take place through a series of steps that follow a six electron donation process [29]. The first step is the dissociative chemisorption of methanol onto the Pt surface. This involves the successive donation of electrons (e^-) to the Pt catalyst according to the following reaction steps:

$$Pt + CH_3OH \rightarrow Pt - CH_2OH + H^+ + e^- \quad \ldots 5.1$$

$$Pt - CH_2OH \rightarrow Pt_2 - CHOH + H^+ + e^- \quad \ldots 5.2$$

$$Pt_2 - CHOH \rightarrow Pt_3 - COH + H^+ + e^- \quad \ldots 5.3$$

A surface rearrangement of the methanol oxidation intermediates (*Pt_3-COH*) from the dissociative chemisorption of methanol on Pt generates carbon monoxide (*CO*) that is linearly or bridge-bonded to the Pt-sites:

$$Pt_3 - COH \rightarrow Pt - CO + 2Pt + H^+ + e^- \quad \ldots 5.4$$

When pure Pt catalyst is used, without a promoting element, the water discharge occurs at high anodic overpotentials (~0.9 V versus reference hydrogen electrode (RHE) [19]) with the formation of *Pt-OH* species, at the platinum surface:

$$Pt + H_2O \rightarrow Pt - OH + H^+ + e^- \quad \ldots 5.5$$

The final step, on Pt sites, is the reaction of *Pt-OH* groups with neighbouring methanolic residues (*Pt-CO*) generated from reaction 5.4 to give carbon dioxide:

$$Pt-OH+Pt-CO \rightarrow 2Pt+CO_2+H^+ +e^- \quad \ldots 5.6$$

Thus as shown in Figure 5.1, on the pure Pt surface, at low potentials, –CO groups are adsorbed while at high potentials, chemisorption of –OH groups takes place during the electro-oxidation of methanol with both processes being distinct. Due to this, Pt alone is not sufficiently active and thus there is a need for a promoter that effectively provides oxygen in some active form to achieve facile oxidation of the chemisorbed CO on Pt.

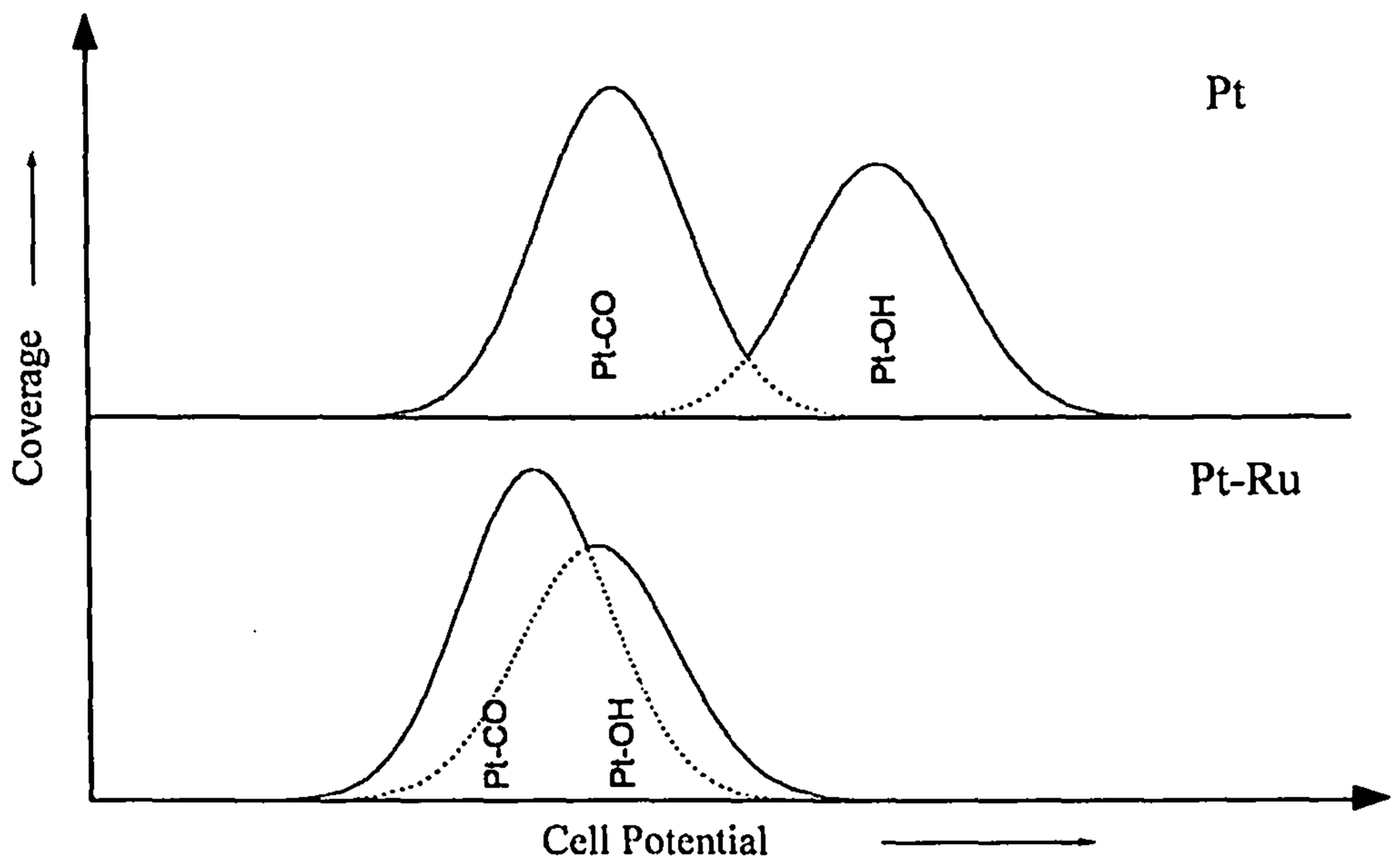

Figure 5.1: Function of binary Pt-Ru catalyst for methanol oxidation

In the literature, a number of approaches for Pt promotion have been proposed [43, 48, 119, 149]. One approach that has been shown to be effective is through the use of alloys of Pt with different metals such as ruthenium (Ru), osmium (Os) or tin (Sn). In these cases, the second metal forms a surface oxide in the potential range for methanol oxidation to occur. Of the various methanol oxidation catalysts Pt-Ru and Pt-Sn have been the most widely studied [9, 19, 143, 146, 148, 149]. It has been shown that the alloying of Sn and Ru with Pt gives rise to electrocatalysts, which promote the oxidation of methanol and related methanolic species. Thus on a Pt-Ru alloy, as shown in Figure 5.1, due to the addition of Ru, water discharge occurs on Ru-sites at much lower potentials (~0.3 V versus RHE [19]) compared to the pure Pt catalyst (reaction 5.5):

$$Ru + H_2O \rightarrow Ru - OH + H^+ + e^- \quad \ldots 5.7$$

The final step on the Ru site in a Pt-Ru alloy is the reaction of the Ru-OH groups with the neighbouring methanolic residues (*Pt-CO*), generated in reaction 5.4:

$$Ru - OH + Pt - CO \rightarrow Ru + Pt + CO_2 + H^+ + e^- \quad \ldots 5.8$$

Overall, for the dual site Pt-Ru catalyst, Figure 5.1, Ru acts as a promoter for methanol oxidation consequently the chemisorption of the –OH groups shifts to lower potentials and overlaps with the region where the –CO groups are adsorbed on the catalyst, thereby facilitating effective oxidation of methanol on Pt-Ru alloy compared to pure Pt.

5.3. Experimental Setup

The experimental data used for validating the models, developed in the subsequent sections was attained from a porous anode type of direct methanol fuel cell [31]. The methodology for the detailed preparation of the membrane electrode assembly is similar to that described in sections 3.3. Anode data were collected using the cathode as a pseudo reference electrode, by feeding 5 %.vol hydrogen in nitrogen stream and polarising the cell between OCP and 700 mV using liquid methanol as the fuel at the anode side. Conditions of temperature and concentration were varied between 30 and 90 °C and, 0.5 and 2 M respectively, and the system was given approximately 2 hours to equilibrate before testing. All experiments were carried out under galvanostatic conditions, i.e. the electrical cell current was fixed and defined as the input variable with the resulting cell voltage being measured and defining the output variable [31].

5.4. Model Formulation

State-of-the-art DMFC applications have reported the use of the Pt-Ru catalyst [6, 9, 19, 143]. It is evident from section 5.2 that the electrochemical oxidation of aqueous methanol is a complex multi-step reaction based on the dual site mechanism. Recent studies have validated the dual site concept using in-situ FTIR spectroscopy and electrochemical mass spectrometry [45, 148, 150]. Thus in this work, a kinetic model

utilising a dual site mechanism of methanol oxidation on Pt-Ru catalyst using the Gasteiger et al., (1994) [119] approach is proposed. The basic steps are:

$$CH_3OH \underset{k_1'}{\overset{k_1}{\longleftrightarrow}} CH_3OH_{ads} \quad \text{... 5.9}$$

$$CH_3OH_{ads} \xrightarrow{k_2} CO_{ads} + 4H^+ + 4e^- \quad \text{... 5.10}$$

$$H_2O \underset{k_{3,1}'}{\overset{k_{3,1}}{\longleftrightarrow}} OH_{ads,Pt} + H^+ + e^- \quad \text{... 5.11}$$

$$H_2O \underset{k_{3,2}'}{\overset{k_{3,2}}{\longleftrightarrow}} OH_{ads,Ru} + H^+ + e^- \quad \text{... 5.12}$$

$$CO_{ads} + (OH_{ads,Pt} + OH_{ads,Ru}) \underset{k_{4,2}}{\overset{k_{4,1}}{\rightarrow}} CO_2 + H^+ + e^- \quad \text{... 5.13}$$

By using the dual site mechanism, it is assumed that reactions 5.9 to 5.11 occur primarily on the Pt site and reaction 5.12 on the Ru site. The dissociative chemisorption of methanol on Pt involves the transfer of four electrons, as observed in reactions 5.1 to 5.4. However in the above simplified reaction mechanism, the dissociative chemisorption of methanol on Pt is combined in one irreversible reaction 5.9. The water discharge reaction 5.11 and 5.12 occurs on both, the Pt and Ru catalyst sites. Finally the surface reaction, 5.13, is believed to occur on both the Pt and Ru sites depending on the hydroxyl ion.

For the kinetic model, the surface coverage of the different species (θ_M, θ_{CO}, $\theta_{OH,Pt}$ and $\theta_{OH,Ru}$) involved in the above reaction steps is of importance. Using the steady state approximation model [151], the rate of change of the surface coverage of the different intermediate species (θ_i) on both catalyst sites for reactions 5.9 to 5.13 can be derived as follows:

$$\Gamma \frac{d\theta_M}{dt} = k_1 C_M (1 - \theta_{OH,Pt} - \theta_{CO} - \theta_M) - k_1' \theta_M - k_2 \theta_M e^{(\frac{\alpha_2 FE}{RT})} \quad \text{... 5.14}$$

$$\Gamma \frac{d\theta_{CO}}{dt} = k_2 \theta_M e^{(\frac{\alpha_2 FE}{RT})} - k_{4,1} \theta_{OH,Pt} \theta_{CO} e^{(\frac{(1-\beta_4)FE}{RT})} - k_{4,2} \theta_{OH,Ru} \theta_{CO} e^{(\frac{(1-\beta_4)FE}{RT})} \quad \text{.... 5.15}$$

$$\Gamma \frac{d\theta_{OH,Pt}}{dt} = k_{3,1} a_{H_2O} (1 - \theta_{OH,Pt} - \theta_{CO} - \theta_M) e^{(\frac{(1-\beta_3)FE}{RT})} - k_{3,1}' \theta_{OH,Pt} e^{(\frac{(-\beta_3)FE}{RT})} - k_{4,1} \theta_{OH,Pt} \theta_{CO} e^{(\frac{(1-\beta_4)FE}{RT})}$$

.... 5.16

$$\Gamma \frac{d\theta_{OH,Ru}}{dt} = k_{3,2} a_{H_2O} (1 - \theta_{OH,Ru}) e^{(\frac{(1-\beta_3)FE}{RT})} - k_{3,2}' \theta_{OH,Ru} e^{(\frac{(-\beta_3)FE}{RT})} - k_{4,2} \theta_{OH,Ru} \theta_{CO} e^{(\frac{(1-\beta_4)FE}{RT})} \quad \text{... 5.17}$$

where, Γ is site density (mol m^{-2}), a_{H_2O} is activity of water, θ_M, θ_{CO}, $\theta_{OH,Pt}$ and $\theta_{OH,Ru}$ are the surface coverage of methanol, carbon monoxide, hydroxyl ion on the Pt site and the hydroxyl ion on the Ru site respectively. C_M is the concentration of methanol (M), F is Faradays constant (96487 As mol^{-1}), E is cell potential (V), R is gas constant (8.314 J mol^{-1} K^{-1}), T is cell temperature (K) and k_i, α_i and β_i are the reaction rate constants, electrochemical transfer coefficient and transfer coefficient for kinetic equation (i) respectively.

The overall rate of anodic reaction (r_4) for the surface reaction 5.13 can be described by:

$$r_4 = k_{4,1}\theta_{OH,Pt}\theta_{CO}e^{(\frac{(1-\beta_4)FE}{RT})} + k_{4,2}\theta_{OH,Ru}\theta_{CO}e^{(\frac{(1-\beta_4)FE}{RT})} \quad \text{.... 5.18}$$

This overall rate of reaction is also related to the cell current density (j) through Faraday's law:

$$r_4 = \frac{j}{nF} \quad \text{.... 5.19}$$

where, j is the cell current density (A m^{-2}) and n is number of electrons transferred in the methanol oxidation reaction.

Substituting Eq. 5.18 into Eq. 5.19:

$$\therefore j = n*F*r_4 = n*F*\left(k_{4,1}\theta_{OH,Pt}\theta_{CO}e^{(\frac{(1-\beta_4)FE}{RT})} + k_{4,2}\theta_{OH,Ru}\theta_{CO}e^{(\frac{(1-\beta_4)FE}{RT})}\right) \quad \text{.... 5.20}$$

From the above equation it can be observed that the anode current density (j) depends on the surface coverage of hydroxyl ions on both the Pt and Ru sites ($\theta_{OH,Pt}$ and $\theta_{OH,Ru}$). On the Pt catalyst sites, depending on the reaction mechanism and cell potential, the adsorption of hydroxyl ions ($\theta_{OH,Pt}$) may be small or almost equal to that of the Ru sites ($\theta_{OH,Ru}$). This theory leads to two important categories of model formulation, described in the subsequent sections by Case A (where adsorption of $\theta_{OH,Pt}$ is considered to be negligible compared to that of $\theta_{OH,Ru}$) and Case B (where adsorption of $\theta_{OH,Pt}$ was considered to be the same as that of $\theta_{OH,Ru}$).

5.4.1 Case A

In this model, it is assumed that the water discharge reaction mainly occurs on the Ru catalyst site. Due to this, the surface coverage of the hydroxyl ion on the Pt sites is much less than on the Ru sites (i.e. $\theta_{OH,Pt} << \theta_{OH,Ru}$) and hence can be neglected ($\theta_{OH,Pt} = 0$). The steady state surface coverage Eq. 5.14 - 5.17, in this case assuming the activity of water is unity, i.e. $a_{H_2O} = 1$, simplify to give:

$$\theta_{CO} = 1 - \theta_M - \left(\frac{k_1' \theta_M}{k_1 C_M}\right) - \left(\frac{k_2 \theta_M e^{(\frac{\alpha_2 FE}{RT})}}{k_1 C_M}\right) \quad \text{.... 5.21}$$

$$\theta_{CO} = \frac{k_2 \theta_M e^{(\frac{\alpha_2 FE}{RT})}}{k_{4,2} \theta_{OH,Ru} e^{(\frac{(1-\beta_4) FE}{RT})}} \quad \text{.... 5.22}$$

$$\theta_{CO} = \frac{k_{3,2} e^{(\frac{(1-\beta_3) FE}{RT})} - k_{3,2} \theta_{OH,Ru} e^{(\frac{(1-\beta_3) FE}{RT})} - k_{3,2}' \theta_{OH,Ru} e^{(\frac{(-\beta_3) FE}{RT})}}{k_{4,2} \theta_{OH,Ru} e^{(\frac{(1-\beta_4) FE}{RT})}} \quad \text{... 5.23}$$

Eq. 5.21 to 5.23 can be resolved to give the surface coverage of $\theta_{OH,Ru}$ and θ_{CO}. By substituting these values and setting $\theta_{OH,Pt} = 0$, in to Eq. 5.20, the cell current density for varying cell potential can be modelled at various methanol concentration and cell temperature:

$$j = n \times F \times \left(\cancel{k_{4,1} \theta_{OH,Pt} \theta_{CO} e^{(\frac{(1-\beta_4) FE}{RT})}}^{\,0} + k_{4,2} \theta_{OH,Ru} \theta_{CO} e^{(\frac{(1-\beta_4) FE}{RT})} \right) \quad \text{... 5.24}$$

$$\therefore j = n \times F \times k_{4,2} \theta_{OH,Ru} \theta_{CO} e^{(\frac{(1-\beta_4) FE}{RT})} \quad \text{... 5.25}$$

5.4.2 Analysis of the Case A Model

Figure 5.2 shows the fit of the model (Eq. 5.25) to the experimental data for various methanol concentrations (0.5, 1 and 2 M) and temperatures (30, 60 and 90 °C) for a conventional porous carbon supported anode. From Figures 5.2.a, 5.2.b and 5.2.c, it can be observed that the anode polarisation experimental data show a strong dependence on cell potential, cell temperature and methanol concentration. This dependence on anode polarisation is captured by the model, since the model and the surface coverage, as seen in equation 5.21 to 5.25, depend on the cell temperature (T), cell potential (E) and methanol concentration (C_M). The transfer coefficients and electrochemical transfer coefficient for the model are taken as, $\beta_3 = \beta_4 = 0.5$, $\alpha_2 = 0.79$

respectively [100]. The remaining kinetic parameter values, obtained by fitting the model to the experimental data, are summarised in Table 5.1.

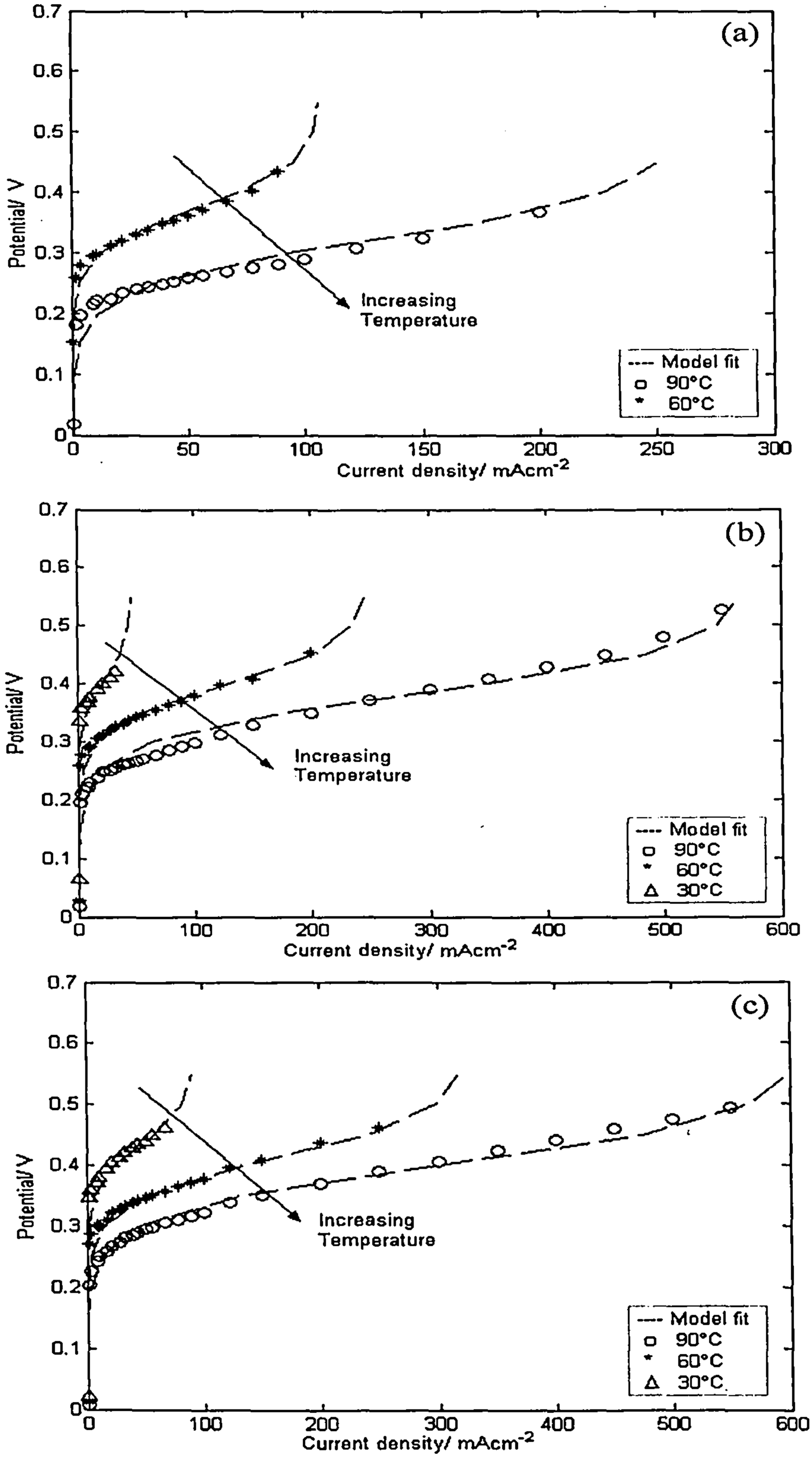

Figure 5.2: Model versus experimental fit for porous anode cell at various temperatures (30, 60 and 90 °C) and methanol concentrations (a) 0.5 M (data for 30 °C was not available [31]), (b) 1 M and (c) 2 M

Parameters	Fit at 30 °C	Fit at 60 °C	Fit at 90 °C
k_1	0.8 X 10^{-6} m s^{-1}	2.8 X 10^{-6} m s^{-1}	5.3 X 10^{-6} m s^{-1}
$k_1^{'}$	0.4 X 10^{-3} mol $m^{-2}s^{-1}$	1 .1X 10^{-3} mol $m^{-2}s^{-1}$	1 .9X 10^{-3} mol $m^{-2}s^{-1}$
k_2	0.3 X 10^{-8} mol $m^{-2}s^{-1}$	8 X 10^{-8} mol $m^{-2}s^{-1}$	4.9 X 10^{-7} mol $m^{-2}s^{-1}$
$k_{3,2}$	4 X 10^{-5} mol $m^{-2}s^{-1}$	4 X 10^{-5} mol $m^{-2}s^{-1}$	5 X 10^{-5} mol $m^{-2}s^{-1}$
$k_{3,2}^{'}$	2 X 10^{-5} mol $m^{-2}s^{-1}$	1.8 X 10^{-5} mol $m^{-2}s^{-1}$	1.8 X 10^{-5} mol $m^{-2}s^{-1}$
k_4	5.3 X 10^{-2} mol $m^{-2}s^{-1}$	5.3 X 10^{-2} mol $m^{-2}s^{-1}$	5.7 X 10^{-2} mol $m^{-2}s^{-1}$

Table 5.1: Kinetic parameters used in dual site Model A

The proposed dual site model is based on kinetics and it is essential that it fits the experimental data at the low current end of the polarisation, i.e. the activation region, where there are no mass transfer limitations and the system is dominated by kinetics [104]. Hence along with the anode polarisation curve in this work, the model was also fitted to the log of cell current density, i.e. the Tafel plot. Figures 5.3, shows the fit of the model for 0.5, 1 and 2 M methanol concentrations for different cell temperatures, 30, 60 and 90 °C. From Figure 5.3 it can be observed that the model fits the anode polarisation curve at the lower end, thus confirming reliable prediction of kinetic behaviour.

Further confirmation that the model captures the behaviour of the system is through examining the correlation of the kinetic currents of the predicted Tafel slope at one potential and three temperatures [29, 119]. The activation energy was derived from the Arrhenius relationship and used to assess whether the solution for the dual site catalyst lay within the range 30 - 70 kJ mol^{-1} [44, 119]. Figure 5.4 shows the Arrhenius plot of the correlation of the log of cell current density (*ln j*) at 0.4 V and the inverse of cell temperature (T^{-1}) for different methanol concentrations. The activation energy (E_a), estimated from the product of the gas constant (R) and the slope from the linear fit to the *ln j* vs. T^{-1} data as utilised in Figure 5.4, was in the range of 40 - 43 kJ mol^{-1}, which further validated the model fit.

The resulting surface coverage of the methanol and hydroxyl ions predicted from Model A for the porous anode cell is shown in Figure 5.5. From Figures 5.5.a, 5.5.b and 5.5.c, it can be observed that the surface coverage of methanol (θ_M) decreases with an increase in cell potential, whereas the surface coverage of hydroxyl ion on

ruthenium ($\theta_{OH,\,Ru}$) increases with an increase in cell potential. The surface coverage of methanol, θ_M and the hydroxyl ion on ruthenium, $\theta_{OH,Ru}$ also increases with an increase in methanol concentration and cell temperature and thus shows a strong dependence on cell temperature and methanol concentration. Consequently due to this dependence on θ_M and $\theta_{OH,Ru}$, it can be concluded that the "whole" anode polarisation curve of a DMFC depends strongly on cell temperature and methanol feed concentration [29, 81, 99-101].

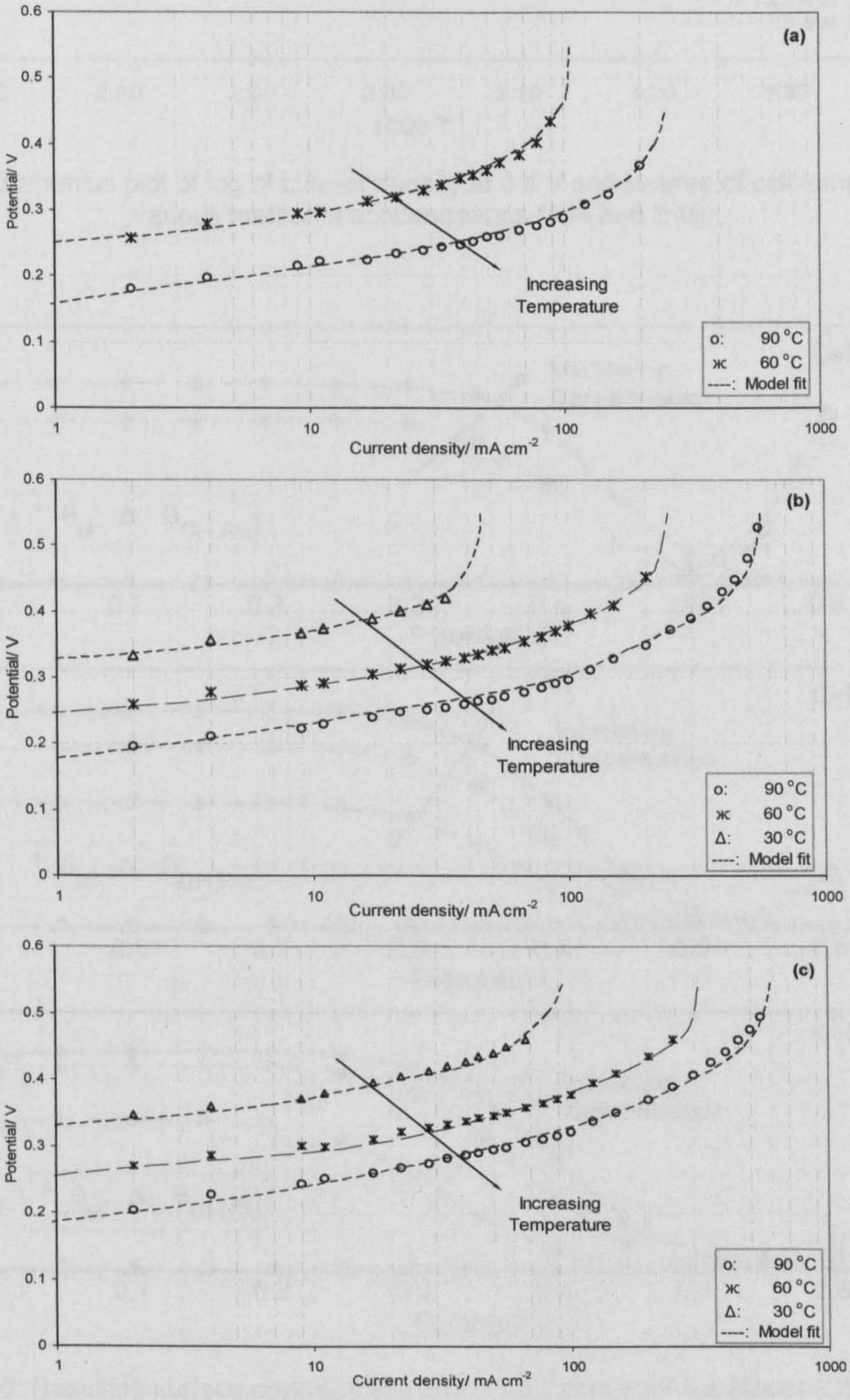

Figure 5.3: Model versus experimental fit on a Tafel plot for various temperatures (30, 60 and 90 °C) and methanol concentrations (a) 0.5 M, (b) 1 M and (c) 2 M

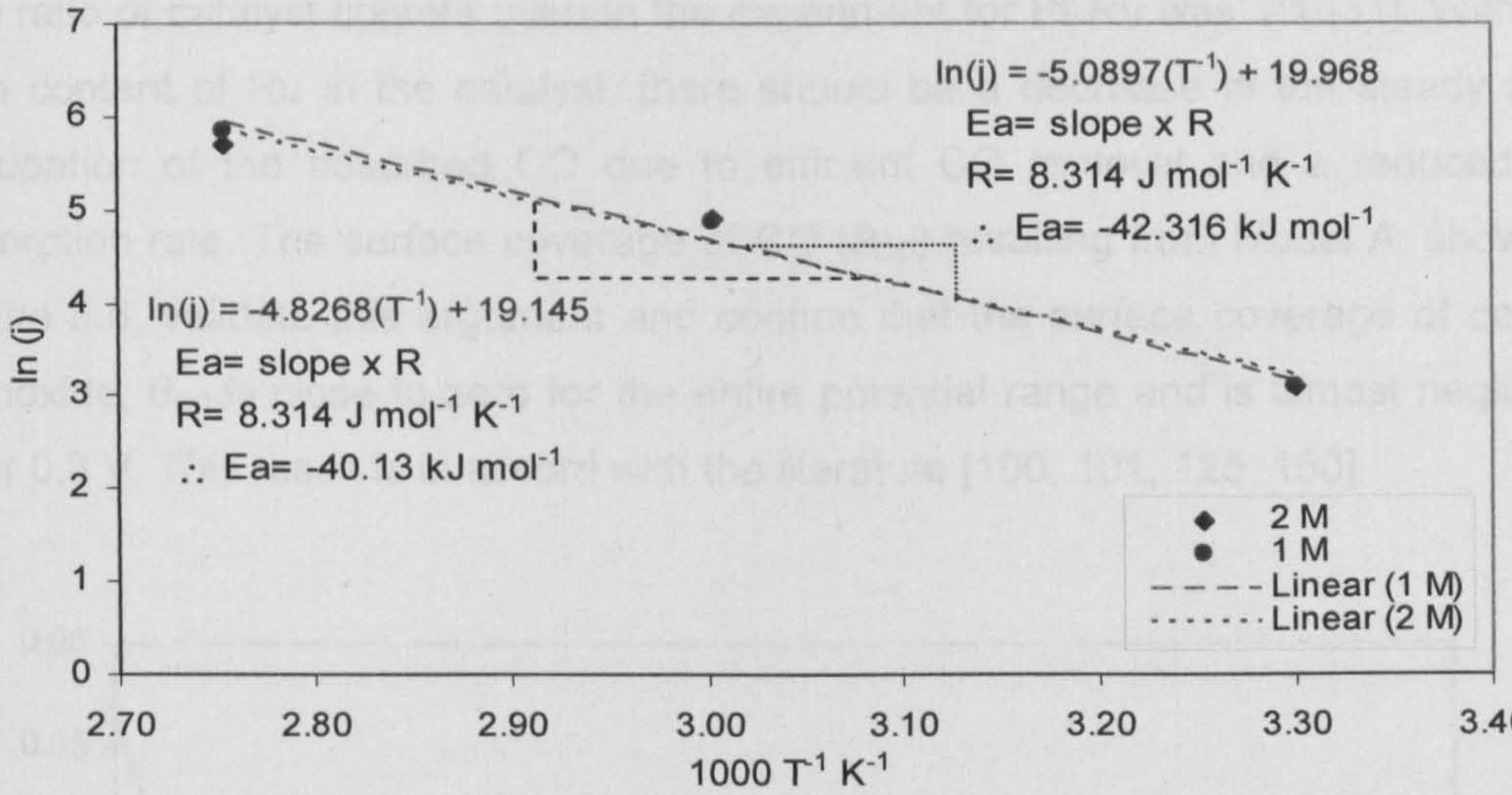

Figure 5.4: Arrhenius plot of log of current density at 0.4 V and inverse of cell temperature for various methanol concentrations (1 M and 2 M).

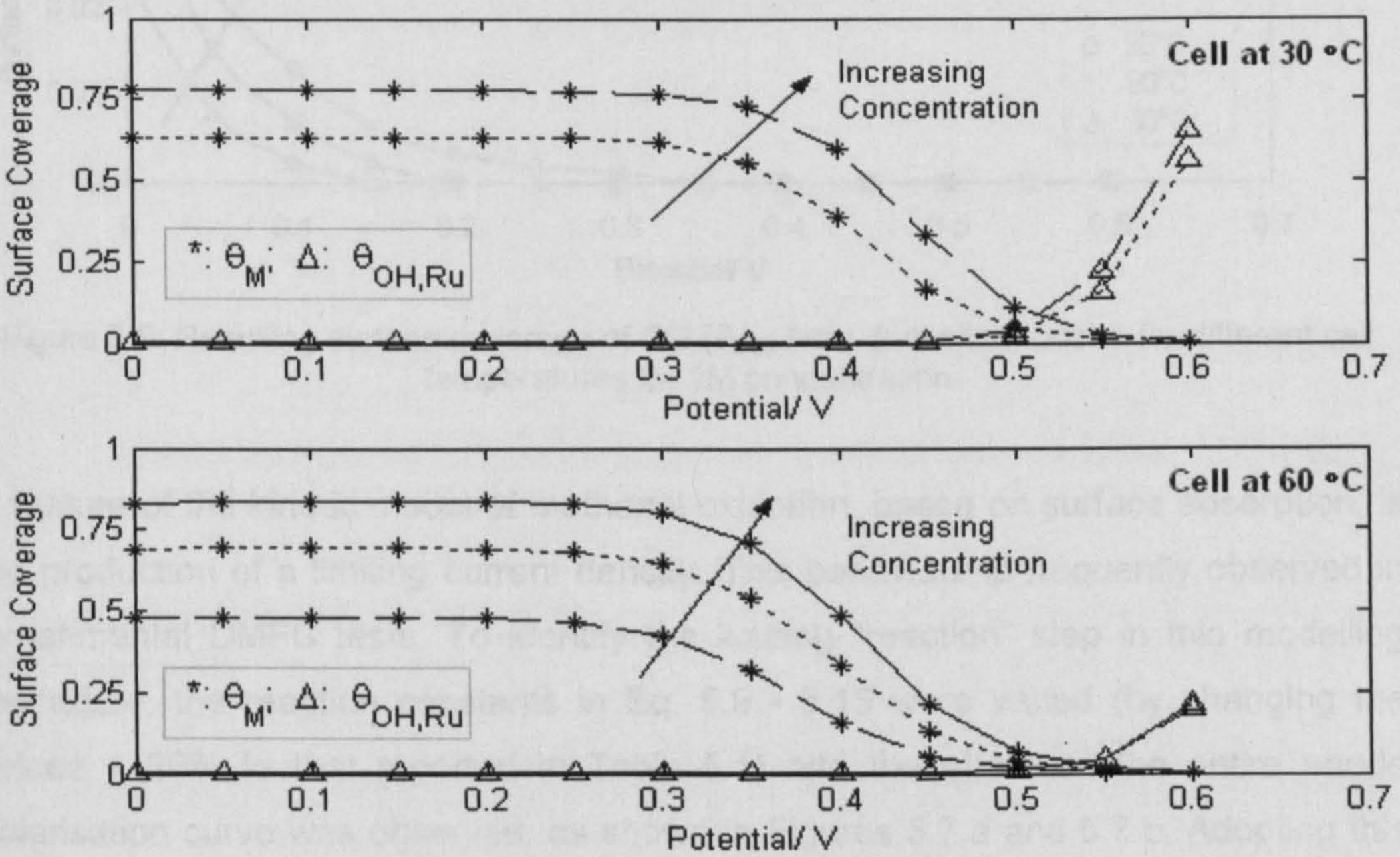

Figure 5.5: Resulting surface coverage (θ_M and $\theta_{OH,Ru}$) from dual site Model A for different temperatures and concentrations (____ 0.5 M; ..... 1 M and — 2 M).

The ratio of catalyst content used in the experiment for Pt-Ru was 1:1 [31]. With this high content of Ru in the catalyst, there should be a decrease in the steady state occupation of the adsorbed CO due to efficient CO removal and a reduced CO adsorption rate. The surface coverage of CO (θ_{CO}) resulting from Model A, shown in Figure 5.6, validate this argument and confirm that the surface coverage of carbon monoxide, θ_{CO} is close to zero for the entire potential range and is almost negligible after 0.3 V. This result is in accord with the literature [100, 101, 125, 150].

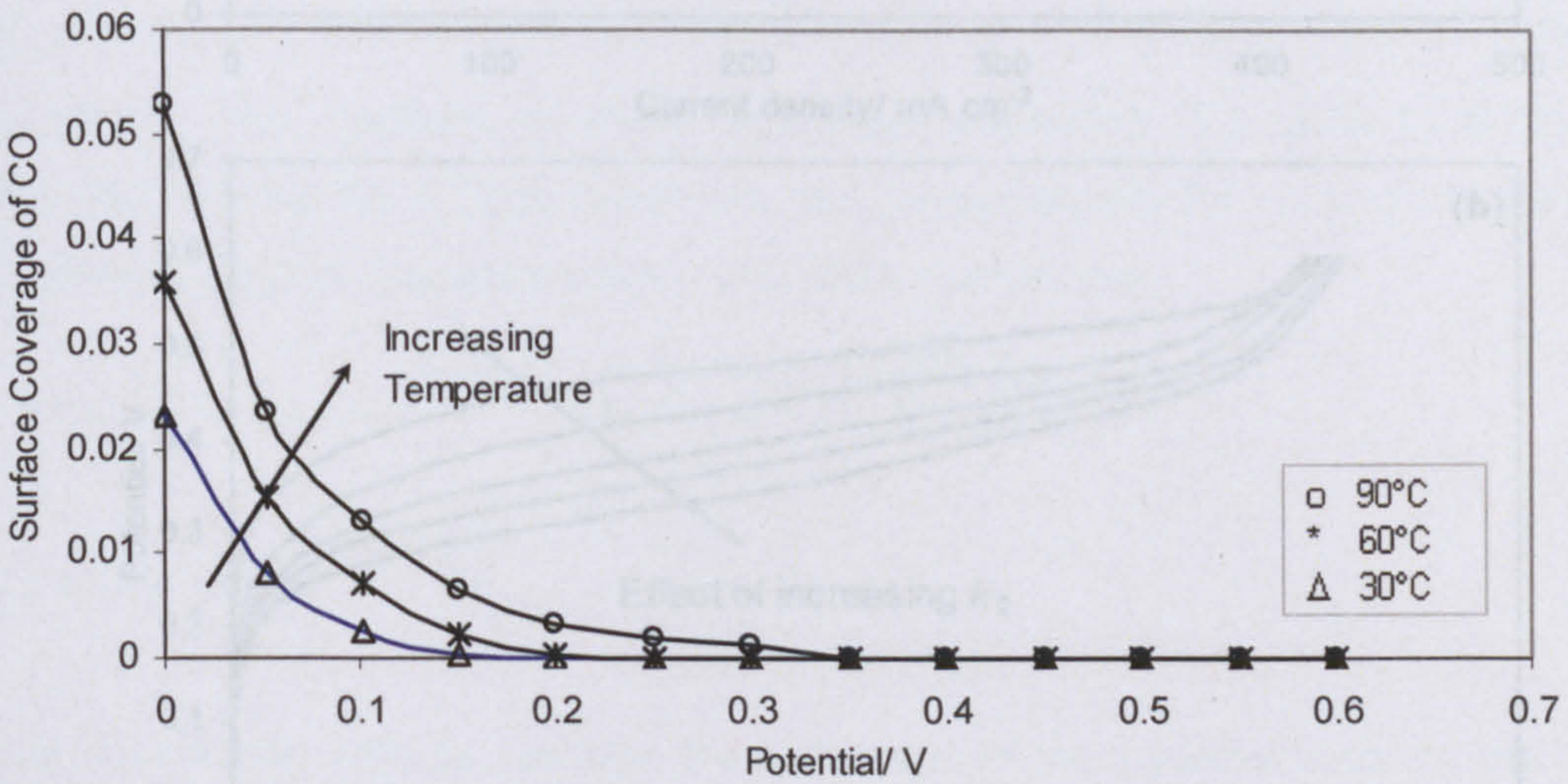

Figure 5.6: Resulting surface coverage of CO (θ_{CO}) from dual site Model A for different cell temperatures for 2M concentration

A feature of the kinetic model of methanol oxidation, based on surface adsorption, is the production of a limiting current density. This behaviour is frequently observed in experimental DMFC tests. To identify the limiting "reaction" step in this modelling procedure, the reaction constants in Eq. 5.9 - 5.13 were varied (by changing the values $\pm$ 20% to that reported in Table 5.1) and the effect on the entire anode polarisation curve was observed, as shown in Figures 5.7.a and 5.7.b. Adopting this method, it was found that reaction 5.9 limits the reaction over the entire potential. The change in the kinetic constant (k_1) for reaction 5.9 primarily affects the tip of the polarisation curve for potentials above 0.4 V (Figure 5.7.a), whilst the change in kinetic constant (k_2) for reaction 5.10 only affects the middle portion of the polarisation curve i.e. between 0 and 0.35 V as shown in Figure 5.7.b. Reaction constants in Eq. 5.11, 5.12 and 5.13 did not have a significant impact on the polarisation curve of the anode compared to k_1 and k_2, but slightly affected the surface coverage of θ_M, θ_{CO} and $\theta_{OH,Ru}$.

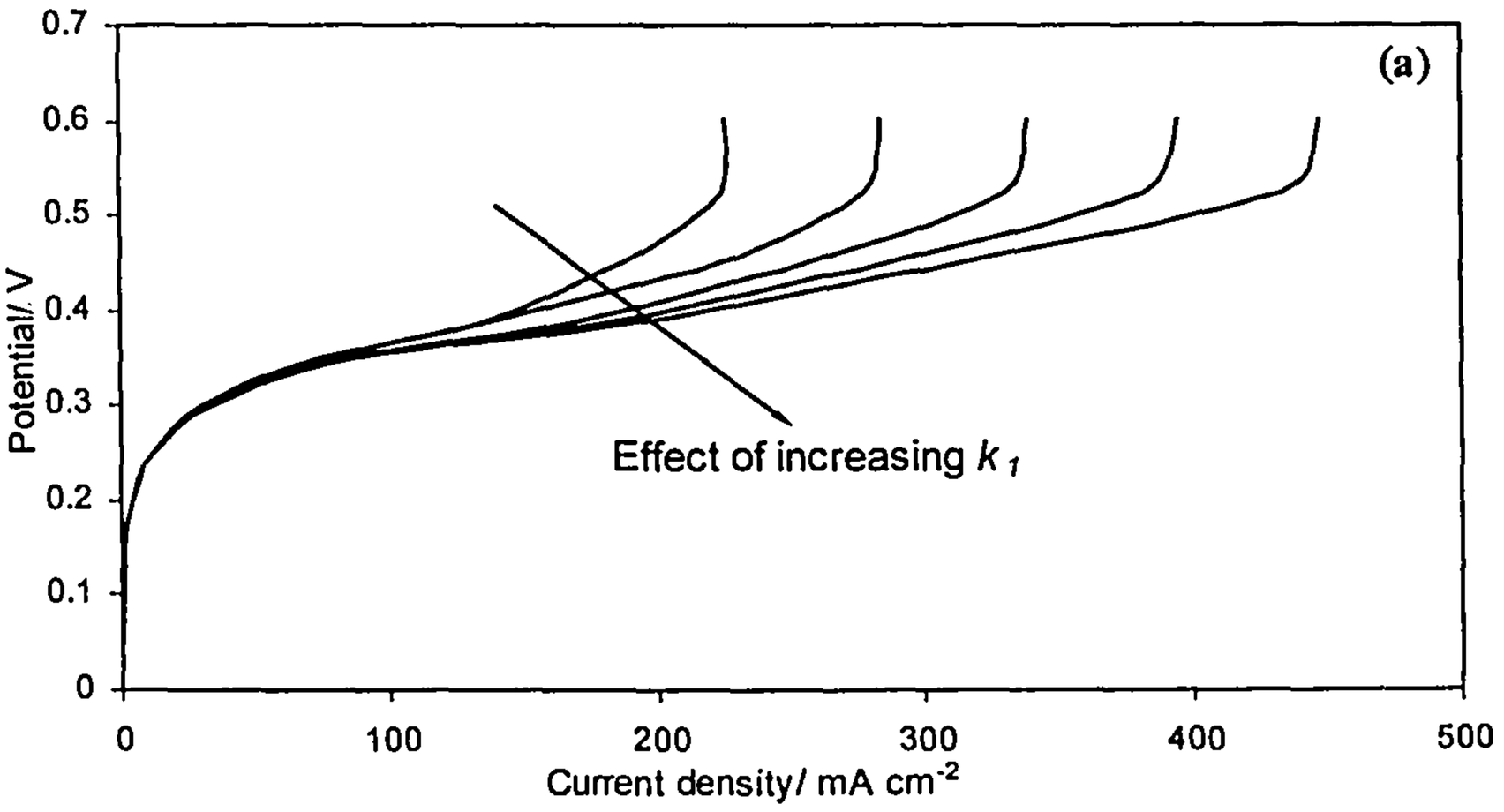

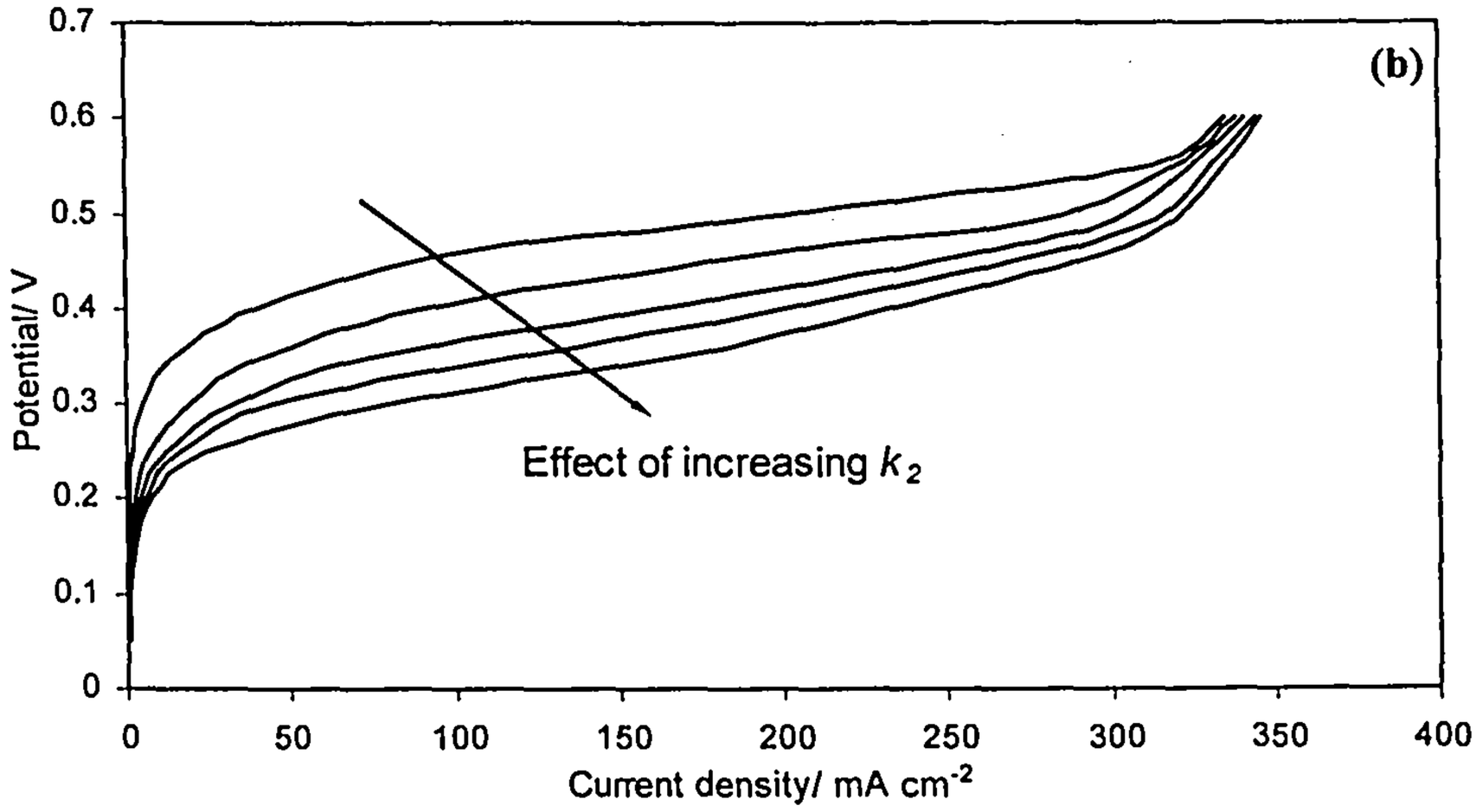

Figure 5.7: Kinetic parameters affecting the anode polarisation cure. (a) Effect of changing k_1 and (b) effect of changing k_2

5.4.3 Case B

For this modelling approach, it is assumed that the surface coverage of the hydroxyl ion on the Pt site and Ru site is approximately the same and for simplicity, it was also assumed that the surface reaction on both the Pt and Ru sites, Eq. 5.13, occur at the same rate (i.e. $k_{4,1} = k_{4,2} = k_4$). Thus the steady state surface coverage, Eq. 5.14 - 5.17, assuming the activity of water is unity, i.e. $a_{H_2O} = 1$, reduce to:

$$\theta_{CO} = 1 - \theta_{OH,Pt} - \theta_M - \left(\frac{k_1'\theta_M}{k_1 C_M}\right) - \left(\frac{k_2\theta_M e^{\left(\frac{\alpha_2 FE}{RT}\right)}}{k_1 C_M}\right) \quad \text{.... 5.26}$$

$$\theta_{CO} = \frac{k_2\theta_M e^{\left(\frac{\alpha_2 FE}{RT}\right)}}{k_4(\theta_{OH,Pt} + \theta_{OH,Ru})e^{\left(\frac{(1-\beta_4)FE}{RT}\right)}} \quad \text{.... 5.27}$$

$$\theta_{CO} = \frac{k_{3,1}(1-\theta_{OH,Pt}-\theta_M)e^{(\frac{(1-\beta_3)FE}{RT})} - k_{3,1}^{'}\theta_{OH,Pt}e^{(\frac{(-\beta_3)FE}{RT})}}{k_{3,1}e^{(\frac{(1-\beta_3)FE}{RT})} + k_4\theta_{OH,Pt}e^{(\frac{(1-\beta_4)FE}{RT})}} \quad \text{.... 5.28}$$

$$\theta_{CO} = \frac{k_{3,2}(1-\theta_{OH,Ru})e^{(\frac{(1-\beta_3)FE}{RT})} - k_{3,2}^{'}\theta_{OH,Ru}e^{(\frac{(-\beta_3)FE}{RT})}}{k_4\theta_{OH,Ru}e^{(\frac{(1-\beta_4)FE}{RT})}} \quad \text{.... 5.29}$$

Inclusion of $\theta_{OH,Pt}$ resulted in the inclusion of two additional kinetic parameters ($k_{3,1}$ and $k_{3,1}^{'}$) in the modelling process, resulting in the above set of non-linear equations. The solutions of these non-linear equations (Eq. 5.26 to 5.29) were incorporated into Eq. 5.20 to model the cell current density for varying cell potentials at different methanol concentrations and cell temperatures:

$$j = n \times F \times \left(k_{4,1}\theta_{OH,Pt}\theta_{CO}e^{(\frac{(1-\beta_4)FE}{RT})} + k_{4,2}\theta_{OH,Ru}\theta_{CO}e^{(\frac{(1-\beta_4)FE}{RT})} \right) \quad \text{...5.30}$$

$$\therefore j = n \times F \times k_4\theta_{CO}e^{(\frac{(1-\beta_4)FE}{RT})}\left(\theta_{OH,Pt}+\theta_{OH,Ru}\right) \quad \text{...5.31}$$

This model was able to describe the behaviour of the hydroxyl ions on the Pt site ($\theta_{OH,Pt}$). However the inclusion of two additional kinetic parameters, ($k_{3,1}$ and $k_{3,1}^{'}$), resulted in a non-linear set of equations, resulting in a more complex modelling procedure than for Model A. To address this, the kinetic parameters from Model A were used as initial estimates in the mathematical software, Maple (version 9) [152], and the remaining kinetic parameters for Model B were then estimated. The two additional kinetic parameters estimated using this procedure are given in Table 5.2.

Parameters	Fit at 30 °C	Fit at 60 °C	Fit at 90 °C
$k_{3,1}$	5 X 10^{-5} mol $m^{-2}s^{-1}$	3.2 X 10^{-5} mol $m^{-2}s^{-1}$	5 X 10^{-5} mol $m^{-2}s^{-1}$
$k_{3,1}^{'}$	2 X 10^{-5} mol $m^{-2}s^{-1}$	1.9 X 10^{-5} mol $m^{-2}s^{-1}$	1.6 X 10^{-5} mol $m^{-2}s^{-1}$

Table 5.2: Additional kinetic parameters used in dual site Model B

5.4.4 Analysis of the Case B Model

Figure 5.8 shows the fit of Model B to the experimental data of the porous anode for varying temperatures and concentrations. From Figures 5.8.a, 5.8.b and 5.8.c, it can be observed that the model adequately explains the dependence of anode current

density on cell temperature, potential and methanol feed concentration. The fit of the model was further validated from Figure 5.9. The model fitted the experimental data well at the lower end of the polarisation curve, Figure 5.9.a, and the resulting activation energy obtained by this modelling procedure lay between 38 to 44 kJ mol^{-1} (Figure 5.9.b). Based on these findings, it can be concluded that the model adequately predicts the kinetic behaviour of the anode.

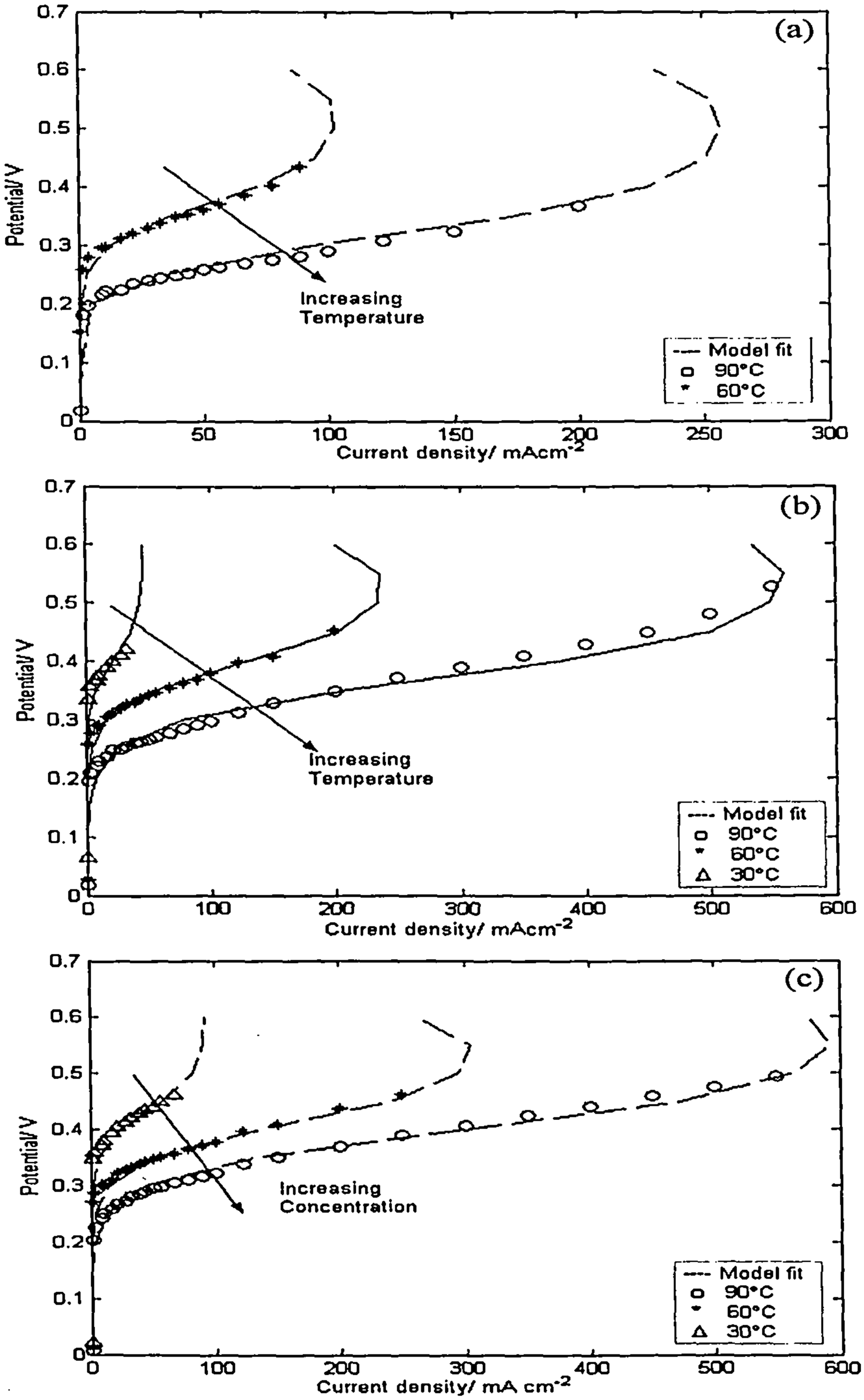

Figure 5.8: Model versus experimental fit for porous anode cell at various temperatures (30, 60 and 90 °C) and methanol concentrations (a) 0.5 M (data for 30 °C was not available [31]), (b) 1 M and (c) 2 M

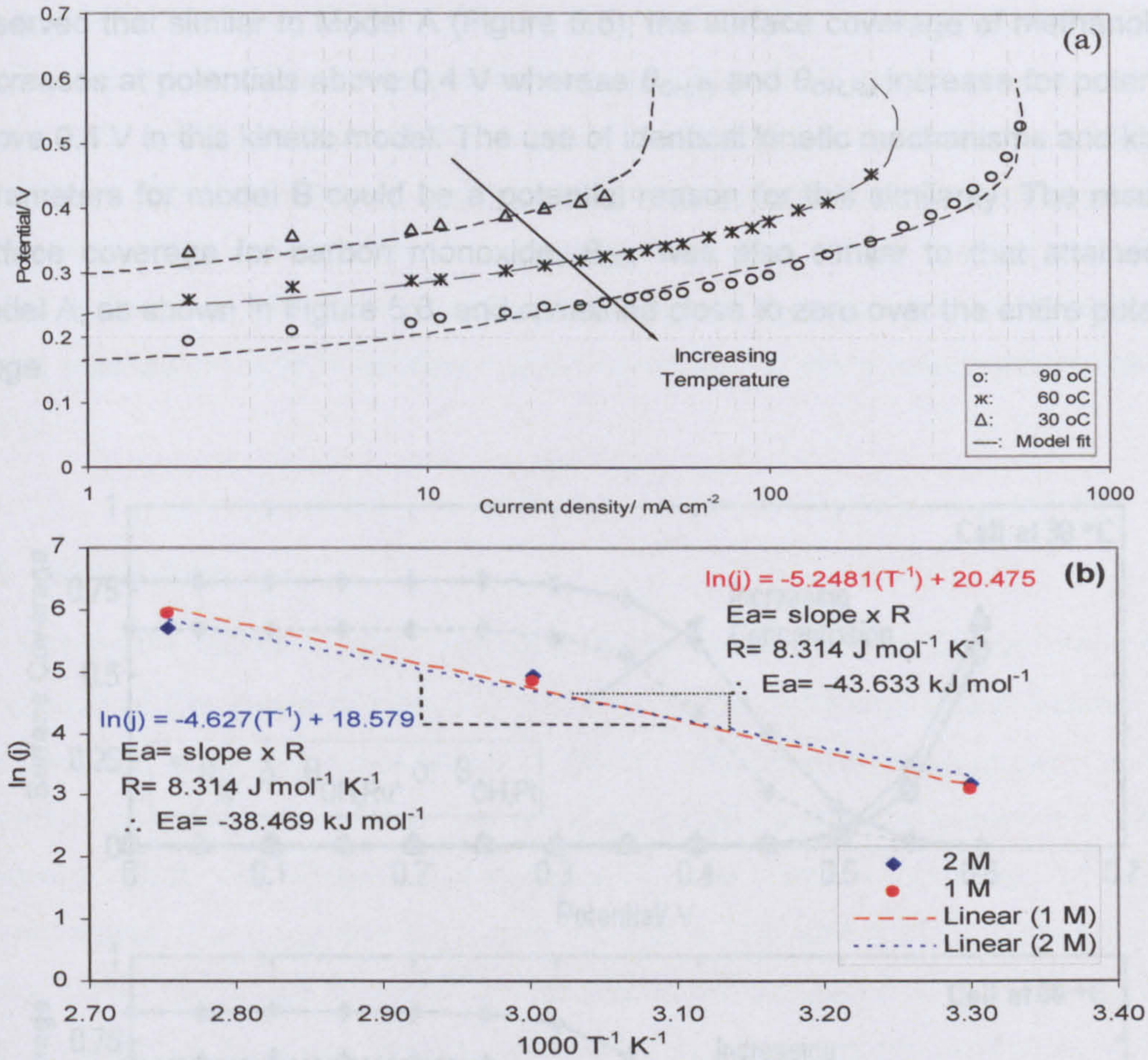

Figure 5.9: Model versus experimental fit (a) Tafel plot at various temperatures (30, 60 and 90 °C) using 1 M methanol concentration and (b) Arrhenius plot at 0.4 V for 1 M and 2 M methanol concentrations.

Comparing the fit of model B (Figure 5.6 and Figure 5.9.a) with model A (Figure 5.2 and 5.3) it can be observed that at low potentials (below 0.4 V) both Model A and B gave approximately similar fits as they were based on the same kinetic mechanism and kinetic parameters. However at high potentials (above 0.5 V), near the region of mass transport, a curving back phenomenon is observed with Model B, especially for higher temperatures (60 and 90 °C). The additional two kinetic parameters may be the reason for this curving back phenomenon. Thus to verify this hypothesis, the surface coverage of different intermediate species, attained by implementing Model B was analysed, Figure 5.10.

The surface coverage plot, Figure 5.10, revealed that the hydroxyl ion intermediate on Pt sites, $\theta_{OH,Pt}$, increased with an increase in potential thereby competing with the surface coverage of methanol (θ_M) and thus causing the curving back of the anode polarisation curve at high potentials (above 0.5 V) in Model B. These results are in agreement with other published work [29, 100, 101]. From Figure 5.10, it can be

observed that similar to Model A (Figure 5.5), the surface coverage of methanol, θ_M, decreases at potentials above 0.4 V whereas $\theta_{OH,Pt}$ and $\theta_{OH,Ru}$ increase for potentials above 0.4 V in this kinetic model. The use of identical kinetic mechanisms and kinetic parameters for model B could be a potential reason for this similarity. The resulting surface coverage for carbon monoxide, θ_{CO}, was also similar to that attained for Model A, as shown in Figure 5.6, and remained close to zero over the entire potential range.

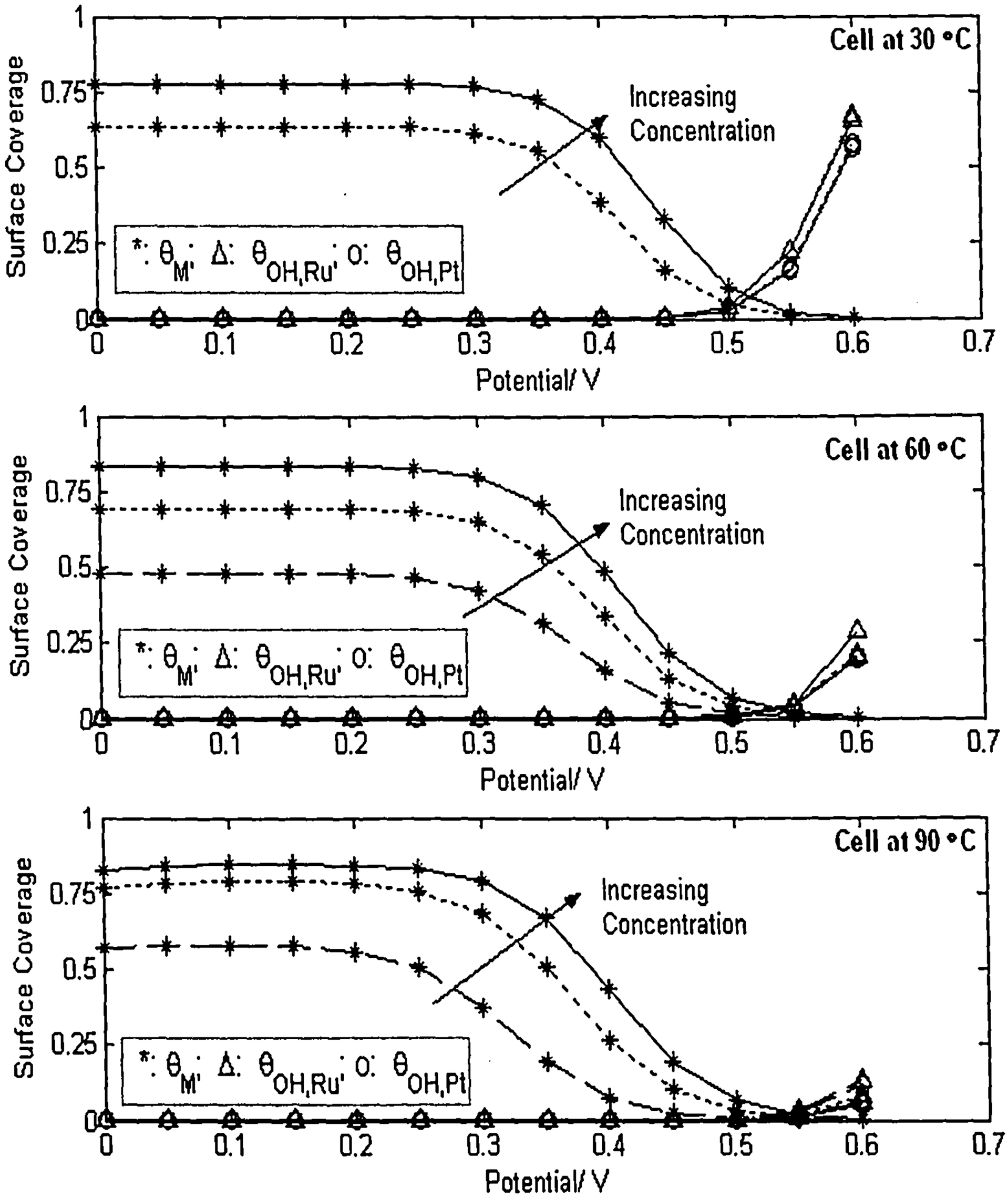

Figure 5.10: Resulting surface coverage from dual site Model B at different temperature (30, 60 and 90 °C) and concentrations (---- 0.5 M; ····· 1 M and —— 2 M).[*: surface coverage of methanol (θ_M); Δ: surface coverage of hydroxyl ion on Pt site ($\theta_{OH,\ Pt}$); o: surface coverage of hydroxyl ion on Ru site ($\theta_{OH,\ Ru}$)]

As illustrated in Figure 5.7, the limiting reactions for this model were identified by varying the reaction kinetic constants. Due to the reaction mechanisms and kinetic parameters being similar to Model A, it was observed that for this modelling procedure, reaction (5.9) was limiting at high anode potentials and reaction (5.10) only affected the anode polarisation at potentials below 0.3 V. The inclusion of two kinetic parameters affected the surface coverage of $\theta_{OH,Pt}$ but overall its impact on anode polarisation was insignificant when compared to other kinetic parameters (k_1 and k_2).

5.5. Simulation

To identify the effect of high methanol concentrations on anode performance, a simulation of the anode polarisation curve for higher methanol concentrations (3M, 4M and 5M) at a cell temperature of 60 °C was generated using both surface-coverage based kinetic models. The resulting anode polarisation curves and surface coverage plots are shown in Figure 5.11. The surface coverage of all the intermediates (θ_M, $\theta_{OH,Pt}$ and $\theta_{OH,Ru}$), in Figures 5.11.b and 5.11.d, reveals that the anode polarises at high anode potentials due to the saturation of methanol (θ_M) and the coverage of the entire catalyst surface by hydroxyl ions ($\theta_{OH,Pt}$ and $\theta_{OH,Ru}$). The simulation results also show a significant curving back of the anode polarisation curve for Model B (Figure 5.11.c). This curving back phenomenon is due to the competition from additional intermediates on the Pt sites in Model B as shown in Figure 5.11.d. The surface coverage of methanol, θ_M, decreases with an increase in the anode potential and both $\theta_{OH,Pt}$ and $\theta_{OH,Ru}$ start covering the surface area on the platinum and ruthenium sites respectively. This increase in $\theta_{OH,Pt}$ on the Pt sites effectively blocks further adsorption of methanol on Pt and thus, with an increase in the potential, the current density starts to decrease, which materialises in the curving back of the polarisation curve.

Compared with Model B, in Model A it is assumed that the surface coverage of the hydroxyl ion ($\theta_{OH,Pt}$) is much less on Pt sites than on Ru sites. The Pt site is thus dominated by methanol and with an increase in potential there is no competition from additional intermediates, like $\theta_{OH,Pt}$, on the Pt sites for surface coverage as shown in Figure 5.11.b. Hence in Model A, with an increase in potential, the anode polarisation curve increases continuously without any curving back, Figure 5.11.a. A feature of the model is that methanol oxidation continues to improve, i.e. lower polarisation is observed, at higher methanol concentrations (i.e. anode polarisation at 5 M> 4 M> 3

M). It would be interesting to explore this behaviour further in real fuel cell tests to improve the overall performance of the DMFC provided the issue of methanol crossover is resolved, i.e. the high cathode polarisation caused by high methanol concentrations.

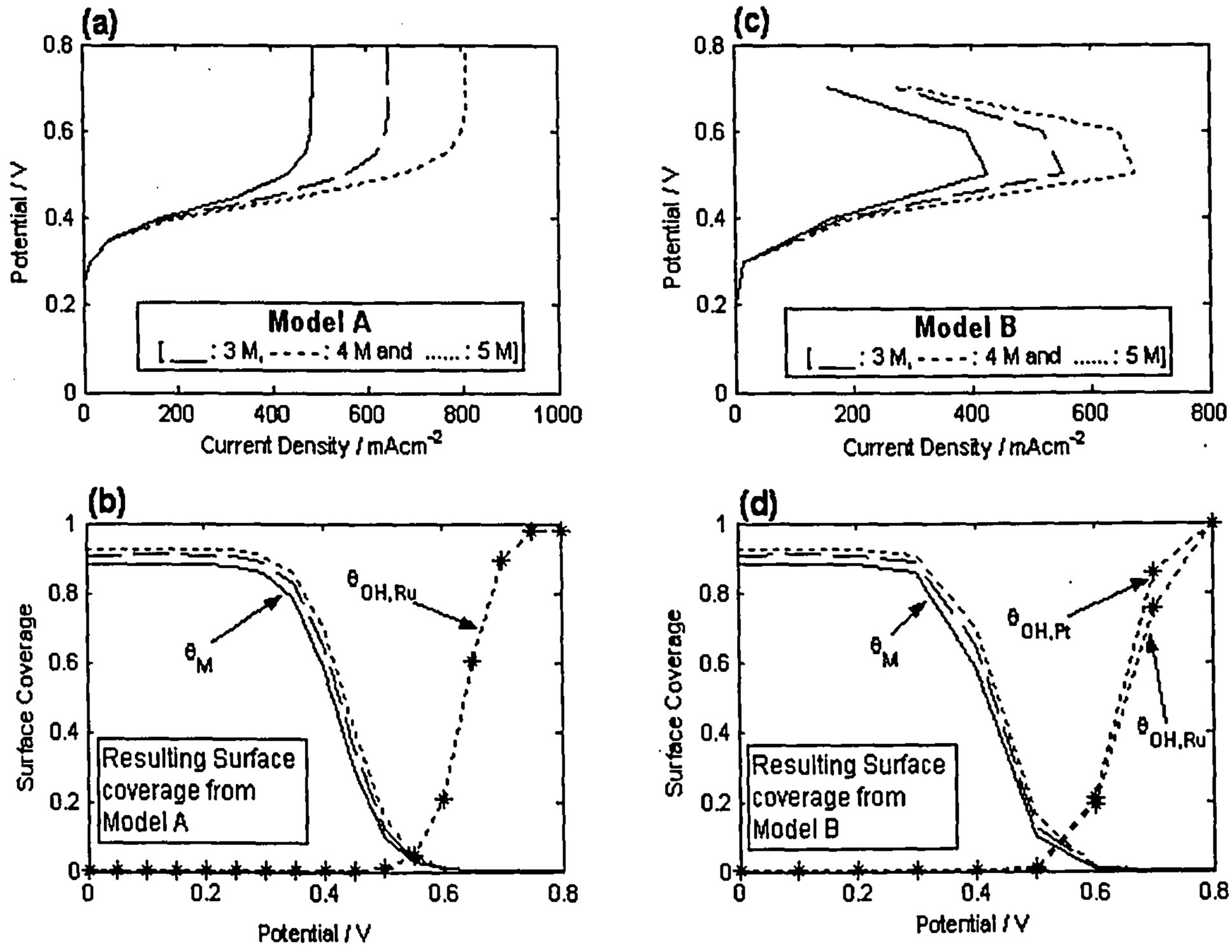

Figure 5.11: Simulation results on both the dual site model at 60 °C with varying methanol concentrations (— 3 M; ----- 4 M; and ····· 5 M) (a) Simulation results from Model A, (b) resulting surface coverage from Model A, (c) simulation results from Model B and (d) resulting surface coverage from Model B.

5.6. Simplified Anode Model

The detailed kinetic models described in section 5.4 fitted the experimental data well but due to the presence of non-linear equations and the determination of 6 to 8 kinetic parameters, the overall model was complex and was computationally intensive. Variations in the kinetic parameters to identify the limiting reaction step, as shown in Figure 5.7, indicated that some of the kinetic parameters, including the reaction constants k_1' and k_2', have less effect or almost no effect on the polarisation curve compared to the reaction constants k_1 and k_2. On the basis of this, the reverse

reaction constants $k_1^{'}$ and $k_2^{'}$, can be assumed to be negligible in comparison to the forward reaction constants in Eqs. 5.9 to 5.12 which simplifies Eq 5.14 for the Case A model further:

$$\Gamma\frac{d\theta_M}{dt} = k_1 C_M(1-\cancelto{0}{\theta_{OH,Pt}}-\theta_{CO}-\cancelto{0}{\theta_M}) - k_1^{'}\theta_M - k_2\theta_M e^{(\frac{\alpha_2 FE}{RT})} \quad \text{....5.32}$$

At steady state:

$$\therefore \theta_M = \frac{k_1 C_M(1-\theta_{CO})}{k_2 e^{(\frac{\alpha_2 FE}{RT})} + k_1 C_M} \quad \text{....5.33}$$

In the detailed kinetic model, it was observed that the surface coverage of CO was very low and is almost negligible above 0.3 V, Figure 5.6. On this basis, it was assumed that, 1-θ_{CO} ≈ 1. Thus the above equation can be further simplified:

$$\therefore \theta_M = \frac{k_1 C_M}{k_2 e^{(\frac{\alpha_2 FE}{RT})} + k_1 C_M} \quad \text{... 5.34}$$

Similarly Eq. 5.15 at steady state can be further simplified:

$$\Gamma\frac{d\theta_{CO}}{dt} = k_2\theta_M e^{(\frac{\alpha_2 FE}{RT})} - k_{4,2}\theta_{OH,Ru}\theta_{CO} e^{(\frac{(1-\beta_4)FE}{RT})} \quad \text{...5.35}$$

$$\therefore k_{4,2}\theta_{OH,Ru}\theta_{CO} e^{(\frac{(1-\beta_4)FE}{RT})} = k_2\theta_M e^{(\frac{\alpha_2 FE}{RT})} \quad \text{... 5.36}$$

Substituting Eq 5.36 into Eq 5.25 for Case A model gives:

$$\therefore j = n * F * k_2\theta_M e^{(\frac{\alpha_2 FE}{RT})} \quad \text{... 5.37}$$

Substituting, θ_M, from Eq. 5.33 into equation 5.37 and simplifying gives:

$$\therefore j = n * F * k_2 e^{(\frac{\alpha_2 FE}{RT})} * \left(\frac{k_1 C_M}{k_2 e^{(\frac{\alpha_2 FE}{RT})} + k_1 C_M}\right) \quad \text{... 5.38}$$

Figure 5.12 demonstrates the fit of this simplified three parameter model to the experimental data of the cell at 30, 60 and 90 °C for varying methanol concentrations. From these figures it can be seen that the simplified model also fits the data well and explains the dependence of anode polarisation on cell temperature and methanol concentration.

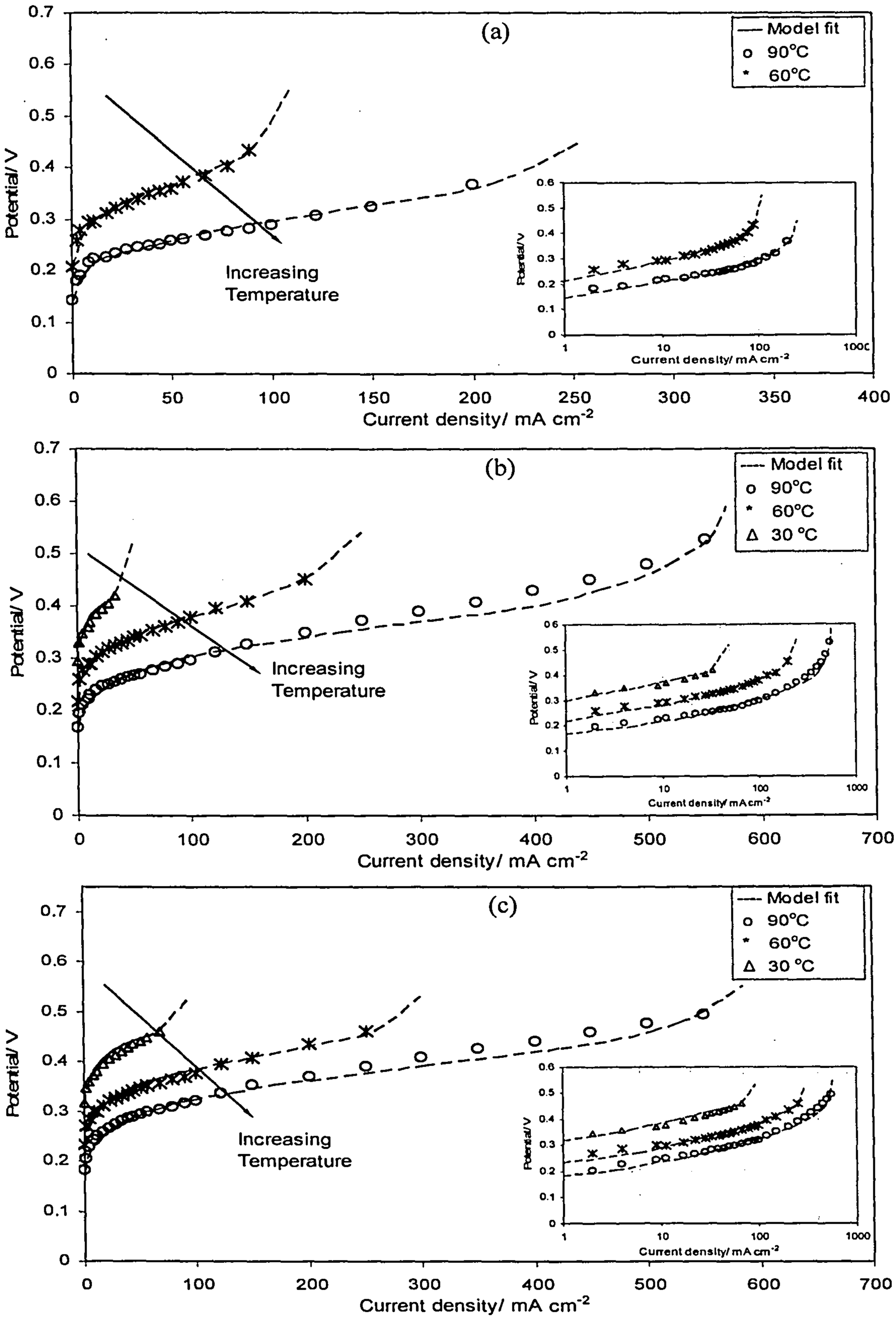

Figure 5.12: Simplified model versus experimental fit for porous anode cell at temperatures (30, 60 and 90 °C) and methanol concentrations (a) 0.5 M, (b) 1 M and (c) 2 M. Inset plots show the fit of the model to lower end of the experimental data (0 to 100 mA cm^{-2}) using a Tafel plot.

The model was also fitted to the Tafel plot, shown as insets in Figure 5.12, which showed that the model was able to predict the experimental data at the lower end of the polarisation curve. The activation energy obtained in this case, by estimating the slope of log of cell current density at 0.4 V and the inverse of cell temperature as shown in Figure 5.13, was in the range of 44 -46 kJ mol^{-1}, which was slightly higher than the detailed model but still within the acceptable range of 30 to 70 kJ mol^{-1} [44, 119].

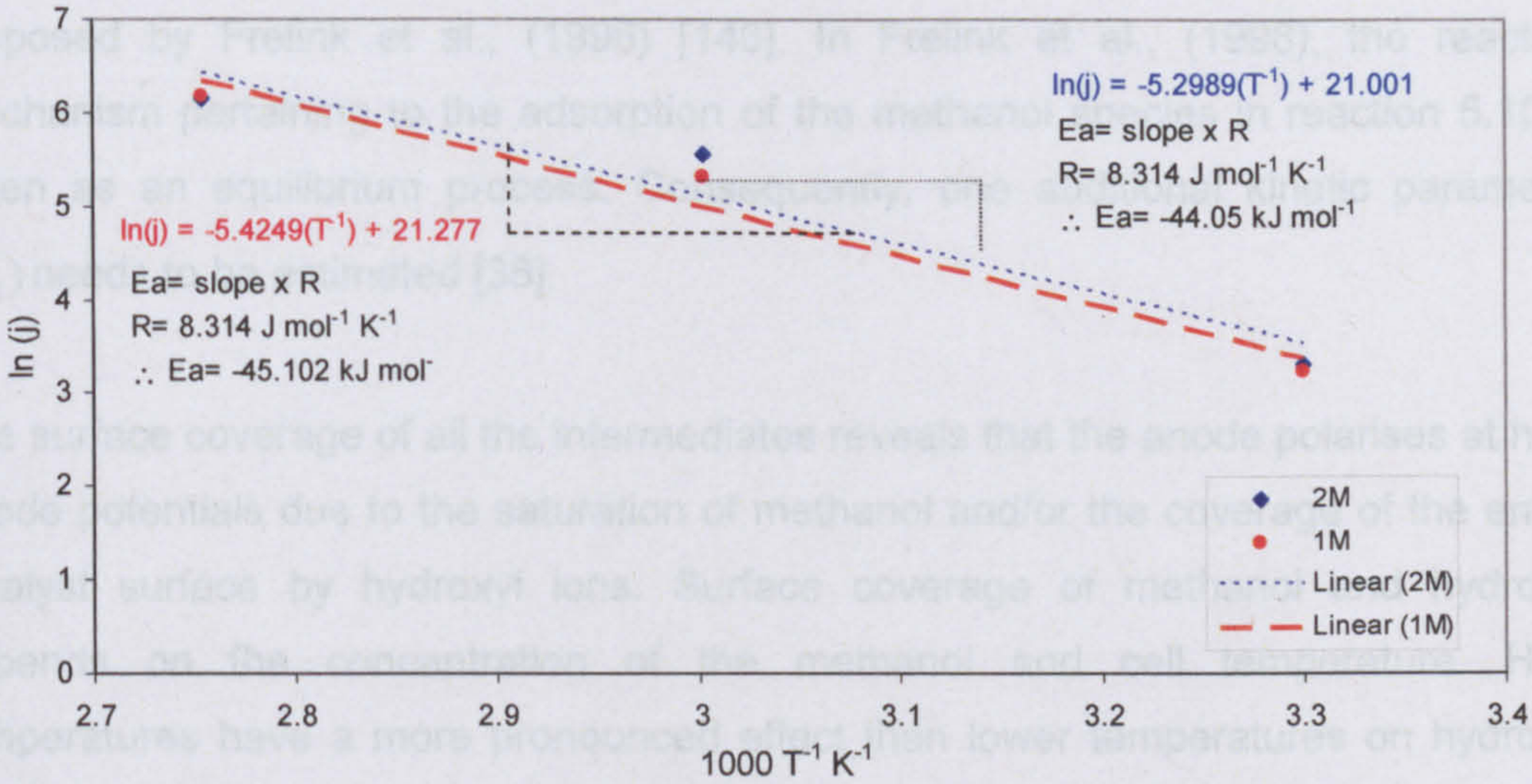

Figure 5.13: Arrhenius plot at 0.4 V for 1 M and 2 M methanol concentrations

The drawback of the simplified model was that it cannot describe the surface coverage of the intermediates involved in the mechanism but on the other hand due to the need to estimate only 3 kinetic parameters to fit the anode polarisation it was not computationally intensive compared to the previous detailed models. The kinetic parameters derived from the simplified model are given in Table 5.3.

Parameters	Fit at 30 °C	Fit at 60 °C	Fit at 90 °C
k_1	3.28 X 10^{-7} m s^{-1}	4.09 X 10^{-7} m s^{-1}	9.73 X 10^{-7} m s^{-1}
k_2	2 X 10^{-10} mol $m^{-2}s^{-1}$	8.82 X 10^{-9} mol $m^{-2}s^{-1}$	1.1 X 10^{-7} mol $m^{-2}s^{-1}$

Table 5.3: Parameters used in the simplified model

5.7. Conclusions

The surface-coverage based detailed kinetic models presented in this chapter describe the anode polarisation curve of the DMFC. It has been observed that the methanol oxidation kinetics depend strongly on cell temperature and methanol

concentration. Both models gave similar results at the lower end of the polarisation curve as they were based on a similar methanol oxidation kinetic mechanism. The resulting surface coverage of all the intermediates (θ_M, θ_{CO}, $\theta_{OH,Pt}$ and $\theta_{OH,Ru}$) from the model supported the hypothesis that the Ru sites act as the centre for CO oxidation and the Pt sites serve as the centre for the adsorption and dehydrogenation of methanol. The proposed surface coverage based modelling approach can also be applied to other generally accepted reaction mechanisms for example those proposed by Frelink et al., (1996) [146]. In Frelink et al., (1996), the reaction mechanism pertaining to the adsorption of the methanol species in reaction 5.10 is taken as an equilibrium process. Consequently, one additional kinetic parameter ($k_2^{'}$) needs to be estimated [38].

The surface coverage of all the intermediates reveals that the anode polarises at high anode potentials due to the saturation of methanol and/or the coverage of the entire catalyst surface by hydroxyl ions. Surface coverage of methanol and hydroxyl depends on the concentration of the methanol and cell temperature. High temperatures have a more pronounced effect than lower temperatures on hydroxyl adsorption on both the Pt and Ru sites. The model highlights the subtle balance between methanol adsorption and the subsequent oxidisation to CO on the dual site catalyst and identifies them as the limiting steps rather than the surface oxidation of CO to CO_2.

Model B provided greater insight than Model A, into the nature of the methanol and hydroxyl surface coverage on both catalyst sites but the addition of two kinetic parameter resulted in four sets of non-linear equations thereby increasing the computational challenges. The use of identical reaction constants for the surface reaction in Model B eliminated one of the additional kinetic parameters and hence the non-linear equations were solvable. However, in real systems the reaction constants will differ depending on the reaction sites. On the other hand, Model A contained six kinetic parameters and due to the absence of non-linear equations it was computationally more straightforward than Model B.

The detailed kinetic models, models A and B, can be used to predict the performance of the electrode and the behaviour of surface coverage of intermediates as a function of cell temperature, anode potential and methanol concentration. However in a complete system or stack studies it is not practical to use such detailed models due

to the slow computational speed [100]. For such studies, the simplified three parameter model derived from the Gasteiger mechanism can rapidly calculate the cell current density for an input of cell potential, cell temperature and methanol concentration. Thus this is a significant advantage of this approach. This is demonstrated in the next chapter where the simplified anode model is combined with the cathode model to understand the effect of methanol crossover on the overall DMFC polarisation characteristics.

Chapter 6
A Model For The Direct Methanol Fuel Cell

6.1. Introduction

The DMFC performance depends on a large number of operating parameters (cell temperature, pressure and reactant flow rates), design parameters (gas diffusion layer morphology, design of flow field and current collectors) and electrochemical and physical parameters (reaction mechanism and MEA formulation). The overall DMFC operation is complex as many of these parameters are strongly coupled and inter-dependent [6, 9, 19, 32, 96] and consequently modelling the cell can be complex. One approach is to combine mathematical modelling with a detailed experimental modus operandi. The literature review in Section 2.7 described a number of semi-empirical models that have been proposed [46, 78-80, 82, 83, 88, 89, 102, 104-107, 153]. For example, a two stage semi-empirical model was proposed to predict the cell voltage with respect to the current density response of a DMFC [79, 80]. In the first stage, an empirical equation similar to Squadrito et al., (1999) [86] was proposed. A semi-empirical model was subsequently developed to explain the significance of each of the parameter. More specified anode and cathode kinetics were given by Tafel equations and methanol oxidation was potentially mass transport limited at higher current density [80]. The generalised model proposed to explain the polarisation characteristics of the DMFC is given by the following expression [79, 80]:

$$E_{cell} = E_O^{\bullet} - b_{cell}\log j - R_e j + C_1 \ln(1 - C_2 j) \qquad \ldots (6.1)$$

where, $b_{cell} = \dfrac{2.303RT}{F}\left(\dfrac{1}{\alpha_a} + \dfrac{1}{\alpha_c}\right)$, $C_1 = \dfrac{NRT}{\alpha_a F}$, $C_2 = \dfrac{1}{nFk_{eff}C_{ME}}$,

$$E_O^{\bullet} = E_{Cell}^{o} - \frac{RT}{\alpha_c F}\ln\left(\frac{p_O^{ref}}{j_{Oc}p_O}\right) - \frac{RT}{\alpha_a F}\left(\ln\frac{C_{ME}^{ref}}{j_o C_{ME}^{N}}\right),$$

E_{cell} is the cell potential (V), E_{Cell}^{o} is the standard cell potential (1.23 V), j is the cell current density (A m^{-2}), R_e is the internal cell resistance (Ω m^2) and R is the gas

constant (8.314 J mol^{-1} K^{-1}). T is cell the temperature (K), F is Faraday's constant (96487 A s mol^{-1}), α_a and α_c are the electrochemical transfer coefficients for methanol oxidation and oxygen reduction reaction respectively, N is a reaction order for methanol oxidation, k_{eff} is an effective mass transport coefficient for the anode side of the cell (m s^{-1}), C_{ME} is the concentration of methanol (M), p_o is the oxygen partial pressure (N m^{-2}), j_o and j_{oc} are the exchange current density at the reference methanol concentration (C_{ME}^{ref}) at the anode and cathode side respectively (A m^{-2}).

This expression (6.1) has a number of limitations including:

i) The open circuit potential does not allow for the influence of methanol crossover [88],

ii) The cathode kinetics do not allow for the influence of methanol crossover which is a function of current density,

iii) The anode kinetics is limited by a simple Tafel equation. This does not capture the true methanol oxidation behaviour [95],

iv) The potential mass transport limitations of oxygen reduction are not taken into account.

The objective of this chapter is to develop a new semi-empirical model which addresses these issues as well as explaining the DMFC polarisation characteristics; taking into account the mixed potential and methanol crossover phenomena. The model was developed in two parts. Initially a model of oxygen reduction at the cathode was developed prior to a second model that takes into account the oxygen reduction in the presence of methanol due to crossover. This combined cathode model will provide an insight into the effect of methanol crossover on the cathode open circuit voltage and overall cell potential.

The overall cell output is the combined effect of the anode and cathode polarisation. Consequently, the cathode model was combined with the three parameter anode model developed in Chapter 5 to describe the DMFC polarisation; taking into account the mixed potential and methanol crossover at the cathode with methanol oxidation kinetics at the anode. To predict the DMFC characteristic curve with respect to methanol concentration across the cell, the methanol concentration profile in both the anode and the cathode region is modelled as a function of cell current density, temperature and methanol concentration. The models were developed in LabVIEW [115] and the parameters were estimated, utilising experimental data from a 9 cm^2

conventional DMFC for various methanol concentrations (0.5, 1 and 2 M) and temperatures (30, 60 and 90 °C) [114] using the test rig and experimental procedure described in Section 3.3.

6.2. Model Formulation

The net cell voltage of a DMFC (η_{Cell}) is the difference between the cell potentials at the cathode ($\eta_{Cathode}$) and anode (η_{Anode}). The electrode potential is a combination of the activation overpotential and concentration overpotential for each electrode. When the ohmic resistance ($\eta_{Ohmic} = R_e \times j_{Cell}$), which predominantly results from internal cell resistance from the polymer electrolyte membrane, is taken into account [89] the overall expression is given by:

$$\eta_{Cell} = \eta_{Cathode} - \eta_{Anode} - \eta_{Ohmic} \quad \ldots (6.2)$$

A model to predict anode polarisation behaviour (η_{Anode}), was developed in Chapter 5 and a relationship that describes the ohmic resistance, with respect to a change in temperature (η_{Ohmic}), having previously been developed [82]. Hence to explain the polarisation behaviour of the DMFC, a cathode model ($\eta_{Cathode}$) is required. The underlying assumptions in the cathode and overall cell models are:

i) the electrodes are at steady state and the fuel cell is operated isothermally with negligible pressure differences between various compartments,
ii) Butler–Volmer kinetics are valid for the charge transfer steps and are adapted to describe methanol oxidation,
iii) the concentration of methanol in the anode feed channel is assumed to be the same as the feed concentration. This is based on the fact that the variation in the flow channel methanol concentration, at the anode side, is almost negligible,
iv) water transport through the membrane, at high current density by diffusion is considered to be negligible compared to the electro-osmotic drag [83],
v) only the liquid phase is considered and CO_2 is assumed to be dissolved in the solution,
vi) for simplicity, the anode and cathode are treated as one-dimensional
vii) water vapour pressure is assumed to obey Dalton's and Raoult's laws [154].

6.2.1 Model for Open Circuit Cathode Potential

A model for the open circuit cathode potential that takes into account the effect of methanol crossover on oxygen reduction is first developed. As a first approximation, in the absence of a well developed mechanism and suitable parameters for the kinetics, it is assumed that the following overall reactions occur simultaneously at the cathode in the presence of methanol:

$$CH_3OH + 0.5O_2 \rightarrow CO_2 + 4H^+ + 4e^- \quad \ldots (6.3)$$

$$O_2 + 4H^+ + 4e^- \rightarrow 2H_2O \quad \ldots (6.4)$$

The model uses the Butler-Volmer equation [155],for kinetics for the oxygen reduction reaction (Eq. 6.4). It assumes that the cathode is essentially at low overpotential and thus uses the Butler-Volmer model for methanol oxidation (Eq. 6.3) at the cathode:

$$j_{O,Cathode} = j_{o,O}\left[\frac{P_O}{P_{Oref}} e^{\left(\frac{-n\alpha_{O2}F(E-E^o_{O_2})}{RT}\right)} - e^{\left(\frac{n(1-\alpha_{O2})F(E-E^o_{O_2})}{RT}\right)}\right] \quad \ldots (6.5)$$

$$j_{M,Cathode} = j_{o,M}\left[\frac{C^c_M}{C_{Mref}}\left(\frac{P_O}{P_{Oref}}\right)^{0.5} e^{\left(\frac{n\alpha_M F(E-E^o_M)}{RT}\right)} - \frac{P_{CO_2}}{P_{CO_2 ref}} e^{\left(\frac{-n(1-\alpha_M)F(E-E^o_M)}{RT}\right)}\right] \quad \ldots (6.6)$$

where, $j_{O,Cathode}$ and $j_{M,Cathode}$ are the current density at the cathode due to oxygen reduction and methanol oxidation (A m^{-2}) respectively, α_M and α_{O_2} are the electrochemical transfer coefficients at cathode due to oxygen reduction and methanol oxidation respectively, n is the number of electrons transferred, E is the cathode potential (V), E^o_M and $E^o_{O_2}$ are the standard potential due to methanol oxidation and oxygen reduction reaction (V), P_{CO_2} is the partial pressure of carbon dioxide formed due to methanol oxidation (N m^{-2}), $j_{o,O}$ and $j_{o,M}$ are the exchange current density at the reference methanol concentration (C_{Mref}) for the methanol oxidation and oxygen reduction reaction respectively (A m^{-2}).

The total current at the cathode ($j_{Cathode}$), is the sum of the two partial currents for methanol oxidation and oxygen reduction, thus

$$j_{Cathode} = j_{O,Cathode} + j_{M,Cathode} \quad \ldots (6.7)$$

For the open circuit condition, the current is zero and hence the solution of Eqs 6.5 and 6.6 is:

$$\therefore -j_{o,O}\left(\frac{P_O}{P_{Oref}}\right) = -j_{o,O}\left(e^{f\eta_{oc}}\right) + j_{o,M}\left[\frac{C_M^C}{C_{Mref}}\left(\frac{P_O}{P_{Oref}}\right)^{0.5} e^{\left(\alpha_M f(E_{oc}-E_M^o)\right)+\alpha_{O_2} f\eta_{oc}}\right] \quad \ldots (6.8)$$
$$- j_{o,M}\frac{P_{CO_2}}{P_{CO_2ref}} e^{\left(-(1-\alpha_M) f(E_{oc}-E_M^o)\right)+\alpha_{O_2} f\eta_{oc}}$$

where, E_{OC} is the open circuit cathode potential, η_{OC} is the cathode over voltage at open circuit $(\eta_{OC} = E_{OC} - E^o_{O_2})$, E^o_{Cell} is the standard cell potential for the DMFC $(E^o_{Cell} = E^o_{O_2} - E^o_M)$ and $f = F/RT$.

In Eq. 6.8, if the influence of carbon dioxide (CO_2) on the right hand side is neglected, then on rearrangement, Eq. 6.8 gives:

$$\therefore e^{f\eta_{oc}} = \left(\frac{P_O}{P_{Oref}}\right) + \frac{j_{o,M}}{j_{o,O}}\left[\frac{C_M^C}{C_{Mref}}\left(\frac{P_O}{P_{Oref}}\right)^{0.5} e^{\alpha_M f(E_{oc}-E_M^o)+\alpha O2 f(E_{oc}-E^o_{cell}-E^o_M)}\right] \quad \ldots (6.9)$$

Taking logarithm of both sides and solving gives:

$$\therefore E_{oc} = \frac{1}{f}\ln\left[\left(\frac{P_O}{P_{Oref}}\right) + \frac{j_{o,M}}{j_{o,O}}\left(\frac{C_M^C}{C_{Mref}}\left(\frac{P_O}{P_{Oref}}\right)^{0.5} e^{\alpha_M f(E_{oc}-E_M^o)+\alpha_{O_2} f(E_{oc}-E^o_{cell}-E^o_M)}\right)\right] + E^o_{O2} \quad \ldots (6.10)$$

The above equation relates the open circuit polarisation at the cathode to the log of methanol concentration at the cathode and is used to calculate the open circuit cathode potential.

6.2.2 Model for Cathode Polarisation

A model for cathode polarization, taking into account the crossover of methanol to the cathode side, is obtained from Eq. 6.8:

$$\therefore j = j_{o,O}\left[\frac{P_O}{P_{Oref}} e^{\left(-\alpha_{O_2} f(E-E^o_{O_2})\right)} - e^{\left(1-\alpha_{O_2} f(E-E^o_{O_2})\right)}\right] \quad \ldots. (6.11)$$
$$+ j_{o,M}\left[\frac{C_M^C}{C_{Mref}}\left(\frac{P_O}{P_{Oref}}\right)^{0.5} e^{\left(\alpha_M f(E-E^o_M)\right)} - \frac{P_{CO_2}}{P_{CO_2ref}} e^{-\left(1-\alpha_M\right) f(E-E^o_M)}\right]$$

Adopting a high field approximation for higher overpotential [155] (i.e. assuming Tafel kinetics) Eq. 6.11 reduces to:

$$\therefore j = j_{o,O}\left[\frac{P_O}{P_{Oref}} e^{-\alpha_{O2} f(E-E^o_{O_2})}\right] + j_{o,M}\left[\frac{C_M}{C_{Mref}}\left(\frac{P_{O_2}}{P_{O_2 ref}}\right)^{0.5} e^{\alpha_M f(E-E^o_M)}\right] \quad \ldots (6.12)$$

Let the cathode overvoltage polarisation due to methanol crossover (η_{Po}) be $\eta_{Po} = E - E_{O^o_2}$ and $E^o_{Cell} = E^o_{O_2} - E^o_M$,

$$\therefore j = j_{o,O}\left[\frac{P_O}{P_{Oref}} e^{-\alpha_{O_2} f \eta_{Po}}\right] + j_{o,M}\left[\frac{C_M}{C_{Mref}}\left(\frac{P_{O_2}}{P_{O_2 ref}}\right)^{0.5} e^{\alpha_M f(\eta_{Po}+E^o_{cell})}\right] \quad \ldots (6.13)$$

Multiplying both sides by $e^{(\alpha_{O_2} f \eta_{Po})}$ and further simplifying gives:

$$\therefore j \times y = j_{o,O}\left[\frac{P_O}{P_{Oref}}\right] + j_{o,M}\left[\frac{C_M}{C_{Mref}}\left(\frac{P_{O_2}}{P_{O_2 ref}}\right)^{0.5} e^{\alpha_M f E^o_{cell}} \times y^{\left(1+\frac{\alpha_M}{\alpha_{O_2}}\right)}\right] \quad \ldots (6.14)$$

where, $y = e^{(\alpha_{O_2} f \eta_{Po})}$

The above equation relates the cathode overvoltage polarisation due to methanol crossover to the log of methanol concentration at the cathode side of the DMFC and is used to model the cathode polarisation in the presence of methanol at the cathode.

6.2.3 Cathode Model taking into account the Methanol Crossover

Let the cathode polarisation $(\eta_{Cathode})$, taking into account the methanol crossover from the anode to cathode, be given by:

$$\eta_{Cathode} = E - E_{oc} \quad \ldots (6.15)$$

The cathode overvoltage polarisation (η_{Po}) due to methanol crossover is the difference between the standard oxidation potential and the cathode potential i.e.

$$\eta_{Po} = E - E^o_{O_2} \quad \ldots (6.16)$$

Adding and subtracting E_{oc} to the right hand side of Eq. 6.6 and rearranging:

$$\eta_{Po} = \eta_{cathode} + E_{oc} - E^o_{O_2} \quad \ldots (6.17)$$

Finally, from the Eq. 6.17, a cathode polarisation model that takes into effect the crossover of methanol from the anode to the cathode is given by:

$$\eta_{Cathode} = \eta_{Po} - E_{oc} + E^{o}_{O_2} \quad \text{... (6.18)}$$

Equation 6.18 is a function of cell current density and methanol concentration at the cathode side of the cell. This equation is then used to model the cathode behaviour in the presence of methanol at the cathode as a function of cell current density, cell temperature and cell voltage.

6.2.4 Simplified Anode Model

The Kinetics of the oxygen reduction reaction can be well described by the Tafel equation whereas the kinetics of methanol oxidation exhibits non-Tafel behaviour [95]. Hence in this work, instead of a Tafel based model, a kinetic based model developed in Chapter 5 is used to model the anode polarisation curve. In Appendix H, the suitability of the kinetic based anode model over Tafel based anode model is shown by comparing the fit of both models to the anode polarisation data.

The anode model, developed in Chapter 5, for methanol oxidation at the anode of a DMFC [38] is given by:

$$j_{M,Anode} = n \times F \times k_2 e^{\left(\frac{\alpha_2 FE}{RT}\right)} \left(\frac{k_1 C^a_M}{k_2 e^{\left(\frac{\alpha_2 FE}{RT}\right)} + k_1 C^a_M} \right) \quad \text{... (6.19)}$$

where, $j_{M,Anode}$ is the current density at the anode (A m^{-2}), k_1 and k_2 are the kinetic parameters for the methanol oxidation reaction at the anode, C^a_M is the concentration of methanol at the anode and α_2 is the electrochemical transfer coefficient for the methanol oxidation reaction at the anode.

Rearranging the above equation gives:

$$e^{\left(\frac{\alpha_2 FE}{RT}\right)} = \left(\frac{j_{M,Anode} . k_1 C^a_M}{nFk_1 k_2 C^a_M - j_{M,Anode} k_2} \right) \quad \text{... (6.20)}$$

Further simplification by taking logarithm on both sides gives:

$$E = \frac{RT}{\alpha_2 F}\ln\left(\frac{j_{M,Anode}}{nFk_2}\right) - \ln\left(1 - \frac{j_{M,Anode}}{nFk_1 C_M^a}\right) + E_M^o \quad \ldots (6.21)$$

Equation 6.21 describes the anode polarisation behaviour as a function of methanol concentration at the anode (C_M^a), cell temperature and anode current density ($j_{M,Anode}$).

6.2.5 Ohmic Resistance

Recent work by Scott et al., (2006) [82] applied the model given in Eq. 6.1 to experimental data and produced a set of electrochemical parameters consistent with the individual cell component. Scott et al., (2006) observed that the values of resistivity (R_e) in Eq. 6.1 can be described by the expression:

$$R_e = R_o \exp\left(\frac{B}{T} - \frac{B}{T_o}\right) \quad \ldots (6.22)$$

where, $R_o = 0.085 \times 10^{-4}\ \Omega\ m^2$, is the resistance at temperature, $T_o = 383.15$ K and $B = 3724$, is a constant.

Based on the above relationship (Eq. 6.22), in this work, the ohmic resistance ($\eta_{Ohmic} = R_e \times j_{Cell}$) which is assumed to be mainly due to the internal resistance from the Nafion® membrane, (Eq. 6.2), was modelled.

6.2.6 Methanol Concentration in Anode and Cathode Region

The characteristic polarization curve for the cathode and anode, taking into account the crossover of methanol, can be obtained from the analytical solution of Eq. 6.10, 6.14 and 6.21 respectively. To obtain the current density versus potential response from these model equations, the concentration of methanol at the anode (C_M^a) and cathode catalyst regions (C_M^c) needs to be estimated. Figure 6.1, describes schematically the methanol concentration profile across the cell. The concentration of methanol at the anode backing layer is assumed to be the same as the feed concentration (C_M^f), since the variation of methanol concentration in the anode feed channel is assumed to be negligible. In addition, the concentration of methanol at the anode and cathode catalyst layer was assumed to be constant [67]. Based on these

assumptions, the relationship for the concentration of methanol at the anode and cathode catalyst layer is developed in the subsequent sections.

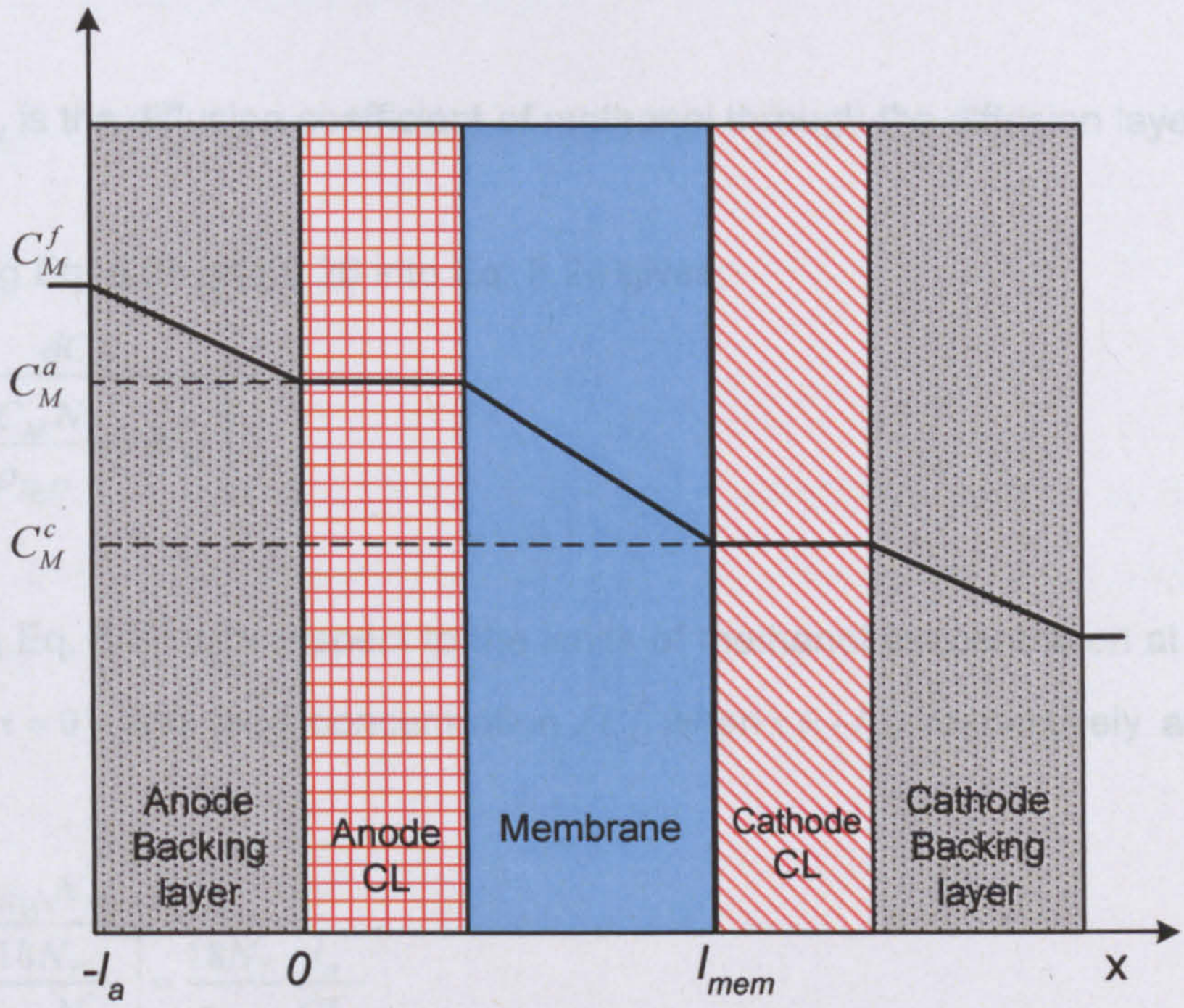

Figure 6.1: Methanol concentration profile across the cell

6.2.6.1 Methanol Concentration at the Anode Side

In a DMFC, at the anode side, the total flow (N_T) is the sum of the methanol $(N_M^{'})$ and water flow (N_{H_2O}):

$$N_T = N_M^{'} + N_{H_2O} \quad \ldots (6.23)$$

The methanol flux through the diffusion layer is a combination of diffusion (N_{Diff}) and convection $(x_M N_T)$:

$$N_M^{'} = N_{Diff} + x_M N_T \quad \ldots (6.24)$$

Generally a dilute methanol solution is used in a DMFC (i.e. $C_M << C_{H_2O}$), hence the local mole fraction of methanol (x_M) can be approximated by:

$$x_M = \frac{C_M}{C_{H_2O} + C_M} \cong \frac{C_M}{C_{H_2O}} \cong \frac{18 \times C_M}{\rho_{H_2O}} \quad \ldots (6.25)$$

The diffusion flux of methanol (N_{Diff}) is given by Fick's law:

$$N_{Diff} = -D_{DL}^{e} \frac{dC_M}{dx} \quad \ldots (6.26)$$

where, D_{DL}^{e} is the diffusion coefficient of methanol through the diffusion layer ($m^2\ s^{-1}$).

Substituting Eq. 6.25 and 6.26 into Eq. 6.24 gives:

$$\frac{dx}{D_{DL}^{e}} = \frac{dC_M}{\left(\frac{18C_M N_T}{\rho_{H_2O}} - N_M^{'}\right)} \quad \ldots (6.27)$$

Integrating Eq. 6.27 with respect to the limits of methanol concentration at the anode ($C_M^a \; when \; x = 0$) and feed concentration ($C_M^f \; when \; x = -l_a$) respectively and solving gives:

$$\ln\left[\frac{C_M^a - \frac{\rho_{H_2O} N_M^{'}}{18N_T}}{C_M^f - \frac{\rho_{H_2O} N_M^{'}}{18N_T}}\right] = \frac{18N_T}{\rho_{H_2O}} \frac{l_a}{D_{DL}^{e}} \quad \ldots (6.28)$$

From this relationship, the anode reaction methanol concentration can be determined subject to determining the total water flow (N_T) in the anode diffusion layer.

6.2.6.2 Methanol Concentration at the Cathode Side

In the cathode side of the DMFC, methanol is consumed by the reaction or is lost by vaporization (N_M^{vap}) due to high temperatures at the cathode:

$$\therefore N_M = \frac{j_M}{4F} + N_M^{vap} \quad \ldots (6.29)$$

The methanol is supplied to the cathode from the anode through the membrane by a combination of diffusion and electro-osmosis as it is dissolved in water [19, 25]. Thus the methanol flux through the membrane is given by:

$$N_M = \frac{\lambda_M j}{F} + \frac{(-D_{Mem}^{e}) dC_M}{dx} \quad \ldots (6.30)$$

where, λ_M is the drag coefficient for methanol obtained from the drag coefficient of water (λ_{H_2O}) using the relationship $\lambda_M = 18\lambda_{H_2O} C_M / \rho_{H_2O}$ and D^e_{Mem} is the diffusion coefficient of methanol through membrane ($m^2\ s^{-1}$).

Substituting the drag coefficient for methanol into Eq. (6.30) gives:

$$\frac{dx}{D^e_{Mem}} = \frac{dC_M}{\frac{18\lambda_{H_2O} j C_M}{\rho_{H_2O} F} - N_M} \qquad \ldots (6.31)$$

Integrating Eq.6.31 with respect to the limits of methanol concentration at the anode $(C^a_M \text{ when } x = 0)$ and methanol concentration at the cathode $(C^c_M \text{ when } x = l_m)$ respectively and solving gives:

$$\ln\left[\frac{C^c_M - \frac{\rho_{H_2O} N_M F}{18\lambda_{H_2O} j}}{C^a_M - \frac{\rho_{H_2O} N_M F}{18\lambda_{H_2O} j}}\right] = j\frac{18\lambda_{H_2O}}{\rho_{H_2O} F}\frac{l_m}{D^e_{Mem}} \qquad \ldots (6.32)$$

This gives the cathode methanol concentration (C^c_M) as a function of the anode methanol concentration (C^a_M) and cell current density (j). The relationship gives the cathode concentration which when coupled to the cathode polarization equation enables the effect of crossover on the cell to be determined.

6.2.7 Water Transport, Methanol Flux and Total Flow

Water transport (N_{H_2O}) and methanol flux (N'_M) at the anode side of the cell are crucial for determining the concentration of methanol at the anode and cathode sides.

Methanol Flux (N'_M):

In a DMFC, the consumption of methanol occurs at both the anode and cathode sides of the cell. The consumption of methanol in the cathode is almost complete with a small quantity of water and carbon dioxide being released into the cathode exhaust stream. As the only source of methanol is from the anode side of the cell, the transfer of methanol in the anode diffusion layer must be equal to the net consumption of methanol in the cell in addition to any methanol evaporated from the

cathode. In general, methanol consumption in a DMFC is through reaction flux at the anode and the consumption of methanol at the cathode, which results in:

$$N_M^{'} = \frac{j}{6F} + \frac{j_M}{4F} + N_M^{vap} \quad \ldots (6.33)$$

To calculate the methanol vapour flux (N_M^{Vap}), it is assumed that the methanol in the air is in equilibrium with the liquid at the cathode, which obeys Dalton's and Raoult's laws [154]:

$$\therefore p_M = y_M P_{cathode} = x_{M,l} \gamma_M p_M^s \quad \ldots (6.34)$$

where, p_M is the partial pressure of methanol, y_M is the mole fraction of methanol vapour in cathode side, $P_{cathode}$ pressure at the cathode, $x_{M,l}$ is the liquid phase mol fraction of methanol, which is a function of the methanol concentration, γ_M activity coefficient of methanol p_M^s is the vapour pressure of pure methanol which is a function of temperature.

The rate of methanol vapour removal is then given by:

$$N_M^{vap} = \left(\frac{p_M}{RT}\right) * \frac{\upsilon_{air}}{A_{membrane}} = \frac{x_{M,l} \gamma_M p_M^s \upsilon_{air}}{RTA_{membrane}} \quad \ldots (6.35)$$

where, υ_{air} is volumetric flow rate of air (6.67 X10^{-6} m^3 s^{-1}), $A_{membrane}$ is the area of membrane 9 X 10^{-4} m^{-2}. Here $x_{M,l}$, γ_M and P_M^s are calculated using equations developed by Argyropoulos et al., (1999) [154].

Water Transport (N_{H_2O})**:**

In a DMFC, water transport results from three factors,

i) Water required for the anode reaction, $(N_a = j/6F)$,

ii) Electro-osmotic water transfer through the membrane with H^+ ions, $(N_{drag} = \lambda_{H_2O} j/F)$,

iii) Diffusion across the membrane, which is assumed negligible at high current density [83].

In addition to these three factors, water is also formed at the cathode by oxygen reduction, $\left(N_{H_2O}^{O_2} = \frac{j}{2F} \right)$ and lost as vapour from the cathode flow channel $(N_{H_2O}^{Vap})$:

$$\therefore N_{H_2O}^{vap} = \left(\frac{p_{H_2O}}{RT} \right) * \frac{\upsilon_{air}}{A_{membrane}} = \frac{x_{H_2O,l} \gamma_{H_2O} P_{H_2O}^{s} \upsilon_{air}}{RTA_{membrane}} \quad \ldots (6.36)$$

where, $x_{H_2O,l}$ is the liquid phase mole fraction which is a function of methanol concentration, γ_{H_2O} is the activity coefficient of water and $P_{H_2O}^{s}$ is the vapour pressure of pure water which is a function of temperature. The loss of vapour from the cathode channel in Eq. 6.36 is calculated by estimating $x_{H_2O,l}, P_{H_2O}^{s}$ and γ_{H_2O} from the equations developed by Argyropoulos et al., (1999) [154].

This formation and loss of water at the cathode side is difficult to assess fully and hence with regard to the total water flow in the anode side of the cell, it is assumed that it is the sum of the electro-osmotic drag (N_{drag}), the net water formation at the anode (N_a) and cathode $(N_{H_2O}^{O_2})$ and that lost by vaporization $(N_{H_2O}^{Vap})$:

$$\therefore N_{H_2O} = \frac{\lambda_{H_2O} j}{nF} + \frac{(-j)}{2F} + \frac{j}{6F} + N_{H_2O}^{vap} \quad \ldots (6.37)$$

This enables the total water flow in the anode, Eq. (6.23), to be estimated approximately by combining Eq. (6.33) and Eq. (6.35) to (6.37).

$$\therefore N_T = N_{ME}^{'} + N_{H_2O} = \frac{j_M}{4F} + \frac{j}{6F} + N_{ME}^{vap} + \frac{\lambda_{H_2O} j}{F} - \frac{j}{3F} + N_{H_2O}^{vap} \quad \ldots (6.38)$$

Combining Eq. 6.38 with Eq. (6.28) and Eq. (6.32) gives the anode and cathode methanol concentration as a function of cell current density (*j*) and temperature.

6.3. Results and Discussion

Figure 6.2, illustrates the methanol concentration profile, obtained from Eqs. 6.28 and 6.32, for both the anode and cathode compartment of the DMFC with respect to the cell current density. The base case and operating parameters for estimating the methanol concentration profile and overall model is given in Table 6.1.

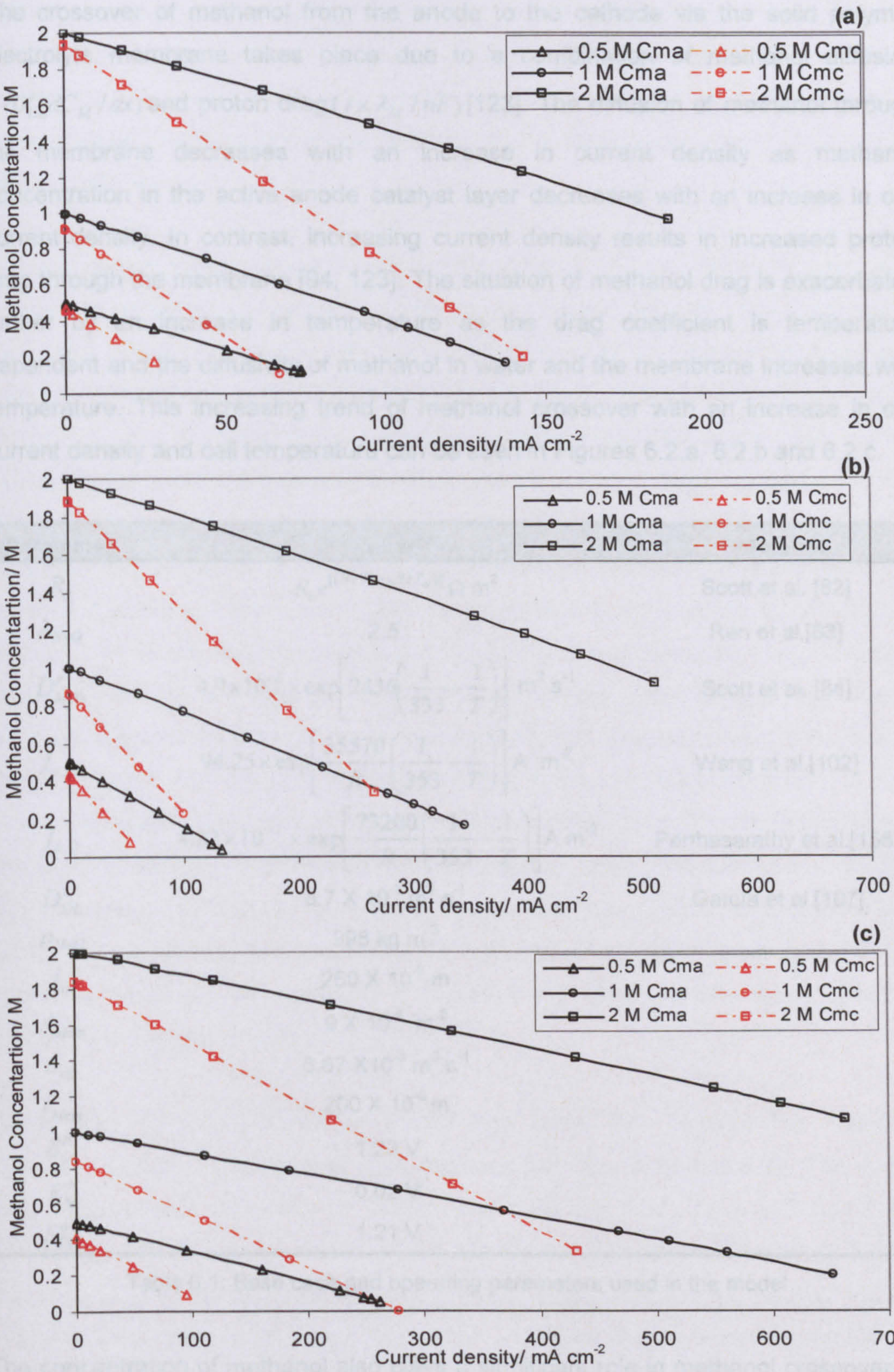

Figure 6.2: Methanol concentration profile at the anode (solid lines) and cathode (dotted lines) compartment with respect to cell current density at varying cell temperatures (a) 30 °C, (b) 60 °C and (c) 90 °C.

The crossover of methanol from the anode to the cathode via the solid polymer electrolyte membrane takes place due to a combination of methanol diffusion ($-D^{e}_{DL} dC_M / dx$) and proton drag ($j \times \lambda_M / nF$) [123]. The diffusion of methanol through the membrane decreases with an increase in current density as methanol concentration in the active anode catalyst layer decreases with an increase in cell current density. In contrast, increasing current density results in increased proton drag through the membrane [94, 123]. The situation of methanol drag is exacerbated further by an increase in temperature as the drag coefficient is temperature dependent and the diffusivity of methanol in water and the membrane increases with temperature. This increasing trend of methanol crossover with an increase in cell current density and cell temperature can be seen in Figures 6.2.a, 6.2.b and 6.2.c.

Parameter	Value	Reference
R_e	$R_o e^{[(B/T)-(B/T_o)]}$ Ω m^2	Scott et al. [82]
λ_{H_2O}	2.5	Ren et al.[63]
D^{e}_{Mem}	$4.9\times10^{-6}\times\exp\left[2436\left(\frac{1}{333}-\frac{1}{T}\right)\right]$ m^2 s^{-1}	Scott et al. [84]
$j_{o,M}$	$94.25\times\exp\left[\frac{35570}{R}\left(\frac{1}{353}-\frac{1}{T}\right)\right]$ A m^{-2}	Wang et al.[102]
$j_{o,O}$	$4.22\times10^{-2}\times\exp\left[\frac{73200}{R}\left(\frac{1}{353}-\frac{1}{T}\right)\right]$ A m^{-2}	Parthasarathy et al.[156]
D^{e}_{DL}	8.7 X 10^{-5} m^2 s^{-1}	García et al.[107]
ρ_{H_2O}	998 kg m^{-3}	
l_a	260 X 10^{-6} m	
A_{Mem}	9 X 10^{-4} m^{-2}	
υ_{air}	6.67 X10^{-6} m^3 s^{-1}	
l_{Mem}	200 X 10^{-6} m	
$E^{o}_{O_2}$	1.23 V	
E^{o}_{M}	0.02 V	
E^{o}_{Cell}	1.21 V	

Table 6.1: Base case and operating parameters used in the model

The concentration of methanol also plays a significant role in methanol crossover as seen in Figures 6.2.a, 6.2.b and 6.2.c. The availability of methanol at the cathode almost doubles with an increase in methanol concentration from 0.5 M to 2 M at the anode. For a 2 M concentration, irrespective of cell temperature, there is sufficient unused methanol available at the anode catalyst layer, which can crossover to the

cathode decreasing cell efficiency due to the mixed potential. Hence to gain the best performance and better fuel economy, 0.5 M and 1 M are suitable choices. These results are in agreement with the results from the parametric study in Chapter 3, which showed that a methanol concentration of 1 M is suitable for attaining optimum DMFC performance.

The analytical solution of Eq. 6.29, Eq. 6.33 and Eq. 6.37 using LabVIEW [115] gave a profile of methanol and water flux with varying current density. The variations in water and methanol flux rates with cell current density for varying temperatures and methanol concentrations are shown in Figures 6.3.a, 6.3.b and 6.3.c. It is clear from Figure 6.3.a that the water flux is higher than the methanol flux at any given current density as the aqueous methanol solution used in a DMFC is predominantly water. With an increase in current density the methanol flux through anode and membrane increases and is higher at higher temperatures and methanol concentrations, as shown in Figures 6.3.b and 6.3.c. This is mainly due to an increase in diffusivity of methanol in water and the membrane [94]. The electro-osmotic drag becomes dominant, with an increase in the cell current density, compared to that due to diffusion of methanol through the membrane [81, 94]. The dominating influence of electro-osmosis can be seen in Figures 6.3.a, 6.3.b and 6.3.c especially at high current densities where the flux increases approximately linearly with an increase in cell current density. Thus this overall increase in drag coefficient, due to high temperatures, as shown in Figure 6.3.b, results in a higher methanol crossover rate across the membrane. The situation is exacerbated even further by the availability of additional methanol, as observed in Figure 6.3.c, at the anode when a higher concentration of methanol is used [72, 94, 123].

Finally, the cathode polarisation model that takes into account the methanol crossover and the anode model were obtained from Eq. 6.18 and 6.21. The output from these models along with the ohmic resistance (Eq. 6.22), on substitution in the overall cell model, Eq. 6.2, resulted in a complete cell model that accounts for the crossover of methanol through the membrane. Figure 6.4 illustrates the fit of the cell model to the experimental data from a 9 cm^2 DMFC at varying temperatures (30, 60 and 90 °C) and methanol concentrations (0.5, 1 and 2 M). From Figure 6.4 it can be seen that the model predictions agree favourably with the experimental data. In particular, the anode model describes the anode polarisation curve accurately. Both the experimental data and model plots, Figures 6.4.a, 6.4.b and 6.4.c, show that the

anode polarisation curve is particularly sensitive to temperature as compared to the cathode polarisation curve. This implies that by increasing the temperature, DMFC performance is improved mainly due to the improvement at the anode side [89]. Higher temperatures increase the kinetics of methanol oxidation on dual site Pt-Ru catalyst. Ru demonstrates increased activity for the methanol oxidation reaction principally during the water discharge reaction at high temperatures, due to which an overall increase in the methanol oxidation kinetics occurs [44, 81, 119]. These results are in accord with the analysis of the anode limiting current from the parametric study in Chapter 3.

The values of different parameters estimated by fitting the model to the experimental data along with the standard values used in the model are given in Table 6.2. The temperature dependence of the kinetic parameters can be observed in Table 6.2, where the fitted kinetic parameters increase exponentially with an increase in temperature in an Arrhenius approximation [29, 100, 101]. In addition, the model fit in Figure 6.4 at different concentration using the fitted kinetic parameters suggests that the electrochemical transfer coefficient and the kinetic parameters are effectively concentration independent.

Parameters	Fit at 30 °C	Fit at 60 °C	Fit at 90 °C
k_1	8 X 10^{-6} m s^{-1}	7.15 X 10^{-5} m s^{-1}	1.24 X 10^{-4} m s^{-1}
k_2	5.3 X 10^{-7} mol $m^{-2}s^{-1}$	1.1 X 10^{-6} mol $m^{-2}s^{-1}$	1.8 X 10^{-6} mol $m^{-2}s^{-1}$
α_2	0.34	0.48	0.6
α_M	0.42	0.45	0.48
α_{O_2}	0.9	0.92	0.94

Table 6.2: Kinetic parameters estimated from the model

The cathode open circuit potential (shown by filled markers in Figure 6.4) indicates that with an increase in methanol concentration, the cathode open circuit potential decreases due to the increase in mixed potential effect caused by an increase in the concentration of methanol at cathode [92]. The situation is exacerbated further with an increase in temperature as high temperatures favour methanol oxidation at the active platinum catalyst site at the cathode catalyst layer.

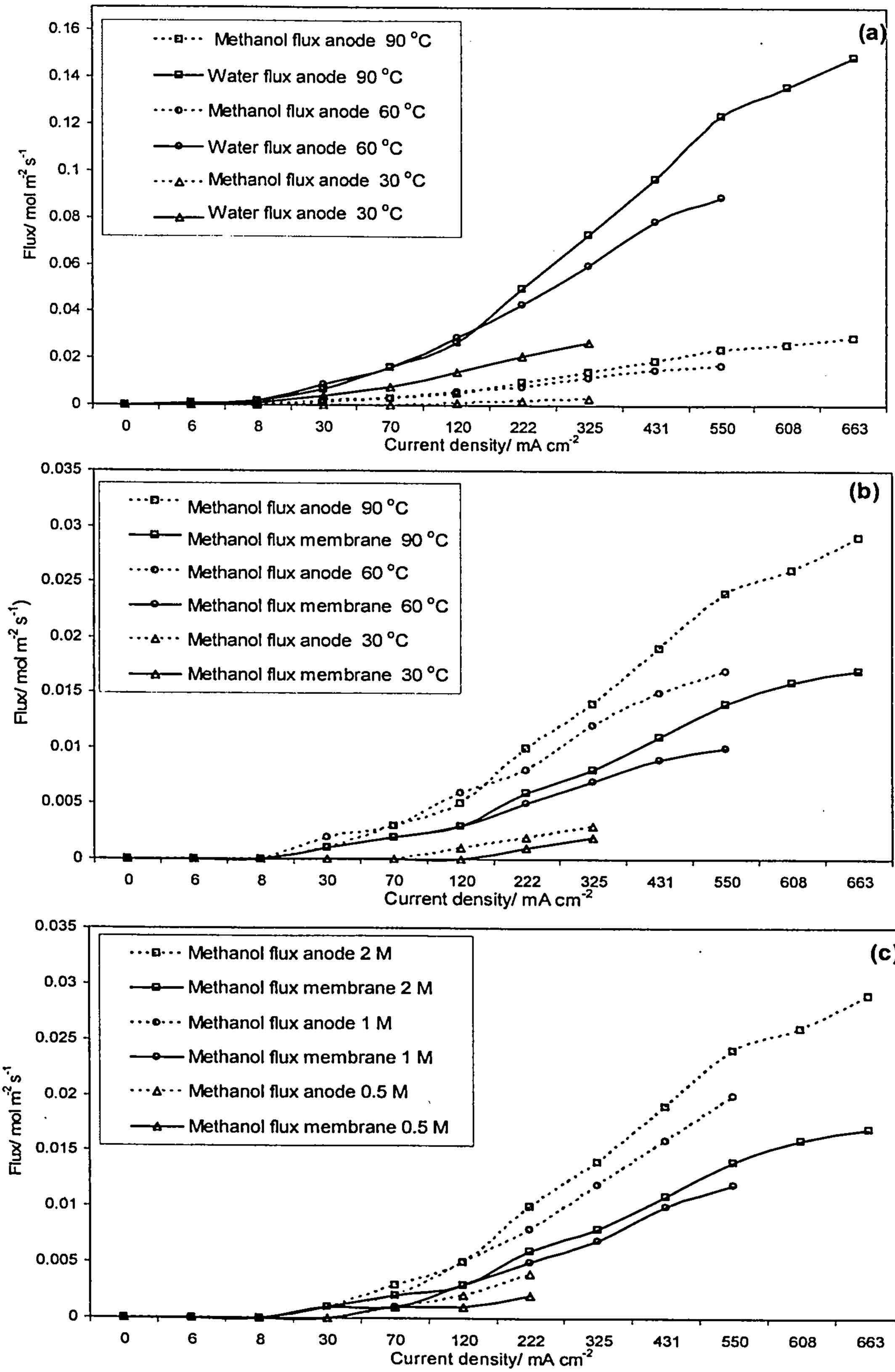

Figure 6.3: Flux across anode and membrane (a) water and methanol flux in anode region for 2 M concentration at varying temperatures, (b) methanol flux across membrane and anode for 2 M concentration at varying temperatures and (c) methanol flux across membrane and anode for 90 °C and various methanol concentrations

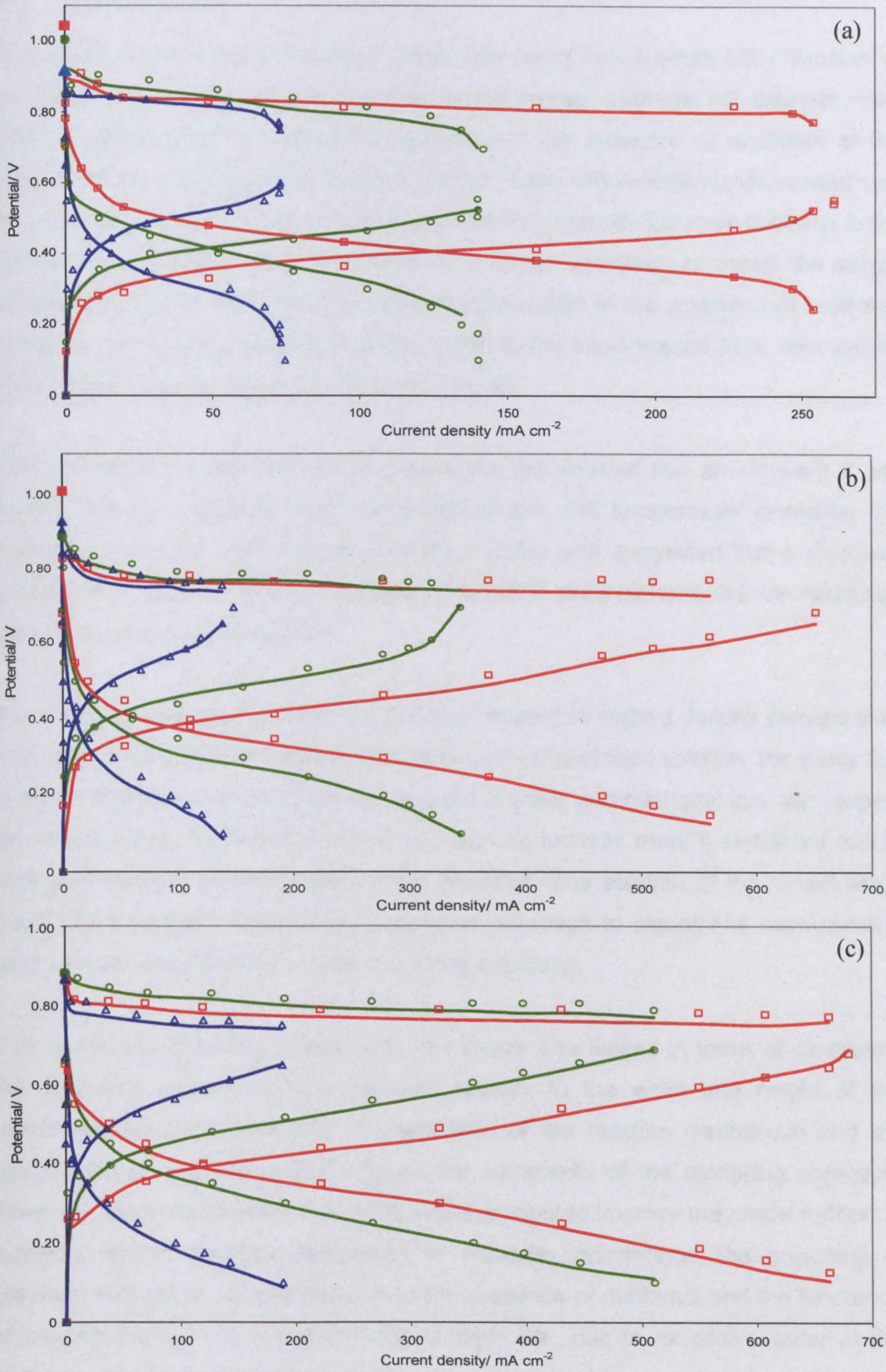

Figure 6.4: Model versus Experimental fit for varying cell temperatures (Δ: 30 °C, ○: 60 °C, □ : 90 °C) and at varying methanol concentrations (a) 0.5 M, (b) 1 M and (c) 2 M. Filled markers are the cathode open circuit potential for respective temperatures and concentrations.

6.4. Conclusions

A semi empirical, one dimensional, model that takes into account the crossover of methanol was developed. The cathode model helped estimate the cathode open circuit potential and the cathode polarisation in the presence of methanol at the cathode. The model predicted that the cathode open circuit obtained decreased with an increase in methanol concentration and cell temperature due to an increase in the mixed potential effect. The application of a kinetic approach to model the anode polarisation and the estimation of cathode polarisation in the presence of methanol crossover gave an acceptable fit of the model to the experimental data, overcoming the limitations of previous published work [79, 80].

The methanol concentration profile across the cell showed that an increase in cell current density, methanol feed concentration and cell temperature increases the methanol crossover rate. The concentration profile also suggested that a methanol concentration above 1 M is not suitable for a DMFC since higher crossover rates and lower fuel economy materialises.

The change in water and methanol flux with respect to current density showed that, due to the dominance of water in the aqueous methanol feed solution, the water flux is higher than the methanol flux. An increase in water and methanol flux with respect to current density implies that the electro-osmotic process plays a significant role in methanol transfer at higher cell current densities. The solution of the model using LabVIEW provided a flexible and interactive approach to algorithmic development, which greatly simplified the overall modelling approach.

Due to the one dimensional approach, the model was limited in terms of computing the methanol concentration profile with respect to the width and height of the membrane electrode assembly. Simplification of the reaction mechanism and the assumption of a single phase reduced the complexity of the modelling approach. However, these parameters should be taken account to improve the model further. In addition, for an accurate description of cathode performance, the poisoning of platinum catalyst at the cathode due to the presence of methanol and the hindrance of oxygen transport to active cathode catalyst site, due to excessive water at the cathode, should also be taken into account.

Chapter 7
CONCLUSIONS AND FUTURE WORK

7.1. Conclusions

The DMFC is a commercially attractive source for power generation with possible applications in the field of transport and portable power supply. However, there are limitations related to the poor methanol oxidation kinetics and methanol crossover restricting its widespread application. The objective of the thesis was to investigate these limitations through the application of statistically designed experiments and steady state modelling techniques. The following sections summarise the main conclusions drawn from the various studies.

7.1.1 Statistical Design of Experiments

In Chapter 3, a parametric study based on a fractional factorial (2^{k-1}) experimental design with the addition of centre points to take account of the variability in the experimentation was utilised to investigate the main effects and interactions of six operating parameters in 36 experiments. The performance of the DMFC took into consideration the anode polarisation and the methanol crossover through the membrane and the traditional measure of peak power response. The analysis indicated that the peak power and anode limiting current response increased with an increase in temperature but at the cost of high methanol crossover. Further examination of the two-way interaction between cell temperature and methanol concentration revealed that a combination of low methanol concentration and high temperature can balance the negative effect of high temperature and optimise the peak power output by taking into account the methanol crossover rate. In addition, the interaction of cell temperature with cathode back pressure and type of oxidant indicated that a high cell temperature in combination with oxygen at a high back pressure increases the peak power due to an increase in partial pressure of oxygen at the cathode and by negating the effect of methanol crossover. Based on these outcomes, an optimisation study was performed which gave a peak power performance of 105.12 mW cm^{-2} using oxygen and 69.03 mW cm^{-2} using air at the cathode, by limiting the negative effect of methanol crossover.

In Chapter 4, a sequential method of applying response surface methodology (RSM) to optimise the membrane electrode assembly (MEA) was demonstrated. The impact of catalyst loading, Nafion® content and PTFE content in the cathode and anode catalyst formulation was investigated through a full factorial design and a central composite design (CCD). The CCD highlighted the importance of high cathode catalyst loading (2 mg cm^{-2}) on both the peak power and cathode response. Moreover it revealed the quadratic behaviour of Nafion® content in the formulation of the catalyst layer and its significance in terms of determining the overall peak power and cathode output. The CCD analysis suggested than an optimum Nafion® loading of 20 to 30 %.wt in combination with a high catalyst loading (2 mg cm^{-2}) will result in the highest peak power and cathode output. In addition, the analysis also showed the negative effect of adding PTFE to the cathode catalyst layer and thus suggested its omission from the formulation of the cathode catalyst layer.

In contrast, the analysis of the anode response showed a positive effect of adding PTFE to the formulation of the anode catalyst layer. The analysis suggested that the addition of PTFE (10 - 20 %.wt), due to its hydrophobic characteristics, promotes the flow of gas and liquid to and from the active anode catalyst site thereby achieving the highest anode response. However in the absence of PTFE, in the anode catalyst layer formulation, the influence of Nafion® loading plays a dominating role in increasing anode performance. The two-way interaction between catalyst loading and Nafion® loading showed that the continuous network for proton conductivity is essential for the effective utilisation of the anode catalyst. Consequently a combination of high catalyst loading with high Nafion® loading results in a higher anode response in the absence of PTFE.

7.1.2 Semi Empirical Modelling

The dependence of the performance of the DMFC on catalyst loading and methanol crossover lead to an in-depth analysis of the methanol oxidation reaction on the dual site Pt-Ru catalyst and the development of a cell model that took into account methanol crossover.

Detailed kinetic models based on the well established dual site Gasteiger mechanism [119] were proposed in Chapter 5. The goal was to predict the performance of the electrode and the behaviour of the surface coverage of intermediates as a function of cell temperature, anode potential and methanol concentration. The models supported

the hypothesis that the Pt sites act as centres for the adsorption and dehydrogenation of methanol whilst the Ru sites act as a centre for CO oxidation. The resulting surface coverage of intermediate species from the detailed kinetic modelling approaches (Case A and Case B models in section 5.4.1 and 5.4.3 respectively) suggested that the anode polarises at a high potential due to the saturation of the methanol and/or the coverage of the catalyst site by hydroxyl ions. In addition, a curving back phenomenon in the anode polarisation was observed when the surface coverage of hydroxyl ions on the Pt site, for one of the modelling approaches (Case B model in section 5.4.3), was assumed to be similar to that of the Ru catalyst site. This curving back phenomenon suggested that the formation of hydroxyl ions at high potentials blocks the further adsorption of methanol on the Pt catalyst site leading to anode polarisation. By varying the reaction rate constants, the detailed kinetic models identified the adsorption of methanol and subsequent oxidisation to CO on the dual site catalyst site as the limiting step. The need for real time responses necessitated the development of simplified three parameter kinetic model (section 5.6) based on the output of the detailed models. This model can be readily applied to a complete system or a stack system.

To understand the effect of mixed potential at the cathode due to the crossover of methanol through the membrane, a model to predict cell performance as a function of cell current density, temperature and concentration was proposed in Chapter 6. The model helped estimate the cathode open circuit potential by taking into account the methanol crossover and the results indicated that it decreases with an increase in cell temperature and methanol concentration. Comparison of the anode and the cathode polarisation models revealed that an increase in temperature mainly increases the anode cell polarisation compared to the cathode polarisation due to the enhanced kinetics of methanol oxidation on the dual site Pt-Ru catalyst.

The methanol concentration profile from the modelling approach supported the results from the parametric study. It illustrated that an increase in the cell current density, methanol feed concentration and the cell temperature increases the methanol crossover rate due to which a methanol concentration above 1 M is not a suitable choice for the DMFC. The application of the kinetic model for the modelling of the anode polarisation as opposed to the Tafel equation, whilst estimating the cathode open circuit potential and polarisation in the presence of methanol crossover, gave an acceptable fit with experimental data.

The models were developed using, LabVIEW [115]. Due to its dataflow modelling structure, the models were straight forward to develop and can be easily associated with LabVIEW test station or controllers for control applications and real time simulation.

7.2. Future Work

In this thesis, the application of experimental design and modelling has been adopted to better understand the phenomena occurring within the DMFC. The results from the statistical analysis showed that the interaction between various electrochemical, design and operating parameters hold the key to optimising the performance of the DMFC by taking into account the negative effect of crossover. In addition, the outcome from the modelling approach identified the significance of various reaction intermediates, kinetic mechanisms and the effect of mixed potential on the overall performance of the DMFC. However, there are still issues related to overall DMFC performance, which need further in-depth investigation. To address this further, the following research is proposed.

7.2.1 Statistical Design of Experiments

A general rule in experimental design is to ensure that the factor levels are sufficiently far apart to allow the effect to be observed [113]. However, the levels should be within the boundaries that are achievable in full scale operation. In addition, by improving the accuracy of the measurement, the ability of the experimental design to detect an effect and interaction can be increased [112]. Hence in future experimental design, an optimum setting for the operating parameters should be investigated by taking into account a range of reactant flow rates and using precise measurements of methanol crossover, such as measuring the carbon dioxide concentration at the cathode exit [157, 158].

In Chapter 4, the objective was to demonstrate the application of RSM. Three factors, catalyst loading, Nafion® content and PTFE content were selected on the basis of a literature review and their significance in terms of the membrane electrode assembly (MEA) fabrication. However, in future a screening experimental design should be investigated where factors such as supported or unsupported catalyst layer, metals loading, type of solvent, etc are induced to identify the key factors and interactions impacting the MEA fabrication.

Analysis of the statistical design for catalyst layer optimisation showed that the addition of PTFE is beneficial for anode catalyst formulation whereas it is ineffective for cathode catalyst layer formulation. In this study, the anode and cathode catalyst formulation were varied simultaneously. However, there may be an interaction between the anode and cathode response as the measurement sytem and overall reaction mechanisms are interrelated. Hence to identify an independent recipe for the cathode and anode catalyst layer, it is proposed to apply RSM by fixing the catalyst layer formulation of one electrode and changing the formulation for the other electrode according to the design. The use of RSM can also be applied in optimising individual single electrode behaviour in alternative studies focused on the interaction of the electrode layer with the ionomer membrane.

The MEA is the heart of the DMFC. To further optimise its performance, the gas diffusion layer (GDL) and the micro-porous layer (MPL) which control the ingress of liquid and gas to and from the active catalyst site should be optimised. A number of factors affect the GDL and MPL composition and thus have a significant influence on the overall performance of the DMFC. These factors include the type of gas diffusion layer (carbon cloth or carbon paper), carbon material (Ketjen Black, Vulcan XC-72 or Acetylene Black), loading of the carbon (1 to 5 mg cm^{-2}), addition of PTFE (0 to 40%), and deposition method (tape casting, screen painting or spraying). To date there has been no published study which systematically optimises the formulation of the GDL and MPL whilst taking into account the variability associated with the experiment [6]. The systematic application of experimental design can be used to screen and optimise the important factors affecting GDL and MPL formulation so that maximum catalyst utilisation can be achieved and the performance of the DMFC further improved.

Finally as shown in Figure 7.1, the performance of the DMFC depends on various electrochemical, design and operating parameters which in turn depend on other key factors. The sheer number of permutations for identifying the critical interactions due to the number of factors involved is not possible to achieve with a one-factor-at-a-time study. The detection of these key interactions utilising a reduced number of experimental runs through the application of experimental design, as shown in Chapter 3 and 4, is the way to further increase the performance of the DMFC.

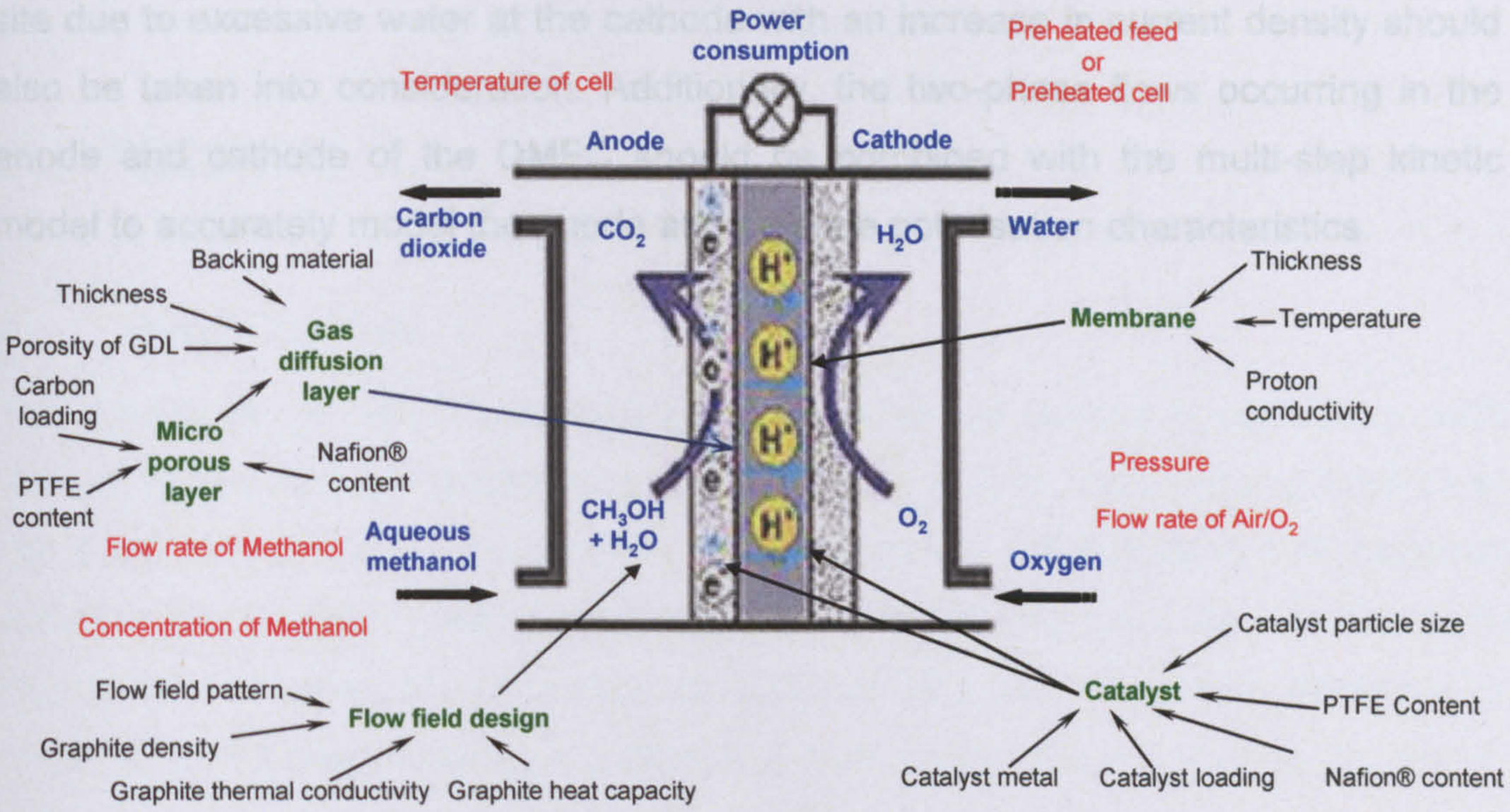

Figure 7.1: Factors affecting the performance of the DMFC

7.2.2 Semi Empirical Modelling

The models presented in this thesis are reduced one-dimensional models, which are valid for the activation controlled and ohmic regions of the DMFC polarisation curve. These can be extended or adapted to different DMFC designs. During the anode modelling simulation, it was observed that by varying the kinetic rate constants the surface coverage of the intermediates species can be manipulated while still obtaining a reasonable fit to the anode polarisation curve. Hence in future, to further validate the kinetic constants and the modelled coverage at particular operating conditions, the behaviour of the intermediate species with respect to temperature, concentration and potential should be estimated through the approach of modern spectroscopic tools such as Fourier Transform Infra-red Spectroscopy (FTIR) [120, 150] and corroborated with the model. Further refinement of the anode models can be achieved by adding more realistic conditions to the original reaction expressions. This could include the non-ideal distribution of the platinum and ruthenium, which would influence the impact of the reaction constants (k_3 and k_4) and the addition of rate expressions for the significantly more complex and stable intermediates.

Similar to the anode model, instead of the Butler-Volmer equation a detailed kinetic model for the cathode that takes taking into account the presence of methanol on the cathode platinum catalyst site should be developed to improve the cathode polarisation model. The inactivity of the platinum catalyst due to adsorbed intermediates and the hindrance of oxygen transport to the active cathode catalyst

site due to excessive water at the cathode with an increase in current density should also be taken into consideration. Additionally, the two-phase flows occurring in the anode and cathode of the DMFC should be combined with the multi-step kinetic model to accurately model the anode and cathode polarisation characteristics.

APPENDIX

A. Durability Test

The stability of the DMFC was tested by monitoring the change in cell voltage with working time during galvanostatic operation, Figure A.1, at loads ranging from 11 to 194.4 mA cm^{-2} at 90 °C for a duration of approximately 145 hrs using 1 M methanol at the anode (5 ml min^{-1}) and oxygen at the cathode (400 ml min^{-1}). As observed from Figure A.1, an open circuit voltage of 623 mV at zero cell current density was obtained during galvanostatic operation and as expected the cell voltage decreased with an increase in cell current density.

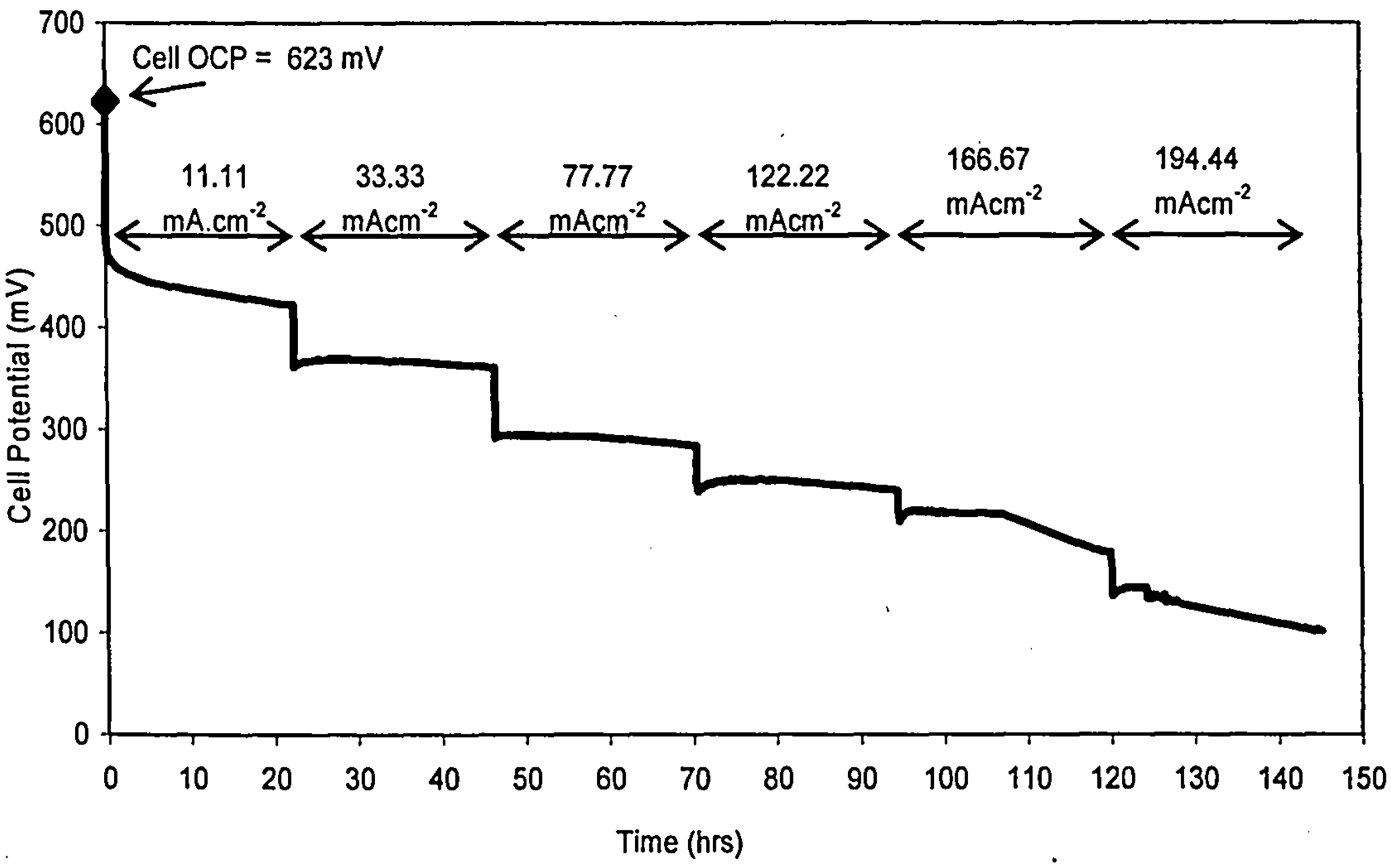

Figure A.1: Durability test at 90 °C under varying load conditions using 1 M methanol at the anode (5 ml min^{-1}) and oxygen at the cathode (400 ml min^{-1})

Similar test results were obtained during potentiostatic operation, Figure A.2, where the current density was monitored and the cell voltage was increased from 100 to 500 mV for duration of approximately 60 hrs. Potentiostatic operation also showed that with an increase in cell voltage there was a decrease in cell current density. Both durability tests, Figures A.1 and A.2, also showed that DMFC performance was relatively stable. The only fluctuation in cell output was when a change in current

density or cell voltage was introduced. Performance started to deteriorate when the cell was operated above 167 mA cm^{-2} or above 200 mV for both the stability studies. This deterioration in performance can be attributed primarily to mass transport limitation in the DMFC. At high loads, the cell generates more carbon dioxide which generally blocks access of the fresh methanol to the reactive catalyst site resulting in a decrease in performance. Hence DMFCs are generally not operated near the mass transport limitation region [10].

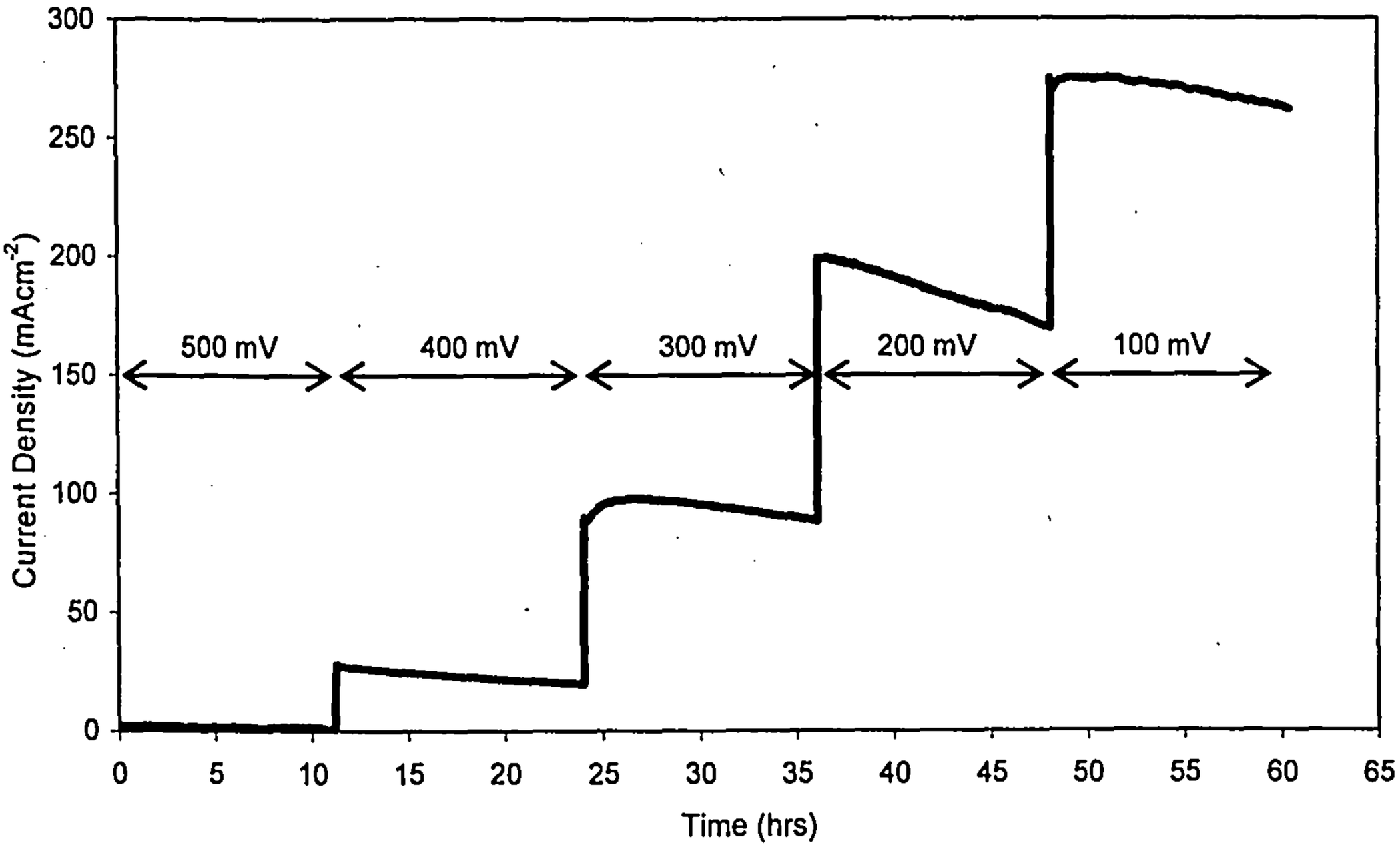

Figure A.2: Durability test at 90 °C under varying cell voltage using 1 M methanol at the anode (5 ml min^{-1}) and oxygen at the cathode (400 ml min^{-1})

B. Parameter Estimation of the DMFC Polarisation Curve

The aim of this work was to estimate different parameters for the model proposed by Scott et al., (2002) [79] and identify limitations with respect to predicting the DMFC polarisation curve. The research also illustrates the application of non-linear regression technique for parameter estimation using the GraphPad software [159].

B.1. DMFC Data

The polarisation curve shown in Figure B.1, is based on data from a DMFC operating at various concentrations and temperatures [79]. In this study, data generated at 0.25 M and 0.5 M concentration of methanol solution supplied at a rate of 1.12 cm^3 min^{-1} with air fed cathode pressurised at 2 bars was utilised. The cell temperature was varied between 343.15 K and 363.15 K.

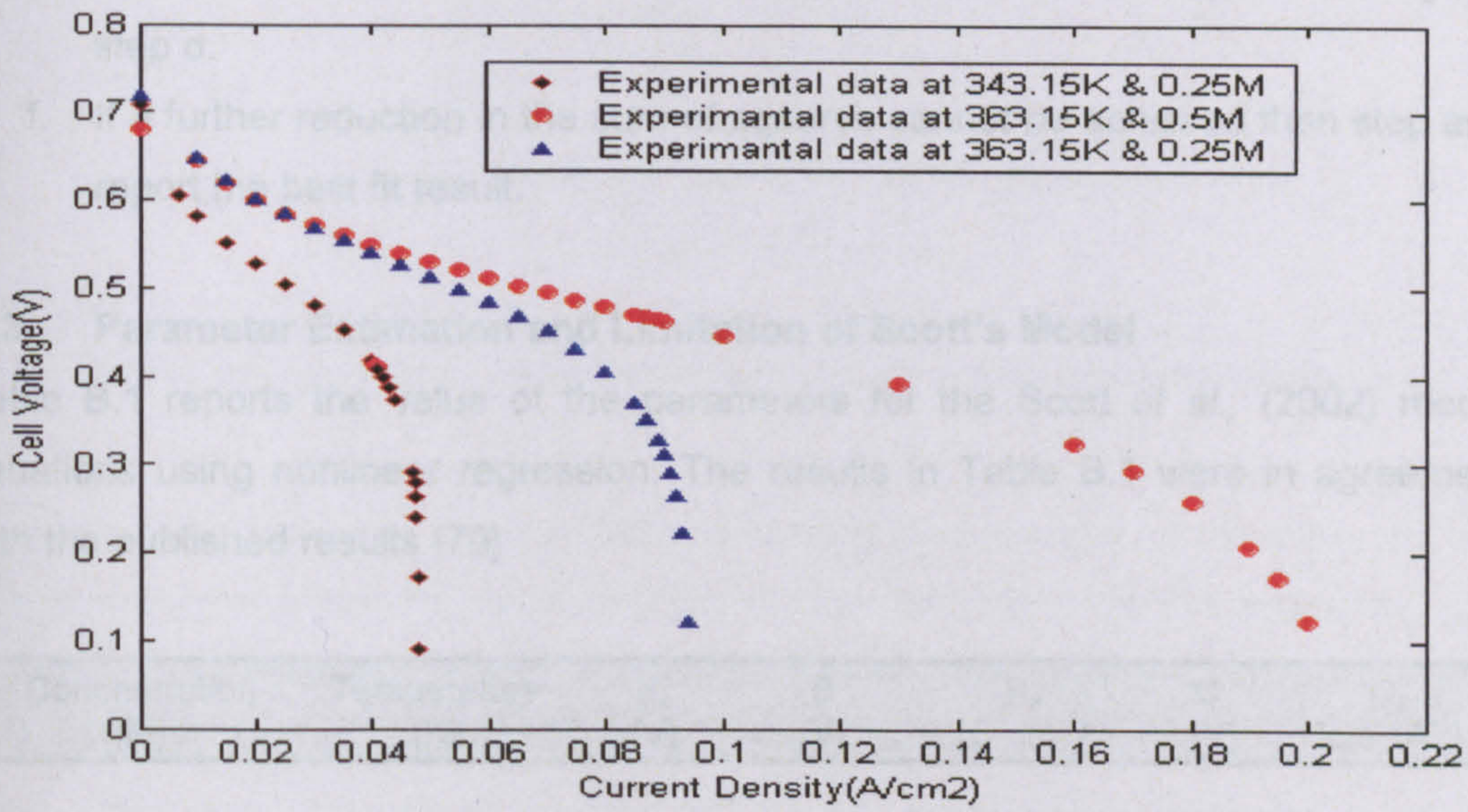

Figure B.1: Polarisation curve from Scott et al., (2002) [79]

The model proposed by Scott et al., (2002), Eq. B.1, was fitted to this data:

$$E_{cell} = E_o - b\log(i) - R_e i + C_1 * \ln(1 - C_2) \quad \ldots (B.1)$$

where,

$$E_o = E_r + b\log(i_o)$$

E_{Cell} is the cell voltage (V), E_r is the reversible cell potential (V), b is the Tafel slope (V dec^{-1}), i is the cell current density (A cm^{-2}), i_o is the exchange current density (A

cm^{-2}), R_e is the cell resistance (Ωcm^{-2}) and C_1, C_2 are the empirical parameters in (V) and (cm^{-2} A^{-1}) respectively. All these parameters were determined using GraphPad software [159].

B.2. Parameter Estimation using Nonlinear Regression

For this study, GraphPad software (*Demo version*) was utilised. It fits a curve to the data and then identifies the best estimates of the parameters using non-linear regression. Typically non-linear regression adapts the following steps [160]:

a. Provide an initial estimate for each parameter.
b. Generate the model fit defined by the initial values.
c. Calculate the sum of squares.
d. Adjust the parameters to improve the fit. A number of algorithms can be used including Steepest Descent, Gauss-Newton or Levenberg-Marquardt.
e. Calculate the sum of squares. If a further reduction in the sum of squares between the initial model fit and the adjusted model fit is required then go to step d.
f. If a further reduction in the sum of squares cannot be achieved then stop and report the best fit result.

B.3. Parameter Estimation and Limitation of Scott's Model

Table B.1 reports the value of the parameters for the Scott *et al.*, (2002) model equations using nonlinear regression. The results in Table B.1 were in agreement with the published results [79].

Concentration [M]	Temperature [K]	E_o [V]	B [V]	R_e [Ω cm^{-2}]	C_1 [V]	C_2 [cm^{-2} A^{-1}]
0.5	363.15	0.400	0.1250	0.02248	0.120	4.750
0.25	363.15	0.4058	0.1250	0.02187	0.073	10.60
0.25	343.15	0.3600	0.1177	0.1267	0.057	20.82

Table B.1: Estimation of the parameters for Scott et al., (2002) model

However the model fit, shown in Figure B.2, highlighted one of the issues with Scott et al., (2002) model fit. For zero current density, the model failed to fit the open circuit voltage (Figure B.2). Additionally, due to the high values of the open circuit voltage

predicted by the model (shown by the red square in Figure B.2) it did not fit the activation area of the cell polarisation curve.

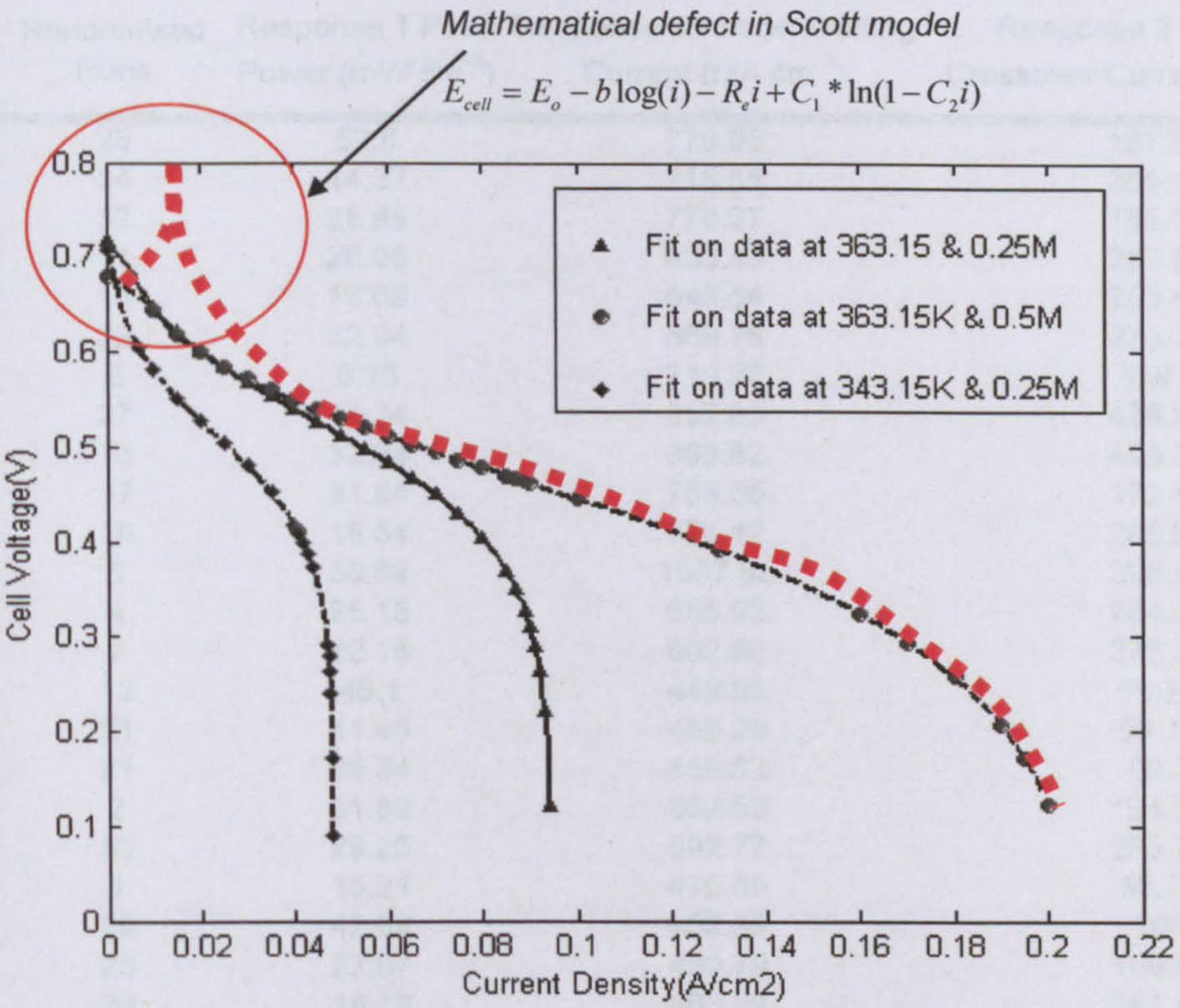

Figure B.2: Model vs. experimental fit for Scott et al., (2002) model (red squares illustrates the limitation of the model in fitting the activation region of the cell polarisation curve)

In Scott et al., (2002) Eq. B.1, the first and second term account for the activation and ohmic overvoltage from the cell respectively. The last term in Eq. B.1 relates to mass transport limitation. The model did not account for the methanol crossover effect, which has been shown to affect cell performance. This mathematical limitation was later addressed by Hwan Kim et al., (2005) [88] by adding a methanol crossover parameter term to Scott et al., (2002) proposed model. However the model proposed by Hwan Kim et al., (2005) failed to explain the physical significance of the parameters included in the equation. To address this, and to overcome the limitation of Scott et al., (2002) a model for DMFC that takes into account the methanol crossover effect is proposed, Chapter 6.

C. Response obtained for the Parametric Fractional Factorial Design

Standard Runs	Randomised Runs	Response 1 Peak Power (mW cm^{-2})	Response 2 Anode Limiting Current (mA cm^{-2})	Response 3 Methanol Crossover Current (mA cm^{-2})
1	23	52.8	778.95	167.02
2	34	44.37	715.55	256.18
3	32	28.98	776.27	185.54
4	11	26.08	636.45	257.89
5	15	16.68	546.54	283.48
6	22	32.94	569.76	275.78
7	6	8.16	710.22	359.6
8	27	44.34	892.85	429.83
9	13	32.94	803.62	408.31
10	17	81.94	763.55	172.41
11	10	15.64	524.42	265.97
12	5	50.62	1037.85	395.81
13	4	25.18	655.93	264.34
14	7	22.18	502.56	276.58
15	12	46.1	449.55	96.29
16	31	41.45	455.29	98.13
17	21	26.84	438.82	99.3
18	2	51.89	862.53	161.28
19	33	29.26	592.77	283.77
20	1	15.21	475.55	98.27
21	29	42.09	452.39	103
22	25	22.07	460.79	100.55
23	26	18.78	603.99	281.47
24	16	11.63	766.78	405.63
25	8	34.33	418.11	96.63
26	18	69.74	689.7	156.75
27	28	30.52	739.33	174.61
28	30	52.39	773.51	167.95
29	14	55.78	451.21	180.08
30	9	24.99	786.46	404.78
31	20	28.24	784.82	376.56
32	35	51.13	729.62	262.82
33	36	54.82	868.9	417.59
34	24	28.07	684.24	257.56
35	3	25.15	663.98	240.6
36	19	26.27	426.78	93.94

Table C.1: Response data for the parametric study design matrix given in Table 3.2

D. Analysis of Variance Table

A detailed description of the statistics [112, 113] used in the analysis of variance (ANOVA) table, Table D.1 has been presented below.

Response: Peak Power
ANOVA for Selected Factorial Model
Analysis of variance table [Partial sum of squares]

Source	Sum of Squares	DF	Mean Square	F Value	Prob > F	Comment
Model[1]	9185.11	7	1312.16	71.36	< 0.0001	.... Significant
A[2]	1794.15	1	1794.15	97.57	<0.0001	.... Significant
B[2]	1753.06	1	1753.06	95.34	< 0.0001	.... Significant
E[2]	1048.71	1	1048.71	57.03	< 0.0001	.... Significant
F[2]	3570.86	1	3570.86	194.20	< 0.0001	.... Significant
AB[2]	310.94	1	310.94	16.91	0.0003	.... Significant
AE[2]	445.59	1	445.59	24.23	< 0.0001	.... Significant
AF[2]	261.80	1	261.80	14.24	0.0008	.... Significant
Curvature[3]	20.72	1	20.72	1.13	0.2978	.... not significant
Residual[4]	496.46	27	18.39			
Lack of Fit[5]	471.63	25	18.87	1.52	0.4734	.... not significant
Pure Error[6]	24.83	2	12.41			
Cor Total[7]	9702.29	35				

Std. Dev.[8]	4.29
Mean[8]	35.27

R-Squared[8]	0.95
Adj R-Squared[8]	0.94

Final Equation in Terms of Coded Factors:[9]
Peak Power = +35.00 +7.49*A -7.40*B +5.72*E +9.96*F -3.12*A*B +3.73*A*E +2.86*A*F
Final Equation in Terms of Actual Factors:[9]
Type of Oxidant (AIR):
Peak Power = + 24.33212 - 0.022188 * A + 8.18437* B - 258.66250*E - 0.20781*AB + 4.97542*AE
Type of Oxidant (OXYGEN):
Peak Power = + 15.64788 + 0.35919*A + 8.18437*B - 258.66250*E - 0.20781*AB + 4.97542*AE

Table D.1: ANOVA output for peak power response

The ANOVA table shows seven columns [113, 117]. The first column shows the 'Source' of variability in the analysis. The second column shows the estimated 'Sum of Squares' due to each source. The third column identifies the 'Degrees of Freedom' associated with each source in the ANOVA. The fourth column represents the 'Mean Square' for each source which is estimated by taking the ratio of sum of squares to degrees of freedom. The 'Fisher statistics' (F-statistics) which is the ratio of mean squares of each source to mean square of residual is estimated in the fifth column, with the resulting 'P-value' for the F-statistics shown in the sixth column (Prob>F). The resulting p-value from F-statistics is compared with the chosen significance level

(α) and if the value is less than chosen significance level then the source of the variability is considered significant as shown in column 7. The significance level (α) refers to the probability of making Type-I error (i.e. rejecting null hypothesis when it is true). Generally smaller value (α =0.05) is assigned so that there is low risk associated with the rejection of the null hypothesis.

Following is the detail description of the sources of variability and the associated statistics.

1. Model:

The model consists of terms (factors and interactions) identified from the ANOVA analysis and half normal plot to infer the response.

- **Sum of Squares (SS_{Model})**: Total sum of squares of all terms included in the model. For peak power:

$$SS_{Model} = SS_A + SS_B + SS_E + SS_F + SS_{AB} + SS_{AE} + SS_{AF}$$

- **DF_{Model}:** The model degrees of freedom is the number of parameters estimated minus one.
- **Mean Square:** It is an estimate of model variance and is calculated using:

$$MS_{Model} = \frac{SS_{Model}}{DF_{Model}}$$

- **F-Value:** It is ratio of model variance to residual variance. It is estimated by:

$$F - value_{Model} = \frac{MS_{Model}}{MS_{\text{Re sidual}}}$$

- **Prob > F**: It is the probability of observing the F-value if the null hypothesis is true. Conventionally, the null hypothesis states that the model is insignificant. Depending on the chosen significance level (generally α =0.05) the critical F-value used in the test is obtained from the F-distribution table using:

$$F_{critical} = F_{\alpha,(DF_{Model},DF_{Residual})}$$

where, α is the significance level i.e. the Type-I error. If the *Prob>F* value is less than the chosen significance level (0.05) then the model is considered significant i.e. the null hypothesis can be rejected.

2. Term:

It's possible to accidentally include an insignificant term (effect and interaction) in the model. Hence to cross verify this individual model term (effect and interaction) are checked for its adequacy in the model.

3. Curvature:

In 2-level factorial design, curvature is used to test the presence of non-linearity in the response by comparing the average response of the factorial points to the average response of the centre points.

4. Residual:

The insignificant effects and interaction not included in the model are used to estimate the residual error associated with model.

5. Lack of Fit (LOF):

The lack of fit test is used to compare the error from the excess design points (i.e. insignificant effects and interaction not included in the model) with the pure error from the replicates.

6. Pure Error:

It is the amount of variation in response identified from the replicated design points.

7. Cor Total:

It is the sum of all information corrected for the mean.

8. Summary statistics for the model:

- **Std Dev:** Calculated by taking square root of the residual mean square.
- **Mean:** It is an overall average of the response data.
- **R-Squared:** It is a measure of the amount of variation about the mean explained by the model.

$$R-Square = 1-\left(\frac{SS_{Residual}}{SS_{Total}}\right)$$

R-square does not take into account the number of terms included in the model hence it is not an accurate estimate compared to Adjusted R-square.

- **Adj R-Squared:** It is a measure of the amount of variation about the mean explained by the model taking into account the number of terms included in the model. Higher the Adj-R-square better is the fit of the model.

$$Adj\ R-Square = 1-\left(\frac{\frac{SS_{Residual}}{DF_{Residual}}}{\frac{SS_{Model}+SS_{Residual}}{DF_{Model}+DF_{Residual}}}\right)$$

9. Model

The model is a mathematical equation developed by using regression method to predict the response. The predictive model is presented both in coded (+1, 0 and -1 for low, centre and high level) and actual (e.g. 30, 75 and 90 °C) terms, Table D.1. The analysis of design is based on coded factors instead of the specified actual levels, as coding of the factors allows the calculations to be performed independent of the units for each factor. The coded predictive model helps in identifying the relative significance of the factors by comparing the factor coefficients whereas with actual model comparison cannot be made as the coefficients are scaled to accommodate the units of each factor. However, on substitution of factor levels (coded or actual) both the equation gives the same predictions.

The relation between actual level and coded level is:

$$Coded = \frac{Actual - \left(\frac{Actual_{High} + Actual_{Low}}{2}\right)}{\left(\frac{Actual_{High} - Actual_{Low}}{2}\right)}$$

E. Least Significant Difference I-bar

The least significance difference I-bar makes use of least significance difference (LSD) test statistics for comparing two means[112, 113]. The general statistics applied is:

$$LSD = t_{\frac{\alpha}{2}} \times \sqrt{MS_E \left(\frac{1}{n_j} + \frac{\sum_{i=1}^{k} \frac{1}{n_{i \neq j}}}{k-1} \right)} \qquad \ldots(E.1)$$

where, k is the number of treatments, n is the number of sample size for a given treatment j, t-value is based on a default risk level of 0.05 for a two-tailed test with the degrees of freedom associated with residual error in the ANOVA table and MS_E is the residual mean square error.

The LSD I-bar resulting from this statistics represents the 95% confidence interval for that particular average value. If these LSD I-bar do not overlap, then the means are significantly different.

F. Effects of Reactant Flow Rates on the Performance of DMFC

The experimental design in Table 3.2 could not identify any significant effect of methanol flow rate and oxidant flow rate on the performance of the DMFC. This was due to the narrow range considered for both factors. For methanol flow rate, the range considered was 3.4 to 6.6 ml min^{-1} whilst for oxidant flow rate it was 300 to 500 ml min^{-1}. Figures F.1 and F.2 illustrates the effect of a wider rage of oxidant flow rate and methanol flow rate on DMFC performance. From both figures, it can be concluded that a change in performance is visible due to the wider range.

In Figure F.1, DMFC performance increases with an increase in oxidant flow rate as a higher oxygen flow rate increases the concentration of oxygen at the cathode catalyst layer due to an elevated supply of oxygen. In addition, a high flow rate plays a critical role in removing water from the gas diffusion layer and flow channels thus avoiding flooding of the cathode compartment which in turn impacts on DMFC performance [33]. However, from Figure F.1, it can be observed that a 10 fold increase in oxidant flow rate from 200 to 2000 ml min^{-1} resulted in only a 10-15% increase in peak power density. Thus this excess supply of oxidant will have a negative impact on overall system efficiency and will not be practical in commercial application.

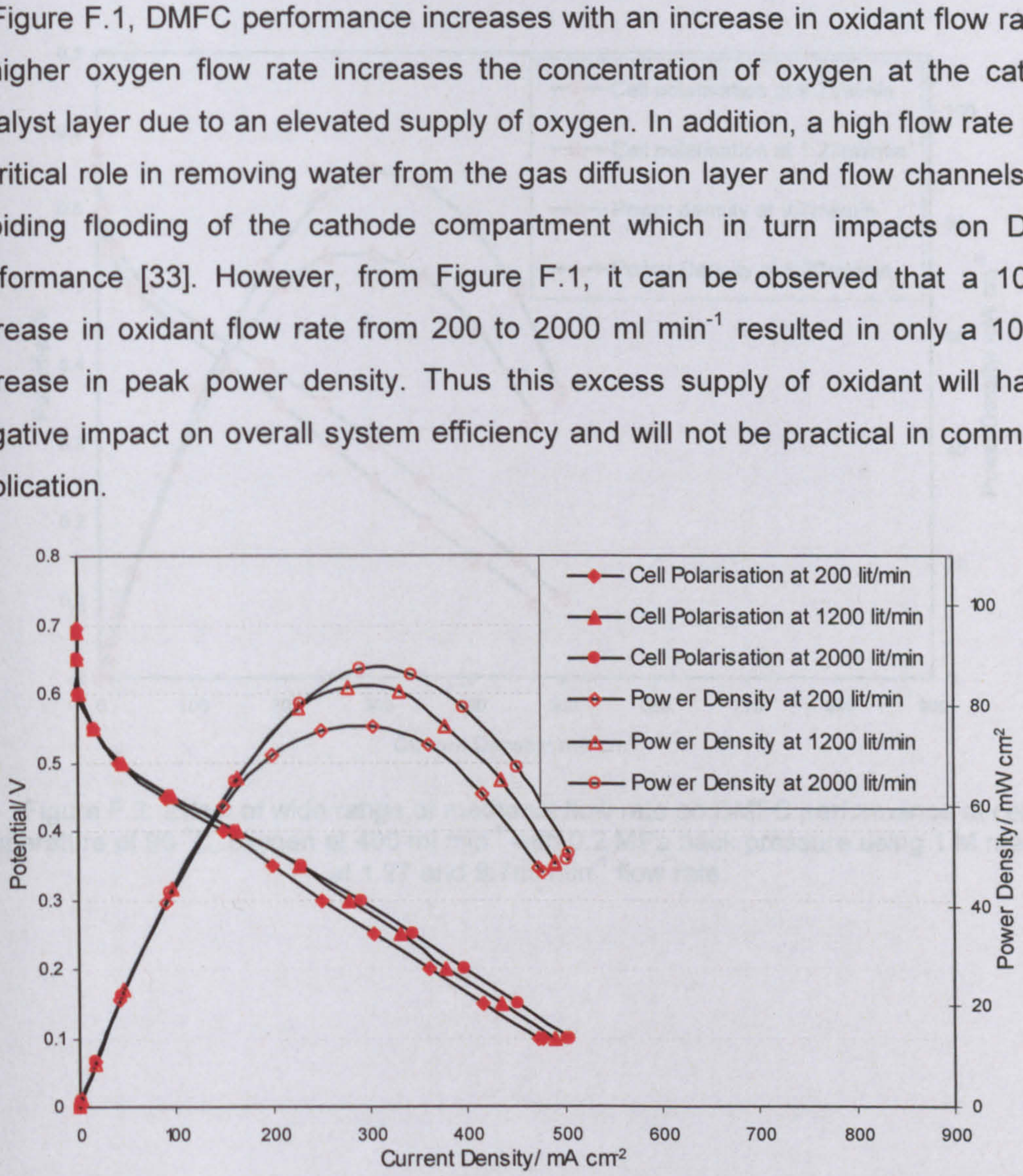

Figure F.1: Effect of wide range of oxidant flow rate on DMFC performance at cell temperature of 90 °C, 1 M methanol at 5 ml min^{-1}, using oxygen with 0.2 MPa back pressure and flow rate of 200, 1200 and 2000 ml min^{-1}.

The effect of a wider range of methanol flow rate on DMFC performance is shown in Figure F.2. The plot shows that DMFC performance increases with an increase in methanol flow rate i.e. from 1.27 to 9.7 ml min^{-1}. High flow rates of methanol results in a more uniform stream of smaller slugs and bubbles due to less surface tension at the anode catalyst layer which in turn increases the cell performance [24, 31]. In addition, an increase in methanol flow rate also provides the anode catalyst with enough fuel, which improves the reaction. However this improvement is as not significant compared to the increase in the flow rate as this increase in the flow rate leads to lower fuel utilisation at anode lowering the overall fuel cell efficiency [33, 157]. Hence a balance between the methanol flow rate and its effective utilisation at the anode requires to be sought.

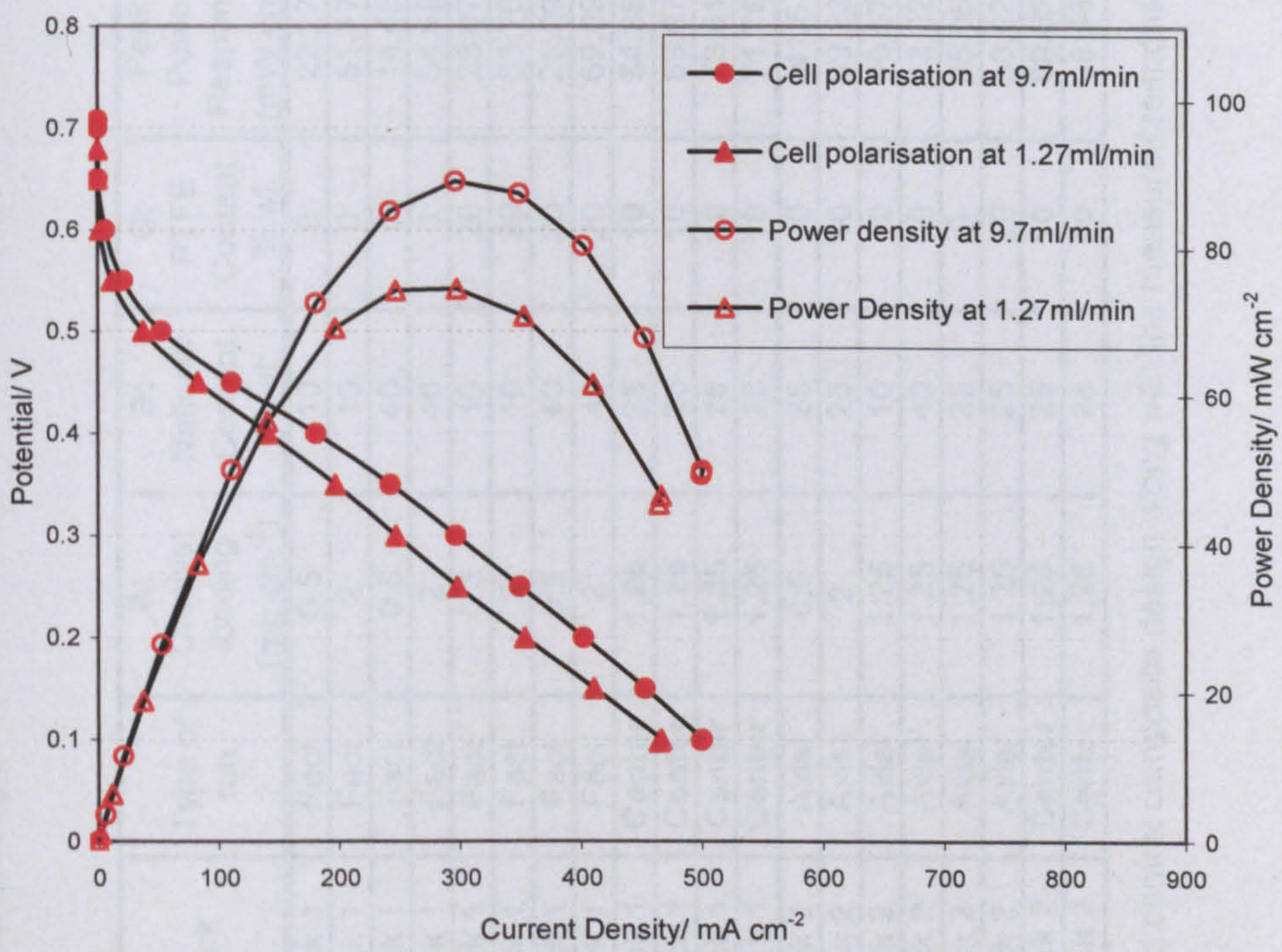

Figure F.2: Effect of wide range of methanol flow rate on DMFC performance at cell temperature of 90 °C, oxygen at 400 ml min^{-1} with 0.2 MPa back pressure using 1 M methanol at 1.27 and 9.7ml min^{-1} flow rate.

G. Response Obtained for the RSM Design

Standard experimental runs	Randomised experimental runs	Block	Type of run	A: Catalyst loading (mg cm^{-2})	B: Nafion® Content %.wt	C: PTFE Content %.wt	Peak Power Response (mW cm^{-2})	Cathode response at 10 mA cm^{-2} (V)	Anode response at 0.25 V (mA cm^{-2})	Crossover Limiting Current (mA cm^{-2})
1	4	Block 1	Fact	0.5	10	0	22.27	0.692	5.956	112.42
2	1	Block 1	Fact	2	10	0	51.17	0.846	5.756	108.55
3	8	Block 1	Fact	0.5	40	0	14.45	0.749	0	95.91
4	9	Block 1	Fact	2	40	0	54.58	0.777	8.178	114.1
5	6	Block 1	Fact	0.5	10	20	23.07	0.784	1.278	90.02
6	10	Block 1	Fact	2	10	20	63.76	0.777	17.306	137.77
7	7	Block 1	Fact	0.5	40	20	29.09	0.743	1.367	134.62
8	5	Block 1	Fact	2	40	20	69.89	0.84	3.367	128.35
9	**2**	**Block 1**	**Center**	**1.25**	**25**	**10**	**54.88**	**0.791**	**3.422**	**139.74**
10	**3**	**Block 1**	**Center**	**1.25**	**25**	**10**	**69.97**	**0.835**	**4.756**	**145.48**
11	**11**	**Block 1**	**Center**	**1.25**	**25**	**10**	**73.51**	**0.837**	**5.511**	**116.8**
12	**12**	**Block 1**	**Center**	**1.25**	**25**	**10**	**71.76**	**0.827**	**5.322**	**130.79**
13	17	Block 2	Axial	0.5	25	10	41.5	0.774	3.422	133.97
14	14	Block 2	Axial	2	25	10	69.22	0.831	7.6	127.09
15	18	Block 2	Axial	1.25	10	10	46.67	0.81	5.689	116.94
16	16	Block 2	Axial	1.25	40	10	23.32	0.718	1.589	133.51
17	19	Block 2	Axial	1.25	25	0	85.06	0.858	5.411	132.8
18	15	Block 2	Axial	1.25	25	20	50.02	0.841	3.733	120.19
19	**13**	**Block 2**	**Center**	**1.25**	**25**	**10**	**68.09**	**0.834**	**1.278**	**123.8**
20	**20**	**Block 2**	**Center**	**1.25**	**25**	**10**	**66.68**	**0.814**	**2.644**	**117.9**

Table G.1: Full factorial and central composite design along with the measured responses for MEA optimization study

H. Kinetic Based Anode Model versus Tafel Model

The overall methanol oxidation reaction at the anode is given by:

$$CH_3OH + H_2O \longrightarrow CO_2 + 6H^+ + 6e^- \quad \text{... (H.1)}$$

Using Butler-Volmer equation, the kinetics of methanol oxidation reaction is given by:

$$j_{Anode} = j_{o,M}\left[\frac{C_M^a}{C_{Mref}} e^{\left(\frac{n\alpha_M F(E-E_M^o)}{RT}\right)} - \frac{P_{CO2}}{P_{CO2ref}} e^{\left(\frac{-n(1-\alpha_M)F(E-E_M^o)}{RT}\right)}\right] \quad \text{... (H.2)}$$

where, j_{Anode} is the anode current density due to methanol oxidation reaction (A m^{-2}), α_M is the electrochemical transfer coefficients, n is number of electrons transferred, C_M^a is the concentration of methanol at anode (M), E is the anode potential (V), E_M^o is the standard methanol oxidation potential (V), P_{CO2} is the partial pressure of carbon dioxide formed due to methanol oxidation reaction (N m^{-2}) and $j_{o,M}$ is the exchange current density at the reference methanol concentration (C_{Mref}) for the methanol oxidation reaction (A m^{-2}).

At high potentials, for a simple one electron process [155], Eq. H.2, reduces to:

$$j_{Anode} = j_{o,M}\frac{C_M^a}{C_{Mref}} e^{\left(\frac{\alpha_M F(E-E_M^o)}{RT}\right)} \quad \text{... (H.3)}$$

The above Tafel type kinetic equation can be used to model the anode polarisation curve. Figure H.1, illustrates the fit of the model to the experimental anode polarisation data for varying methanol concentrations (1 and 2 M) and cell temperatures (30, 60 and 90 °C) [114]. To highlight the fit of the model at the lower end of the polarisation curve, a plot of log current density with respect to the anode potential is shown in Figure H.2. From both plots it can be observed that the Tafel based model fits the experimental data well at the lower end of the polarisation curve however it fails to predict the anode polarisation data above 0.4 V as the kinetics of methanol oxidation exhibits non-Tafel behaviour [95]. The parameters obtained from fitting the model to the experimental data are summarised in Table H.1.

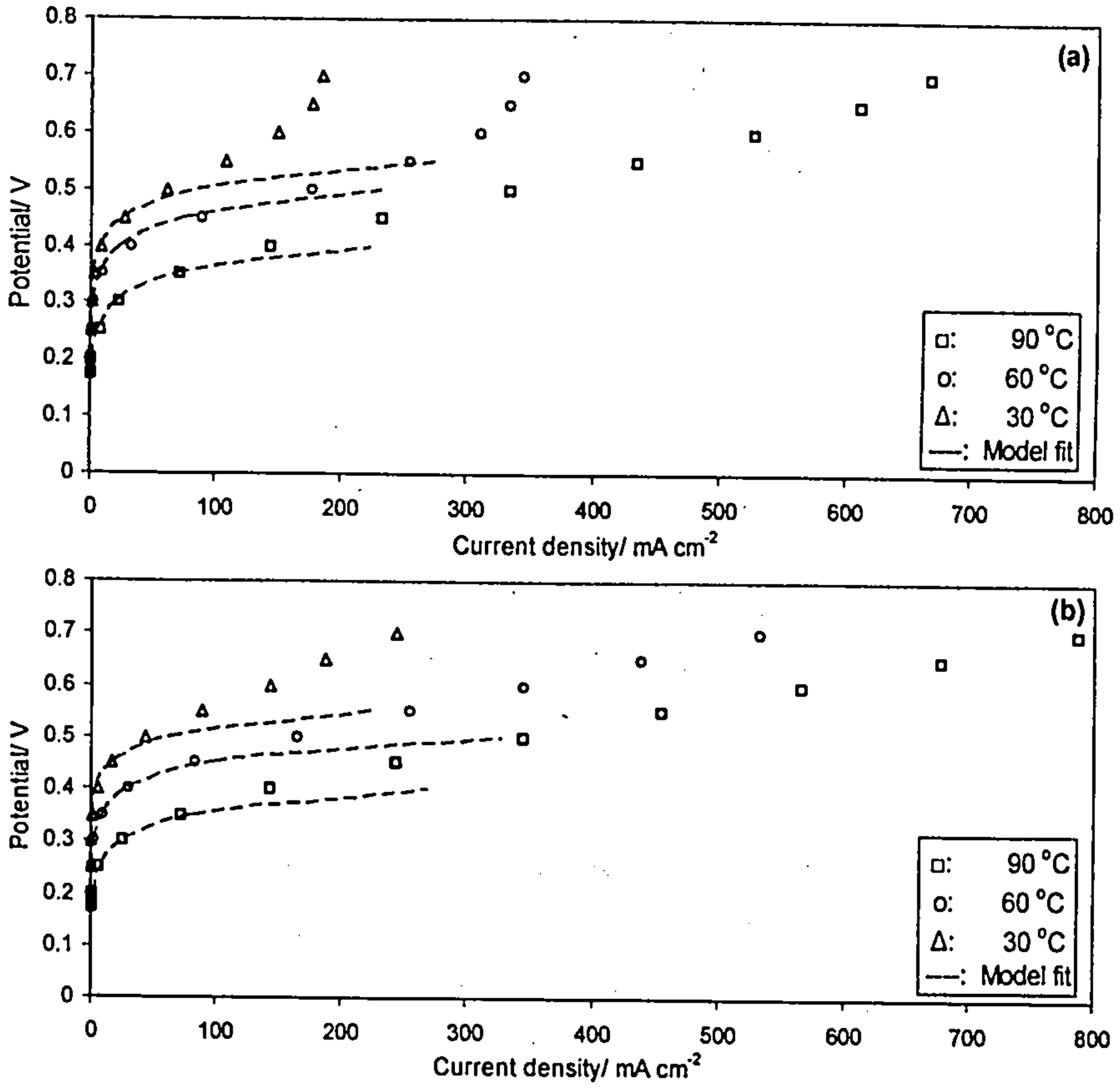

Figure H.1: Tafel model versus experimental fit for porous anode cell at various temperatures (30, 60 and 90 °C) and methanol concentrations (a) 1 M and (b) 2 M

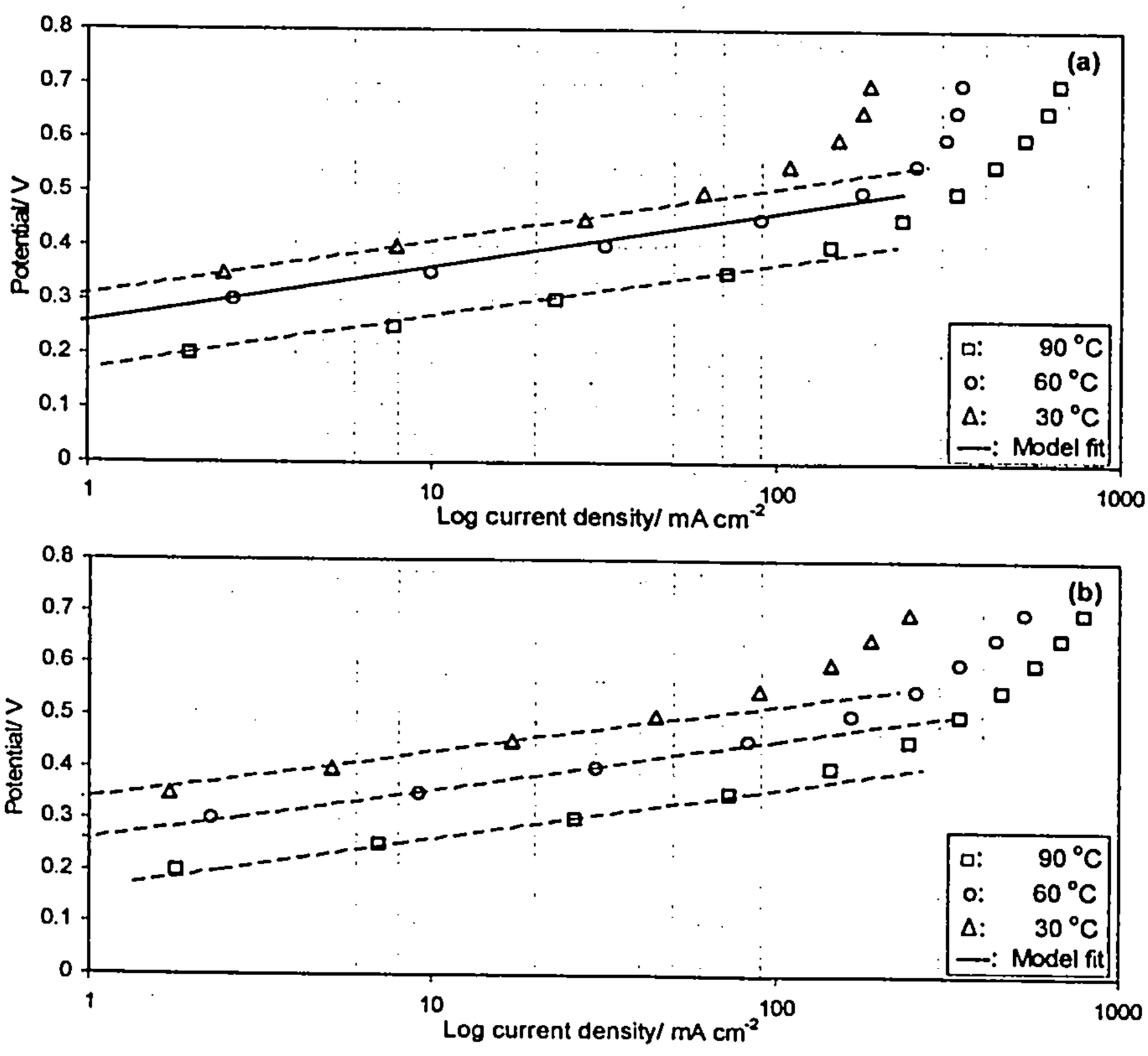

Figure H.2: Tafel model versus experimental fit on a Tafel plot at various temperatures (30, 60 and 90 °C) and methanol concentrations (a) 1 M and (b) 2 M

To overcome the limitation of simple Tafel model, the kinetic based model developed in Chapter 5 is used to model the anode polarisation curve. More specifically the anode model for methanol oxidation at anode of DMFC is given by:

$$j_{Anode} = n \times F \times k_2 e^{(\frac{\alpha_2 FE}{RT})} \left(\frac{k_1 C_M^a}{k_2 e^{(\frac{\alpha_2 FE}{RT})} + k_1 C_M^a} \right) \quad \ldots (H.3)$$

where, j_{Anode} is the current density at anode (A m^{-2}), k_1 and k_2 are the kinetic parameters for the methanol oxidation reaction at anode, C_M^a is the concentration of methanol at the anode and α_2 is the electrochemical transfer coefficient for the methanol oxidation reaction at anode.

Figure H.3 and H.4, illustrates the fit of the kinetic model to the experimental anode polarisation data for varying methanol concentrations (1 and 2 M) and cell temperatures (30, 60 and 90 °C) and the parameters obtained by fitting the model to the experimental data are summarised in Table H.1. Compared to Tafel model, it can be observed that the kinetic model predicts the anode polarisation curve over the entire range. The three parameters included in the kinetic model α_2, k_1 and k_2 affect the lower, top and middle portion of the anode polarisation curve respectively, as observed in Figure 5.7, and thus help to model the entire anode polarisation curve accurately. In contrast, the Tafel based model contains only one parameter (α_M), which helps to model mainly the lower end (below 0.4 V) of the polarisation curve.

Parameters	Fit at 30 °C	Fit at 60 °C	Fit at 90 °C
α_M	0.61	0.66	0.70
k_1	8 X 10^{-6} m s^{-1}	7.15 X 10^{-5} m s^{-1}	1.24 X 10^{-5} m s^{-1}
k_2	5.3 X 10^{-7} mol $m^{-2}s^{-1}$	1.1 X 10^{-6} mol $m^{-2}s^{-1}$	1.8 X 10^{-6} mol $m^{-2}s^{-1}$
α_2	0.34	0.48	0.6

Table H.1: Kinetic parameters estimated from the model

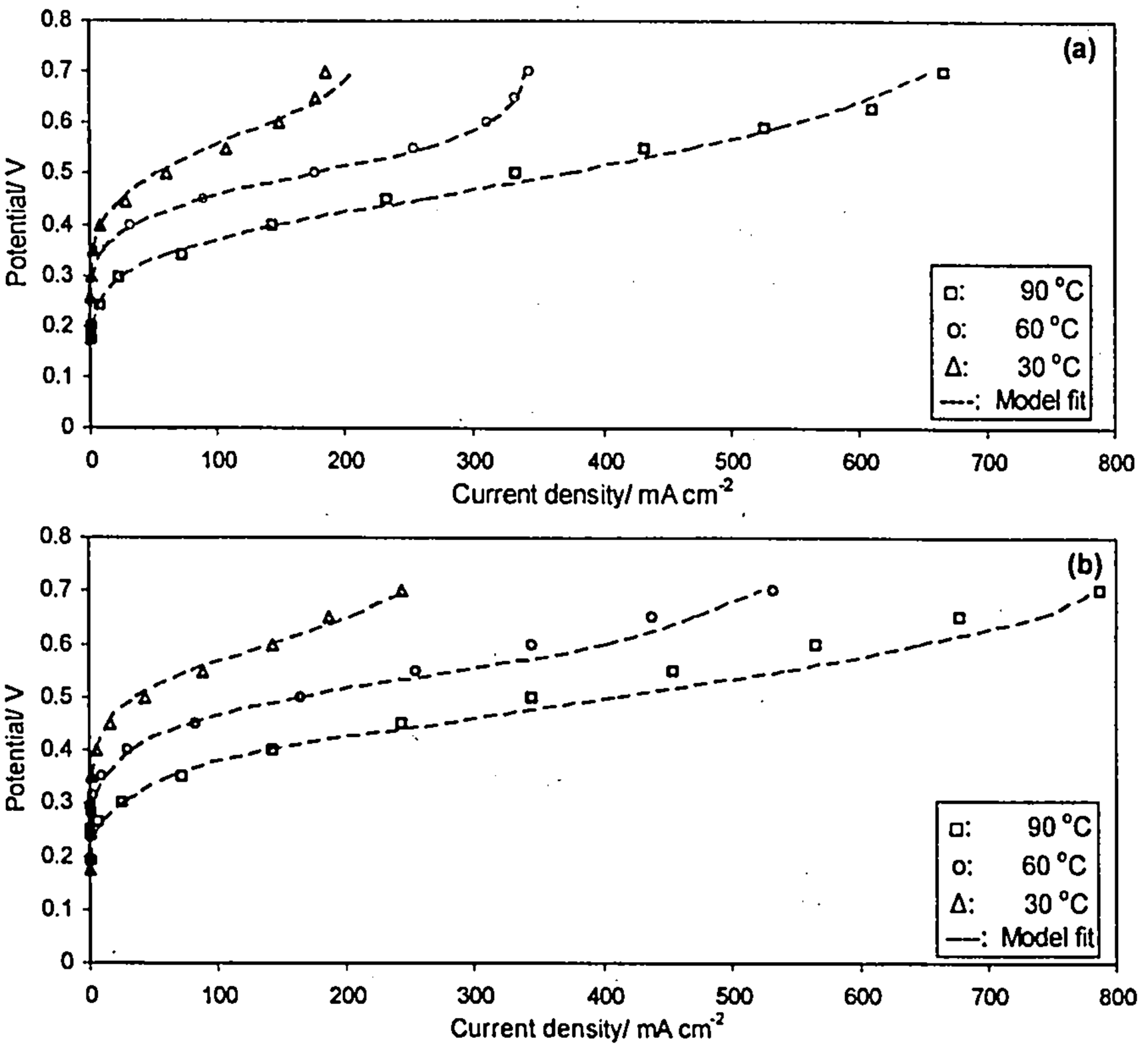

Figure H.3: Kinetic model versus experimental fit for porous anode cell at various temperatures (30, 60 and 90 °C) and methanol concentrations (a) 1 M and (b) 2 M

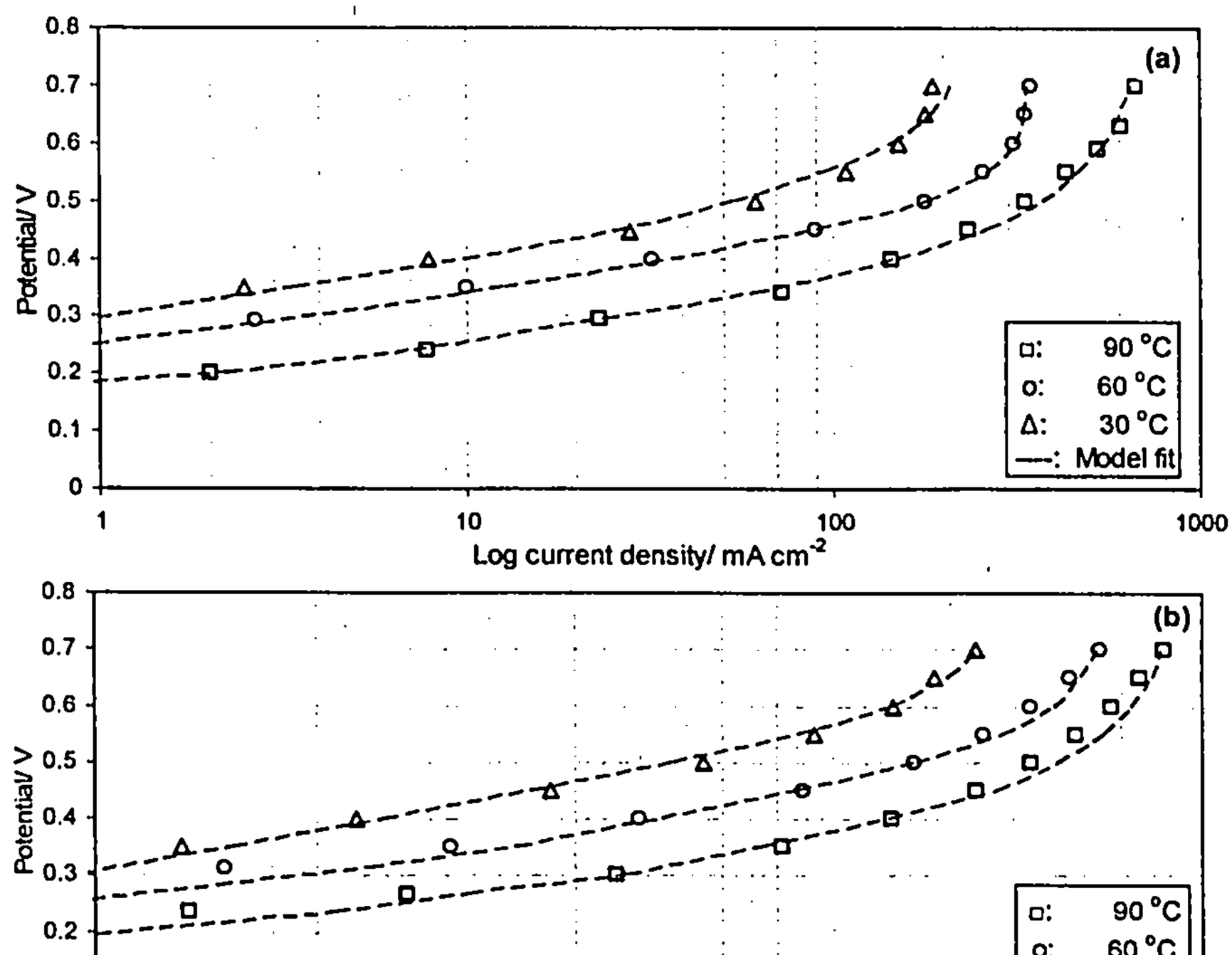

Figure H.4: Kinetic model with respect to the experimental fit on a Tafel plot at various temperatures (30, 60 and 90 °C) and methanol concentrations (a) 1 M and (b) 2 M

I. Raw Material Specification

Raw Material Specification	Manufacturer	Batch No.
Pt-Ru/C catalyst (60 %wt) 1:1 a/o on Vulcan XC-72R	E-TEK	Lot# D1260912
Pt/C Catalyst on Vulcan XC-72R	E-TEK	Lot# B0660604
Nafion® perfuorinated ion-exchange resin, 5 wt% solution in lower aliphatic alcohols/H_2O mix	Aldrich®	Lot # 07416HD
Nafion® 117 perfluorinated membrane	Aldrich®	
Polytetrafluoroethylene, 60 wt.% dispersion in water	Aldrich®	Lot # 077208PA
Ketjen Black Carbon Powder	Cabot	Lot # 032215CB
Carbon paper 20% wet proof TGP-120	Aldrich®	
Methanol (purity 99.9%)	Aldrich®	
Isopropyl Alcohol (purity 99.9%)	Aldrich®	
Flexible electric heaters	Watson Marlow	
Graphite Fuel Cell assembly with seven parallel channels (30mm x 1mm x 2mm)	Ralph Coiden	
Spray Gun A4309 Airbrush Sets	Aztek	

REFERENCES

1. *International Energy Outlook, Energy Information Administration*. May 2007, U.S. Department of Energy: Washington DC. p. 5-18.
2. *Summary of policymakers: contribution of working group I to the fourth assessment report of the intergovernmental panel on climate change*, in *Climate Change 2007: The Physical Science Basis*. Feb 2007, Intergovernmental Panel on Climate Change. p. 1-18.
3. *The Kyoto protocol - A brief summary*, http://unfccc.int/kyoto_protocol/items/2830.php. [cited 13 Jul 2007].
4. Los Alamos National Laboratory, *Fuel cells - Green power*. 2003, Los Alamos National Laboratory. p. 4-25.
5. Apanel G. and Johnson E., *Direct methanol fuel cells - ready to go commercial?* 2004, Fuel Cells Bulletin. p. 12-17.
6. Aricó A.S., Srinivasan S., and Antonucci V., *DMFC's: From fundamental aspects to technology development*. Fuel Cells, 2001. 1(2): p. 133-161.
7. Barrett S., *Progress in the European hydrogen and fuel cell technology platform*. Fuel Cells Bulletin, April 2005: p. 12-17.
8. Bruijn F., *The current status of fuel cell technology for mobile and stationary applications*. Journal of the Royal Society of Chemistry, 2005. 7: p. 132-150.
9. Dillon R., Srinivasan S., Aricó A.S., and Antonucci V., *International activities in DMFC R&D: Status of technologies and potential applications*. Journal of Power Sources, 2004. 127: p. 112-126.
10. Larmine J. and Dicks A., *Fuel cell systems explained*. 2001: John Wiley and Sons Ltd. p. 3-75.
11. *Handbook of fuel cells: Fundamentals and survey of systems*, ed. Vielstich W., Lamm A., and Gasteiger H.A. Vol. 1. 2003: John Wiley & Sons Ltd.
12. *Fuel Cell Handbook*, ed. EG&G Technical Services Inc. Vol. 7. 2004: U.S. Department of Energy.
13. Katz E., Shipway A.N., and Willner I., *Biochemical fuel cells*. Handbook of Fuel Cells- Fundamentals, Technology and Applications, ed. Vielstich W., Gateiger A., and Lamm A. Vol. 1. 2003: John Wiley and Sons Ltd. 1-27.

14. Costamagna P. and Srinivasan S., *Quantum jumps in the PEMFC science and technology from the 1960s to the year 2000. Part I: Fundamental scientific aspects.* Journal of Power Sources, 2001. 102: p. 242-252.
15. Costamagna P. and Srinivasan S., *Quantum jumps in the PEMFC science and technology from the 1960s to the year 2000. Part II: Engineering, technology development and application aspects.* Journal of Power Sources, 2001. 102: p. 253-269.
16. Litster S. and McLean G., *PEM fuel cell electrodes.* Journal of Power Sources, 2004. 130: p. 61-76.
17. Vishnyakov V.M., *Proton exchange membrane fuel cells.* Vacuum, 2006. 80: p. 1053-1065.
18. Lamy C., Lima A., LeRhun V., Delime F., Coutanceau C., and Leger J.M., *Recent advances in the development of direct alcohol fuel cells (DAFC).* Journal of Power Sources, 2002. 105: p. 1283-1296.
19. Schultz T., Zhou S., and Sundmacher K., *Current status of and recent developments in the direct methanol fuel cells.* Chemical Engineering Technology, 2001. 12: p. 1223-1233.
20. Chetty R. and Scott K., *Direct ethanol fuel cells with catalysed metal mesh anodes.* Journal of Electrochemica Acta, 2007. 52(12): p. 4073-4081.
21. Pavela T.O., Annales Academiæ Scientiarum Fennicæ Ser. AII Chem., 1954. 59.
22. Lamy C., Leger J.M., and Srinivasan S., *Modern aspects of electrochemistry*, ed. Bockris J. O'M. and Conway B. E. Vol. 34. 2001, New York, USA: Plenum Press.
23. Li Xianguo, *Principles of fuel cells*. 2006, New York, USA: Taylor & Francis Group. p. 507-523.
24. Argyropoulos P., Scott K., and Taama W.M., *Gas evolution and performance in direct methanol fuel cell.* Journal of Applied Electrochemistry, 1999. 29: p. 661-669.
25. Heinzel A. and Barragan V.M., *A review of the state-of-the-art of the methanol crossover in direct methanol fuel cells.* Journal of Power Sources, 1999. 84(1): p. 70-74.
26. Jiang R. and Chu D., *Comparative studies of methanol crossover and cell performance for a DMFC.* Journal of the Electrochemical Society, 2004. 151(1): p. A69-A76.

27. Lindermeir A., Rosenthal G., Kunz U., and Hoffman U., *On the question of MEA preparation for DMFCs.* Journal of Power Sources, 2004. 129(2): p. 180-187.

28. Piela P., Fields R., and Zelenay P., *Electrochemical impedance spectroscopy for direct methanol fuel cell diagnostics.* Journal of the Electrochemical Society, 2006. 153(10): p. A1902-A1913.

29. Kauranen P.S., Skou E., and Munk J., *Kinetics of methanol oxidation on carbon-supported Pt and Pt + Ru catalysts.* Journal of Electroanalytical Chemistry, 1996. 404(1): p. 1-13.

30. Carlson E., Kopf P., Sinha J., and Yang Y. *PEM fuel cell cost status-2005.* in *Fuel Cell Seminar.* 2005. California..

31. Allen R.G., *New anodes for the direct methanol fuel cell.* PhD Thesis, 2005, University of Newcastle upon Tyne.

32. Aricó A.S., Creti P., Antonucci P.L., Cho J., Kim H., and Antonucci V., *Optimization of operating parameters of a direct methanol fuel cell and physico-chemical investigation of catalyst-electrolyte interface.* Journal of Electrochemica Acta, 1998. 43(24): p. 3719-3729.

33. Ge J. and Liu H., *Experimental studies of a direct methanol fuel cell.* Journal of Power Sources, 2005. 142(1-2): p. 56-69.

34. Nakagawa N. and Xiu Y., *Performance of a direct methanol fuel cell operated at atmospheric pressure.* Journal of Power Sources, 2003. 129(2): p. 248-255.

35. Oedegaard A., Hebling C., Schmitz A., Møller-Holst S., and Tunold R., *Influence of diffusion layer properties on low tempreature DMFC.* Journal of Power Sources, 2004. 127: p. 187-196.

36. Shukla A., Christensen P. A., Hamnett A., and Hogarth M. P., *A vapour-feed direct-methanol fuel cell with proton-exchange membrane electrolyte.* Journal of Power Sources, 1995. 55(1): p. 87-91.

37. Shivhare M. R., Allen R. G., Scott K., Morris A. J., and Martin E. B., *A kinetic model for the direct methanol fuel cell anode based on surface coverage.* Journal of Electroanalytical Chemistry, 2006. 595: p. 145-151.

38. Shivhare M. R., Jackson C.L., Scott K., and Martin E.B., *Simplified model for the direct methanol fuel cell anode.* Journal of Power Sources, 2007. 173: p. 240–248.

39. *LabVIEW course manual, Basics I and II.* 1993-2004, National Instruments Corporation.

40. Dohle H. and Stolten D. *DMFC systems - state of the art and future trends.* in *Fuel Cell Seminar.* 2005. California.

41. Thomas S.C., Ren X., Gottesfeld S., and Zelenay P., *Direct methanol fuel cells: progress in cell performance and cathode research.* Journal of Electrochimica Acta, 2002. 47: p. 3741-3748.

42. Argyropoulos P., Scott K., and Taama W.M., *Dynamic response of the direct methanol fuel cell under variable load conditions.* Journal of Power Sources, 2000. 87: p. 153-161.

43. Gasteiger H. A., Markovic N., Ross P. N., and Cairns E. J., *Methanol electrooxidation on well characterized Pt-Ru alloys.* Journal of Physical Chemistry, 1993. 97(46): p. 12020-12029.

44. Gojković S.Lj., Vidaković T.R., and Durović D.R., *Kinetic study of methanol oxidation on carbon supported PtRu electrocatalyst.* Journal of Electrochimica Acta, 2003. 48: p. 3607-3614.

45. Lai C.M., Lin J.C., Hsueh K.L., Hwang C.P., Tsay K.C., Tsai L.D., and Peng Y.M., *On the electrochemical impedance spectroscopy of direct methanol fuel cell.* Jounal of Hydrogen Energy, 2007. 32(17): p. 4381-4388.

46. Kulikovsky A. A., *On the nature of mixed potential in a DMFC.* Journal of the Electrochemical Society, 2005. 152(6): p. A1121-A1127.

47. Frelink T., Visscher W., and Van Veen J.A.R., *On the role of Ru and Sn as promoters of methanol electro-oxidation over Pt.* Surface Science, 1995. 335: p. 353-360.

48. Ley K. L., Liu R., Pu C., Fan Q., Leyarovska N., Segre C., and Smolkin E. S., *Methanol Oxidation on Single-Phase Pt-Ru-Os Ternary Alloys.* Journal of the Electrochemical Society, 1997. 144(5): p. 1543-1548.

49. Akyalçýn L. and Kaytakoðlu S., *Performance comparison of sputter deposited PEM fuel cell MEAs with an E-TEK® MEA*, in *NORDIC 2006 PEMFC*. 2006: Stockholm, Sweden.

50. Gülzow E., Kaz T., Reissner R., Sander H., Schilling L., and Bradke M., *Study of membrane electrode assemblies for direct methanol fuel cells.* Journal of Power Sources, 2002. 105(2): p. 261-266.

51. Yang L.X., Allen R.G., Scott K., and Christensen P., *A new PtRu anode formed by thermal decomposition for the direct method fuel cell.* Journal of Fuel Cell Sciences and Technology, 2005. 2(2): p. 142-149.

52. Neergat M. and Shukla A.K., *Effects of diffusion-layer morphology on the performance of solid-polymer-electrolyte direct methanol fuel cells.* Journal of Power Sources, 2002. 104: p. 289-294.

53. Aricó A.S., Creti P., Modica E., and Antonucci V., *Influence of flow field design on the performance of a direct methanol fuel cell.* Journal of Power Sources, 2000. 91: p. 202-209.
54. Tüber K., Oedegaard A., Hermann M., and Hebling C., *Investigation of fractional flow-fields in portable proton exchange membrane and direct methanol fuel cells.* Journal of Power Sources, 2004. 131: p. 175-181.
55. Dohle H., Jung R., Kimiaie N., Mergel J., and Müller M., *Interaction between the diffusion layer and the flow field of polymer electrolyte fuel cells-experiments and simulation studies.* Journal of Power Sources, 2003. 124(2): p. 371-384.
56. Argyropoulos P., *Performance and modelling of the direct methanol fuel cell (DMFC).* PhD Thesis, 1999, University of Newcastle upon Tyne.
57. Heinzela A., Mahlendorf F., Niemzigb O., and Kreuza C., *Injection moulded low cost bipolar plates for PEM fuel cells.* Journal of Power Sources, 2004. 131(1-2): p. 35-40.
58. *Fuel Cells*, in *Electrochemistry Encyclopaedia*, Nagy Z., Editor. cited: 13 July 2007, http://electrochem.cwru.edu/ed/encycl/.
59. Evertz J. and Gunthart M., *Structural concepts for lightweight and cost effective end plates for fuel cell stacks*, in *Tribecraft*. 2003.
60. Kordesh K. and Simader G., *Fuel cells and their applications.* 1st ed. 1996: Wiley VCH.
61. Scott K., Taama W. M., Argyropoulos P., and Sundmacher K., *The impact of mass transport and methanol crossover on the direct methanol fuel cell.* Journal of Power Sources, 1999. 83(1-2): p. 204-216.
62. Qi Z. and Kaufman A., *Open circuit voltage and methanol crossover in DMFCs.* Journal of Power Sources, 2002. 110: p. 177-185.
63. Ren X., Springer T. E., Zawodzinski T. A., and Gottesfeld S., *Methanol transport through Nafion membranes -Electro-osmotic drag effects on potential step measurements.* Journal of the Electrochemical Society, 2000. 147(2): p. 466-474.
64. Narayanan S.R., Frank H., Nakamura J., Smart M., Chun W., Halpert G., Kosek J., and Cropley C. *First international symposium on proton conducting membrane fuel cells.* 1995. Chicago, USA: The Electrochemical Society Proceedings Series.
65. Ling J. and Savadogo O., *Comparison of methanol crossover among four types of Nafion membranes.* Journal of the Electrochemical Society, 2004. 151(10): p. A1604-A1610.

66. Ren X., Springer T.E., and Gottesfeld S., *Water and methanol uptakes in Nafion membranes and membrane effects on direct methanol cell performance.* Journal of the Electrochemical Society, 2000. 147(1): p. 92-98.

67. Kulikovsky A. A., *The voltage-current curve of a direct methanol fuel cell: "exact" and fitting equations.* Journal of Electrochemistry Communications, 2002. 4: p. 939-946.

68. Ren X., Henderson W., and Gottesfeld S., *Electro-osmotic drag of water in ionomeric membranes.* Journal of the Electrochemical Society, 1997. 144(9): p. L267-L270.

69. Dohle H., Divisek J., Mergel J., Oetjen H.F., Zingler C., and Stolten D., *Recent development of the measurement of the methanol permeation in a direct methanol fuel cell.* Journal of Power Sources, 2002. 105: p. 274-282.

70. Cruickshank J. and Scott K., *The degree and effect of methanol crossover in the direct methanol fuel cell.* Journal of Power Sources, 1998. 70: p. 40-47.

71. Divisek J., Fuhrmann J., Gärtner K., and Jung R., *Performance modelling of a direct methanol fuel cell.* Journal of the Electrochemical Society, 2003. 150(6): p. A811-A825.

72. Meier F., Denz S., Weller A., and Eigenberger G., *Analysis of direct methanol fuel cell (DMFC) performance via FTIR spectroscopy of cathode exhaust.* Fuel Cells, 2003. 3(4): p. 161-168.

73. Ravikumar M.K. and Shukla A.K., *Effect of methanol crossover in a liquid-feed polymer-electrolyte direct methanol fuel cell.* Journal of the Electrochemical Society, 1996. 143(8): p. 2601-2606.

74. Wang J.T., Wasmus S., and Savinelle R.F., *Real-time mass spectrometric study of methanol crossover in a direct methanol fuel cell.* Journal of the Electrochemical Society, 1996. 143: p. 1233.

75. Oliveira V.B., Falcao D.S., Rangel C.M., and Pinto A.M.F.R., *A comparative study of approaches to direct methanol fuel cells modelling.* Journal of Hydrogen Energy, 2007. 32: p. 415-425.

76. Sousa R Jr. and Gonzalez E.R., *Mathematical modelling of polymer electrolyte fuel cells.* Journal of Power Sources, 2005. 147(1-2): p. 32-45.

77. Wang C.Y., *Fundamental models for fuel cell engineering.* Chemical Reviews, 2004. 104(10): p. 4753-4760.

78. Yao K.Z., Karan K., McAuley K.B., Oosthuizen P., Peppley B., and Xie T., *A review of mathematical models for hydrogen and direct methanol polymer electrolyte membrane fuel cells.* Fuel Cells, 2004. 4(2): p. 3-29.

79. Argyropoulos P., Scott K., Shukla A.K., and Jackson C.L., *Empirical model equations for the direct methanol fuel cell.* Fuel Cells, 2002. 2(2): p. 78-82.

80. Argyropoulos P., Scott K., Shukla A.K., and Jackson C.L., *A semi-empirical model of the direct methanol fuel cell performance. Part I: Model development and verification.* Journal of Power Sources, 2003. 123: p. 190-199.

81. Scott K. and Argyropoulos P., *A one dimensional model of a methanol fuel cell anode.* Journal of Power Sources, 2004. 137(2): p. 228-238.

82. Scott K., Jackson C.L., and Argyropoulos P., *A semi-empirical model of the direct methanol fuel cell performance. Part II: Parametric analysis.* Journal of Power Sources, 2006. 161(2): p. 885-892.

83. Scott K., Argyropoulos P., and Sundmacher K., *A model for liquid feed direct methanol fuel cell.* Journal of Electroanalytical Chemistry, 1999. 477: p. 97-110.

84. Scott K., Taama W.M., and Cruickshank J., *Performance and modelling of a direct methanol solid polymer electrolyte fuel cell.* Journal of Power Sources, 1997. 65: p. 159-171.

85. Kim J., Srinivasan S., Lee S.M., and Chamberlin C.E., *Modelling of proton exchange membrane fuel cell performance with an empirical equation.* Journal of the Electrochemical Society, 1995. 142(8): p. 2670-2674.

86. Squadrito G., Maggio G., Passalacqua E., and Patti A., *An empirical equation for polymer electrolyte fuel cell (PEFC) behaviour.* Journal of Applied Electrochemistry, 1999. 29: p. 1449-1455.

87. Srinivasan S., Ticianelli E.A.,Derouin C.R., and Redondo A., *Advances in solid polymer electrolyte fuel cell technology with low platinum loading electrodes.* Journal of Power Sources, 1988. 22: p. 359-375.

88. Kim T. H. and Bae Y.C., *A semi-empirical cell voltage model for the direct methanol fuel cell: the methanol crossover effect.* Journal of Polymer, 2005. 46: p. 6494–6499.

89. Tu H.C., Wang Y.Y., Wan C.C., and Hsueh K.L., *Semi-empirical model to elucidate the effect of methanol crossover on direct methanol fuel cell.* Journal of Power Sources, 2006. 159(2): p. 1105-1114.

90. Simoglou A., Argyropoulos P., Martin E.B., Scott K., Morris A.J., and Taama W.M., *Dynamic modelling of the voltage response of direct methanol fuel cells and stacks Part I: Model development and validation.* Chemical Engineering Science, 2001. 56: p. 6761-6772.

91. Simoglou A., Argyropoulos P., Martin E.B., Scott K., Morris A.J., and Taama W.M., *Dynamic modelling of the voltage response of direct methanol fuel cells*

and stacks Part II: Feasibility study of model-based scale-up and scale-down. Chemical Engineering Science, 2001. 56: p. 6773-6779.

92. Dohle H., Divisek J., and Jung R., *Process engineering of the direct methanol fuel cell.* Journal of Power Sources, 2000. 86: p. 469-477.
93. Dohle H., Mergel J., and Stolten D., *Heat and power management of a direct methanol fuel cell system.* Journal of Power Sources, 2002. 111: p. 268-282.
94. Dohle H. and Wippermann K., *Experimental evaluation and semi-empirical modeling of U/I characteristics and methanol permeation of a direct methanol fuel cell.* Journal of Power Sources, 2004. 135(1-2): p. 512-164.
95. Kulikovsky A. A., *A method for analysis of DMFC performance curves.* Journal of Electrochemistry Communications, 2003. 5: p. 1030-1036.
96. Kulikovsky A. A., *Analytical Model of the anode side of DMFC: the effect of non-Tafel kinetics on cell performance.* Journal of Electrochemistry Communications, 2003. 5: p. 530-538.
97. Kulikovsky A. A., *Model of the flow with bubbles in the anode channel and performance of a direct methanol fuel cell.* Journal of Electrochemistry Communications, 2005. 7: p. 237-243.
98. Baxter S.F., Battaglia V.S., and White R.E., *Methanol fuel cell model: Anode.* Journal of the Electrochemical Society, 1999. 146: p. 437-447.
99. Sundmacher K., Schultz T., Zhou, S., Scott K., Ginkel M., and Gilles E. D., *Dynamics of the direct methanol fuel cell (DMFC): experiments and model-based analysis.* Chemical Engineering Science, 2001. 56(2): p. 333-341.
100. Nordlund J. and Lindbergh G., *A Model for the porous direct methanol fuel cells anode.* Journal of the Electrochemical Society, 2002. 149(9): p. A1107-A1113.
101. Nordlund J. and Lindbergh G., *Temperature dependent kinetics of the anode in the DMFC.* Journal of the Electrochemical Society, 2004. 151(9): p. A1357-A1362.
102. Wang Z. H. and Wang C.Y., *Mathematical modelling of liquid-feed direct methanol fuel cells.* Journal of the Electrochemical Society, 2003. 150(4): p. A508-A519.
103. Murgia G., Pisani L., Shukla A.K., and Scott K., *A numerical model of a liquid feed solid polymer electrolyte DMFC and Its experimental validation.* Journal of the Electrochemical Society, 2003. 150(9): p. A1231-A1245.
104. Meyers J. P. and Newman J., *Simulation of the direct methanol fuel cell-II. Modeling and data analysis of transport and kinetic phenomena.* Journal of the Electrochemical Society, 2002. 149(6): p. A718-A728.

105. Meyers J. P. and Newman J., *Simulation of the direct methanol fuel cell-I. Thermodynamic framework for a multicomponent membrane.* Journal of the Electrochemical Society, 2002. 149(6): p. A710-A717.

106. Meyers J. P. and Newman J., *Simulation of the direct methanol fuel cell-III. Design and optimization.* Journal of the Electrochemical Society, 2002. 149(6): p. A729-A735.

107. García B.L., Sethuraman V.A., Weidner J.W., and White R.E., *Mathematical model of a direct methanol fuel cell.* Journal of Fuel Cell Sciences and Technology, 2004. 1: p. 43-48.

108. Jung D.H., Lee C.H., Kim C.S., and Shin D.R., *Performance of a direct methanol polymer electrolyte fuel cell.* Journal of Power Sources, 1998. 71: p. 169-173.

109. Shukla A., Jackson C.L., Scott K., and Murgia G., *A solid-polymer electrolyte direct methanol fuel cell with a mixed reactant and air anode.* Journal of Power Sources, 2002. 111(1): p. 43-51.

110. Lim C. and Wang C.Y., *Development of high-power electrodes for a liquid-feed direct methanol fuel cell.* Journal of Power Sources, 2003. 113: p. 145-150.

111. Tsotridis G. *Fuel cell testing, safety and quality assurance FCTESQA: European Commission.* in *International Energy Agency (IEA) Annex XVI Fall 2006 meeting.* 2006. Jülich, Germany.

112. Anderson M.J. and Whitcomb P.J., *DOE Simplified: Practical tools for effective experimentation.* 2nd ed. 2007, New York: Productivity Press.

113. Montgomery D.C., *Design and analysis of experiments* 5th ed. 2004, New York: John Wiley & Sons, Inc,.

114. Jackson C.L., *Performance and optimisation of the direct methanol fuel cell (DMFC).* PhD Thesis, 2006, University of Newcastle upon Tyne.

115. *LabVIEW (version 7.1), 2004, National Instruments Corporation*: Texas.

116. *Design Expert (Version 6.0.11).* 2005, Stat-Ease, Inc: Minneapolis.

117. *NIST/SEMATECH e-Handbook of Statistical Methods, http://www.itl.nist.gov/div898/handbook/, Ed. Croarkin C., and Tobias P., date accessed March 2006.*

118. Aricó A.S., Cretí P, Modica E., Monforte G., Baglio V., and A. V, *Investigation of direct methanol fuel cell based on unsupported Pt-Ru anode catalysts with different chemical properties.* Journal of Electrochimica Acta, 2000. 45(25-26): p. 319-4328.

119. Gasteiger H. A., Markovic N., Ross P. N., and Cairns E. J., *Temperature dependent methanol electro-oxidation on well characterized Pt-Ru alloys.* Journal of the Electrochemical Society, 1994. 141(7): p. 1795-1803.

120. Krewer U., Christov M., Vidakovic T., and Sundmacher K., *Impedance spectroscopic analysis of the electrochemical methanol oxidation kinetics.* Journal of Electroanalytical Chemistry, 2006. 589: p. 148-159.

121. Gogel V., Frey T., Yongsheng Z., Friedrich K.A., Jörissen L., and Garche J., *Performance and methanol permeation of direct methanol fuel cells: Dependence on operating conditions and on electrode structure.* Journal of Power Sources, 2004. 127: p. 172-180.

122. Anderson M.J. and Whitcomb P.J., *How to use graphs to diagnose and deal with bad experiment data*, in *Stat-Ease, Inc. www.statease.com, date accessed March 2008.*

123. Han J. and Liu H., *Real time measurements of methanol crossover in a DMFC.* Journal of Power Sources, 2006. 164: p. 166-173.

124. Hamnett, A., *Mechanism and electrocatalysis in the direct methanol fuel cell.* Catalysis Today, 1997. 38(4): p. 445-457.

125. Markovic N. M., Gasteiger H. A., Ross, P. N. and Jiang X., *Electro-oxidation mechanisms of methanol and formic acid on Pt-Ru alloy surfaces*, in *Surface Structure and Electrochemical Reactivity.* 1995, Pergamon Press. p. 91-98.

126. Dohle H., Schmitz H., Bewer T., Mergel J., and Stolten D., *Development of a compact 500 W class direct methanol fuel cell stack.* Journal of Power Sources, 2002. 106(1-2): p. 313-322.

127. Furuukawa K., Okajima K., and Sudoh M., *Structural control and impedance analysis of cathode for direct methanol fuel cell.* Journal of Power Sources, 2005. 139(1-2): p. 9-14.

128. Kim J.H., Ha H.Y., Hong S.A., and Lee H.I., *Influence of the solvent in anode catalyst ink on the performance of a direct methanol fuel cell.* Journal of Power Sources, 2004. 135(1-2): p. 29-35.

129. Lee J.S., Han K.I., Park S.O., Kim H.N., and Kim H., *Performance and impedance under various catalyst layer thickness in DMFC.* Journal of Electrochimica Acta, 2004. 50(2-3): p. 803-806.

130. Liu F. and Wang C.-Y., *Variations in interfacial properties during cell conditioning and influence of heat treatment of ionomer on the characteristics of direct methanol fuel cells.* Journal of Electrochimica Acta, 2005. 50(6): p. 1413-1422.

131. Wang S., Sun G., Wang Z., Zhou Z., Zhao X., Sun X., Fan X., Yi B., and Xin Q., *Improvement of direct methanol fuel cell performance by modifying catalyst coated membrane structure.* Journal of Electrochemistry Communications, 2005. 7(10): p. 1007-1012.

132. Zhao X., Fan X., Wang S., Yang S., Yi B., Xin Q., and Sun G., *Determination of ionic resistance and optimal composition in the anodic catalyst layers of DMFC using AC impedance*. Journal of Hydrogen Energy: Fuel Cells, 2005. 30(9): p. 1003-1010.

133. Zhou W.J., Zhou W.Z., Li Z.H., Song S.Q., Sun G.Q., Xin Q., Douvartzides S., Goula M., and Tsiakaras P., *Performance comparison of a low temperature direct alcohol fuel cells with different anode catalysts.* Journal of Power Sources, 2004. 126(1-2): p. 16-22.

134. Schmidt T. J., Gasteiger H. A., and Behm R. J., *Methanol electrooxidation on a colloidal PtRu-alloy fuel-cell catalyst.* Electrochemistry Communications, 1999. 1(1): p. 1-4.

135. Frey T. and L. M., *Effects of membrane electrode assembly preparation on the polymer electrolyte membrane fuel cell performance.* Journal of Electrochimica Acta, 2004. 50(1): p. 99-105.

136. Nordlund J., Roessler A., and Lindbergh G., *The influence of electrode morphology on the performance of a DMFC anode.* Journal of Applied Electrochemistry, 2002. 32: p. 259-265.

137. Hogarth M., Christensen P., Hamnett A., and Shukla A., *The design and construction of high-performance direct methanol fuel cells. 2. Vapour-feed systems.* Journal of Power Sources, 1997. 69(1-2): p. 125-136.

138. Tang H., Wang S., Pan M., Jiang S.P., and Ruan Y., *Performance of DMFCs prepared by hot-pressed MEA and catalyst-coated membrane.* Fuel Cells Bulletin, 2007. 2007(5): p. 12-16.

139. Anderson M.J. and Whitcomb P.J., *RSM Simplified: Optimizing process using response surface methos for design of experiments.* 2005, New York: Productivity Press.

140. Passalacqua E., Lufrano F., Squadrito G., Patti A., and Giorgi L., *Nafion content in the catalyst layer of polymer electrolyte fuel cells: effects on structure and performance.* Journal of Electrochimica Acta, 2001. 46(6): p. 799-805.

141. Gamburzev S. and Appleby A.J., *Recent progress in performance improvement of the proton exchange membrane fuel cell (PEMFC).* Journal of Power Sources, 2002. 107(1): p. 5-12.

142. Qi Z. and Kaufman A., *Improvement of water management by a microporous sublayer for PEM fuel cells.* Journal of Power Sources, 2002. 109(1): p. 38-46.

143. Wasmus S. and Kuver A., *Methanol oxidation and direct methanol fuel cells: A selective review.* Electroanalytical Chemistry, 1999. 461: p. 14-31.

144. Bagotzky V. S., Vassiliev Yu. B., and Khazova O. A., *Generalized scheme of chemisorption, electrooxidation and electroreduction of simple organic compounds on platinum group metals.* Journal of Electroanalytical Chemistry, 1977. 81(2): p. 229-238.

145. Burstein G.T., Barnett C.J., Kucernak A.R., and Williams K.R., *Aspects of the anodic oxidation of methanol.* Catalysis Today, 1997. 38: p. 425-437.

146. Frelink T., Visscher W., and Van Veen J.A.R., *Measurement of the Ru surface content of electrocodeposited PtRu electrodes with the electrochemical quartz crystal microbalance: Implications for methanol and CO electrooxidation.* Langmuir, 1996. 12(15): p. 3702-3708.

147. Lizcano-Valbuena W. H., Paganin V. A., and Gonzalez E. R., *Methanol electro-oxidation on gas diffusion electrodes prepared with PtRu/C catalysts.* Electrochimica Acta, 2002. 47(22-23): p. 3715 - 3722.

148. Munk J., Christensen P. A., Hamnett A., and Skou E., *The electrochemical oxidation of methanol on platinum and platinum + ruthenium particulate electrodes studied by in-situ FTIR spectroscopy and electrochemical mass spectrometry.* Journal of Electroanalytical Chemistry, 1996. 401: p. 215-222.

149. Raman R. K., Shukla A. K., Gayen A., Hegde M. S., Priolkar K. R., Sarode P. R. and Emura S., *Tailoring a Pt-Ru catalyst for enhanced methanol electro-oxidation.* Journal of Power Sources, 2006. 157(1): p. 45-55.

150. Kabbabi A., Faure R., Durand R., Beden B., Hahn F., Leger J. M., and Lamy C., *In situ FTIRS study of the electrocatalytic oxidation of carbon monoxide and methanol at platinum-ruthenium bulk alloy electrodes.* Journal of Electroanalytical Chemistry, 1998. 444(1): p. 41-53.

151. Atkins P.W., *Concepts in physical chemistry*. 1998: Oxford University Press.

152. *Maple (version 9), 2004, Maplesoft Inc,* . 1981-2003: Waterloo, Canada.

153. Liu F. and Wang C Y., *Mixed potential in a direct methanol fuel cell.* Journal of the Electrochemical Society, 2007. 154(6): p. B514-522.

154. Scott K., Taama W.M., and Argyropoulos P., *Engineering aspects of the direct methanol fuel cell system.* Journal of Power Sources, 1999. 79: p. 43-59.

155. Mann R.F., Amphlett J.C., Peppley B.A., and Thurgood C.P., *Application of Butler-Volmer equations in the modelling of activation polarization for PEM fuel cells.* Journal of Power Sources, 2006. 161: p. 775-781.

156. Parthasarathy A., Srinivasan S., Appleby A. J., and Martin C. R., *Temperature dependence of the electrode kinetics of oxygen reduction at the Platinum/Nafion interface -a microelectrode investigation.* Journal of the Electrochemical Society, 1992. 139(9): p. 2530-2537.

157. Casalegno A., Grassini P., and Marchesi R., *Experimental analysis of methanol cross-over in a direct methanol fuel cell.* Applied Themal Engineering, 2007. 27: p. 78-754.

158. Han J. and Liu H., *Real time measurements of methanol crossover in a DMFC.* Journal of Power Sources, 2007. 164(1): p. 166-173.

159. *GraphPad Prism (version 4), GraphPad Software Inc.* 2004: California.

160. Motulsky H. and Christopoulos A., eds. *Fitting models to biological data by using linear and nonlinear regression.* GraphPad. Vol. 4. 2004, Prism. 13-159.